Dissertation

submitted to the

Combined Faculties for the Natural Sciences and for Mathematics

of the Ruperto-Carola University of Heidelberg, Germany

for the degree of

Doctor of Natural Sciences

presented by

Aleksandra Karolina Balwierz, M.Sc. in Medical Biotechnology

born in Kraków, Poland

Oral examination date:

ERBB2 as a driver of an invasive phenotype of cells grown in 3D culture and an important regulator of oncogenic miRNAs' expression in breast cancer

Referees: Prof. Dr. Stefan Wiemann
Prof. Dr. Bruce Edgar

Declaration

I hereby declare that the work reported in this thesis was carried out between April 2010 and December 2014 under the joint supervision of Prof. Dr. Stefan Wiemann and Assist. Prof. Dr. Özgür Şahin at German Cancer Research Center, Heidelberg, Germany. The data described here has not yet been presented as a part of a university examination, is original and all the sources used have been referenced.

Heidelberg, ……

……..

Aleksandra Balwierz

Acknowledgements

Firstly, I would like to express my sincerest gratitude to both of my supervisors. Dr. Özgür Şahin was my supervisor in the first years of my PhD studies and guided my first steps in the field of ERBB signaling and miRNAs. He was a great teacher and I am thankful for his time spent on thoroughly understanding my daily challenges and his readiness to give practical and useful advice to me. Prof. Dr. Stefan Wiemann, my supervisor for the last three years, and my examiner, gave me an invaluable opportunity to develop as a scientist by giving me the chance to work independently, participate in international meetings and pursue my own ideas. I would like to thank him for his constant support and encouragement, remarkable patience, respect and last but not least for critically reading my manuscript.

I would like to thank my other thesis advisory committee members and examiners, Prof. Dr. Bruce Edgar, Dr. Aurelio Telemann, Prof. Dr. Rüdiger Hell and Prof. Dr. Oliver Gruss as well as the DKFZ Graduate School for giving me their time and input.

I am also grateful to Prof. Dr. Yosef Yarden, who agreed to host and supervise me during my research stay in his laboratory. He and his group not only shared their scientific expertise with me but they also created a welcoming atmosphere and made me feel at home.

I thank the members of the DKFZ Core Facilities for their excellent technical help and professional discussions, especially: PD Dr. Karin Muller-Decker, Dr. Christopher Previti, Klaus Hexel, Brigitte Steinbauer, and Dr. Rainer Will whose interest kept me going forward.

I would like to thank all the present and past members of the Molecular Genome Analysis department, most notably: Dr. Johanna Sonntag, Dr. Ulrike Korf, Afsheen Yousaf, Dr. Aoife Ward and Dr. Kirti Sharma – who either directly or indirectly contributed to the project; Angelika Wörner and Heike Wilhelm – for their excellent technical support; Dr. Stefan Uhlmann, Chiara Giacomelli, Moritz Küblbeck, Alexander Bott, Dr. Cindy Körner, Dr. Ioanna Keklikoglou, Dr. Christian Breunig, Dr. Sabine Klauck, Ewald Münstermann, Ute Ernst, Rita Schatten and Daniela Fischer – for creating an enjoyable working environment.

Finally, I want to thank my family, Robert Kreuzer and Dr. Marta Faryna for their constant support, encouragement and readiness to cheer me up when I needed it. I also thank the group of Polish scientists in Heidelberg, who became my good friends during this time.

For my Family

Table of contents

1. Summary

1.1 Abstract

Breast cancer is often associated with deregulated activity of two receptor tyrosine kinases (RTKs) from the ERBB family: EGFR and ERBB2 (HER2/Neu). Whereas the EGF receptor is often mutated in breast cancer, ERBB2 is up-regulated in up to 20% of invasive breast tumors and plays a triggering role in cell proliferation, invasion and metastasis. Patients overexpressing ERBB2 are treated with targeted therapies and in particular with the monoclonal antibody trastuzumab, which binds an extracellular domain of the receptor and abrogates receptor-kinase activation. However, ERBB2-positive breast cancer patients overexpress ERBB2 to different extent. The expression range is very wide, raising the question whether the tumors expressing moderate, high and very high ERBB2 levels have different outcome and patients carrying them can be treated as one entity or not.

To better understand the impact of different ERBB2 levels I developed stable cell line pools overexpressing ERBB2 at different levels. I observed that in 3D culture as well as in matrigel-based invasion assays, cells expressing very high ERBB2 levels showed more invasive properties than those expressing moderate ERBB2 levels, even in the absence of EGF. This was accompanied by disruption of cell polarity in 3D-grown spheroids and anchorage-independent growth which occured only when ERBB2 expression was very high. These phenotypes could be at least partially explained by ERBB2-dose dependent epithelial-mesenchymal transition (EMT), an increase in HB-EGF transcription and constitutive ERK and AKT signaling pathway activation at the very high ERBB2 levels.

As recently several miRNAs have been reported to regulate EMT-related processes and because their expression is frequently deregulated in cancer, I also hypothesized that their expression would change with the ERBB2 expression level in 3D culture. To verify my hypothesis, I performed small RNA sequencing from stable cell line pools grown in matrigel. This identified several miRNAs which are ERBB2-level dependent. I focused then on the functional characterization of miR-301b and miR-130b whose expressions were ERBB2-dependent in 3D, but not in 2D culture. Overexpression of these miRNAs phenocopied ERBB2 effects on cell invasion and proliferation as well as induction of EMT, as did overexpression of the related miR-301a.

1.2 Zusammenfassung

Brustkrebs wird oft in Verbindung gebracht mit deregulierter Aktivität von EGFR und ERBB2 (HER2/Neu), zwei Rezeptor-Tyrosinkinasen der ERBB Familie. Während der EGF Rezeptor bei Brustkrebs oft Mutationen aufweist, ist ERBB2 in bis zu 20% aller Fälle von invasiven Brusttumoren hochreguliert und spielt eine auslösende Rolle für Zellteilung, Zellinvasion und Metastasen. Patienten, die ERBB2 überexprimieren, werden mit zielgerichteten Therapien behandelt, insbesondere mit dem monoklonalen Antikörper Trastuzumab, welcher eine extrazelluläre Domäne des Rezeptors bindet und eine Aktivierung der Rezeptor-Tyrosinkinase verhindert.

ERBB2-positive Brustkrebs Patienten überexprimieren ERBB2 jedoch unterschiedlich stark. Die großen Unterschiede der Expression werfen die Fragen auf, ob die moderate, hohe oder sehr hohe ERBB2-Tumorexpressionslevel zu unterschiedlichen Krankheitsverläufen führen und ob Patienten mit diesen Tumoren als eine Gruppe betrachtet werden können oder nicht. Um den Effekt verschieden starker ERBB2-Level besser zu verstehen, habe ich stabile Zelllinien entwickelt, welche ERBB2 in unterschiedlichem Ausmaß überexprimieren. Ich konnte beobachten, dass Zellen mit hohen und sehr hohen ERBB2-Leveln, sowohl in 3D-Kulturen als auch in Matrigel-basierten Invasionstests stärkere invasive Eigenschaften aufwiesen, als solche mit moderaten ERBB2-Leveln, selbst wenn kein EGF vorhanden war. Dies wurde von Störungen der Zell-Polarität in 3D-gezüchteten Spheroiden und von verankerungsunabhängigem Wachstum begleitet, welches nur bei sehr hoher ERBB2-Exprimierung auftrat. Diese Phänotypen können zumindest teilweise durch die von der ERBB2-Dosis abhängige epithelial-mesenchymale Transition (EMT), einem Anstieg der HB-EGF Transkription und konstitutiver Aktivierung von ERK und AKT Signalwegen bei sehr hohen ERBB2-Leveln erklärt werden.

Da vor Kurzem mehrere miRNAs gefunden wurden, die EMT-abhängige Prozesse regulieren, und weil deren Exprimierung häufig bei Krebs dereguliert ist, habe ich die Hypothese aufgestellt, dass die Überexprimierung dieser miRNAs die ERBB2-Level in 3D-Kulturen verändern würde. Um meine Hypothese zu verifizieren habe ich kleine RNAs von stabilen Zelllinien sequenziert, welche in Matrigel gezüchtet wurden. Dadurch konnte ich mehrere miRNAs identifizieren, die abhänging von den ERBB2-Leveln sind. Ich habe mich dann auf die funktionale Charakterisierung von miR-301b und miR-130b fokussiert, wessen Expression in

3D-Kulturen - jedoch nicht in 2D-Kulturen - ERBB2-abhängig war. Überexprimierung dieser miRNAs induzierte ERBB2-gleiche phänotypische Effekte auf Zellinvasion, Zellvermehrung und auf die Induktion von EMT. Dies konnte auch für das verwandte miR-301a beobachtet werden.

2. Abbreviations

°C	degrees Celsius
AGO	argonaute
AKT1	v-akt murine thymoma viral oncogene homolog 1
APS	ammonium peroxodisulphate
AR	AREG, amphiregulin
ATP	adenosine triphosphate
a.u.	arbitrary units
BCA	bicinchoninic acid
bp	base pairs
BSA	bovine serum albumin
CDH1	E-cadherin
CDH2	N-cadherin
cDNA	complementary DNA
CDS	coding sequence
CISH	chromogenic in situ hybridization
cm	centimeter
CTTN	cortactin
DAPI	4′,6-Diamidino-2-phenylindole
DAVID	Database for Annotation, Visualization and Integrated Discovery
DICER1	dicer 1, ribonuclease type III
DMSO	dimethyl sulfoxide
DNA	deoxyribonucleic acid
dNTPs	deoxyribonucleotide triphosphates
E. coli	Escherichia coli
ECL	enhanced chemiluminescence
EGF	epidermal growth factor
EGFP	enhanced green fluorescent protein
EGFR	EGF receptor
EMT	epithelial-mesenchymal transition

ER	estrogen receptor
ERBB2	v-erb-b2 avian erythroblastic leukemia viral oncogene homolog 2
ERBB3	v-erb-b2 avian erythroblastic leukemia viral oncogene homolog 3
ERBB4	v-erb-b2 avian erythroblastic leukemia viral oncogene homolog 4
ERK1	MAPK3, mitogen-activated protein kinase 3
ERK2	MAPK1, mitogen-activated protein kinase 1
FACS	fluorescence activated cell sorting
FAK	Focal Adhesion Kinase, PTK2, protein tyrosine kinase 2
FBS	fetal bovine serum
FISH	fluorescence in situ hybridization
FN1	Fibronectin 1
g	gram
GM130	protein encoded by GOLGA2 (golgin A2) gene
h	hours
HB-EGF	heparin-binding EGF-like growth factor
hluc+	firefly luciferase
hRluc	renilla luciferase
IHC	immunohistochemistry
kbp	kilobase pair
KRT5	keratin 5, cytokeratin 5
KRT6	keratin 6, cytokeratin 6
l	liter
LB Medium	Luria Bertani Medium
M	molar
MEK1	MAP2K1, mitogen-activated protein kinase kinase 1
MEK2	MAP2K2, mitogen-activated protein kinase kinase 2
mg	milligram
min	minute
miRNA	microRNA
ml	milliliter
mRNA	messenger RNA

MTDH	metadherin
MUC1	mucin 1, cell surface associated
NEAA	non-essential aminoacids
ng	nanogram
nm	nanometer
nM	nanomolar
NRG1-4	neuregulin 1-4
nt	nucleotide
PAGE	polyacrylamide gel-electrophoresis
PBS	phospahte buffered saline
PCR	polymerase chain reaction
Pen/Strep	penicillin/streptomycin
PFA	paraformaldehyd
PI3K	phosphoinositide 3-kinase
PKA	protein kinase A
PLCG1	phospholipase gamma 1
polyHEMA	poly(2-hydroxyethyl methacrylate)
PTEN	phosphatase and tensin homolog
qRT-PCR	quantitative realtime PCR
RHOA	ras homolog family member A
RISC	RNA induced silencing complex
RNA	ribonucleic acid
rpm	revolutions per minute
RPPA	reverse phase protein array
RTCA	real time cell analyzer
SDS	sodium dodecylsulphate
sec	second
siRNA	short interfering RNA
SISH	silver in situ hybridization
SRC	sarcoma viral oncogene homolog
SRC	v-src avian sarcoma (Schmidt-Ruppin A-2) viral oncogene homolog

TBS-T	Tris-buffered saline-Tween 20
TEMED	tetramethylethylenediamine
TGFα	transforming growth factor, alpha
TP53INP1	tumor protein p53 inducible nuclear protein 1
U	units
UPL	universal probe library
UTR	untranslated region
V	volt
v/v	volume/volume
VIM	vimentin
w/v	weight/volume
WST1	Water soluble Tetrazolium salt 1, (2-(4-Iodophenyl)-3-(4-nitrophenyl)-5-(2,4-disulfophenyl)-2H-tetrazolium, monosodium salt)
ZEB1	zinc finger E-box-binding homeobox 1
µl	microliter
µM	micromolar

3. Introduction

3.1 Breast cancer

Breast cancer is the most frequently diagnosed cancer and the second leading cause of cancer deaths, after lung cancer, in women.[1] In 2012 around 500 thousand women in Europe, 233 thousand women in the United States, and in total approximately 1.67 million breast cancer cases worldwide have been diagnosed with the disease.[2,3] Out of them, one third is estimated to eventually die of breast cancer (522 thousand deaths in 2012). Currently, the ratio between breast cancer mortality and incidence varies depending on the world region and is much higher in less developed countries (Figure 1).[3]

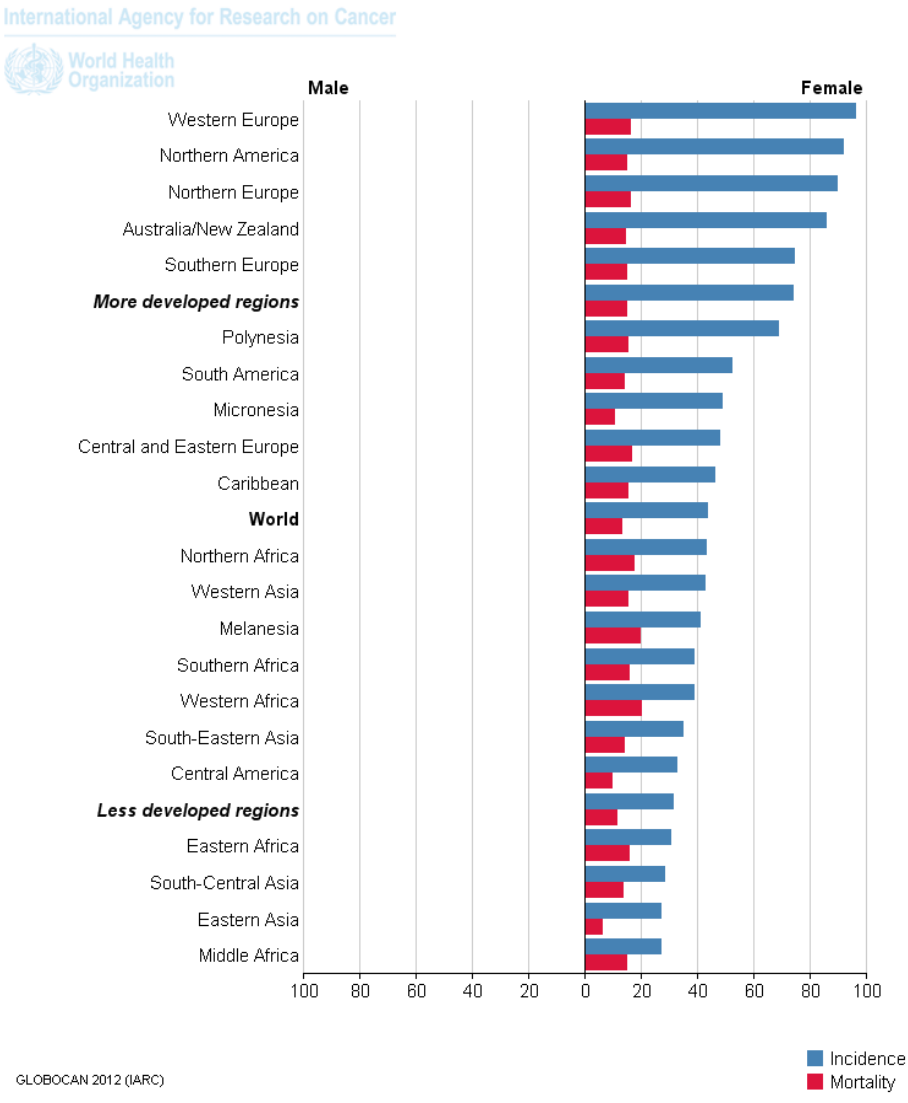

Figure 1

Breast cancer incidence and mortality rates per 100,000 people depending on the world region in 2012. (adapted from GLOBOCAN 2012, http://globocan.iarc.fr)[3]

While breast cancer can affect men as well and is associated with poorer survival rate in men compared to women, male breast cancer is rare and accounts for less than 1% of all breast cancer cases and less than 0.1% of cancer deaths in men.[4,5]

Breast cancer is a very heterogenous disease. Half a century ago clinicians had observed diverse responses to breast cancer treatment in different patients without finding a good explanation for that phenomenon. The recognition of the impact hormone receptor presence in tumor samples has on hormone therapy efficiency was one of the first breakthroughs in the breast cancer field.[6,7,8] The tumors expressing estrogen receptor showed "addiction" to estrogen and blockage of the estrogen receptor (ER) with the ER targeting drug tamoxifen has brought a significant improvement to the patients' survival.[9,10] However, treatment of ER-negative (ER-) tumors with such drugs proved to be less effective and more aggressive radiation therapy and/or chemotherapy had to be administred.

The recent emergence of new highthroughput technologies to study the molecular background of tumor samples has triggered a number of attempts to find common traits among breast cancer patients. Technologies used involve studies at DNA level – genotyping, sequencing; RNA level – gene expression profiling (both using either microarrays or deep sequencing methods), as well as at the protein level – using protein microarrays.[11,12,13,14]

Today one of the most widely accepted classifications of breast cancer is founded on the discovery by Sorlie et. al, who reported that five main molecular subtypes of breast cancer can be distinguished mostly based on particular expression patterns of ~500 intrinsic genes.[15,16] These molecular subtypes are: basal-like, HER2-overexpressing, normal breast tissue-like, estrogen/progesterone receptor (ER/PR) positive luminal A (good differentiation; low Ki67 staining) and luminal B (poor differentiation; high Ki67 staining).[15,16,17]

The best prognosis is associated with the luminal A subtype, followed by normal breast-like and luminal B. Much more aggressive tumors belong to the basal-like subtype, consisting mainly of HER2-/ER-/PR- (so called triple negative; TN) breast cancers and to the HER2 overexpressing subtype.[15,16,18] Most of the patients with BRCA1 gene mutation – a heritable mutation increasing the risk of developing breast cancer to 50-85% in women by age 70 – are of the TN subtype as their tumors show striking similarities to the basal-like subtype, including lack of estrogen/progesterone receptor expression and HER2 overexpression.[19]

It is estimated that around 15-20% of invasive primary breast cancer cases bear genomic amplifications of ERBB2 and/or otherwise overexpress this receptor tyrosine kinase.[20,21]

They are associated with increased resistance to standard anti-cancer therapies and with shorter overall survival.[22,23,18] ERBB2-overexpressing tumors are, however, not homogeneous. If they do not express hormone receptors then they are classified into the ERBB2-overexpressing breast cancer subtype, if they do, then they are classified as luminal B and associated with relatively better overall survival (Figure 2).[18]

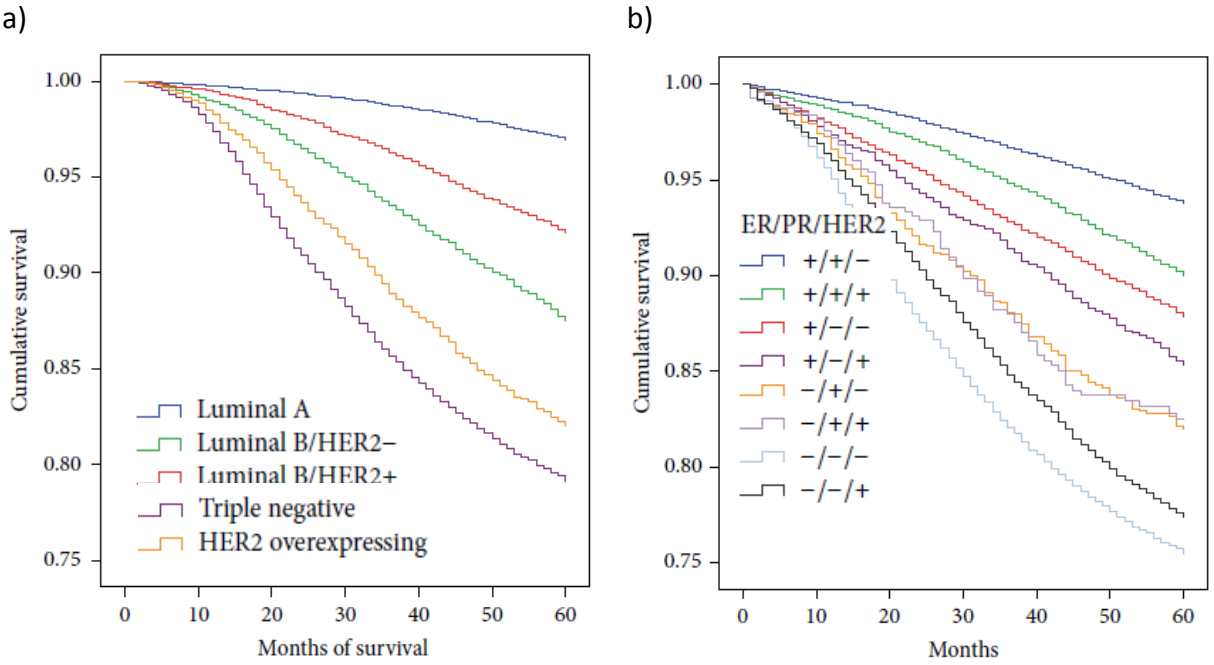

Figure 2
Kaplan-Meier 5-year survival rates for combined breast cancer stages 1-3 with respect to a) breast cancer subtype; b) ER/PR/HER2 status. (adapted from C.A. Parise et al., 2014)[18]

In the last years several tests have been developed to stratify breast cancer patients as well as to discover novel molecular signatures.[12] Their aim is to assist clinicians in choosing the adequate personalized therapy by predicting patients' outcome and response to particular treatments. The most advanced tests in the clinical setting are MammaPrint (NKI-70, based on a 70 genes signature)[24,25,26,27], OncotypeDX (Recurrence Score, 21 genes)[28] and Prosigna (PAM50, 50 genes)[29]. There are also other tests at various phases of development and with varying complexities, like BluePrint[30,31], TargetPrint[32], Molecular Grade Index (MGI)[33], Breast Cancer Index (BCI)[34,35], SCMGENE[36,37], IHC4[38], Mammostrat[39], Nottingham Prognostic Index Plus (NPI+)[40,41], Randox Breast Cancer Array[42], Genomic Grade Index (GGI)[43], Basal 14[44], Core Serum Response (CSR/wound) signature[45], 14-gene metastasis score (MS-14)[46], 76-gene Veridex signature (EMC-76)[47], expression signature for p53 status[48], hormone

receptor negative/triple negative signatures IR-7[49] and Buck-14[50] and Integrated Cytokine Score (ICS).[51]

Although the number of tests/molecular signatures of breast cancer increases rapidly, the main types of treatment have remained largely unchanged. Most patients undergo conventional surgery, radiation therapy, chemotherapy, and/or anti-hormone therapy. However, the emergence and efficiency of first targeted therapy drugs in breast cancer treatment (inspired by development of ERBB2-directed monoclonal antibody trastuzumab) brings hope to overcome the need of unselective and more aggressive treatments for hormone negative tumors.[52,53,54]

Currently, tumor specimens obtained during the surgical procedure or biopsy samples are routinely analyzed by in-situ hybridization (ISH) or immunohistochemistry (IHC) for overexpression of ERBB2 (HER2) in parallel with IHC tests for the presence of estrogen and progesterone receptors.[55,21,56] Patients positive for estrogen receptor can be then treated with hormone therapy using the ER-targeted drug tamoxifen or aromatase inhibitors, like anastrozole, in either a neadjuvant (before surgery) or in the more commonly applied adjuvant (post-surgery) setting.[57,58,59] Patients who are classified as ERBB2-positive can, on the other hand, undergo targeted therapy treatment with trastuzumab or with combination of trastuzumab and pertuzumab in the adjuvant setting for early breast cancer or in neoadjuvant setting for metastatic breast cancer.[6061] In case of more advanced breast cancer stages lapatinib and an improved version of trastuzumab, trastuzumab emtansine (T-DM1), are also in clinical use.[62] Although the most common treatment for HER2-positivie patients – trastuzumab – has been shown to improve patients' overall survival by 33% in early stage breast cancers and by 20% in metastatic breast cancers[63,64], the de novo resistance rate in both groups is very high and most of the metastatic patients who show primary response to the treatment eventually develop resistance within one year.[53,65] The ERBB2-overexpressing breast cancer subtype remains therefore responsible for a large portion of breast cancer deaths.

3.2 Structure and function of ERBB2 and ERBB-family receptors

3.2.1 ERBB2 and other ERBB-family members' structure

ERBB2 (v-erb-b2 avian erythroblastic leukemia viral oncogene homolog; also called HER2/Neu) is a 185kDa member of the human epidermal growth factor receptor (HER/ERBB) family, along with EGFR (HER1), ERBB3 (HER3) and ERBB4 (HER4).[66] ERBB family members are classified as receptor tyrosine kinases (RTKs) due to the presence of three characteristic domains in their structure: ligand-binding extracellular domain (~620 residues), a single alpha-helical transmembrane domain (~23 residues) and a tyrosine kinase intracellular domain (~260 residues) which is flanked by juxtamembrane (~40 residues) and C-terminal (~232 residues) regulatory elements.[67,68] Two of the receptors, ERBB2 and ERBB3, are however not fully autonomous. ERBB2 lacks a known ligand and ERBB3 possesses only very weak kinase activity.[69,70,71,72] For the activation of any ERBB family receptor, homo- or heterodimerization with another family member and the resulting transphosphorylation is required.[71,68] This is possible when the conformation of the receptor changes into an active, dimerization-ready conformation upon ligand binding to its extracellular domain.[73,74,75] The extracellular part of the receptor consists of four smaller fragments. Domains I and III (L1 and L2) are capable of ligand binding and domains II and IV (cystein-rich domains CR1 and CR2) are required for receptor dimerization. In a monomeric state, domains II and IV interact with each other playing an autoinhibitory role. Ligand binding to domains I and III induces a conformational change and exposure of domains II and IV for dimerization.[68]

ERBB2 is specific in this protein family. Its extracellular domain is believed to be in a constitutively active conformation, as revealed by crystallography studies, which makes ERBB2 a preferential dimerization partner for other family members.[76] It is therefore often referred to as a coreceptor for other ERBB receptors or the "amplifier" of their signaling as it induces their stronger and prolonged activation once they bind their respective ligands. The signaling from EGFR homodimers, for example, is usually transient and receptor becomes quickly (within few minutes) internalized and degraded following ligand binding.[77,78,79] Heterodimerization with ERBB2 not only increases the ligand affinity and prolongs the duration of signaling, but also slows down the internalization of EGFR and enhances its recycling.[80,81] In spite of this suggested coreceptor role of ERBB2, its recently revealed structural similarity to the *Drosophila* EGFR receptor, which nevertheless requires ligand (incl.

Spitz, *Gurken*, *Keren*, *Vein*) binding for its activation, raises the question if the ERBB2 also possesses an autoinhibitory mechanism which needs to be disrupted by ligand binding to activate the receptor.[82,83] Although it seems that such ERBB2 ligand is yet to be identified, membrane-bound mucin 4 (MUC4), which contains an EGF-like domain in its structure could potentially play the role of an 'unorthodox' ligand, as it was demonstrated that it forms a complex with ERBB2, promotes its autocatalysis, relocates it from the lateral to the apical cell surface and stabilizes ERBB2-ERBB3 heterodimers.[84,85,86]

3.2.2 Regulation of ERBB receptor family signaling activity

ERBB-family signaling is one of the longest-studied protein-protein interaction networks in the history of molecular biology. Yet, the level of complexity of ERBB-signaling still opens new questions the more knowledge is accumulated. There are several factors contributing to this complexity. **1)** There are multiple combinations of receptor dimers which can be formed by ERBB-family members. All possible receptor combinations have been detected *in vivo* – six different heterodimers and four homodimers.[67,87] **2)** The number of activating ligands is high. Four of them bind both EGFR and ERBB4: betacellulin (BTC), epiregulin (EREG), heparin-binding EGF (HB-EGF)[88,89] and epithelial mitogen (epigen; EPGN).[90] Additionally, EGFR can bind epidermal growth factor (EGF), amphiregulin (AREG) and transforming growth factor α (TGFα), whereas ERBB4 can bind all four neuregulins (NRG1-4). Known ERBB3 ligands are NRG1-2.[90,91,92] Moreover, few EGF-like domain containing transmembrane proteins have been shown to directly interact with and activate ERBB receptors, including tomoregulin (TMEFF2; NRG5) activating ERBB4, neuroglycan C (CSPG5) activating ERBB3, and MUC4 activating ERBB2.[90,93,94,86] Around 3000 different proteins are encoded in the human genome that contain EGF-like domains. It is therefore very likely that more ligands will eventually be found to interact with ERBB-family members[95], like the recently found transmembrane Ephrin B1 (EFNB1) which binds ERBB2 in complex with non-receptor tyrosine kinase SRC.[96] **3)** On top of the sheer number of soluble ligands, also their availability is strictly regulated. Their transmembrane precursors' ectodomain is shed by ADAM family metallopeptidases (e.g. ADAM9, ADAM10, ADAM12 and ADAM17 shed proHB-EGF) producing a soluble extracellular ligand and membrane-bound carboxy terminal fragment (CTF) which can be subsequently internalized and participate in intracellular signaling.[97] **4)** ERBB ligands can have more than one splice variants. Among them the leader seems to be neuregulin 1 with

at least six different transcription start sites and up to 19 splice variants reported in ENSEMBL release 76.[98,95,99] **5)** ERBB-receptors themselves can also be alternatively spliced and shed by metalloproteases. E.g. ERBB2 is known to have at least 6 alternative isoforms: Δ16HER2, 648-CTF, 611-CTF, 687-CTF, p100 and herstatin (Figure 3).[100] Two soluble isoforms, p100 and herstatin function as HER2 inhibitors by binding to other full-length ERBB receptors and preventing them from forming functional dimers.[101]

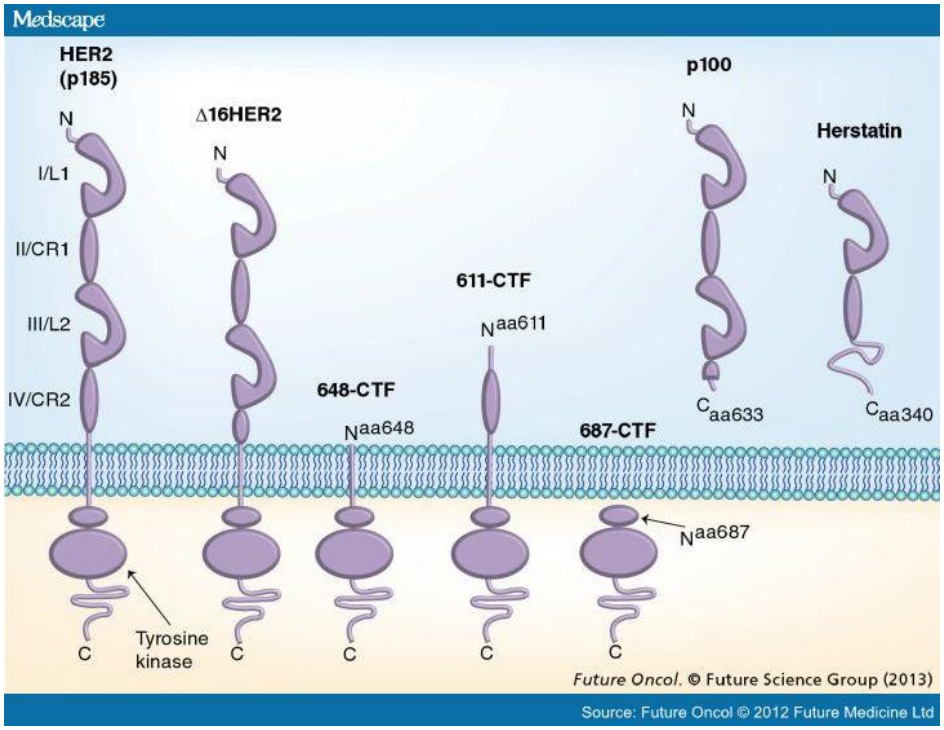

Figure 3
The ERBB2 isoform. From the left: full length p185 HER2 receptor, its Δ16HER2 (lacking exon 16) isoform, membrane-anchored C-terminal fragment 648-CTF and 611-CTF, cytoplasmic/nuclear protein 687-CTF and soluble isoforms p100 and herstatin.(adapted from J. Wang et al., 2013) [100]

Δ16HER2 lacks exon 16 and retains an oncogenic capability of the receptor.[101,102] The other 3 isoforms lack the extracellular domain and are collectively called p95HER2.[103] 648-CTF which is a cleavage product of ERBB2 by ADAM10[104] and possibly a matrix metalloprotease (MMP)[105], can function similarly to full length ERBB2. 611-CTF can increase the metastatic potential of the receptor, and the only non-membrane bound isoform, 687-CTF, is believed to be inactive in the initiation of signaling.[106,101,107] However, 687-CTF is found in the nucleus, which does not exclude its role in intracellular signaling.[106] Full length EGFR, ERBB2, ERBB3

and ERBB4 as well as a few of their isoforms, like e.g. mini-LEEK (EGFR isoform)[108], $ERBB3_{80kDa}$[109] and 4ICD ($ERBB4_{80kDa}$ intracellular domain)[110] have also been detected in the nucleus, where they serve as transcription factors or coactivators.[111] **6)** ERBB receptors can interact with other transmembrane and cytoplasmic proteins which can regulate their function. Full length ERBB2 and p95, for example, can be found in complex with a molecular chaperone – heat shock protein 90 (HSP90) - which stabilizes the receptor by preventing it from ubiquitination.[112] It can also be bound by ERBB2IP (ERBB2-interacting protein; ERBIN), ERRFI1 (ERBB receptor feedback inhibitor 1; MIG6), CHK (Csk homologous kinase; MATK), PICK1 (protein interacting with PRKCA 1), IGF1R (insulin-like growth factor 1 receptor), SRC and IL6R (interleukin 6 receptor). ERBB2IP directs it to basolateral membrane of epithelial cells and inhibits the MAPK activation by ERBB2 through inhibition of RAF1 interaction with activated Ras.[113,114] ERRFI1 and CHK are feedback inhibitors of ERBB2 mitogenic activity and PICK1 is believed to participate in clustering of the receptor.[115,116,117,118] Interaction with IGF1R, also belonging to the RTK superfamily, was shown to occur in breast cancer cells (SKBR3) where heterotrimers ERBB2/ERBB3/IGF1R are formed and contribute significantly to the trastuzumab resistance.[119,120] Another tyrosine kinase bound by EBB2, SRC, also affects trastuzumab sensitivity.[121] ERBB2 can also associate with gp130 subunit of IL-6 receptor in prostate carcinoma cells. This interaction increases the intrinsic kinase activity of ERBB2, which next leads to autophosphorylation and activation of ERBB3 and MAPK pathway.[122]

Each combination of two ERBB-family members with one or two ligands and possibly with additional interaction partners can result therefore in differential auto- and trans-phosphorylation of their tyrosines within the intracellular domains. These can then serve as docking sites for multiple interacting proteins.[123] Phosphorylated tyrosines of ERBB family receptors (altogether 89) appear to be the exclusive docking sites for Src homology domain 2 (SH2) and phosphotyrosine binding (PTB) domain-containing proteins with 40 sites bound by these classes of coreceptors and the rest remaining unbound or not yet well characterized.[123] ERBB2 has 19 tyrosine residues of which eight are recognized by at least four adaptor proteins. Five of them are bound by Src homology domain consensus protein (SHC), two by SH3 domain binding glutamate-rich protein like (SH3BGRL) and one by growth factor receptor-bound 2 protein (GRB2) and protein tyrosine phosphatase non-receptor type 11 (PTPN11/PTP2C).[123]

3.2.3 ERBB2 downstream signaling

ERBB2 is known to be involved in activation of RAS-MAPK, PI3K/AKT, PLCγ/PKC and JAK/STAT signaling pathways (Figure 4).[124]

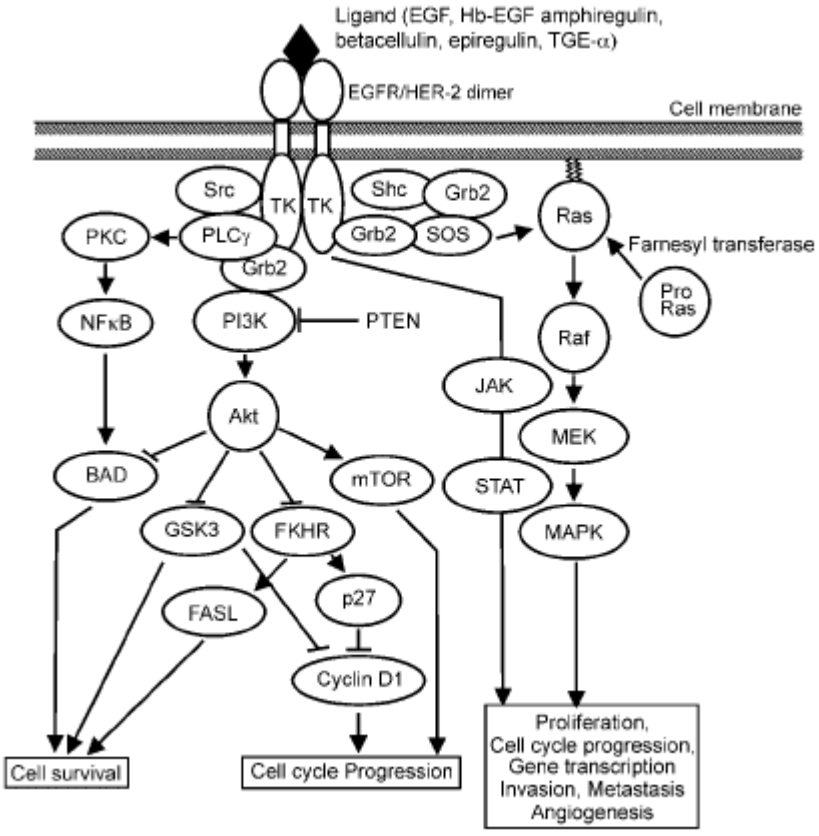

Figure 4
The EGFR/ERBB2 heterodimer signaling pathway. EGF receptor is activated by ligand binding, including EGF, TGF-α, heparin-binding EGF-like growth factor (HB-EGF), amphiregulin, betacellulin, epiregulin and epigen (not shown), followed by receptor dimerization. In turn, the intracellular tyrosine kinase domain becomes activated by auto- and transphosphorylation of the receptors on multiple tyrosine residues. This leads to recruitment of adaptor proteins, such as Shc, Grb-2, and activation of three main downstream signaling pathways: RAS-MAPK, PI3K/AKT, JAK/STAT and PLCγ/PKC. Those pathways induce cell proliferation and enhance cell survival as well as drive invasion, metastasis, and angiogenesis in breast cancer cells. (adapted from R. Saxena and A. Dwivedi, 2010)[124]

Activation of RAS-MAPK signaling pathway

The activation of RAS-MAPK signaling is started by recruitment of GRB2-SOS complex to the receptor at the plasma membrane which is facilitated by tyrosyl phosphorylated GRB2 associated binder 1 and 2 (GAB1/2).[125,126,127] GRB2 can bind either directly to ERBB2 or to

receptor-bound phosphorylated SHC.[123,128] Son of sevenless (SOS), a guanine nucleotide exchange factor (GEF), further activates membrane-associated GTPase superfamily of RAS by stimulating the release of their GDP and binding of GTP.[129] GTP-bound RAS proteins activate the mitogen-activated protein kinase (MAPK) pathway via phosphorylation of serine/threonine kinase C-RAF (MAPK kinase kinase kinase; MAPKKK) at a tyrosine residue followed by subsequent MEK1/2 (MAP kinase kinases; MAPKK) and ERK1/2 activation (MAP kinases; MAPK3 and MAPK1, respectively).[130,131] ERK in turns drives both: the phosphorylation of cytoplasmic growth-factor responsive targets and, upon translocation to the nucleus, also activation of several transcription factors regulating gene expression. The MAPK pathway is involved in cell proliferation, differentiation, survival and apopotosis.[131]

Activation of PI3K signaling pathway

Whereas ERBB2 can directly stimulate the MAPK pathway, it cannot bind p85, the regulatory subunit of PI3K, and requires either adaptor proteins GRB2/GAB1 or heterodimerization with ERBB3 or ERBB4 to activate PI3K/AKT signaling that further triggers cell growth, proliferation, regulation of metabolism, survival and inhibition of apoptosis.[123,132,133] PI3K activation can be also independent of p85 and occur via RAS.[134] The p110 catalytic subunit of PI3K generates phosphatydylinositol 3,4,5-trisphosphate (PIP_3) from the plasma membrane-bound phosphatydylinositol 4,5-bisphosphate (PIP_2). This action can be reverted by the tumor suppressor phosphatase and tensin homolog (PTEN).[135] PIP_3 is then recognized by and brings together two important pleckstrin homology (PH) domain-containing proteins: phosphoinositide-dependent kinase 1 (PDK1) and AKT (protein kinase B; PKB). Membrane-associated PDK1 then activates AKT through phosphorylation at threonine 308.[136] For full activation of AKT, additional phosphorylation at serine 473 is required. This is accomplished by mammalian target of rapamycin mTOR in a complex with rapamycin-insensitive companion of mTOR (RICTOR).[137] AKT has 3 genetic isoforms: AKT1, AKT2 and AKT3.[133] AKT1 is mostly involved in inhibition of apoptosis via inactivating of pro-apoptotic BAD and BAX, and phosphorylation of MDM2 resulting in binding to and degradation of pro-apoptotic p53.[138,139,140] AKT2 and AKT3 regulate glucose homeostasis and control the growth of mice.[141] In ERBB2 overexpressing breast cancer cells, AKT1 was reported to suppress ERBB2-induced invasion by inhibition of ERK and epithelial-to-mesenchymal transition (EMT), but in

the same time to induce cell proliferation.[133,142] AKT2 overexpression, on the other hand, was shown to induce cell invasion in vitro and metastasis *in vivo*.[143]

Activation of PLCγ and JAK/STAT signaling

Activation of PLCγ by ERBB2 takes place by its direct association with the receptor and tyrosine phosphorylation.[144] PLCγ can then cleave phosphatidylinositol 4,5 bisphosphate (PIP2) to 1,4,5-trisphosphate (IP3) and diacyloglycerol (DAG). As a consequence IP3 directs the release of Ca2+ from the endoplasmic reticulum which, together with DAG, leads to activation of protein kinases C (PKCs).[145] Activation of PKCs can also take place via the ERBB2-SRC axis, and is independent of PLCγ.[146] PKCs in turn regulate proliferation, differentiation and apoptosis.[147] STAT transcription factors 3 and 5 (signal transducers and activators of transcription) were shown to be phosphorylated via Janus kinases TYK2 and JAK3 associated with NRG1-bound ERBB2/ERBB3 heterodimers.[148] STAT3 was also reported to be activated by ERBB2 in a SRC and JAK2-dependent manner.[149] STAT3 and STAT5 stimulate cell pro- liferation, regulate cell cycle and inhibit apoptosis.[148]

Whereas EGFR undergoes endocytosis and becomes degraded shortly after activation, ERBB2 was shown to be endocytosis-resistant.[103] First reports have suggested that ERBB2 undergoes basal endocytosis and very rapid and efficient recycling to the plasma membrane. However, recent studies have shown that ERBB2 blocks its own endocytosis through negative regulation of clathrin-coated pits and vesicle formation.[150,151] The increased stability of EGFR when heterodimerized with ERBB2 is also caused by blocking formation of endocytotic pits by ERBB2.[78] The main ways of ERBB2 deactivation are therefore receptor dephosphorylation and/or degradation. PTPN9 and PTPN13 (protein tyrosine phosphatases, non-receptor types 9 and 13) were shown to dephosphorylate tyrosine residues in the intracellular domain of ERBB2.[152,153] Further, ERBB2 degradation is proteasome-mediated and occurs upon receptor K48 and K63 polyubiquitination by E3 ubiquitin ligases CBL (negatively regulated by SPRY2[154]) and CHIP.[155,156, 157] Also LRIG1 (leucine-rich repeats and immunoglobulin-like domains 1) directly interacts with ERBB2 and enhances the ubiquitination of the receptor.[158] USP9x/FAM which coprecipitates with ERBB2 plays the opposite role and is responsible for its deubiquitination.[155]

3.2.4 The role of ERBB2 and other ERBB-family receptors in breast development

In the final stages of female embryonic development, mammary epithelial cells start to proliferate and the mammary bud sprouts into the fat pad within the dermis. That results in a formation of the rudimentary ductal system consisting of 15-20 branches that stem from a primary duct.[159] During adolescence, production of estrogen (ERα) in mammary epithelium controls ductal elongation and branching to fill the fat pad.[160] Cell proliferation takes place at the end of the ducts that are enlarged and form bulbous structures referred to as terminal end buds (TEBs). When TEBs bifurcate, the secondary branches are formed.[161] During adulthood, progesterone levels change repeatedly in the estrous/menstrual cycle and control the ductal network complexity via regulating the outgrowth of side branches. Progesterone plays also a role in alveoli (acini) formation during pregnancy along with prolactin which is required for alveologenesis and later for differentiation of mammary epithelial cells into milk-secreting cells (Figure 5).[160] Alveoli are hollow structures organized in lobules with epithelial cells forming the inner acinar layer and myoepithelial cells forming the outside layer. Milk secretion takes place when myoepithelial cells contract in response to oxytocin and milk drains through the terminal ducts into the lactiferous duct and sinus.[162]

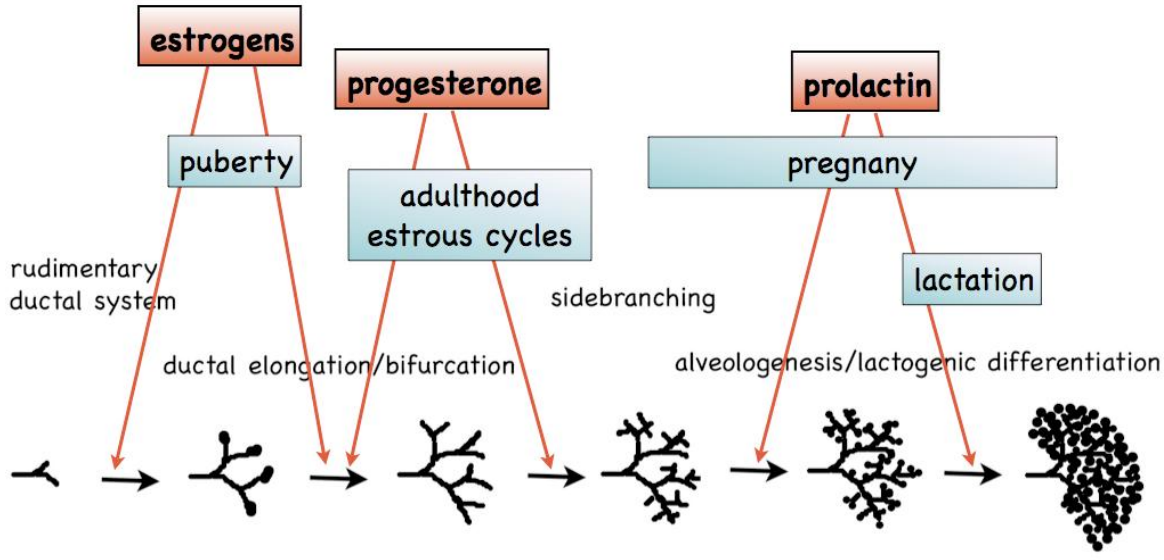

Figure 5
Mammary gland development consists of four main stages: rudimentary ductal system formation, ductal elongation/bifurcation, side branching and alveologenesis/lactogenic differentiation. Estrogen, progesterone and prolactin are key players regulating these processes. (apted from C. Brisken and B. O'Malley, 2010)[160]

Development of the mammary gland is regulated by several signaling pathways, including ERBB-, FGFR- (fibroblast growth factor receptor), IGFR- and WNT/β-catenin signaling.[161,163] As ERBB family-deficient mice are embryonic lethal due to severe cardiac deffects, studies of the ERBB receptors in breast development required either the transplantation of mammary buds from ERBB deficient embryos into immunodeficient mice or expressing ERBB receptors under control of a cardiac-specific promoter in knockout mice to overcome cardiac-specific lethality. Introduction of these and other methods led to the discovery that, although EGFR and ERBB2 are expressed throughout the whole breast development process, their levels are the highest in the initial stages of mammary gland morphogenesis.[164] Interestingly, it was shown that EGFR in the fad pad, but not in the epithelium plays a critical role in supporting ductal growth. Whereas EGFR-deficient epithelial cells could still grow beyond rudimentary structures in the presence of wild-type fat pad, wild-type epithelial cells in the presence of EGFR defficient fat pad could not.[165] ERBB2 knockout in mammary buds transplanted into immunodeficient but ERBB2 wild-type mice, on the other hand, indicated an important role of ERBB2 in the epithelium. In those transplants, terminal bud ends were severly impaired resulting in ductal elongation and branching defects. The lobuloalveolar structure formation as well as lactation were however not affected.[166,167] Expression of ERBB3 and ERBB4 is highest in pregnancy and lactation and much lower during puberty and involution.[164] Nevertheless, ERBB3 deficiency has already an impact early in mammary gland development, resulting in an impairment of the ductal outgrowth that persists into adulthood and pregnancy. Incomplete filling of the mammary fat pad by the ductal trees was accompanied by a decrease in size of the terminal end buds but an increase in their number as well as the number of luminal spaces and ductal density.[168] ERBB4 plays a role in the latest stage of mammary development and its knockout is associated with abberant lobuloalveolar development; alveoli do not differentiate properly resulting in insufficient milk secretion.[169]

3.2.5 ERBB2 and other ERBB-family members in breast cancer

ERBB-family receptors in cancer

ERBB-family receptors and their ligands strictly control development and cell signaling. Their alterations either in terms of mutation, gene amplification or protein overexpression play therefore pivotal roles in the initiation and preservation of several tumors.[67,170] Directly responsible for the tumorigenesis is an excessive and constitutive activation of downstream

signaling, including above mentioned RAS-MAPK, PI3K/AKT, PLCγ/PKC and JAK/STAT pathways. The disregulated signaling, as a consequence, drives uncontrollable cell proliferation, survival and migration/invasion.

The EGFR is the best characterized receptor regarding the number of different oncogenic mutations found in human cancers. Mutations are most commonly seen in non-small cell lung adenocarcinomas (NSCLC) and gliomas. Amplification of the gene have been additionally reported in squamous NSCLCs, gliomas, esophageal, colorectal, head and neck, as well as in triple negative breast cancers.[170,171] ERBB2 mutations are reported less often than EGFR mutations, but a subset of lung adenocarcinomas, breast (lobular), gastric, bladder and endometrial cancers have been reported to carry ERBB2 mutations. Amplification of the ERBB2 gene is more common and takes place in breast, ovarian, gastric and esophageal cancers. ERBB2 aberrations have also been reported to be found in tumors of colon, cervix, germ cells, head and neck, liver, pancreas, salivary duct and in glioblastomas. ERBB3 and ERBB4 are more often mutated than amplified and affect mainly breast and gastric tumors, or NSCLCs, melanomas, and medulloblastomas, respectively.[170] Breast cancer patients overexpressing EGFR have poor prognosis and their resistance to radiotherapy is relatively high.[172] Similarly, patients overexpressing ERBB2 are associated with radioresistance, worse prognosis, shorter overall survival and aggressive phenotype of cancer.[173,174]

ERBB2-positive breast cancer

The ERBB2 gene maps to chromosome 17q12, within a region which is frequently amplified in breast cancer (17q11-21). The minimal ERBB2 amplicon overlapping in different ERBB2-positive breast cancer patients spans 85.92 kbp and includes the TCAP, PNMT, PERLD1, ERBB2, C35 (C17orf37) and GRB7 genes.[175] Whereas TCAP, PNMT and PERLD1 seem to be amplified as “passengers” in this region and have not been shown to play a role in tumorigenesis, GRB7 and C35 were reported as oncogenes in breast cancer. Similar to GRB2, GRB7 serves as an adaptor protein for ERBB2 and its amplification contributes to ERBB2-driven migration via interaction with focal adhesion kinase (FAK).[176,177] C35, when overexpressed in cells grown in three-dimentional (3D) cultures induces formation of enlarged acinar structures and invasion into collagen matrix, which is accompanied by downregulation of epithelial markers E-cadherin (CDH1) and keratin-8 (KRT8).[178] Apart from

alterations in the genetic vicinity of ERBB2, the ERBB2-enriched breast cancers are predominantly accompanied by tumor suppressor p53 mutations (72%) and often carry structural changes in the catalytic subunit alpha of PI3K (PIK3CA; 39%).[14] The ERBB2-overexpressing breast cancer subtype is, therefore, in practice not a simple single gene-disease. The contribution of genes/mutations involved in tumor formation requires separate experimental studies.

According to American Society of Clinical Oncology – College of American Pathologists (ASCO-CAP) guidelines regarding ERBB2 testing in breast cancer, ERBB2-positive status is assigned to a cancer with an evidence of either protein overexpression or gene amplification.[21] Consequently, two methods have been developed and standardized throughout the last decade(s) to correctly test ERBB2 overexpression in all cases of invasive breast cancers (including metastatic ones) to determine the ERBB2 status from formalin-fixed, paraffin-embedded (FFPE) tissue.[179,21] In immunohistochemical assessment of ERBB2 receptor levels, IHC scores 0 and 1+ are reffered to as ERBB2-negative, 2+ as equivocal and 3+ as positive. The guidelines from 2007 recommended classification of invasive cancers as IHC3+ if >30% of invasive tumor cells strongly and uniformly stain for ERBB2.[179] However, more recent guidelines from 2013 have changed that threshold back to the >10% that had also previously been the cut-off for trastuzumab treatment. This change has been introduced due to potential benefits of using trastuzumab in the small number of patients with >10% and <30% of cells staining for ERBB2.[21,180] In situ hybridization (ISH) is another method to assess the ERBB2 status. There either a single probe measurement of ERBB2 copy numbers or a dual probe measurement of ERBB2/CEP17 (centromeric probe for chromosome 17) ratios is carried out. For single probe measurments the cut-offs are: ≥6.0 (for positive status), ≥4.0 and <6.0 (for equivocal), <4.0 (for negative). For dual probes the ratio needs to be either ≥2.0 or copy number ≥6.0 to be classified as ERBB2-positive, ratio <2.0 and copy number ≥4.0 and <6.0 for equivocal status and ratio <2.0 and copy number <4.0 for negative status. Tumors considered equivocal by one of these two methods (IHC or ISH) require retesting with another one.[21] The most commonly used FDA approved diagnostic test kits are immunohistochemical test - HercepTest (Dako Denmark A/S) and fluorescent *in situ* hybrydization test - PathVysion HER2 DNA Probe Kit (Abbot Molecular Inc.).[181] Apart from four IHC and six ISH tests, one HER2/neu ELISA test (Siemens Healthcare Diagnostics) has also been approved by the FDA.[182]

All above mentioned tests measure total ERBB2 levels and not active (phosphorylated or dimer forming) receptors. This refers especially to in-situ hybridization which measures gene amplification and not the amount of functional receptor. Protein detection by immunohistochemistry is, however, not a very good method in terms of quantitative receptor analysis. It is rather considered a semi-quantitative method.[182] Recently, however, more tests are being developed to address this issue. One such example is a proximity-based technology developed by Monogram Biosciences (VeraTag), able to measure: total receptor levels (EGFR, ERBB2 or ERBB3); their phosphorylated forms; EGFR-, ERBB2-, and ERBB3-homodimers; p95HER2; as well as EGFR/ERBB2, ERBB2/ERBB3 and ERBB3/PI3K heterodimers.[183,184,185] In these assays two antibodies are used which recognize two different epitopes on one receptor or two identical ones on two receptor molecules. One of each pair is tagged with fluorescent reporter (fluorescein) and the other one is biotinylated. Upon addition of a photosensitizer molecule (streptavidin-conjugated methylene blue) and its activation with 670 nm light, a free radical - singlet oxygen - is released and cleaves only Ab-fluorescein conjugates located in very close proximity. This liberates fluorescein which can then be quantitatively measured by capillary electrophoresis.[186] Although this and other similar methods measuring protein levels, like e.g. proximity ligation assay (PLA)[187], quantum dots-coupled antibodies[188] or reverse phase protein arrays (RPPAs)[189,190] are not yet FDA approved as diagnostic tests, they go one step further and raise a few important questions. Is clinical measurement of total ERBB2 (in combination with ER and PR) in invasive tumors sufficient to predict patient outcome and decide on proper treatment? Would the more detailed information about the activity of ERBB-family receptors in ERBB2-overexpressing patients bring additional improvement to their healthcare? And if so, what should a "perfect" quantitative test look like and how would it compare to the currently applied gene expression signatures? Recent studies indicate that, indeed, testing activation states of ERBB-family receptors could potentially bring more treatment-relevant information. In a subset of patients with even low or moderate amounts of ERBB2 the activated receptor (e.g. upon ligand overexpression) can contribute to worse disease outcome without the receptor being overexpressed.[191,192,193] Moreover, quantitative assessments of ERBB2 levels suggest that a pool of patients with very high ERBB2 levels (top 13-16% percent) may be less sensitive to trastuzumab treatment than the majority of ERBB2-overexpressing patients for whom higher ERBB2 levels correlate with increased response to trastuzumab.[194,195,196]

ERBB2 levels in breast cancer

In the past, Denis Slamon and colleagues have shown that the number of copies can vary greatly between patients and ~5% of breast cancer patients carry more than 20 ERBB2 gene copies.[174] Moreover, in one of the following studies, the average ERBB2 copy number in ERBB2-postive patients, measured by FISH, was 14. However, the distribution varied between 1.5 and 40.9 copies.[197] Another study pointed out that, whereas usually the average copy number of ERBB2 is calculated for a given tumor, different cell populations within the tumor may carry distinct copy numbers.[198] That study reports the detection of highly amplified cell subpopulations in ERBB2-overexpressing tumors with at least 25 and up to 100 ERBB2 copies per cell.[198] Importantly, established breast cancer cell lines were also shown to have subpopulations with varying ERBB2 copy numbers.[199]

In a more recent study of ERBB2 protein levels in breast cancer patients, Joensuu and colleagues, using the quantitative HERmark technology, showed that the range of total receptor levels in their subset of tumors varied greatly by 1808-fold in all of the patients and by 69-fold in patients classified as both: IHC3+ and CISH-positive.[200] In a related study which used the same technology to quantify ERBB2 at protein level in trastuzumab-treated patients, the authors suggested that there could additionally be a discrepancy in drug reponse between patients with different ERBB2 levels. In particular, they argued that patients with very high ERBB2 levels (top 13% of ERBB2-positive patients) could be less responsive to the given dosage and administration time of trastuzumab therapy (note that in this study the administration time was shorter than currently recommended).[194] The wide range of receptor levels in ERBB2-overexpressing patients, hence, raises the question if and how the increasing ERBB2 levels affect ERBB2-positive patients' outcome and if and how the molecular features of ERBB2 overexpressing cells change with the increasing ERBB2 levels.

Targeted treatment of ERBB2- positive cancer

According to an ASCO guideline from 2014, HER2-targeted treatment is recommended for all patients "with HER2-positive advanced breast cancer, except for those with clinical congestive heart failure or significantly compromised left ventricular ejection fraction".[60] This restriction is due to an increased risk of class III or IV congestive heart failure in HER2-treated patients with pre-existing heart injury.[63]

As a first-line treatment, currently a combination of trastuzumab, pertuzumab and taxane is recommended for at least 4-6 months.[60] Trastuzumab is a humanized monoclonal antibody which binds to the extracellular domain IV of ERBB2 and prevents the activation of the tyrosine kinase domain (Figure 6).[202] Its action is most potent in inhibiting the activation of ERBB2 homodimers.[201]

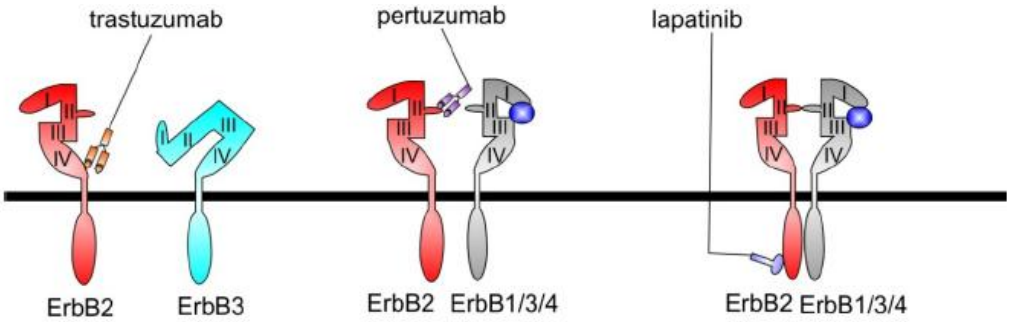

Figure 6
Drugs used in the treatment of ERBB2 overexpressing cancers. Trastuzumab is a monoclonal antibody that binds to an extracellular part of domain IV of ERBB2. Upon its binding, signal from the receptor cannot be transduced. Pertuzumab is also an antibody but mechanism of its action is different – it prevents receptor dimerization by binding to domain II of ERBB2. Lapatinib is a small molecule tyrosine kinase inhibitor and targets tyrosine kinase domain of EGFR and ERBB2 (here binding to ERBB2 is shown). Blue circle symbolizes a ligand binding to domains I and III of EGFR/ERBB3/ERBB4. (adapted and modified from A.S Hervent at al., 2012)[202]

Trastuzumab is known to upregulate cyclin-dependent kinase inhibitor - p27 and PI3K/AKT pathway inhibitor - PTEN, as well as to induce endocytotic degradation of ERBB2 receptor and antibody-dependent cellular cytotoxicity (ADCC)[203]. The second recommended drug, pertuzumab, is also a therapeutic antibody and acts through inhibiting homo- and heterodimerization of ERBB2 via blocking extracellular doman II.[204] Resistance to these drugs has, however, been frequently observed with trastuzumab resistance occurring in most of the metastatic patients within one year of treatment. It occurs in ~15% patients treated in an adjuvant setting.[203] Resistance to trastuzumab has been linked to PI3K mutations as well as the presence of IGF1R and p95HER2 or absence of PTEN.[203,205] Combinatorial treatment of patients with trastuzumab and pertuzumab, however, has been shown to revert trastuzumab resistance.[206] Taxanes (paclitaxel or docetaxel) are diterpenes that work as mitotic inhibitors by stabilizing GDP-bound tubulin in the microtubules.[207] Interestingly, due to the inhibition of cell division, the presence of giant cells with polyploidy after use of

taxanes is observed. This can affect correct ERBB2 status determination in metastases and therefore testing ERBB2 levels before chemotherapy is suggested.[208]

As a second-line treatment, ASCO guideline recommends the trastuzumab derivative T-DM1, a recently (February 2013) FDA approved drug.[60] Before its approval lapatinib was the preferred second-line treatment for patients who progressed on trastuzumab or was used in combination with trastuzumab in first-line treatment.[209,210] Lapatinib is a small-molecule tyrosine kinase inhibitor that binds the ATP-binding pocket of EGFR and ERBB2 protein kinase domains and leads to decreased activation of MAPK and PI3K signaling cascades. However, lapatinib as a monotherapy was often insufficient and patients progressed frequently.[211,212] T-DM1 is a novel and very promising antibody drug conjugate that proved its superiority over trastuzumab plus docetaxel in direct comparison by prolonging patients' progression free survival from 9.2 months to 14.2 months.[213] T-DM1 consists of trastuzumab connected with a linker to DM1, a maytansinoid derivative, which prevents microtubule assembly and leads to a block of mitosis.[214,215] For those patients who progressed on trastuzumab/pertuzumab as well as on lapatinib, T-DM1 is suggested as a third-line treatment.[60]

ERBB2-overexpressing tumors are usually ER/PR-negative and only ~10% of luminal B breast cancers overexpress ERBB2.[216] However, according to the new ASCO guideline, the therapy of those patients may include endocrine therapy as well – either alone or in combination with ERBB2-targeted therapy.[60]

3.3 Cell migration and invasion and its role in breast cancer

3.3.1 Cell migration and invasion in breast cancer

Cell migration plays an important role in several natural processes, like embryonic development, wound healing, tissue repair, regeneration and immune response.[217,218] It requires, however, precise control which is lost or altered when cells become tumorigenic due to signaling abnormalities. [219,220] In the earliest stage of breast cancer, cells show excessive localized growth and initate ductal carcinoma in situ (DCIS). Eventually, these cells gain the ability to move and to degrade the extracellular matrix proteins that form the basal membrane thus contributing to cancer progression into invasive ductal carcinoma (IDC).[221,222] Moreover, to form metastases, tumor cells need to acquire the ability to

intravasate small blood vessels, survive in the blood stream, extravasate and to form colonies in distant organs.[223,219] The ability of cancer cell to migrate and invade is therefore critical in tumor progression.

Tumor cells can migrate individually (mesenchymal or ameboidal migration), as multicellular streaming, or collectively in small groups spreading from the original site of tumor growth.[224] Tumor cell migration/invasion is regulated by integrins, matrix-degrading proteins (e.g. matrix metalloproteinases), cell-cell adhesion molecules (e.g. E-cadherin), as well as several cytokines and growth factors.[225] The mechanism of cell migration involves a few important processes and factors, namely: polarization, formation of protrusions (lamellipodia or filopodia), adhesion and protrusion of the cell body followed by retraction of the rear.[226,225] These processes are strictly coordinated by local and transient signaling that is initiated by integrins and other receptors.[227,228] In migrating cells, signaling molecules are organized in large scaffolds which localize active kinases and phosphatases to the appropriate parts of the cell. They control microtubule dynamics, drive local actin polymerization, and actomyosin bundling and contraction, which are the actual factors responsible for cell movement.[225] Focal adhesion-associated protein kinase (FAK) serves as an important example of a locally activated kinase involved in cellular adhesion and spreading processes.[229]

3.3.2 Signaling pathways in ERBB2-induced migration and invasion

As mentioned before, cell migration is strictly dependent on cellular signaling pathways. In EGFR-driven migration, blocking of PI3K/AKT and PLCγ signaling substantially reduces the ability of cells to move.[230] In melanoma and epithelial cell lines, simultaneous inhibition of the RAS-MAPK and PI3K/AKT pathways leads to almost complete loss of cell migration, as does the knockdown of EGFR.[231,232,233] It has been shown that cells with higher levels of ERBB2/ERBB3 and EGFR/ERBB2 heterodimers have higher potential of activating PI3K and hence migration than ERBB2 homodimers.[132,123] This is in line with the fact that PIP_3 is one of the first molecules which becomes polarized in response to the exposure to chemotactic agents.[225] EGFR/ERBB2 heterodimers induce migration also more efficiently than homodimers via PLCγ signaling activation.[234] The RAS-MAPK pathway is, in contrary, similarly activated by ERBB2 homo- or heterodimers, which was confirmed in three-dimensional cell cultures.[235]

In the initial phase of cell migration, PI3K becomes activated by integrins at the leading edge of the cell, which results in local accumulation of PIP_3.[236] Consequently, RHO family members of RAS GTPases superfamily RAC1 (RAS-related C3 botulinum toxin substrate 1) and CDC42 (cell division cycle 42), are phosphorylated and induce actin polymerization. RAC1 drives formation of lamellipodia, whereas CDC42 induces filopodia formation.[225] In EGF-stimulated cells RAC1 and CDC42 were shown to synergistically induce lamellipodia and membrane ruffles.[237] Integrin-mediated FAK signaling plays an important role in adhesion-triggered migration as it is activated at the retracting end of migrating cells along with PTEN that dephosphorylates PIP_3. Phosphorylated FAK induces disassembly of adhesions by recruitment of SRC. SRC further phosphorylates FAK and promotes GRB2 interaction with FAK.[229] At last, GRB2 activates RAS-MAPK signaling, including a RAS-family member present in higher concentration at the back of migrating cells, RHOA (RAS homolog family member A), which works as a RAC1 antagonist.[238,239] SRC acts also at the leading edge of the cell were it activates cortactin which induces and stabilizes actin branching via direct actin-related protein 2/3 (ARP2/3) complex regulation.[240,241]

A recent screening for proteins involved in migration in ERBB2-overexpressing MCF10A cells has revealed engagement of three major signaling nodes of networks regulating this process: β-catenin (CTNNB1), β1-integrin (ITGB1) and actin (ACT).[233] The involvement of β-catenin in EGF-induced migration was confirmed by showing the ability of EGFR to activate β-catenin via the PI3K/AKT pathway and to further stimulate the Wnt pathway. Additionally, EGFR and ERBB2 can directly interact with β-catenin.[242] In normal cells, β-catenin provides a mechanical linkage between cell-to-cell junctional (e.g. E-cadherin), and cytoskeletal proteins.[243] Upon EGFR activation and in tumors, however, β-catenin translocates to the nucleus, where it forms a complex with TCF/LEF family proteins and activates transcription of proliferation-associated genes, like MYC (v-myc avian myelocytomatosis viral oncogene homolog) and CCND1 (cyclin D1). This jointly leads to epithelial-mesenchymal transition (EMT) of the cell.[244,242]

3.3.3 Epithelial-mesenchymal transition

EMT is a strictly regulated cellular mechanism that allows cells to gain the necessary motility to drive the normal developmental program. However, in cancer it can get out of control and contribute to the malignancies by promoting tumor cells escape from its origin, leading to

invasion and metastasis. While epithelial cells undergo EMT process they lose cell-cell adhesion, reorganize their cytoskeleton and gain the ability to move.[245] This is accompanied by the loss of apico-basal polarity, change of shape (elongation) and gain of front-back polarity.[246] During the process, the cells decrease their epithelial gene expression and increase mesenchymal, which is driven by β-catenin and mesenchymal-specific transcription factors including Snail (snail family zinc finger), and ZEB (zinc finger E-box binding homeobox). Upon transition, the expression of EMT molecular markers, E-cadherin (CDH1) and cytokeratins (KRTs), is reduced while the expression of N-cadherin (CDH2), vimentin (VIM) and fibronectin (FN1) is increased (Figure 7).[246,247] Cells also often gain the ability to degrade the extracellular matrix (ECM), become insensitive to apoptosis and are associated with stem cell-like phenotype.[248] ERBB2-transformed cells have been reported to bear the characteristic of cells that underwent EMT - at least partially induced through activation of STAT3 and TGFβ-Snail (transforming growth factor beta) signaling arms by ERBB2.[249,250,251] Signs of EMT were detected also in ERBB2-overexpressing metastatic breast cancer patients.[252,253] This cell reprogramming contributes to increased trastuzumab resistance in HER2+ patients.[254,253]

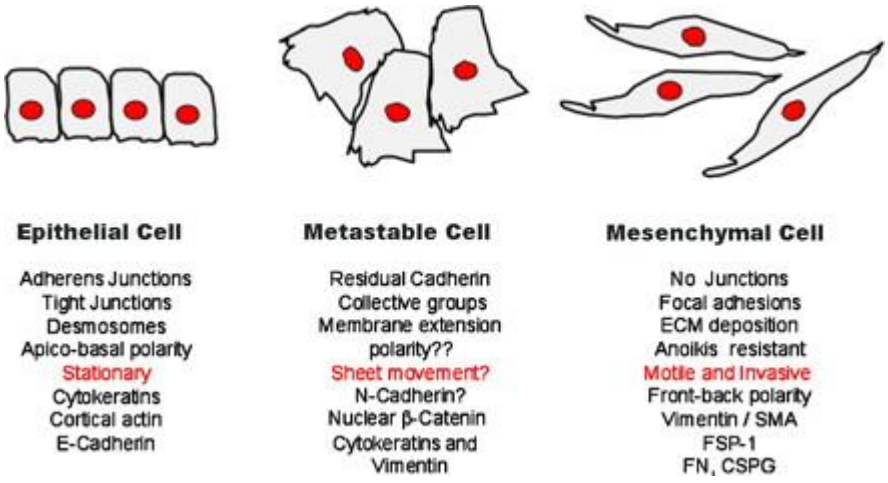

Figure 7

The characteristics of epithelial, mesenchymal and metastable cell phenotypes. In the process of epithelial-mesenchymal transition (EMT) cell features change from left to right and in the reverse process, called MET, from right to left. The differentiation of cells between both end states is not a rapid process but a plastic one that allows existence of metastable cells bearing both epithelial and mesenchymal traits. (adapted from J.M. Lee et al., 2006)[247]

3.3.4 Three-dimensional cell cultures as a model to study breast cancer

For the last three decades researchers have studied the role of extracellular matrix (ECM) in gene expression regulation and cell behaviour.[255] Throughout this time, it has been discovered that *in vivo* cell migration and invasion are strictly dependent on the microenvironment. Several three-dimensional (3D) cell and tissue models have been therefore developed and subsequently proved superior to 2D cell cultures in which cells are grown in monolayers on plastic dishes.[256] In the most commonly applied 3D culture type cells are partially or fully embedded in ECM-like collagen gels like Matrigel, collagen I or mix of them. Matrigel is a solubilized basement membrane extract from the Engelbreth-Holm-Swarm (EHS) mouse sarcoma, composed mainly of laminin, nidogen 1 (entactin 1; NID1), collagen IV, glycoproteins and proteoglycans (heparan suflate proteoglycans).[257] Cells grown in 3D cultures can attach to them and activate their integrin-dependent signaling, resembling the situation observed *in vivo*.[258]

In breast cancer studies, 3D model systems enable phenotypic discrimination between non-malignant and malignant mammary cells. Whereas different breast cancer cell lines grown in monolayers show phenotypes hardly distinguishable from each other, their morphologies in laminin-rich ECM-like gels differ dramatically. Depending on a genetic context the cells can form either round, mass, grape-like or stellate colonies.[259] Moreover, signaling pathways which function in parallel in breast cells cultured in 2D system (e.g. EGFR and β1-integrin) become coupled and bidirectional in 3D system as a result of contacting basement membrane-like gel.[260,261,262] Thus appropriate 3D cell culture provides a more physiologically relevant approach to study signaling pathways ex-vivo.

Non-malignant mammary epithelial cell line, MCF10A, is frequently used to study oncogenesis in breast.[263,264] This cell line is of particular interest among researchers as it forms polarized, growth-arrested acini-like spheroids with a hollow lumen, when grown in 3D cultures. On the contrary, malignant cells form disorganized, proliferative and non-polar colonies, which can invade through the matrix.[265,266] Overexpression or inhibition of different genes in this cell line can help, thus, to identify potential oncogenes or tumor suppressors.

3.4 The role of miRNAs in breast cancer

3.4.1 miRNAs' biogenesis and function

miRNAs are small, single-stranded non-coding RNAs of the average length 22 bp (17-24 bp), which negatively regulate gene expression at the postranscriptional level in a sequence-specific manner.[267] According to the latest miRNA database release (miRBase 21, June 2014) there are 1881 annotated human miRNA loci present in the human genome and 2588 mature miRNAs encoded by them.[268] Their expression is often tissue-specific.

The first step of most miRNAs' production is polymerase II-driven transcription from either intergenic or intronic miRNA-specific promoters. In case of intronic miRNAs, polymerase III can be alternatively involved in transcription.[269,270] Original, long, often policistronic transcripts (e.g. microRNA cluster miR-17-92), are therefore usually capped and polyadenylated and can undergo splicing.[269,271,272] These primary transcripts are called pri-miRNAs and contain stem loop structures. The cleavage of them out of long transcripts by RNase III enzyme DROSHA, in complex with DGCR8 (DGCR8 microprocessor complex subunit), produces ~70 nt long miRNA precursors (pre-miRNAs).[273,274] In the next step of miRNA maturation, exportin 5 (XPO5) binds to and transports pre-miRNAs to cytoplasm where further cleavage of the loop by RNase III endonuclease Dicer (DICER1) complex takes place.[275,276] Dicer is a component of an RNA-induced silencing complex (RISC) together with an RNA binding protein TRBP (TARBP2; TAR (HIV-1) RNA binding protein 2) and an endonuclease AGO2 (argonaute RISC catalytic component 2). RISC selects the guide strand from the double-stranded RNA formed by Dicer cleavage and the mature miRNA helps Ago2 to recognize and to cleave the target mRNAs (Figure 8).[277,278] The choice of guide strand depends on the thermodynamic stability of pre-miRNA - the strand with lower stability at its 5' end is preserved within RISC and the passenger strand is degraded.[279]

One miRNA can target hundreds of mRNAs and one mRNA can be targeted by several miRNAs. For the target recognition the most important is the pairing of miRNA's "seed sequence" embracing nucleotides 2-7 (or 2-8) at the 5' end of a mature miRNA with the target site(s) within mRNA. Additionally, at least a few nucleotides should pair within positions ~13-18 whereas nucleotides ~9-12 should ideally form a loop to achieve higher targeting efficiency.[280] If the miRNA shows perfect homology to the target mRNA then

degradation of the transcript takes place, like in the situation described above. On the other hand, if the complementarity is not perfect then the inhibition of translation occurs.[281,282]

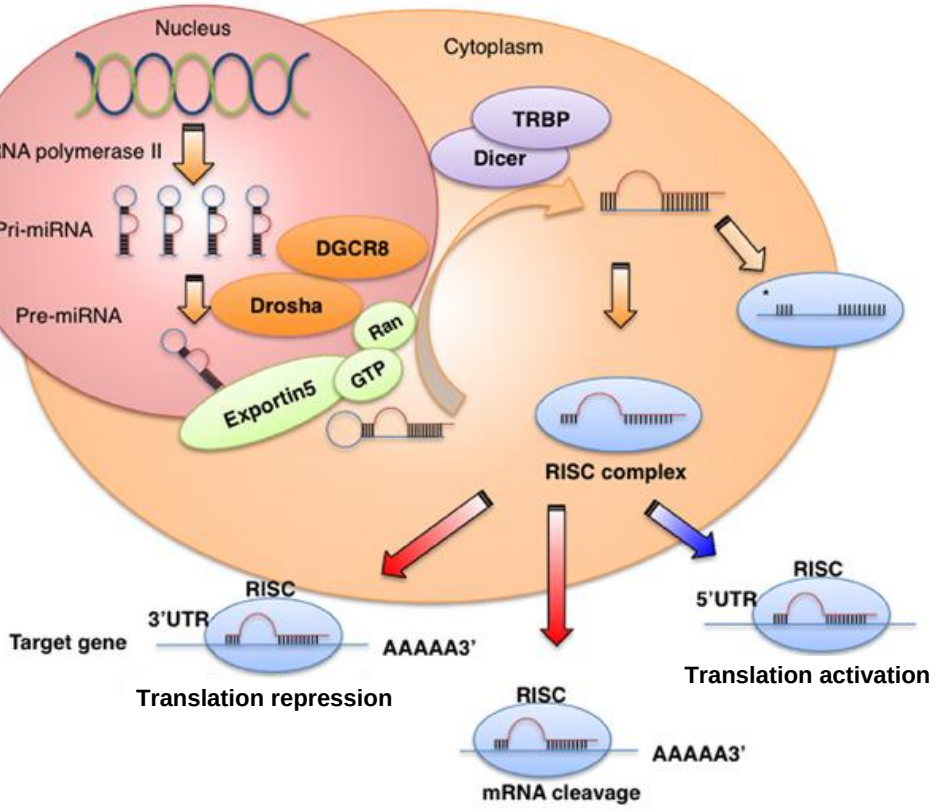

Figure 8
miRNAs' biogenesis. Polymerase II transcribes the miRNA gene forming pri-miRNA, which is cleaved by Drosha complex into hairping loop-structured double-stranded pre-miRNA. The transport of pre-miRNA into cytoplasm is facilitated by exportin 5. Dicer recognizes and cleaves pre-miRNA removing the RNA loop. RISC complex further selects the single guide strand of pre-miRNA. This mature miRNA drives silencing of target mRNA either by translational repression or deadenylation and degradation. In certain situations miRNA can enhance translation. (adapted from R. Takahashi et al., 2014; slight changes introduced)[283]

Although miRNAs are often involved in inhibition (and sometimes enhancement under certain conditions)[284] of mRNA translation upon binding to the complementary sequences, it has been shown that the majority of miRNA-bound mRNAs are directed for degradation.[285] miRNAs target mRNAs mostly by binding to their 3'UTRs. The miRNA target sites have also been reported in 5'UTRs and in the coding sequences, however, they have been shown to have lower effectiveness and rather inhibit translation of mRNAs than induce their degradation.[286] This is in part due to lower AU content in these regions, leading to more complex RNA secondary structures and to hampered site accessibility by miRNAs as well as

due to ribosome sliding along mRNA starting from 5' end and removing of silencing complexes.[287] Interestingly, miRNAs were also shown to be able to regulate stability of non-coding RNAs.[288]

3.4.2 miRNAs in breast cancer

In human malignancies miRNA expression patterns are altered and specific miRNA signatures have been associated with particular types of cancers.[289] In breast cancer, it has been shown that miRNAs are differentially expressed between different intrinsic subtypes, especially between low-proliferative luminal A and high-proliferative basal subtypes. The pattern of miRNA expression differs also between cancers with wild type or mutant p53 as well as ER-positive and ER-negative breast cancers. Other miRNAs show also specific association with proliferation (like e.g. miR-17-92), cell adhesion and immune response.[290] In breast cancer certain miRNAs function as oncogenes, while others behave like tumor suppressors. This depends on the complex interplay of the downregulated target genes. Supposing that all targets of a certain miRNA were known, their combined impact on the cell behaviour would still be very hard to predict, and therefore functional studies involving overexpression of artificially synthesized miRNA mimics and/or their inhibitiors are commonly applied to determine miRNAs' function. Additionally, a few bioinformatic platforms enabling biologists to find a potential target genes of a given miRNA or miRNA-families, based on seed sequence complementarity, site conservation and context score, like e.g. TargetScan, miRanda, Elmmo, miRWalk, Diana-microT or PITA.[291,292,293294,295,296]

Well-studied miRNAs with oncogenic potential in breast cancer include: miR-10b, miR-21, miR-22, miR-27a/b, miR-29b, miR-17-92, miR-155, miR-204, miR-221/222, miR-373/520c and miR-510, while those with tumor suppressor properties are: let-7, miR-17-5p, miR-31, miR-34a/b/c, miR-125a/b, miR-145, 146a/b, miR-193b, miR-200, miR-205, miR-206 and miR-335.[297,298,299,300] Out of them, only miR-34a replacement therapy (MRX34 by Mirna Therapeutics) reached clinical trial phase I in 2013 and its safety is currently being tested in healthy volunteers. If it proves safe, it will be further tested for the treatment of patients with liver cancers and those with liver metastasis from other cancers.[299] This is the first miRNA-based cancer therapeutic and the second miRNA-based therapeutic ever which reached the clinics. The first one was an anti-miR-122 (miravirsen, Santaris Pharma) which is being tested for its capability of reducing Hepatitis C virus (HCV) infection - currently in

phase 2 clinical trial.[299,301] Pioneering miRNA-based drugs, thus, seem to be promising alternatives to current treatments and as several miRNAs are deregulated in breast cancer, it is very likely that they will be considered as potential therapeutics for this disease in future.

Similar to breast cancer signatures based on expression profiles of protein-coding genes, biomarker miRNAs' expression levels can also predict patients' outcome and response to specific drug treatments.[302] In particular, miR-210 has been shown to predict the sensitivity and response to trastuzumab therapy.[303] Moreover, reduced expression of miR-375 (targets IGF1R) and increased expressions of miR-21 and miR-221 (both target PTEN) have been shown to directly increase trastuzumab resistance.[304,305,306] In recent years several researchers pointed out that circulating miRNAs (e.g. miR-19a, miR-24, miR-133a, miR-148b, miR-155 and miR-181b) detected in serum/plasma could be also of a great help for early detection of breast cancer.[307,308]

The increase or decrease of miRNAs' levels is usually controlled on transcriptional, post-transcriptional and epigenetic level and rarely their expression is affected by genomic alterations (i.e. mutations).[309] Although single nucleotide polymorphisms (SNPs) are rarely found in miRNA seed sequences, SNPs are more common in target sites (mostly in the 3'UTRs) in mRNAs and block mRNA regulation by miRNA.[310] This mechanism was shown also to be used by viruses. Viral v-FOS mRNA of Finkel-Biskis-Jinkins (FBJ) murine osteosarcoma virus, for example, carries in its 3'UTR a deletion of miR-101 binding site and single nucleotide change in a sequence recognized by miR-155 evading the control by these miRNAs.[311]

Although there are a lot of miRNAs known to regulate migration and invasion, their function can vary in different cancers and tissues depending on the cellular context. Below a few examples of miRNAs involved in both ERBB signaling and migration/invasion are presented.

3.4.3 miRNAs' role in ERBB-regulated tumor cell migration and invasion

A lot of evidence exists that implicate the role of miRNAs in cancer cell migration, invasion and metastasis. One of the best known miRNAs known to regulate ERBB2-induced migration is miR-21. It is highly expressed in several types of cancers and modulates tumor cell apoptosis, cell adhesion and motility via control of actin cytoskeleton.[312,313] Interestingly, miR-21 expression correlates with ERBB2 upregulation in breast cancer and its induction occurs upon activation of ERBB2-activated MAPK pathway.[314] miR-21 downregulates several

tumor suppressors including AKT pathway suppressor – PTEN and key matrix metalloproteinase inhibitors – RECK and TIMP3, contributing to invasiveness of tumor cells.[315]

microRNAs: miR-125a/b, miR-128b and miR-146a/b, miR-205, on the other hand, play the opposite role and inhibit ERBB-driven migration by directly targeting EGFR (miR-128b, miR-146a/b), ERBB2 (miR-125a) or ERBB3 (miR-125b, miR-205).[316,317,219,318,319] Moreover, miR-200b, miR-200c and miR-429 inhibit EGF-induced invasion by targeting PLCγ1.[320] Most of these miRNAs target additionally other mRNAs coding for proteins involved in regulation of metastatic process, which renders the signal more intense.[321]

Currently available high-throughput techniques like microarrays and next generation sequencing (NGS) enable researchers to study the changes in the whole transcriptome upon miRNA overexpression or inhibition. In this way, they aid determination of all direct and indirect effects of miRNA. However, the similar study of translation inhibition presents a big challenge, as the high throughput methods for protein level determination are despite big progress still in their infancies. In one of the successful attempts to study the effects of miRNAs on protein levels, a different scientific approach has been therefore adopted.[322] Instead of investigating the effect of one miRNA on all proteins, the effects of all miRNAs on a restricted pool of proteins involved in the indicated cellular processes (EGFR signaling and cell-cycle) have been studied using reverse phase protein arrays. The results show that single miRNAs can coordinate specific cellular actions by targeting several proteins within the same network. Thus, miRNAs play role of very important signaling molecules.

3.5 Aims of the study

The global aim of my PhD-project has been to contribute to the understanding of female breast cancer overexpressing HER2 (further interchangeably referred to as ERBB2/HER2). To this end, I carried out two subprojects that dealt with phenotypic alterations and miRNA regulation, respectively:

1) Determination of the influence of different ERBB2 levels on molecular features in a non-malignant immortalized breast cell line to model the first steps of oncogenesis in normal breast tissue upon ERBB2 upregulation to different extents.

To achieve this goal, I overexpressed the ERBB2 receptor to four different levels using a retroviral system in MCF10A cells. I further characterized the resulting stable cell line pools in 2D and 3D cell cultures, focusing on ERBB2-induced migration/invasion, ERBB-signaling activation, and epithelial-mesenchymal transition.

2) Identification of miRNAs differentially regulated by ERBB2 in three-dimensional context that are critically associated with ERBB2 function in vitro as well as *in vivo*.

The next goal of my PhD project was to find miRNAs engaged in conducting ERBB2 function in a system that would closely resemble the situation *in vivo*. I performed therefore miRNA and mRNA expression profiling, using next generation sequencing and microarrays, respectively, from the cells expressing four levels of ERBB2, which had been grown in 3D cell culture. Consecutively, I performed correlation studies using publically available clinical datasets to assess the role of differentially expressed miRNAs in breast cancer. Finally, I carried out a functional characterization of the most promising candidates.

4. Materials

4.1 Instruments and equipment

Name	Company
Abi Prism 7900HT	Life Technologies (Applied Biosystems)
Agarose gel casting chamber	Peqlab Biotechnologie
Agarose gel electrophoresis chamber	Peqlab Biotechnologie
Agilent 2100 Bioanalyzer	Agilent
Axiovert 25 light microscope with built-in camera Axiocam MRc	Carl Zeiss
Axiovert 40 CFL microscope with built-in camera Axiocam MRc	Carl Zeiss
Bacteria shaking platform	GFL
Benchtop centrifuges: Labofuge 200, Biofuge fresco	Thermo Fisher Scientific Heraeus
Cell counter CASY	Casy, Innovatis
Cell culture hood - HERAsafe Safety Cabinet KS12	Thermo Fisher Scientific Heraeus
Cell culture incubator (37^{o}C, 5% CO_2)	Binder
Cell sorter FACSAria	BD Biosciences
Centrifuge for PCR tubes	Labnet International
Computers	LG, Apple, Fujitsu Siemens
Contact spotter	Aushon BioSystems
Electrophoresis power supply BioRad-Power-Pac-200	Bio-Rad Laboratories
Electrophoresis power supply Consort E835	Sigma-Aldrich
Floor centrifuges - Heraeus Multifuge 4KR, Heraeus Sepatech Varifuge 3.0 R	Thermo Fisher Scientific Heraeus
Flow Cytometer FACSCalibur	BD Biosciences
Freezer -20^{o}C	Liebherr, Bosch
Freezer -80^{o}C	Sanyo
Freezing container (Nalgene, Mr. Frosty)	Sigma-Aldrich
Fridge 4^{o}C	Liebherr

High throughput sequencer HiSeq 2000	Illumina
Horizontal roller shaker (RM5)	neoLab
Ice machine	Hoshizaki
Infinite M200 microplate reader	Tecan
Light microscope Wilovert S	Hund Wetzlar
Liquid nitrogen storage system CHRONOS	Cryotherm
LSM 510 Meta confocal microscope	Carl Zeiss
Magnetic stirring hotplate MR 3001 K	Heidolph
Microwave	Panasonic
MilliQ Biocel Water Purification System	Millipore
Mini-PROTEAN Tetra Cell Electrophoresis System	Bio-Rad Laboratories
Multichannel pipette	Eppendorf
Multistep pipette Biohit (5-100 µl)	Biohit
Multistep pipette Ripette (200 µl - 5 ml)	Ritter Medical
Nanodrop ND-1000 spectrophotometer	NanoDrop Technologies
Odyssey Infrared Imaging System	Li-Cor Biosciences
Olympus Scanning microscope	Olympus
Peltier Thermal Cycler PTC-200	MJ Research
pH meter	inoLab
Pipetboy	Integra Biosciences
Pipettes (0.5-1000 µl)	Gilson, Eppendorf
Room 37^{o}C	Viessmann
Room 4^{o}C	Integra
Safety/exhaust hood	Waldner
Scale HL-200i (max. 200 g)	A&D Company, Limited
Scanner	Epson
Suction device for cell culture	neoLab
Thermomixer comfort	Eppendorf
Tissue lyser	Qiagen
Topload balance	Mettler Toledo
Trans-Blot SD semi-dry transfer cell	Bio-Rad Laboratories

UV imager	Herolab
UV transilluminator	Renner GmbH
Vortexes: Genie 2, Reax top	neoLab, Heidolph
Water bath TW20	Julabo
Waving platform shaker (Polymax 1040)	Heidolph
xCelligence Real-time cell analyzer (RTCA)	Roche
X-ray cassette	Angewandte Gentechnologie Systeme, GmbH
X-ray film developing machine	Amersham Pharmacia

4.2 Consumables

Name	**Company**
384-well plates	Life Technologies (Applied Biosystems)
10 cm Ø tissue culture dishes	TPP
200 µl PCR tubes	Eppendorf
6-well plates, flat bottom, transparent	Nunc, SPL Life Sciences
96-well OptiPlates, flat bottom, white	PerkinElmer
96-well plates, flat or round bottom, transparent	Greiner Bio-One
Adhesive Optically Clear Plate Seal	Thermo Scientific
Amersham Hybond-P PVDF membrane	GE Healthcare
Amersham Hyperfilm ECL	GE Healthcare
Bacteria plating glass beads	Merck Millipore
BeadChip Sentrix arrays Human HT-12 v4	Illumina
Cell culture flasks T25, T75, T175	Greiner Bio-One, TPP
Cell scrapers	TPP
Cell Strainer in FACS Tubes	BD Biosciences
Combitips (different sizes)	Eppendorf
Costar ultra low attachment 6-well plates	Corning B.V.
Cryovials 1.8mL	Nunc
Culture slides, 8-well, glass bottom	BD Biosciences
FACS tubes	BD Biosciences

Filter pipette tips (10 µl, 20 µl, 100 µl, 200 µl, 1000 µl)	Starlab, Neptune
Glass coverslips	R. Langenbrinck
Glass slides	R. Langenbrinck
Immersion oil	Sigma-Aldrich (Fluka)
Latex gloves	Blossom
Lens cleaning paper	neoLab
Matrigel invasion chambers	BD Biosciences
Microcentrifuge tubes (1,5 ml, 2 ml)	Eppendorf
nitrocellulose-coated glass slides (Oncyte Avid)	Grace-Biolabs
Parafilm	Pechiney Plastic Packaging
Powder-free nitrile gloves FreeForm SE	Microflex
PVDF membrane Immobilon-FL	Merck Millipore
Reagent reservoir 50 ml	Corning
RTCA CIM-plates	Roche
RTCA E-plates	Roche
Scalpel Faether	Pfm medical
Serological pipettes (5 ml, 10 ml, 25 ml, 50 ml)	Corning
Silicon culture inserts	Ibidi
Soft tissues Kimtech Science	Kimberly-Clark Proffesional
Tubes (15 ml, 50 ml)	Greiner Bio-One, Corning
Whatman 3 MM blotting paper	GE Healthcare

4.3 Chemicals

Name	**Company**
Acetic acid	Fluka
4’,6-Diamidin-2-phenylindol (DAPI)	Sigma-Aldrich
Acrylamide/bisacrylamide 37.5:1	Roth
Agar	Fluka
Agarose	Sigma-Aldrich
Aminohexanoic acid	Sigma-Aldrich
Ammonium peroxodisulfate (APS)	Roth
Ampicillin	Sigma-Aldrich

Bacto-Agar	Fluka
Bacto-Trypton	Roth
Bovine Serum albumine powder (BSA)	PAA Laboratorien
Chloroform	Merck
Dimethylsulfoxide (DMSO)	Sigma-Aldrich
Dithiothreitol (DTT)	Roth
Ethanol	Sigma-Aldrich
Ethidium bromide (EtBr)	Sigma-Aldrich
Ethylenediaminetetraacetic acid (EDTA)	Acros Organics
Glycerol solution	Sigma-Aldrich
Glycine	Gerbu
HCl	Sigma-Aldrich
Isopropanol	Sigma-Aldrich
KCl	Roth
KH_2PO_4	Sigma-Aldrich
Methanol	Sigma-Aldrich
Na_2HPO_4 x $2H_2O$	Sigma-Aldrich
Paraformaldehyde (PFA)	Sigma-Aldrich
Skimmed milk powder	Roth
SOC medium	Life Technologies (Invitrogen)
Sodium chloride (NaCl)	Merck
Sodium dodecyl sulfate (SDS)	Roth
Sodium fluoride (NaF)	Sigma-Alrich (Fluka)
Sodium hydrogen carbonate ($NaHCO_3$)	AppliChem
Sodium hydroxide (NaOH)	Fluka
Sodium orthovanadate (Na_3VO_4)	Sigma-Aldrich
TEMED	Roth
Tris-base	Sigma-Aldrich
Tris-HCl	Sigma-Aldrich
Triton X-100	AppliChem
Tween 20	Gerbu

Yeast extract	Gerbu

4.4 Molecular biology reagents, kits and enzymes

Name	**Company**
ABsolute qPCR ROX mix	Thermo Fisher Scientific
Alexa Fluor® 488 phalloidin	Life Technologies (Invitrogen)
Alexa Fluor® 647 phalloidin	Life Technologies (Invitrogen)
Ampicillin	Sigma-Aldrich
BCA protein assay kit	Thermo Fisher Scientific (Pierce)
Cell proliferation reagent WST-1	Roche
CellTiter Glo Luminescent Cell Viability Assay	Promega
Complete Mini, EDTA free Protease Inhibitor Cocktail Tablets	Roche
Gateway LR Clonase II Enzyme Mix	Life Technologies (Invitrogen)
deoxynucleoside triphosphates (dNTPs), 10 mM	New England Biolabs
DNA loading dye (6x)	Thermo Fisher Scientific (Fermentas)
Dual-Luciferase Reporter Assay	Promega
Easy Prep Pro - plasmid isolation kit	Biozym
ECL Western Blotting Detection Reagents	GE Healthcare
Fast Green FCF	Sigma-Aldrich
GeneRuler 1 kb DNA Ladder	Thermo Fisher Scientific (Fermentas)
GeneRuler 100 bp DNA Ladder	Thermo Fisher Scientific (Fermentas)
Human Total ERBB2/HER2 DuoSet IC (ELISA kit)	R&D Systems
InSolution Staurosporine, *Streptomyces sp*.	Merck KGaA (EMD Millipore, Novagen)
microRNA LNA™ PCR primer sets	Exiqon
miRCURY LNA™ Universal RT microRNA PCR, Polyadenylation and cDNA synthesis kit	Exiqon
miRNeasy Mini kit	Qiagen

M-PER (Mammalian Protein Extraction Reagent)	Thermo Fisher Scientific (Pierce)
PCR Mycoplasma Test Kit	PromoCell
PhosSTOP (Phosphatase Inhibitor Cocktail Tablets)	Roche
Phusion HF buffer (10x)	Thermo Fisher Scientific (Finnzymes)
Phusion Hot Start High-Fidelity DNA Polymerase	Thermo Fisher Scientific (Finnzymes)
Poly-hydroxyethylmethacrylate (polyHema)	Sigma-Aldrich
Ponceau S staining solution	Sigma-Aldrich
Precision Plus Protein™ Dual Color Standards	Bio-Rad Laboratories
Prolong Gold Antifade Reagent	Life Technologies (Invitrogen)
QiaAmp DNA Maxi Kit	Qiagen
QIAprep Spin Midiprep Kit	Qiagen
QuickChange site-directed mutagenesis kit	Promega
Restore Western Blot Stripping Buffer	Thermo Fisher Scientific
Restriction enzymes and their buffers	New England Biolabs
RevertAid™H Minus First Strand cDNA synthesis kit	Thermo Fisher Scientific (Fermentas)
RNeasy Mini Kit	Qiagen
Rockland Blocking Buffer for Fluorescent applications/Western Blotting	Rockland Immunochemicals
Roti Load (4x)	Roth
Shrimp alkaline phosphatase (SAP)	Roche
Streptavidin, Alexa Fluor 680 conjugate	Life Technologies (Invitrogen)
SYBR Green master mix, Universal RT	Exiqon
T4 DNA ligase and buffer (10x)	New England Biolabs
T-PER	Thermo Fisher Scientific
Universal Probe Library (UPL)	Roche
Wizard SV Gel and PCR Clean-Up System	Promega

4.5 Bacterial strains and media

Subcloning Efficiency DH5α Competent Cells and Library Efficiency DB3.1 Competent Cells were purchased from Life Technologies (Invitrogen). DH5α was used to propagate all plasmids apart from gateway compatible empty vectors containing ccdB gene (e. g. pMXs-gw-CMV-EGFP).

LB medium

10 g Tryptone

5 g Yeast extract

10 g NaCl

Add dH_2O till 1 l, set pH to 7 by adding NaOH, autoclave

1,5% LB agar medium

1 g Tryptone

0.5 g Yeast extract

1 g NaCl

Add dH_2O till 100 ml, set pH to 7 by adding NaOH, then add 1.5 g agar. After autoclaving, mix was cooled down to 55^{o}C and appropriate amount of antibiotic was added (e.g. 100 mg/l ampicillin or kanamycin) before pouring the LB agar medium into sterile Petri dishes to solidify.

4.6 Cell lines, cell culture reagents and media

4.6.1 Cell lines

Cell line	Origin
MCF10A (CRL-10317™)	Human epithelial cell line derived from fibrocystic mammary tissue; ATCC (Manassas, VA, USA)
BT474 (HTB-20™)	Human breast ductal carcinoma; ATCC (Manassas, VA, USA)
SKBR3 (HTB-30™)	Human breast adenocarcinoma; ATCC (Manassas, VA, USA)
T47D (HTB-133™)	Human breast ductal carcinoma; ATCC (Manassas, VA, USA)
UACC-812 (CRL-1897™)	Human breast ductal carcinoma; ATCC (Manassas, VA, USA)
HEK293FT	Human embryonic kidney cells; Invitrogen (Carlsbad, CA, USA)

MDA-MB-231 (HTB-26™)	Human breast adenocarcinoma; ATCC (Manassas, VA, USA)
MCF7 (HTB-22™)	Human breast adenocarcinoma; ATCC (Manassas, VA, USA)

4.6.2 Cell culture reagents

Name	Company
0,5% and 0,25% Trypsin-EDTA solution	Life Technologies (Invitrogen)
5-aza-2'deoxycytidine	Sigma-Aldrich
7-Aminoactinomycin D (7-AAD) staining solution	BD Pharmingen
BadStabil	NeoLab
Basement Membrane Matrix, Growth Factor Reduced	BD Biosciences
Cholera toxin from Vibrio cholerae	Sigma
DMEM/F12 medium	Life Technologies (Invitrogen)
Doxorubicin hydrochloride	Sigma
Dulbecco's Modified Eagle Medium (DMEM)	Life Technologies (Invitrogen)
Fetal Bovine Serum (FBS), heat inactivated	Life Technologies (Invitrogen)
Geneticin	Life Technologies (Invitrogen)
Horse Serum, heat inactivated	Life Technologies (Invitrogen)
Human recombinant Epidermal Growth Factor (EGF)	Sigma-Aldrich
Hydrocortisone	Sigma
Insulin from bovine pancreas	Sigma-Aldrich
Lapatinib	GlaxoSmithKline
Leibovitz's L-15 medium	Life Technologies (Invitrogen)
L-glutamine	Life Technologies (Invitrogen)
Lipofectamine 2000	Life Technologies (Invitrogen)
McCoy's 5A medium	Life Technologies (Invitrogen)
MEK1/2 inhibitor (U0126)	New England Biolabs
microRNA mimics	Thermo Fisher Scientific (Dharmacon)
Minimum Essential Medium (without phenol red)	Life Technologies (Invitrogen)
Non-essential aminoacids (100x)	Life Technologies (Invitrogen)
Nuclease Free Water	Ambion
OptiMEM	Life Technologies (Invitrogen)

Paclitaxel from Taxus yannanensis	Sigma
Penicillin-streptomycin (Pen-Strep)	Life Technologies (Invitrogen)
Phosphate buffered saline (PBS)	Life Technologies (Invitrogen)
PI3K inhibitor (LY294002)	Calbiochem
Polybrene	Santa Cruz Biotechnology
Poly-L-lysine solution	Sigma
Sodium pyruvate	Life Technologies (Invitrogen)
Trastuzumab/Herceptin	Roche

4.6.3 Cell culture media

MCF10A Growth (full) Medium – DMEM/F12 supplemented with 5% horse serum, 10 ng/ml EGF, 0.5 µg/ml hydrocortizone, 100 ng/ml cholera toxin, 1% Pen-Strep (final conc. 50 U/ml penicillin, 50 µg/ml streptomycin) and 10 µg/ml insulin

MCF10A Assay Medium - DMEM/F12 supplemented with 2% horse serum, 0.5 µg/ml hydrocortizone, 100 ng/ml cholera toxin, 1% Pen-Strep (final conc. 50 U/ml penicillin, 50 µg/ml streptomycin) and 10 µg/ml insulin

MCF10A Transfection Medium - DMEM/F12 supplemented with 5% horse serum, 10 ng/ml EGF, 0.5 µg/ml hydrocortizone, 100 ng/ml cholera toxin and 10 µg/ml insulin

MCF10A Starvation Medium 1 - DMEM/F12 supplemented with 1% Pen-Strep (final conc. 50 U/ml penicillin, 50 µg/ml streptomycin); used for signaling pathways analysis

MCF10A Starvation Medium 2 - DMEM/F12 supplemented with 0.9% horse serum, 0.5 µg/ml hydrocortizone, 100 ng/ml cholera toxin, 1% Pen-Strep (final conc. 50 U/ml penicillin, 50 µg/ml streptomycin) and 10 µg/ml insulin; used in migration/invasion assays

MCF7 Growth Medium – MEM without phenol red supplemented with 10% FBS, 1% L-glutamine, 1% sodium pyruvate and 1% Pen-Strep (final conc. 50 U/ml penicillin, 50 µg/ml streptomycin). For tamoxifen resistant cells 5 µM 4-hydroxytamoxifen was additionally added.

MCF7 Transfection Medium - MEM without phenol red supplemented with 10% FBS, 1% L-glutamine, 1% sodium pyruvate.

MDA-MB-231 Growth Medium – Leibovitz's L-15 medium supplemented with 10% FBS, 1% Pen-Strep (final conc. 50 U/ml penicillin, 50 µg/ml streptomycin) and freshly added 3g/l sodium hydrogen carbonate.

MDA-MB-231 Transfection Medium – Leibovitz's L-15 medium supplemented with 10% FBS and freshly added 3g/l sodium hydrogen carbonate.

HEK293FT Growth Medium – DMEM high glucose medium supplemented with 10% FBS, 1% Pen-Strep (final conc. 50 U/ml penicillin, 50 µg/ml streptomycin) and 500 µg/ml geneticin

HEK293FT Transfection Medium – DMEM high glucose medium supplemented with 10% FBS

SKBR3 Growth Medium – McCoy's 5A medium supplemented with 10% FBS, 1x non-essential amino acids and 1% Pen-Strep (final conc. 50 U/ml penicillin, 50 µg/ml streptomycin)

SKBR3 Transfection Medium – McCoy's 5A medium supplemented with 10% FBS and 1x non-essential amino acids

BT474 Growth Medium – DMEM high glucose medium supplemented with 10% FBS and 1% Pen-Strep (final conc. 50 U/ml penicillin, 50 µg/ml streptomycin)

BT474 Transfection Medium – DMEM high glucose medium supplemented with 10% FBS

4.7 Plasmids

Name	Description	Origin
pENTR223.1-ERBB2	Gateway compatible Entry vector containing ERBB2 cDNA sequence (NCBI Reference Sequence: NM_004448.3, CDS: 262..4029)	DKFZ, Genomics and Proteomics Core Facility
pHIT60	gag/pol packaging plasmid	Sonoeka et. al. (1995)
pMD2.G	Vsv-G envelope plasmid	Didier Trono lab (Addgene)
pMXs-gw-CMV-EGFP	Gateway compatible retroviral vector based on pMXs-IRES-GFP, containing gateway cassette from pDEST22 and CMV promoter in place of IRES	Kindly provided by Dr. Cindy Körner and Dr. Ulrich Tschulena
psiCHECK2	Firefly/Renilla luciferase reporter vector	Promega

4.8 Software and databases

Cell Quest Pro	BD Biosciences
Microsoft Office 2010	Microsoft
SDS Software 2.2	Life Technologies (Applied Biosystems)
xCelligence RTCA Software 1.2	Roche Diagnostics
Sigma Plot	Systat Software Inc.
GraphPad Prism 6	GraphPad Software
Lasergene: SeqMan Pro, EditSeq, SeqBuilder	DNASTAR Inc
Adobe Photoshop CS5	Adobe Systems Inc.
TargetScanHuman 6.2	http://www.targetscan.org/
miRBase	http://www.mirbase.org/
miRanda	http://www.microrna.org/
Adobe Illustrator CS5	Adobe Systems Inc.
Gene Expression Omnibus: GEO22220, GEO19783	http://www.ncbi.nlm.nih.gov/geo/
NCBI	http://www.ncbi.nlm.nih.gov/
Odyssey software	Li-cor Biosciences
CellProfiler	http://www.cellprofiler.org/
Software for axiovert40	AxioVision Software (Zeiss)
Software for axiovert25	AxioVision Software (Zeiss)
Software for confocal microscope	ZEN Software (Zeiss)
ImageJ software	http://rsb.info.nih.gov/ij/
BreastMark	http://glados.ucd.ie/BreastMark/
NCI60 Cancer Cell line Microarray expression data	http://dtp.nci.nih.gov/
i-control 1.6 software	TECAN
METABRIC dataset (gene expression profiling/miRNA expression profiling)	Curtis, Shah et. al. (Nature 2012)
TCGA miRNA sequencing dataset	The Cancer Genome Atlas Network (Nature, 2012)
ISMARA	http://ismara.unibas.ch

4.9 UPL Primers

All primers were purchased from Sigma-Aldrich.

primer name	UPL probe number	sequence
HB-EGF_left	55	tggggcttctcatgtttagg
HB-EGF_right	55	catgcccaacttcactttctc
CDH1_left	35	cccgggacaacgtttattac
CDH1_right	35	gctggctcaagtcaaagtcc
CDH2_left	74	ctccatgtgccggatagc
CDH2_right	74	cgatttcaccagaagcctctac
ZEB1_left	3	gggaggagcagtgaaagag
ZEB1_right	3	tttcttgcccttcctttctg
FN1_left	32	ctggccgaaaatacattgtaaa
FN1_right	32	ccacagtcgggtcaggag
MMP9_left	53	gaaccaatctcaccgacagg
MMP9_right	53	gccacccgagtgtaaccata
MMP2_left	70	ataacctggatgccgtcgt
MMP2_right	70	aggcacccttgaagaagtagc
ZO-1_left	66	cagagccttctgatcattcca
ZO-1_right	66	catctctactccggagactgc
SNAI2_left	7	tggttgcttcaaggacacat
SNAI2_right	7	gttgcagtgagggcaagaa
CAV1_left	42	acagcccagggaaacctc
CAV1_right	42	ggatgggaacggtgtagaga
GAPDH_left	60	agccacatcgctcagacac
GAPDH_right	60	gcccaatacgaccaaatcc
HPRT1_left	73	tgaccttgatttattttgcatacc
HPRT1_right	73	cgagcaagacgttcagtcct
TFRC_left	61	ttgagaaaacaatgcaaaatgtg
TFRC_right	61	cccagttgctgtcctgatataga

ERBB2IP_left	75	tgattacttgatgctgaaagtgg
ERBB2IP_right	75	ttttcaaccctcactcgaatc

4.10 miRNA mimics

All miRNA mimics were purchased from Thermo Fisher Scientific (Dharmacon).

Name	**sequence**	**Catalogue number**
Negative Control #2	Based on cel-miR-239b: uuguacuacacaaaaguacug	CN-002000-01
hsa-miR-130b	cagugcaaugaugaaagggcau	C-300660-05
hsa-miR-301b	cagugcaaugauauugucaaagc	C-301252-01
hsa-miR-301a-3p	cagugcaauaguauugucaaagc	C-300657-03
hsa-miR-519a-3p	aaagugcauccuuuuagagugu	C-300835-05

4.11 Antibodies

4.11.1 Primary antibodies used for Western blotting and immunofluorescence

Protein target	**Company**	**Ordering number**
AKT	BD Biosciences	610860
pAKT (S473)	Cell Signaling Technology	CST_4058
ERK	Santa Cruz Biotechnology	sc_94
pERK1 (T202/Y204)/ pERK2 (T185/Y187)	R&D systems	AF1018
ERBB2 [Ab-17]	Thermo Fisher Scientific (NeoMarkers)	MS-730-P
pERBB2 (Y1248)	Merck Millipore	06-229
EGFR - antibody 1	Santa Cruz Biotechnology	sc_03
EGFR - antibody 2	Cell Signaling Technology	CST_2646
pEGFR (Y1068) [1H12]	Cell Signaling Technology	CST_2236L
GM130	BD Biosciences	610823
Fibronectin 1	BD Biosciences	610077
E-cadherin	Santa Cruz Biotechnology	sc-21791

Tubulin	Kind gift from Prof. Michael Boutros' lab	not commercial
Actin (clone C4)	MP BioMedicals	691001

4.11.1 Primary antibodies used for Reverse Phase Protein Arrays (RPPA)

Protein target	**Company**	**Ordering number**
Cortactin	Merck Millipore	05-180
EGFR	Cell Signaling Technology	CST_2646
pERK1 (T202/Y204)/pERK2 (T185/Y187)?	Cell Signaling Technology	CST_4370
pbCatenin (S33/S37/T41)	Cell Signaling Technology	CST_9561
profilin-1	Abcam	ab124904
Cdc42	Santa Cruz Biotechnology	sc-87
pIRS1 (S636/S639)	Cell Signaling Technology	CST_2388
MTSS1	Abnova	H00009788
LAMB1	Cell Signaling Technology	CST_3575-1
AKT1/AKT2	Santa Cruz Biotechnology	sc-1619-R
ERBB2 [AB-17]	Thermo Fisher Scientific (NeoMarkers)	MS-730-P
pEGFR (Y1068)	Cell Signaling Technology	CST_2236
EGR1	Cell Signaling Technology	CST_4154
MTDH	Cell Signaling Technology	CST_9596
FAK	Cell Signaling Technology	CST_3285
pPTEN (T366/S370)	Cell Signaling Technology	CST_2195-1
pRPS6 (S235/S236)	Cell Signaling Technology	CST_4858
R-cadherin	GeneTex Inc.	GTX62825
CAV1	Abcam	ab32577
Cyclin D1	Santa Cruz Biotechnology	sc-718
ROCK1	Cell Signaling Technology	CST_4035
Pan-Cadherin	Cell Signaling Technology	CST_4068
pSRC (Y416)	Cell Signaling Technology	CST_2101
IRS	Cell Signaling Technology	CST_3407

Integrin beta 1	Cell Signaling Technology	CST_4706
PTEN	Cell Signaling Technology	CST_9552
pMEK (S217/S221)	Sigma-Aldrich	M7683
pEGFR (Y845)	Cell Signaling Technology	CST_2231
ZO-1	Cell Signaling Technology	CST_8193
bCatenin	Cell Signaling Technology	CST_9562
EpCAM	Cell Signaling Technology	CST_2929
ROCK2	Sigma-Aldrich	HPA007459
BAX	Cell Signaling Technology	CST_2772
Integrin beta 3	Cell Signaling Technology	CST_4702
NFkB	Santa Cruz Biotechnology	sc-372
pERBB2 (Y1248)	Abcam	ab47755
pMEK (T286)	Cell Signaling Technology	CST_9127
Actin	MP BioMedicals	691001
AKT1	BD Biosciences	610860
pERBB2 (Y1112)	Merck Millipore	04-294
E-cadherin	Cell Signaling Technology	CST_4065
RhoA	Cell Signaling Technology	CST_2117
pMEK (S298)	Cell Signaling Technology	CST_9128
GAPDH	Santa Cruz Biotechnology	sc-47724
ERBB3 [AB-2]	Thermo Fisher Scientific (NeoMarkers)	MS-201-P0
p27	BD Biosciences	610241
N-cadherin	Cell Signaling Technology	CST_4061
PI3K (p110)	Cell Signaling Technology	CST_4249
MET	Cell Signaling Technology	CST_3148
pEGFR (Y1173)	Cell Signaling Technology	CST_4407
pSRC (Y416)_neu	Cell Signaling Technology	CST_2101
PI3K (p85)	Abcam	ab40755
MEK1	BD Biosciences	610122
ERK1/ERK2	Merck Millipore	06-182
pERBB2 (Y877)	Cell Signaling Technology	CST_2241

PKA	Santa Cruz Biotechnology	sc-903
ERK1	R&D Systems	AF1575
pERBB3 (Y1197)	Cell Signaling Technology	CST_4561
CDK6	Santa Cruz Biotechnology	sc-177
pERBB3 (Y1222)	Cell Signaling Technology	CST_4784
pEGFR (Y1148)	Cell Signaling Technology	CST_4404
pFAK (Y397)	Cell Signaling Technology	CST_3283
pCortactin (Y421)	Cell Signaling Technology	CST_4569
Vimentin	Cell Signaling Technology	CST_3932
MUC1	Cell Signaling Technology	CST_4538
ARP2	Cell Signaling Technology	CST_5614
Cytokeratin 5/6	Dako	M7237
pCytokeratin 8 (S23)	Abcam (Epitomics)	2147-1

4.11.1 Secondary antibodies

Antibody	Company	Detection system used	Cat. Nr.
goat anti rabbit IgG-HRP	Santa Cruz Biotechnology	Enhanced Luminescence (ECL)	sc-2004
goat anti mouse IgG-HRP	Santa Cruz Biotechnology	Enhanced Luminescence (ECL)	sc-2055
Alexa Fluor 647 donkey anti-rabbit IgG (H+L)	Life Technologies (Invitrogen)	LSM 510 Meta confocal microscope	A31573
Alexa Fluor 647 donkey anti-mouse IgG (H+L)	Life Technologies (Invitrogen)	LSM 510 Meta confocal microscope	A21235
Alexa680 F(ab')2 fragment of goat anti-rabbit IgG	Life Technologies (Invitrogen)	Odyssey Infrared Imaging System	A21077
Alexa680 F(ab')2 fragment of goat anti-mouse IgG	Life Technologies (Invitrogen)	Odyssey Infrared Imaging System	A21059
goat anti-rabbit IgG (H+L) DyLight 680 conjugated	Thermo Fisher Scientific	Odyssey Infrared Imaging System	35568
goat anti-mouse IgG (H+L)	Thermo Fisher Scientific	Odyssey Infrared	35518

DyLight 680 conjugated		Imaging System	
goat anti-rabbit IgG (H+L) DyLight 800 conjugated	Thermo Fisher Scientific	Odyssey Infrared Imaging System	35571
goat anti-mouse IgG (H+L) DyLight 800 conjugated	Thermo Fisher Scientific	Odyssey Infrared Imaging System	35521

4.12 Mice

In the experiment involving mice, 32 female mice from strain NOD.Cg-Prkdcscid Il2rgtm1Wjl/SzJ were used. These immunodeficient mice, commonly known as NSG (NOD scid gamma) mice, do not express the Prkdc gene as well as the X-linked Il2rg gene and are characterized by the absence of mature T cells, B cells, and natural killer (NK) cells. They are also deficient in multiple signaling pathways activated by cytokines. These features and additional limitation of innate immunity render them long-lived, susceptible to engraftment of human cells mouse model. NSG mice used in my work for engraftment of MCF10-derived cell line pools were bred in Animal Laboratory Services Core Facility at DKFZ.

4.13 Tumor specimens from ERBB2-positive breast cancer patients

Tumor specimens from patients diagnosed with primary invasive breast carcinoma were collected at the time of surgery between 2009 and 2010 at the Department of Gynecology and Obstetrics/National Center for Tumor Diseases, Heidelberg. None of the patients had received neoadjuvant therapy. Institutional Review Board approval was received as ethics vote no. S039/2008 and informed consent was obtained from all the patients. Tumor specimens were processed within 20 min after surgery. Samples were stored flash frozen at −80 °C until further use. Each tumor specimen contained at least 70% tumor cells and was classified as ERBB2 receptor positive as assessed by routine immunohistochemistry/*in situ* hybridization.

5. Methods

5.1 Stable cell line pools production

- **ERBB2 cloning into pMXs-gw-CMV-EGFP vector**

To obtain ERBB2-carrying retroviral vector, Homo sapiens v-erb-b2 avian erythroblastic leukemia viral oncogene homolog 2 (ERBB2), transcript variant 1 cDNA sequence possessing a stop codon has been recloned in LR reaction from gateway compatible entry vector (pENTR223.1-ERBB2) obtained from the International ORFeome Collaboration resources at DKFZ core facility to the gateway compatible destination retroviral vector pMXs-gw-CMV-EGFP. The destination vector has previously been obtained in our laboratory from pMXs-IRES-GFP vector via replacement of multicloning site and IRES sequence with a Gateway cassette from pDEST22 and CMV promoter. Therefore EGFP is expressed completely independently of ERBB2 and serves as a positive control for transfection of packaging cells as well as for target cell infection (Figure 9).

LR reaction

The following components were mixed at room temperature in a 1.5 ml tube: entry clone (50-150 ng), destination vector (150 ng) and TE buffer pH 8.0 to reach 8 µl. 2 µl of LR Clonase II was then added and mix was briefly vortexed and incubated at 25°C for 1 h. Later, 1 µl of proteinase K solution was added and mix was incubated at 37°C for 10 min to terminate the reaction.

Bacteria transformation and plasmid amplification

5 µl of LR reaction mix was added to 100 µl half-frozen competent DH5α bacteria and incubated 30 min on ice. After that time bacteria were incubated for 50 s in 42°C followed by 5 min incubation on ice to cool down the bacteria after heat shock. 500 µl of SOC medium was then added and bacteria were incubated in 37°C for 45-60 min. They were then centrifuged briefly (3 min, 1000 rpm), 350 µl of medium was removed and the remaining medium was used to resuspend the bacteria pellet and spread evenly on LB agar plate containing 100 mg/l ampicilin using glass beads. After 24 hours incubation in 37°C, 5 single colonies were picked up and each of them was inoculated into 5 ml LB medium with 100 µg/ml ampicilin and shaken for 20-24 hours in 37°C at 200 rpm. Plasmids were isolated

with Easy Prep Pro kit according to manufacturer's instructions. DNA concentration and purity was then measured with Nano-Drop.

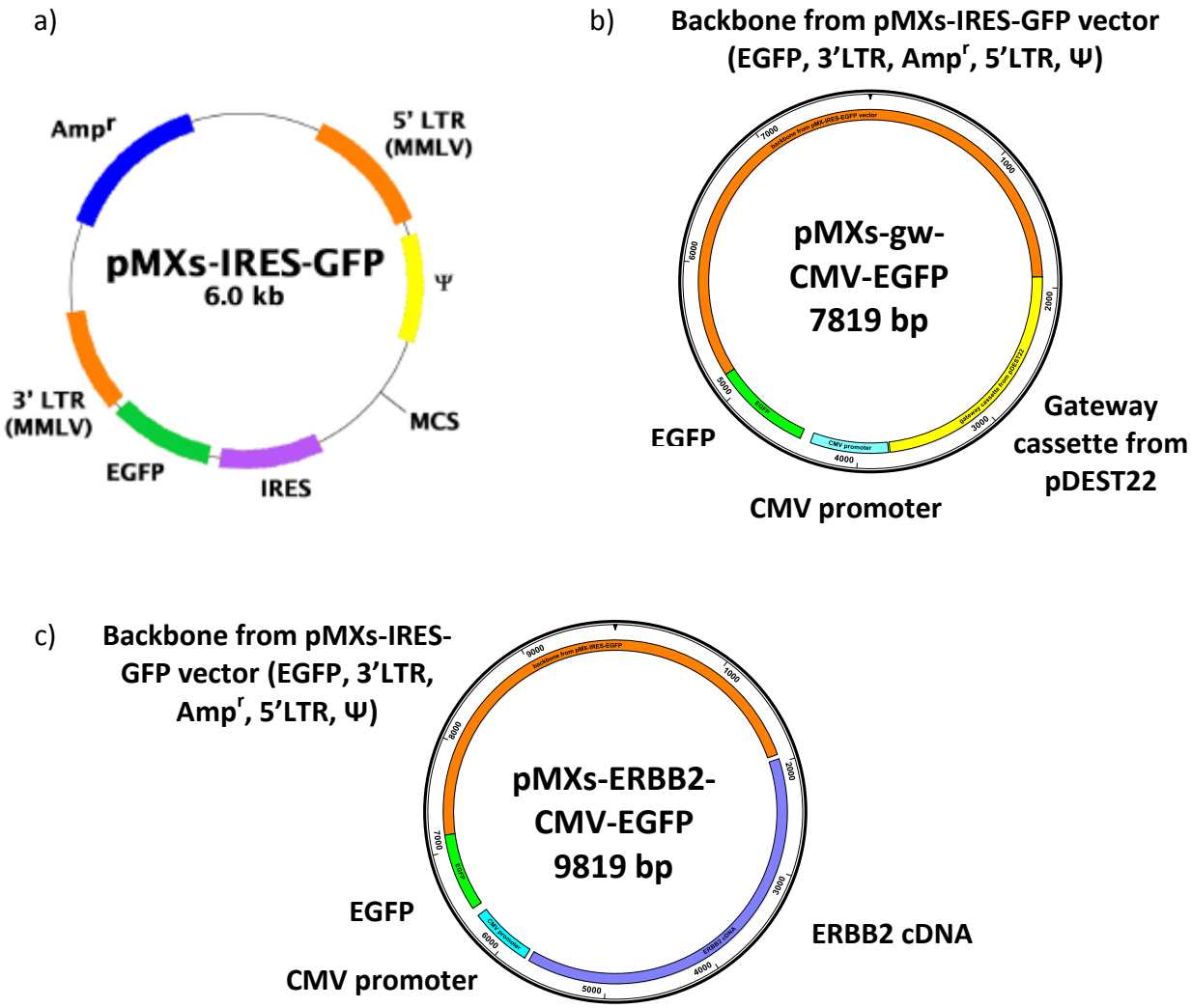

Figure 9
Retroviral vectors used for cloning ERBB2 cDNA. a) The map of commercially available retroviral pMXs-IRES-GFP vector (Cell Biolabs INC.), which served as basis to obtain b) gateway compatible retroviral destination pMXs-gw-CMV-EGFP vector. In this vector MCS and IRES sequences were replaced by gateway cassette from pDEST22 and CMV promoter driving expression of EGFP; c) The map of retroviral destination pMXs-ERBB2-CMV-EGFP vector in which ERBB2 cDNA was cloned from gateway compatible pENTR223.1 vector.

To check if ERBB2 cDNA was successfully cloned into destination vector, restriction digest was performed on each bacteria clone. For a 20 µl reaction 1 µg DNA, 0.2 µl SpeI restriction enzyme, 0.2 µl SbfI restriction enzyme, 2 µl NEBuffer 4, 0.2 µl 100x BSA and H_2O were used. Restriction mix was incubated 3 h at 37 ^oC and then electrophoretically separated in 1% agarose gel at 130 V for 45-60 min. Samples for electrophoresis were prepared by mixing

4 µl of 6x Loading Dye with 20 µl of the digested plasmids. For size control GeneRuler 1 kb DNA Ladder was used. The plasmids showing expected fragments sizes (1436 and 8383 bp) were sent to GATC company for sequencing. Plasmid with correct sequence was then amplified using Qiagen MidiPrep Plasmid Midi Kit according to the manufacturer's instructions.

50x TAE

242 g Tris base

57.1 ml 100% Acetic acid

100 ml 0.5 M EDTA

Added dH_20 to 1 l, set pH to 8.0 with HCl or NaOH

Agarose gel

1 g agarose

100 ml 1x TAE buffer

Heated up to solve, then cooled down to ~50-60 ^{o}C, poured into gel preparation chamber and left to solidify in room temperature for ~45 min.

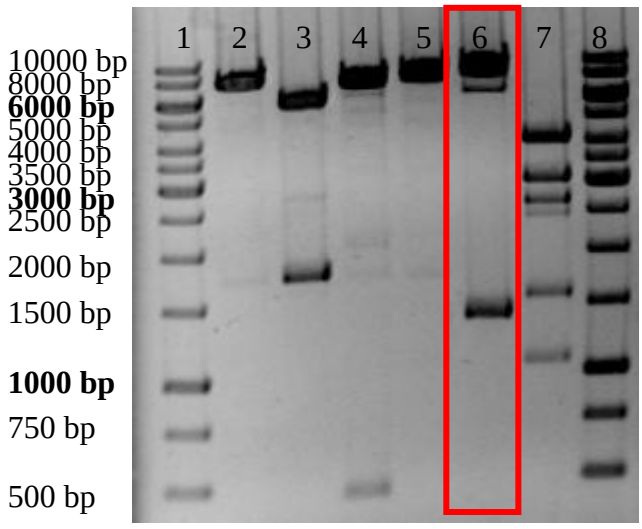

Figure 10

Restriction analysis of plasmids obtained in LR reaction. Lanes 1 and 8: GeneRuler 1kb DNA ladder; Lanes 2-7: plasmids obtained in LR reaction were cut with SpeI and SbfI restriction enzymes and DNA fragments were separated electrophoretically in 1% agarose gel. Lane 6 – the plasmid which showed expected bands' sizes and was sent for further validation by sequencing.

- **Retrovirus production**

For retrovirus production I worked with duplicates. Experiments were performed in S2 laboratory.

On day 1 HEK293FT cells (2 million cells) were seeded in 10 cm plates in full growth medium. On day 2 cells were transfected as described below:

Mix 1 was prepared by mixing 625 µl OptiMEM with 10 µl lipofectamine, vortexing and leaving it in room temperature for 5 minutes.

Mix 2 was prepared by mixing 625 µl OptiMEM with:

3.5 µg pHIT60 (gag/pol packaging vector)

3.5 µg retroviral vector (either pMXs-gw-CMV-EGFP as control or pMXs-ERBB2-CMV-EGFP)

800 ng pMD2.G (Vsv-G envelope vector)

Next, mix 1 and mix 2 were combined, vortexed for 1 minute and incubated in room temperature. In the meantime HEK293FT cells' medium was replaced by 2500 µl OptiMEM. After 20 minutes of 1250 µl of mix1+2 was added to cells. Transfection mix was removed from cells after 5 hours and full growth medium was added. On day 3 medium was changed for MCF10A full growth medium, so that virus can be excreted to the medium used later for infection of MCF10A cells.

- **Infection**

On day 3 early passage of MCF10A cells (500 000 cells) was seeded in 10 cm plates in full growth medium. On day 4, after 24 hours since medium change of HEK293FT cells the medium was collected to 15 ml tube and centrifuged to remove dead cells. Supernatant was mixed with polybrene 4 µl/ml and added to MCF10A cells. New MCF10A full growth medium was added to HEK293FT cells. The procedure was repeated again after 24 hours on day 5. After 8 hours since second infection medium of MCF10A was changed for fresh full growth medium. After a few passages cells were transferred from S2 to S1 laboratory and then collected for cell sorting. As an alternative to cell sorting (obtaining pools of cells with different virus integration site), part of the cells was serially diluted to single-cell suspension and cells were seeded on poly-L-lysine coated 96 well plates to obtain one cell per well. This approach allows to obtain clones of cells with the same virus integration sites.

- **Cell sorting**

Infected cells were trypsinized and after centrifugation the pellet was resuspended in 700 µl PBS containing 10% horse serum. Prior to cell sorting cell suspensions were pipetted through

cell strainer in FACS tubes to avoid cell clumps blocking the instrument. Sorting was done according to the level of EGFP in the cells transduced with a virus at the Imaging and Cytometry Core Facility in DKFZ by Mr. Klaus Hexel. Sorted cells were collected in 2 ml full MCF10A growth medium containing 10% horse serum and subsequently seeded in 24-well plates covered with poly-L-lysine.

5.2 Cell culture

2D cell culture

Different cell types were cultured in appropriate growth medium (see "Materials"). Stable cell line pools and single clones derived from MCF10A cell line were cultured in MCF10A growth medium. Mycoplasm contamination tests were performed routinely in the laboratory using PCR Mycoplasma Test Kit. Additionally, multiplex human cell authentication and thorough contamination tests of the cell lines were performed at the DKFZ Core Facility. Cells were passaged every 3-4 days as follows:

Medium was removed from the cells, cells were washed once with PBS and trypsinized with low amount of 0.05% or 0.25% trypsin in 37^{o}C, 5% CO_2 incubator for 15 minutes (for MCF10A and MCF10A-derived cell line pools) or 3 minutes (for other cell lines). After detachment of cells they were collected with larger volume of growth medium into a 15-50 ml tubes and centrifuged for 5 minutes at room temperature at 1200 rpm speed. Supernatant was removed, cell pellet thoroughly resuspended in 6-7 ml of growth medium and cells were counted by CASY. 4x10^5 cells (MCF10A) or 5x10^5 (other cell lines) were seeded on 10 cm plates. If cells were grown in bigger culture flasks (T75, T175) the amount of cells seeded was proportional to the plate surface.

Preparation of poly L-lysine coated plates

Poly L-lysine coated plates were used to increase cell adherence, e.g. after cell sorting. Poly L-lysine was diluted 1:50 with H_2O to achieve working concentration of 0.1 mg/ml before using. Plates were covered with this solution and incubated for 1 hour in room temperature. After that plates were washed once with H_2O and once with appropriate full growth medium before cell seeding.

Cryopreservation of cells

To freeze cells special freezing medium was prepared. For a particular cell line growth medium was supplemented with 20% of either FBS or horse serum and 10% DMSO, and kept on ice before usage. Trypsinized cells (brought down to single-cell suspension) were collected to 15-50 ml tubes and counted with CASY. The desired amount of cells was then spinned down and supernatant was removed. Cell pellet was resuspended in appropriate volume of ice-cold freezing medium and suspension was aliquoted into cryovials at $1x10^6$-$2x10^6$ cells/ml concentrations. Cryovials were then instantly placed into -80^oC freezer in freezing container filled with isopropanol to ensure slow cooling rate of cells (1°C/min). One day later cells were transferred to liquid nitrogen storage tank.

To thaw frozen cells, a cryovial was placed in a 37°C water bath and quickly after thawing transferred to 10 ml growth medium-containing tube. Cells were then spinned down (5 min, 1200 rpm), supernatant removed, cell pellet resuspended in growth medium and cell seeded in 10 cm plate as desribed before. One day later medium was changed to remove dead cells.

3D cell culture of MCF10A-derived cell line pools in Matrigel

8-well glass bottom chambers were covered with 40 µl/well of ice-cold liquid growth factor reduced matrigel and left 30 minutes to solidify in 37^oC, 5% CO_2 cell culture incubator. In the meantime cells grown in 2D culture in 10 cm Ø plastic dishes were washed 1 x 3 ml PBS, trypsinized with 1,5 ml 0,05% trypsin, collected with 4,5 ml of Assay Medium to a new tube, spinned down to remove trypsin and resuspended to single cell suspension in Assay Medium (containing 2% horse serum and no EGF). Cells were then counted using CASY, further diluted to 25000/ml using Assay Medium and cooled down on ice. In separate tubes Assay Mediums with addition of 2x higher concentrations of EGF or serum than desired for the experiment were prepared. Equal volumes of cell line/cell line pools suspension and assay mediums were then mixed and 2% of matrigel was added just before plating 400 µl/well (containing 5000 cells) on the top of matrigel in 8-well chambers. Assay Mediums containing desired experimental concentrations of growth factors was changed every 4 days, each time with addition of 2% Matrigel. Cells were grown in matrigel for 9-16 days, depending on an experiment.

5.3 Transfections

For transfections with lipofectamine 2000 transfection reagent cells were seeded in growth medium. For MCF10A cell line or MCF10A-derived cell line pools $1,2x10^5$ cells were seeded per well in 6-well plates, for other cell lines $2,5x10^5$. After 24 hours medium was replaced by 1 ml of appropriate transfection medium (see "Materials") without antibiotics and cells were transfected with 500 ml transfection mix prepared in OptiMEM. Transfection mix contained 4 ul lipofectamine and additionally one of the following: 25 nM miRNA or 20 nM siRNA. After 6-8 hours transfection medium was replaced by growth medium.

5.4 Direct cell counting

Direct cell counting was performed to measure the proliferation rate of cells. Specified cell number was seeded in 6-well plates in triplicates. After 48 hours cells were harvested by trypsinization (as previously described) and cell pellet was resuspended in 1 ml medium. Cells were counted using CASY. Alternatively, cells were seeded on 96 well plates and 48h post-transfection were fixed 15 minutes with 2% PFA and incubated for 10 minutes with DAPI. After washing 2x with PBS, the total amount of nuclei was counted using Olympus microscope.

5.5 Cell viability assay

Based on ATP measurement (using CellTiter-Glo reagent)

3000 (MCF10A and MCF10-derived cell line pools), 5000 (SKBR3) or 6000 (BT474) cells were seeded in white 96-well OptiPlates in the respective full growth medium. At least five biological replicates were used per condition. If the cells were going to be transfected, the transfection was done 24 h after seeding. If the drug was added to the cells, then it was done 48 h after seeding, irrespective whether the cells were previously transfected or not. For this purpose 100 µl full growth medium containing desired drug concentration was added to the cells for 72 hours, prior to ATP measurement. The viability of cells was measured using the CellTiter-Glo Luminescent Cell Viability assay according to manufacturer's protocol. Briefly, CellTiter-Glo Buffer was mixed with CellTiter-Glo Substrate prior to addition to cells to obtain CellTiter-Glo Reagent. Cells were taken out of incubator 30 minutes prior to reagent addition to equilibrate them to room temperature. 100 µl of the reagent was then added per well, plates were shaken for 2 minutes and incubated for

10 minutes protected from light at room temperature. Following incubation luciferase activity was measured using Infinite M200 microplate reader. In this assay luminescent signal is proportional to ATP amount present in the cells as the beetle luciferin present in the reagent requires ATP to be transformed into oxyluciferin and produce the light as a byproduct.

Based on NADPH measurement (using WST-1 reagent)

Cells were seeded, transfected and treated with a respective drug similarly as described above. However, in place of white OptiPlates, 96-well transparent plates were used. Prior to NADPH measurement, 10 µl of ready-to-use tetrazolium salt solution (WST-1) was added directly to cells. Cells were then incubated additional 2-4 hours at 37^{o}C, 5% CO_2 to allow WST-1 cleavage to a soluble formazan in the presence of NAD(P)H in viable cells. The amount of formazan dye formed in this colorimetric reaction, which directly correlates with the number of metabolically active cells, was quantitated by measuring formazan absorbance using Infinite M200 microplate reader.

5.6 Immunofluorescence staining and microscopy

Staining cells in 2D culture

For staining of MCF10A and MCF10A-derived cell line pools, 200 000 cells (or 120 000 cells if they were going to be transfected) were seeded on cover slips in 6-well plates (at least two replicates per condition). For other cell lines 250 000 cells were seeded. 48 hours after seeding (or after transfection) cells were fixed on cover slips by addition of 2% PFA in PBS for 15 minutes in room temperature. Cells washed 3x with PBS were permeabilized by incubation in 0.2% Triton X-100 in PBS for 5 minutes. Cover slips, 3x washed in PBS, were then blocked in 3% BSA/PBS and subsequently incubated with primary antibody diluted (1:100- 1:200) in blocking solution overnight at 4^{o}C. Next day cells were washed again and incubated with Alexa647-coupled secondary antibody, diluted 1:1000 in blocking solution, for 1 hour at room temperature. To achieve efficient antibody binding and later detection plates were shaken on waving platform, protected from light. If the cells were stained for actin filaments, cover slips were washed 3x with PBS and incubated with Alexa647-coupled phalloidin, diluted 1:40 in blocking solution for 30 minutes at room temperature. For DAPI staining cover slips were washed 3x with PBS and incubated for 10 minutes with 1:5000

diluted reagent in 3% BSA/PBS on waving platform. Cover slips, washed again with PBS, were then mounted on microscopy slides using ProLong Gold antifade reagent. Slides were kept overnight at room temperature in the dark to dry before proceeding with fluorescent/confocal microscopy. If necessary, slides were stored at 4^{o}C.

If the cells were not stained using antibodies, the whole procedure was performed till "mounting the slides" step within the same day.

Staining cells in 3D culture

Cells grown in Matrigel for 9-11 days as described in "Cell culture" section were washed 2x with PBS and fixed with 4% PFA for 45 minutes at room temperature prior to staining. Both solutions were pre-warmed to 37^{o}C before usage. Cell were then rinsed 3x with PBS:Glycin solution for 10 minutes on a waving platform. This step reduces the background staining as glycin binds to free aldehyde groups (originating from PFA) preventing primary and secondary antibodies from unspecific binding to them. To permeabilize the cells 0.5% Triton X-100 was incubated with cells for 5-10 minutes at room temperature. They were then washed 3x for 10 minutes with 1x IF wash buffer. If not specified differently cell were washed always with the same type of buffer throughout the procedure and all aspirations were performed with mild suction to avoid disruption of matrigel. Fixed cells were then blocked with blocking solution for 1 hour 15 minutes and then additionally for 30 minutes with refreshed blocking solution. Primary antibody was diluted (1:100-1:200) in the blocking solution and incubated with cells overnight at 4^{o}C on a very gentle rocker. Next day, cell culture chambers were equilibrated to room temperature and cells washed 3x 20 minutes. Secondary antibody, Alexa647-conjugated, was added to cell culture chambers, diluted to 1:1000 in blocking solution, and incubated for 50-60 minutes at room temperature in the dark on waving platform. Washed cells were then incubated with 0.5 ng/ml DAPI in PBS for 5-10 minutes, rinsed 2x with PBS and cell culture chambers were disassembled to obtain microscopy slides covered with matrigel containing stained cells. Cover slips were mounted on the top of the slides using ProLong Gold antifade reagent and allowed to dry overnight at room temperature in the dark. Confocal microscopy was performed next day.

Buffers and solutions

10x PBS (pH 7.4)

80.1 g NaCl (final conc. 1370 mM)

2g KCl (final conc. 27 mM)

2.7 g KH_2PO_4 (final conc.20 mM)

17.8 g Na_2HPO_4 x $2H_2O$ (final conc. 100 mM)

ad 1 l dH_2O, pH adjusted to 6.8-7.2 with NaOH or HCl (upon dilution to 1x PBS pH increases)

1x PBS (pH 7.4)

8.01 g NaCl (final conc. 137 mM)

0.2 g KCl (final conc. 2.7 mM)

0.27 g KH_2PO_4 (final conc. 2 mM)

1.78 g Na_2HPO_4 x $2H_2O$ (final conc. 10 mM)

Ad 1 l dH_2O, pH adjusted to 7.4

4% Paraformaldehyde (PFA)

4g PFA

100 ml PBS (warmed up in a microwave)

800 µl 1 M NaOH

After solving pH was neutralised with 800 µl 1 M HCl to 7-8

1x IF wash buffer (35 ml):

35 mg BSA

35 ml PBS

70 µl Triton X-100

17.5 µl Tween-20

1x PBS:Glycine (10ml):

75 mg Glycine

10 ml PBS

blocking solution:

1x IF wash buffer + 10% goat serum

5.7 Anchorage-independent growth assay

Low-attachement plates

250 000 cells/well were seeded on Costar ultra low attachment 6-well plates and kept in 37^{o}C, 5% CO_2 for 72 hours. Microscopy pictures were then taken to capture the structures formed by cells.

PolyHEMA assay

For preparation of 96-well polyHEMA-covered plates, polyHEMA powder was first dissolved to 120 mg/ml in 95% ethanol by incubation at 37^{o}C for 3 days on a horizontal roller shaker. Next 50 µl of the solution was pipetted into each well of 96-well plate and allowed to dry at 37^{o}C, 5% CO_2 for 5-6 days. 8000 cells were then seeded per well in 100 µl of growth medium. After 3-4 days the pictures of cells were taken, followed by addition of 10 µl WST-1 to each well and incubation for additional 2-4 hours at 37^{o}C and 5% CO_2. Absorbance was then measured at 450 nm by Infinite M200 microplate reader. 6 biological replicates were used.

5.8 Migration assays

Wound healing assay using Ibidi chambers

In this type of migration assay, Ibidi culture inserts were used (Figure 11). 15 000 of MCF10A/MCF10A-derived cell line pools were seeded in two chambers of the insert. If the cells were going to be transfected, the transfection took place 24 hours after cell seeding. After reaching a homogenous monolayer, the cells were starved with "MCF10A Starvation Medium 2" containing 0.9% serum and devoid of EGF (for details see chapter "Materials"). 20-24 h later insert was removed to form an empty area ("wound") between the cells and the medium changed for a desired migration conditions (e.g. with the addition of EGF or serum). The migration ability of the cells was quantified by picture capturing of the scratch at different time points starting at time "0" which then can was compared to later time points (Figure 11). The faster a wounded area is covered by the cells, the higher is the cells' migratory potential. The pictures were done using Axiovert 25 microscope, then areas not covered by cells were marked black using Adobe Photoshop software and quantified using Cellprofiler software. Three independent biological replicates were used.

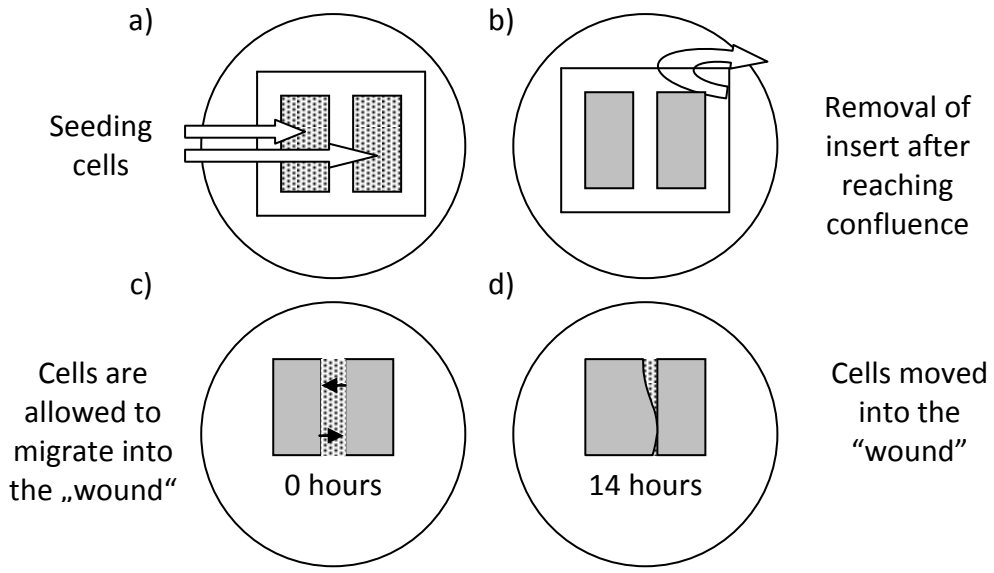

Figure 11

Migration assay using Ibidi chambers. For the migration assay the culture insert is placed into a well in 6-well plate. Cells are seeded in each of the two chambers of the migration insert (a) and after reaching confluency the insert is removed (b), fresh culture medium is added and the migration process is started (c). Pictures of the scratch area are taken for different time points (c, d).

Migration assay using real time cell analyzer (RTCA)

120 000 MCF10A/MCF10A-derived cells were seeded in 6-well plates. If the cells were going to be transfected, the transfection was done 24 hours after seeding. 48 hours after seeding cells the medium was changed for an "Assay medium" with reduced (2%) serum level and no EGF (for details see "Methods"). 20-24 hours later cells were harvested by trypsinization, counted with CASY and 55000 cells were seeded in 100 µl of "Assay medium" in the upper chamber of a CIM plate. The lower chamber was filled with 175 µl of "Assay medium" with addition of chemoattractant – either 20 ng/ml EGF or 3% of horse serum (to achieve final concentration 5%). The CIM plate was then placed in real time cell analyzer (RTCA) machine and cells were allowed to migrate for 24-48h hours depending on the experiment. The cell index was measured every 15 minutes. Four biological replicates were used. The CIM plate's upper chamber is cover at the bottom with microporous polyethylene terephthalate (PET) membrane (8 µm pores) containing microfabricated gold electrode arrays on the bottom side. When the cells move through the membrane and touch the electrodes on the bottom side of the membrane, the changes in impedence are registered. Therefore the cell migration can be measured in real time.

5.9 Invasion Assays

Invasion assay using real time cell analyzer (RTCA)

Invasion assay using RTCA was performed similarly to migration assay described above. However, the upper chambers of CIM plate were covered with matrigel prior to the cell seeding. For this purpose 50 µl of 1:40 dilution of matrigel in DMEM/F12 medium was added to the middle of 4 wells in CIM plate. Immediately 30 µl was then removed from each well and procedure continued until all the wells were covered. Plate was incubated at 37^{o}C for 3-4 hours before cell seeding. Covering the membrane with matrigel, which contains main extracellular matrix components, provides the barrier which only cells with invasive properties can cross. Cells were seeded in assay medium containing 2% of Matrigel.

Invasion assay using matrigel invasion chambers

Prior to the assay, cells were seeded and treated similarly as described for migration assay using RTCA system. Matrigel invasion chambers were rehydrated before the usage according to manufacturer's instructions. For invasion assay 150 000 cells were seeded on the top of

matrigel-covered microporous membrane (8 µm) of the upper chamber and allowed to invade through matrigel towards the lower chamber containing chemoattractant (20 ng/ml EGF or 5% horse serum) for next 48-72 hours. Invaded cells were then trypsinized and counted using flow cytometry and Cell Quest Pro software.

5.10 Cell adhesion

Cell adhesion assay was performed using RTCA system as well. 60 000 cells were seeded in E-plates, which contain microfabricated gold electrode arrays on the bottom of the wells, and the changes in the impedance (resembled by "cell index") were measured every 15 minutes for 24 hours.

5.11 Dual luciferase reporter assay using psiCHECK2

3'UTRs of ESR1, CDKN1A (p21), CDKN2B (p15) and PTEN were cloned previously in our laboratory by Dr. Aoife Ward into a multiple cloning region located downstream of the Renilla luciferase translational stop codon in psiCHECK2 luciferase reporter vector. In this vector the cloned 3'UTR of a desired gene serves therefore as a regulatory sequence for Renilla luciferase gene expression. Additionally the psiCHECK2 vector codes for a Firefly luciferase, which, by its constitutive expression in transfected cells, enables normalization of the Renilla luciferase signal to the Firefly luciferase signal (that corresponds to the cell number). Both luciferases use different substrates to produce luminescence, thus their activity can be sequentially measured in the same cells using dual luciferase reporter assay system kit (Promega).

For luciferase reporter assay 5000 MCF7 cells were seeded in white 96-well OptiPlates in the respective full growth medium. The cells were transfected 24 hours after seeding with 25 nM miRNA mimics and 100 ng/ml of psiCHECK2 reporter vector. Five biological replicates were used per condition. 48 hours post-transfection cells were lysed and dual luciferase reporter assay was performed following manufacturer's instructions and using Inifnite M200 microplate reader for luminescence measurement. Renilla signal was double normalized: to firefly luciferase signal measured in the same cells and to the Renilla/Firefly ratio of cells transfected with the same miRNA but with an empty psiCHECK2 vector to reduce the effect of certain miRNA on psiCHECK2 backbone. The changes in luciferase activity upon miRNA

mimic overexpression are presented as fold changes compared to overexpression of control miRNA mimic.

5.12 ELISA

"Sandwich" enzyme-linked immunosorbent assay (ELISA) was used to measure ERBB2 levels in MCF10A-derived cell line pools and in SKBR cell line. For this purpose Human Total ErbB2/Her2 DuoSet IC was used, apart from streptavidin-HRP which was replaced by streptavidin-Alexa680. Briefly, capture antibody was diluted first with PBS to 4 µg/µl and 100 µl of the solution was added per well to coat 96-well microplates. The plates were then incubated overnight at RT. Next day the antibody solution was removed and each well was washed 3x with 400 µl of washing buffer before addition of 300 µl blocking buffer. After 1.5 hours of blocking the plates at room temperature the blocking buffer was removed and samples as well as standards were added in technical duplicates, diluted with buffer A. As standards ERBB2 protein serial dilutions (4 ng/ml, 2 ng/ml, 1 ng/ml, 0.5 ng/ml, 0.25 ng/ml, 0.125 ng/ml, 0.067 ng/ml, 0 ng/ml) were used. SKBR3 protein lysate and lysates from MCF10A-derived cell line pools were obtained in the similar manner as previously described for Western Blot method. SKBR3 protein lysate was diluted to 100 µg/ml, 50 µg/ml, 10 µg/ml and 5 µg/ml. Protein lysates from MCF10A cell line pools were diluted to 1 µg/ml, 500 ng/ml, 250 ng/ml and 125 ng/ml as high ERBB2 expression was expected. 100 µl of each dilution was applied per well and incubated at RT for 2 hours. The lysates were then removed and wells were washed as described before. 100 µl/well of the detection antibody diluted to 200 ng/ml with buffer B was then incubated for 2 hours at RT with the captured protein, washed as before and incubated for 20 minutes with 100 µl of 1:5000 diluted in wash buffer streptavidin-Alexa680 solution. Plates washed 3x with 400 µl of washing buffer were then scanned using Odyssey Infrared Imaging System.

Buffer A

20 mM Tris, pH 7.2-7.4

137 mM NaCl

0.05% Tween 20 (v/v)

0.1% BSA (w/v)

Buffer B

20 mM Tris, pH 8.0

137 mM NaCl

10% Glycerol (v/v)

2 mM EDTA

Complete Mini Protease Inhibitor Cocktail and PhosStop tablets were added to 10 ml of buffer before use

ELISA wash buffer

0.05% Tween 20 in PBS (v/v)

pH 7.2-7.4

ELISA blocking buffer

1% BSA (w/v) in PBS

0.05% sodium azide

pH 7.2-7.4

5.13 Immunobloting (Western Blot)

Protein isolation

For protein isolation cells were washed once with cold PBS containing 1 mM sodium orthovanadate (Na_3VO_4) - general inhibitor for protein phosphotyrosyl phosphatases (PTPs), and 10 mM sodium fluoride (NaF) - general inhibitor for protein phosphoseryl and phosphothreonyl phosphatases (PSPs). Cells were then lysed using M-PER lysis buffer containing 1x Complete Mini Protease Inhibitor Cocktail, 1x PhosSTOP phosphatase inhibitor, 1 mM Na_3VO_4 and 10 mM NaF. After 10 minutes incubation on ice, lysates were centrifuged at 13000 rpm at 4^{o}C, pellet was removed and concentration of the protein in the supernatant was measured using Pierce BCA protein assay kit. Cell lysates were diluted further with lysis buffer to obtain desired concentrations and then denatured for 5 minutes at 95^{o}C in the presence of 1x Roti-Load.

Gel preparation

Proteins were separated by sodium dodecyl sulfate polyacrylamide gel electrophoresis (SDS-PAGE) according to their molecular weight. For this purpose different percentage (8%, 10%) separating polyacrylamide gels were prepared accompanied by 4% stacking gels. 5-10 µg protein was loaded on the gel and separated by SDS-PAGE at 130 V for 75 minutes in the

1x SDS-PAGE running buffer. A prestained protein ladder (Precision Plus Protein™ Dual Color Standards) was used as molecular weight marker. The buffers and gels were prepared as follows:

4x Separation gel buffer

90.9 g Tris base (final conc. 1.5 M)

add 500 ml dH_2O, pH adjusted to 8.8 with concentrated HCl/NaOH

4x Stacking gel buffer

30.3 g Tris base (0.5 M)

add 500 ml dH_2O, pH adjusted to 6.8 with concentrated HCl/NaOH

4% SDS-PAGE stacking gel (for 4 gels)

6 ml ddH_2O

2.6 ml of 0.5 M 4x stacking gel buffer

1.33 ml acrylamide/bisacrylamide 37.5:1

100 µl 10% SDS

200 µl 10% APS

10 µl TEMED

8% SDS-PAGE separating gel (for 4 gels)

9.4 ml ddH_2O

5 ml of 1.5 M 4x separation gel buffer

5.4 ml acrylamide/bisacrylamide 37.5:1

400 µl 10% SDS

400 µl 10% APS

26.8 µl TEMED

10% SDS-PAGE separating gel (for 4 gels)

8 ml ddH_2O

5 ml of 1.5 M 4x separation gel buffer

6.6 ml acrylamide/bisacrylamide 37.5:1

400 µl 10% SDS

400 µl 10% APS

26.8 µl TEMED

10% APS

1000 mg ammonium persulfate (APS) dissolved in 10 ml dH_20

10% SDS

10 g sodium dodecyl sulfate (SDS) dissolved in 100 ml dH_20 at 55^oC

10x SDS-PAGE running buffer (without SDS)

30.3 g Tris base (250 mM)

144 g Glycine (1.92 M)

add 1 l dH_20

1x SDS-PAGE running buffer

500 ml 10x SDS-PAGE running buffer

50 ml 10% SDS

Add dH_20 to 5 l

Western blotting – using Amersham Hybond-P PVDF membrane

To transfer the protein on a membrane, a "sandwich" - containing 4 Whatman papers soaked with Anode buffer I, 2 Whatman papers soaked with Anode buffer II, polyvinylidene fluoride (Amersham Hybond-P PVDF) membrane activated with methanol and washed a few times with Anode buffer II, polyacrylamide gel with separated proteins and 6 Whatman papers soaked with Cathode buffer - was placed in the semi-dry transfer apparatus. The transfer was done for 75 minutes at 25 V and directly afterwards membrane was stained with Ponceau S solution to check the quality of transfer. If the transfer worked well, the membrane was washed 3x with TBST and then incubated on a waving platform for 1 hour in 5% milk or 5% BSA in TBST depending on antibody. Blocked membrane was exposed to primary antibody (diluted 1:200 - 1:1000 depending on antibody) in blocking solution overnight at 4^{o}C in a 50 ml falcon tube on a horizontal roller shaker. Next day membrane was washed 3x 15 minutes with TBST and then incubated for 1 hour at room temperature with respective HRP-conjugated secondary antibody (anti-mouse or anti-rabbit), diluted 1:10000 in blocking buffer. Membrane, washed again 3x 15 minutes with TBST, was then covered with Enhanced Chemiluminescence (ECL) reagent and immediately exposed to X-ray films. Signal on X-ray films can be detected due to the horseradish peroxidase catalyzed oxidation of luminol present in the ECL reagent. Following oxidation, luminol is in an excited state and quickly goes back to the ground state by emission of light. If the membrane needed to be probed with another primary antibody, it was incubated for 30-45 minutes in Restore Western Blot Stripping Buffer on a waving platform. Membrane was then blocked again and followed by steps described above.

Western blotting – using Millipore's PVDF membrane Immobilon-FL

If the blots were to be probed with DyLight 680 or DyLight 800 – conjugated secondary antibodies compatible with an Infrared Odyssey scanner system (LI-COR), the Immobilon-FL PVDF membrane was used instead of Hybond-P PVDF membrane and Rockland blocking buffer, diluted 1:2 with TBS was used to block the membrane and to dilute primary antibody. Secondary antibody was diluted in TBST. The membrane was scanned with Odyssey scanner at 700 and 800 nm. Using this Western blotting system allows detection of two different proteins on the same membrane at the same time even if their molecular weights are similar without the need of stripping the membrane. Thus, simultaneous detection of

"housekeeping gene" and protein of interest is possible in contrary to detection of protein with X-ray film. For some antibodies, X-ray film detection was, however, more sensitive.

Anode buffer I:
72.8 g Tris Base (final conc. 300 mM)
400 ml methanol (final conc. 20%)
ad 2 l dH_20

Anode buffer II:
6 g Tris Base (final conc. 25 mM)
400 ml methanol (final conc. 20%)
ad 2 l dH_20

Cathode buffer:
10.4 g aminohexanoic acid (final conc. 40 mM)
400 ml methanol (final conc. 20%)
ad 2 l dH_2O

Washing buffer (TBST):
0.1% Tween 20 in 1x TBS

10x TBS
88 g NaCl (final conc. 1,5 M)
24 g Tris base (200 mM)
Ad 1 l dH_20, set pH to 7.6 with concentrated HCl

1x TBS
8.8 g NaCl (final conc. 150 mM)
2.4 g Tris base (final conc. 20 mM)
Ad 1 l dH_20, set pH to 7.6 with concentrated HCl

5.14 Reverse phase protein arrays (RPPA)

Reverse phase protein arrays (RPPA) were used for detection and quantification of proteins as well as their phosphorylated forms in different MCF10A-derived cell line pools and five ERBB2-positive invasive breast cancer specimen.

Protein isolation

The protein from cell lines/cell line pools was extracted from four biological replicates in a similar manner described for Western Blot analysis. For protein extraction from the tumor specimens frozen samples were homogenized using a bead mill (TissueLyser) and tissue protein extraction reagent (T-PER) supplemented with 1 mM EDTA, 5 mM NaF, 2 µM staurosporine, PhosSTOP Phosphatase Inhibitor Cocktail, and Complete Mini Protease Inhibitor Cocktail. Total protein concentration was determined by BCA assay kit.

Reverse Phase Protein Arrays

The proteins of interest were detected and quantified as previously described by Dr. Johanna Sonntag (PhD Thesis; 2013) and Dr. Frauke Henjes (Oncogenesis; 2012)[323]. In brief:

Prior to spotting, tumor lysates were mixed with 4× SDS sample buffer (10% glycerol, 4% SDS, 10 mM DTT, 125 mM Tris–HCl, pH 6.8) and boiled for 5 min at 95°C. Tumor lysates, lysates from ERBB2-overexpressing cell line pools (both with total protein concentration 2 μg/μl) and dilution series of ERBB2-C cell line pool serving as a control were spotted as technical triplicates on identical subarrays on nitrocellulose-coated glass slides (Oncyte Avid) using a contact spotter (Aushon BioSystems). Slides were blocked with Rockland blocking buffer for fluorescent applications in TBS (50%, v/v) containing 5 mM NaF and 1 mM Na_3VO_4 for 2 h at RT, prior to incubation with target-specific primary antibodies at 4°C over night. Primary antibodies (*n* = 69, for the list of antibodies used in RPPA see "Materials") were selected to recognize proteins involved in migration/invasion/cytoskeleton regulation as well as the most important proteins and their phosphorylated forms involved in ERBB2 signaling regulating the above mentioned cellular processes, with a special focus on breast cancer biology. Only highly target-specific antibodies were used and their validation was carried out using previously described method in our laboratory.[324] Detection of primary antibodies was done with Alexa Fluor 680 F(ab')2 fragments of goat anti-mouse IgG or anti-rabbit IgG in 1:8000 dilution. In addition, to be able to compare particular protein levels across sample set, representative slides were stained for total protein quantification using the protein dye Fast Green FCF as described before.[325] Images of the slides were obtained using an excitation wavelength of 685 nm and at a resolution of 21 μm using the Odyssey Infrared Imaging System (LI-COR). Signal intensities of each individual spot were quantified using GenePixPro 5.0 software. Data preprocessing and quality control were performed with the R-package RPPanalyzer.[326]

5.15 Quantitative real time PCR (qRT-PCR)

For RNA quantification qRT-PCR method was used. In this method, RNA is first reverse transcribed into cDNA and then real time polymerase chain reaction is performed using cDNA as a template. Abi Prism 7900HT Sequence Detection System was used to perform sequence amplification and fluorescent signal detection.

5.15.1 qRT-PCR for protein-coding genes

RNA isolation and reverse transcription

150000-250000 cells were seeded in 6-well plates in biological triplicates. The cells from

single wells were lysed 48 hours after transfection (or after cell seeding). RNA was isolated according to manufacturer's instructions using Qiagen's RNeasy Mini Kit or miRNeasy Mini Kit if also miRNA expression was going to be analyzed from the same samples. Elution was done with 40 µl of nuclease-free water. For reverse transcription, RevertAid™H Minus First Strand cDNA Synthesis Kit was used. First, 2 µl (up to 1 µg) of isolated RNA was mixed with 1 µl of oligo dT-primer and 9 µl of water and denatured for 5 minutes at 70^{o}C. Next, 4 µl of 5x reaction buffer, 1 µl of RiboLock ribonuclease inhibitor (20 u/µl), 2 µl of 10 mM dNTPs mix and 1 µl of RevertAid™H Minus M-MuLV reverse transcriptase (200 u/µl) were added to the reaction and incubated as follows: 5min at 37^{o}C, 60 min at 42^{o}C, 10 min at 70^{o}C and 5 min at 4^{o}C.

Quantitative Real time PCR

TaqMan probes from Roche's universal probe library (UPL) were used in qRT-PCR reaction for protein-coding genes to enhance the specificity of amplified DNA detection. These LNA-based probes are 8-9 nucleotides long and are labeled at the 5' end with fluorescein (FAM) and at the 3' end with a quencher dye. The probes are binding to all complementary sequences in the amplified material but are cleaved by Taq polymerase's 5'-3' exonuclease activity only during primer extension. Therefore released fluorescent signal directly corresponds to the amount of DNA accumulated during PCR reaction.

The UPL probes were designed using Roche's web-based ProbeFinder Assay Design Center (http://lifescience.roche.com/shop/CategoryDisplay?catalogId=10001&tab=&identifier=Universal+Probe+Library#tab-3).

The reaction was performed in technical triplicates as follows: cDNA was diluted to 2ng/µl based on RNA concentration used for reverse transcription, then 5 µl (10 ng) of these solution was mixed in a single well of a 384-well plate with 5.5 µl 2x ABgene SYBR Green PCR Master Mix, 0.11 µl forward primer, 0.11 µl reverse primer, 0.11 µl TaqMan probe and 0.17 µl water. Plate was then covered with optical adhesive cover and real time PCR was started:

2 minutes – 50^{o}C

15 minutes – 95^{o}C

15 seconds – 95^{o}C
60 seconds – 60^{o}C
} 45 cycles

Ct (cycle threshold) values obtained were analyzed with the comparative (ΔΔCt) method. In this method it is assumed that the gene of interest and housekeeping genes are amplified with close to 100% efficiency. The fold change in a particular gene expression between the experimental and control sample is estimated by first calculating in both samples the differences between the Ct values obtained for this gene and the average of Ct values obtained for housekeeping genes (ΔCt) and then calculating the differences between ΔCt in experimental and control sample. The fold change equals then $2^{(-\Delta\Delta Ct)}$. As "housekeeping" genes GAPDH, HPRT and TFRC or their combinations were used. For experiments involving miRNA-301a, miR-301b and miR-130b overexpression HPRT gene was not used as its expression was shown to be regulated by these miRNA.

For the list of primers used in qRT-PCR see "Methods".

5.15.2 qRT-PCR for miRNAs

RNA isolation and reverse transcription

RNA was isolated from cells grown in single wells in 6-well plates using miRNeasy Mini Kit according to manufacturer's protocol with elution volume of 40 µl. This kit allows isolation of total RNA with enrichment of miRNAs and RNAs shorter than 200 nucleotides. For detection of miR-301a, miR-301b, miR-130b the Exiqon's Universal cDNA sythesis kit was used, which allows to reverse transcribe all miRNAs in one step. For the reaction 4 µl of RNA diluted with nuclease free water to 5 ng/µl was used and mixed with 4 µl reaction buffer, 2 µl reverse transcriptase enzyme and 10 µl of nuclease-free water. The reaction mix was then incubated for 1 hour at 42^{o}C and then enzyme was heat-inactivated for 5 minutes at 95^{o}C.

Quantitative Real time PCR

For real time PCR reaction to detect miRNAs the following reagents were used per well in 384-well plates: 4 µl of cDNA diluted 1:20 in water, 5 µl Exiqon's SYBR Green Master Mix Universal RT and 1 µl of Exiqon's LNA-enhanced miRNA-specific primer mix. The PCR reaction program was then started:

10 minutes – 95^{o}C

10 seconds – 95^{o}C
60 seconds – 60^{o}C
} 45 cycles

The Ct values were obtained from raw data using SDS software and analyzed as described for protein-coding genes. As “housekeeping” genes SNORD38B and SNORD48 were used.

5.16 Genome-wide mRNA expression profiling and miRNA sequencing

RNA isolation

Total RNA including miRNAs was isolated from 4 biological replicates of either 2D or 3D cell culture using Qiagen’s miRNeasy Mini kit according to manufacturer’s protocol. In case of isolation of RNA from 2D culture, cells from 1 well of 6-well plate were applied per one RNeasy Mini spin column and eluted with 40 µl of nuclease free water. For 3D culture cells from 4 wells of 8-well glass bottom culture slides were used and then during the RNA purification procedure the material from 4 wells was combined on the RNeasy Mini spin column and eluted as one biological replicate with 30 µl of nuclease free water to gather enough material for further steps – whole genome mRNA expression profiling and miRNA sequencing. The concentration and quality of RNA was checked by Genomics and Proteomics Core Facility of DKFZ using Nanodrop ND-1000 and Agilent 2100 Bioanalyzer, respectively. Three biological replicates with verified quality (half of the samples with RIN values 10, the rest in the range of 7.6-9.4) were then submitted for whole genome profiling (800 ng at 80 ng/µl concentration and/or short RNA sequencing (1 µg at >100ng/µl).

Whole genome profiling

Whole genome profiling was done using Illumina’s Sentrix HumanHT-12 v4 Expression BeadChip human array. This array allows analysis of 31000 annotated genes with its ~47000 probes derived mainly from the NCBI RefSeq Release 38 (November 2009). Sample labeling and hybridization was performed by Genomics and Proteomics Core Facility at DKFZ. mRNA profiling from 3D culture of four MCF10A-derived cell line pools was done using 3 technical replicates similarly to mRNA profiling from 2D culture of MCF10A transfected with 4 miRNA mimics (miR-ctrl2, miR-301a, miR-301b and miR-130b). Therefore, in both cases total number of 12 samples were submitted for microarray analysis. This amount of samples could be applied on one HumanHT-12 v4 array because one physical array consists of 12 identical but independent chips. The data obtained was quantile normalized using Chipster "Illumina – lumi” pipeline and differential gene expression between each two conditions was determined.

Whole genome short RNA sequencing

For highthroughput sequencing of short RNAs, i.e. equal or shorter than 50 bp, Illumina HiSeq 2000 was used. The small RNA library was prepared for sequencing using "NEBNext® Multiplex Small RNA Library Prep Set" at Genomics and Proteomics Core Facility of DKFZ. In the course of analysis of raw sequencing results the adaptor sequences were trimmed and sequences mapped to mature miRNA sequences in miRBase (Release 21, June 2014). The differential expression analysis of miRNAs between each two cell line pools was performed using a DEseq program. This tool has a "normalization by variance stabilization" step built-in. For calculation of the miRNAs' expression fold changes, the mean of three replicates was used. P-values were adjusted using Benjamini-Hochberg method to control the false discovery rate. Those miRNAs for which the differential expression between at least two different cell line pools was significant were then clustered together - the log(fold change) values were used - and the heatmap was made using "heatmap.2" function in R.

5.17 miRNA target prediction

For miRNA target prediction as the main target prediction softwares TargetScan 6.2 and miRanda were used.

5.18 Analysis of patients' data

All datasets used were microarray datasets. For determination of the effect of ERBB2 and particular miRNAs on patients' survival METABRIC validation dataset, encompassing mRNA and miRNA expression data from the same tumor samples for close to 1000 breast cancer patients was used. This dataset was also used to correlate miRNAs' expression with ERBB2 level, estrogen receptor and p53 status. Two additional, smaller publically available breast cancer patients' datasets were obtained from NCBI GEO database (GSE19783 and GSE22220) and were used to correlate all miRNAs' expression levels with ERBB2. The Cancer Genome Atlas (TCGA) dataset encompassing over 500 samples from breast cancer patients and healthy controls was used to determine the expression of miRNAs in tumors versus normal patients and to verify whether the particular miRNAs are expressed *in vivo*. All of these datasets consist of whole genome transcriptome and miRNA profiling, which allows to analyze mRNA/miRNA relations.

Correlations of miRNAs' expression levels with ERBB2 expression levels in GSE2220, GSE19783 and METABRIC datasets

The data collected from GEO platform were processed data. GSE19783 data were log2-transformed and quantile normalized using R package *limma*. GSE2220 data were first print-tip loess normalized and then quantile adjusted to adjust for the differing scale of measurements across arrays. The correlation coefficients between levels of all miRNAs vs. ERBB2 mRNA for both datasets were calculated using R function "cor.test" with Pearson's method which gave as an output the list of correlation values along with their respective p-values. The miRNAs profiled on each individual microarray were then arranged from highest to lowest correlation coefficient. Correlations of expression levels of individual miRNAs with ERBB2 expression levels in METABRIC dataset was done with Pearson method as well.

Survival analysis using METABRIC dataset

The METABRIC expression dataset was already pre-processed and quantile normalized using *limma* package in R. An R script was generated to extract the patients having an ERBB2 status IHC3+ from the clinical dataset. Median/quantiles of ERBB2 expression in these subset of patients were calculated using R to classify the patients into two groups: with higher or lower ERBB2 expression than the median/quantile. Survival times of these patients were retrieved by using "Surv" function from *survival* package in R. To test the difference between the two survival curves, "survdiff" function from R package *survival* was used. The survival object returned a chisq value with the degree of freedom. P-value was calculated by using the function in R: 1-pchisq(test statistic, df). To determine effect of miRNA expression levels on patients' survival, the patients were divided into two groups according to their miRNA expression levels and Kaplan-Meier curves were plotted (Q1-Q2 vs. Q3-Q4, or alternatively Q1 vs Q4). Further analyses were preformed as described above.

miRNAs' expression levels in ERBB2-positive and ERBB2-negative, ER-positive and ER-negative, as well as p53-wild type and p53-mutated patients in METABRIC or TCGA datasets

Patients in the METABRIC validation dataset (995 patients) were divided based on their ERBB2, ER or p53 statuses into two groups, i.e. ERBB2-positive and ERBB2-negative or

ER-positive and ER-negative or p53-wild type and p53-mutated. A short R-script was written to perform the comparison of each miRNA expression levels between the indicated two groups and generate p-value to test the significance of the comparison. The p-values were calculated using pchisq function mentioned in the previous section. Boxplot for each miRNA was created using "boxplot" function in R. miRNA expression levels were determined in the TCGA dataset in ER-positive and ER-negative patients in a similar manner. To determine miRNA expression levels in patients with different ERBB2 statuses, patients were divided according to their ERBB2-status into four groups: Null, IHC1+, IHC2+ and IHC3+.

miRNAs' expression levels in tumors vs. normal tissues in TCGA dataset

Patients in the TCGA clinical data were separated based on their barcodes and their miRNAs' expression values were retrieved from the expression dataset. The expression data were pre-processed and normalized prior to use from the TCGA consortium. The patients were divided into "Tumor" and "Normal" groups. Comparison between these two groups were performed using t.test. P-values for each miRNA group of normal vs. tumor were collected from the t.test. Boxplot for each miRNA was created using "boxplot" function in R.

5.19 Mouse model

32 female 7-week-old NSG mice, bred in the animal facility of the German Cancer Research Center, Heidelberg, were maintained at a 12 h light–dark cycle with unrestricted diet and water. Animal handling and experimentation was done in accordance with GV-Solas guidelines and approval by regional regulatory authorities (Regierungspräsidium Karlsruhe, reference number G193/10). NSG mice were used for subcutaneous injection of cells (n = 5 mice/group). Mycoplasma-free MCF10A-ERBB2 cell line pools and MCF10A control cells were detached from culture dishes using trypsin/EDTA, washed twice with PBS and resuspended in PBS. Under isoflurane anesthesia (1–1.5 % in O_2, 0.5 l/min), 5×10^6 cells suspended in 100 µl PBS/Matrigel (v/v) were injected subcutaneously into both flanks, each. Growth of subcutaneous xenografts was monitored each week. Mice were sacrificed and lungs were dissected and partially snap-frozen in liquid nitrogen for RNA isolation. For histological and immunohistochemical analysis, lung was embedded in TissueTek OCT compound and frozen in isopentane that had been precooled in liquid nitrogen.

6. Results

6.1 Part I: Very high ERBB2 level as a sole sufficient factor required for invasive growth of non-tumorigenic mammary cell line in vitro

6.1.1 Very high ERRB2 mRNA levels in ERBB2+ breast cancer patients correlate with worse overall survival compared to ERBB2+ patients with moderate ERBB2 levels

As the previously reported studies (see chapter 3.2.5 in "Introduction") indicated the wide range of the ERBB2 receptor levels either on DNA or protein level, I first wanted to determine if the range of ERBB2 mRNA levels detected in patients is also broad and if it is associated with the patients' survival. For the analysis I used the data from the METABRIC study which is currently the biggest gene expression study of breast tumors and consists of discovery and validation datasets from 997 and 995 tumors, respectively.[327] None of the patients involved had been treated with trastuzumab, since enrollment into the study had been prior to introduction/FDA approval of trastuzumab, and therefore ERBB2 levels in tumors should not be affected. The expression range for ERBB2 at the mRNA level was indeed broad in the validation set (6.37-14.46 a.u. on the $\log_2$ scale) and patients with the highest ERBB2 levels expressed almost 16 times higher receptor levels than the median (10.53 a.u.)(Figure 12a).

A similar range of ERBB2 mRNA levels was observed in several other independent breast cancer datasets, e.g. GSE7390, GSE1456 or GSE3493 (data not shown).[328,329,48] ERBB2 transcript levels slightly increased with the tumor grade, however a significant difference was observed only between grades 1 and 3 (p=0.0255) (Figure 12b). This result suggests that ERBB2 mRNA measurement cannot well predict the histological grade. As expected, and previously reported, mRNA levels were correlated with the protein levels measured by immunohistochemistry (Figure 12c).[330,331] The subdivision of patients according to their IHC status, however, was not sufficient to distinguish between better and worse survivers (Figure 12d).

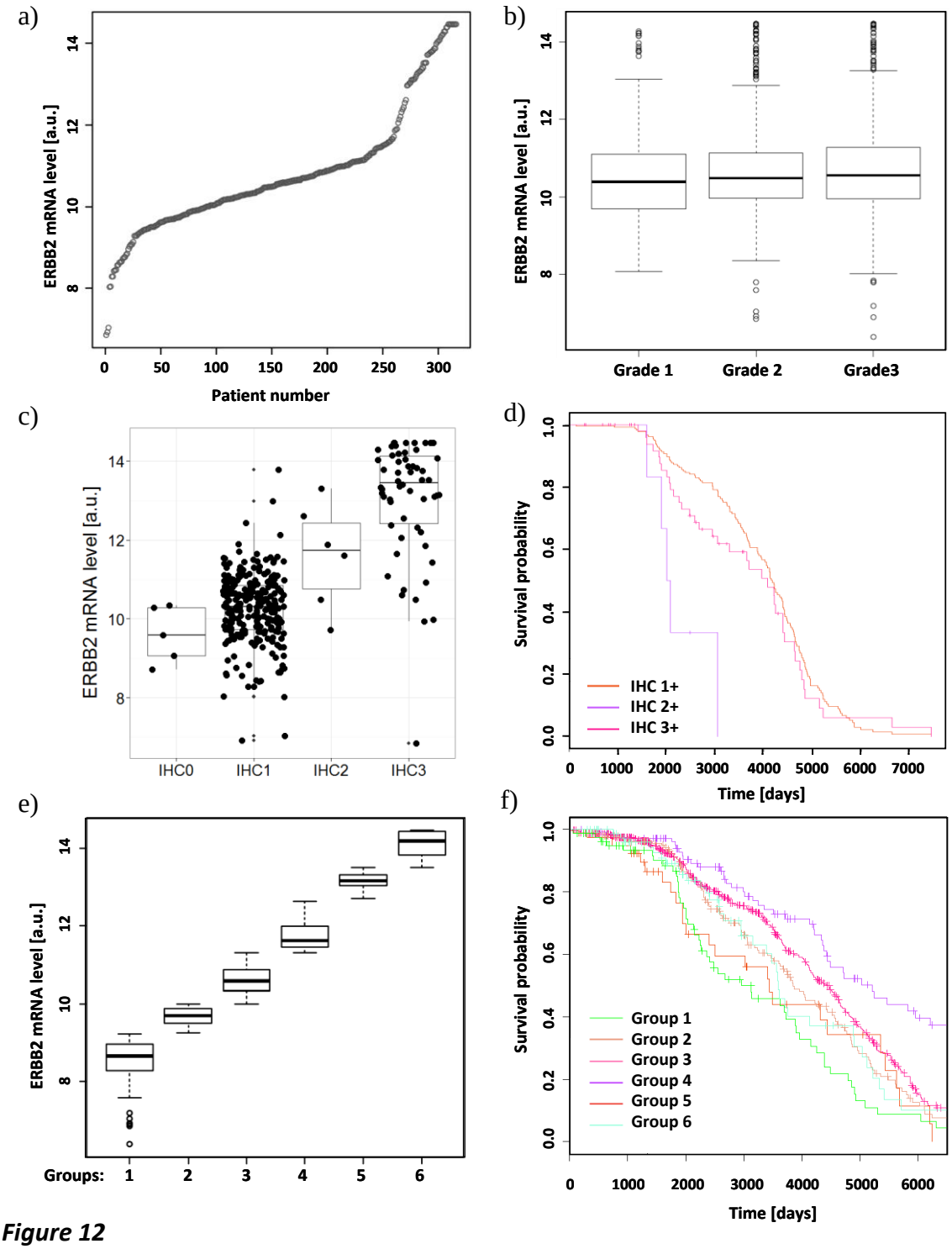

Figure 12

ERBB2 mRNA expression levels (log2 scale) in patients of METABRIC validation dataset and their association with tumor grade, IHC status and patients' survival. a) ERBB2 mRNA levels in 995 patients. b) ERBB2 mRNA levels in 995 tumors categorized as grade 1 (n=98), grade 2 (n=360) and grade 3 (n=447). c) ERBB2 mRNA levels in patients with immunhistochemically determined ERBB2 expression statuses: IHC0 (n=5), IHC1+ (n=252), IHC2+ (n=6), IHC3+ (n=58). d) Survival probability of patients subdivided into 3 groups based on their ERBB2 IHC statuses. e) Arbitrary division of patients into 6 groups based on their ERBB2 mRNA expression levels: group 1 (n=81, range 0-9.25 [a.u.]), group 2 (n=196, range 9.25-10 [a.u.]), group 3 (n=487, range 10-11.3 [a.u.]), group 4 (n=109, range 11.3-12.7 [a.u.]), group 5 (n=39, range 12.7-13.5 [a.u.]), group 6 (n=83, range 13.5-14.5 [a.u.]). f) Survival probability of patients in groups 1-6.

Interestingly, when patients were arbitrarily divided into six groups based on their ERBB2 mRNA expression patterns (Figure 12a), the survival length initially gradually increased with elevated ERBB2 levels until group 4 (expression range 11.3-12.7) and then suddenly decreased for groups 5 and 6 (Figures 12e and 12f). This suggests that patients with low/moderate level of ERBB2 mRNA survive better than those with very high ERBB2 and patients with ERBB2-negative tumors.

Although the correlation of mRNA with IHC status was in general good, the ERBB2-positive patients (with IHC3+ status) showed high mRNA level variation. I wanted to see if this variation leads to different outcomes of ERBB2-overexpressing patients. To assess the effect of ERBB2 mRNA level on patients' overall survival, the ERBB2-positive patients in either validation or discovery datasets of METABRIC study were first divided into two groups: expressing higher or lower ERBB2 mRNA levels than median (Figures 13a and 13b), or belonging to 25% or 75% quantile (figures 13c and 13d) and then Kaplan-Meier curves were plotted. The median and quantiles were calculated only for ERBB2-positive patients. High/very high ERBB2 mRNA levels were associated with worse overall survival than moderate levels in the validation dataset ($p = 0.0495$ and $p = 0.0179$ for median or quantile division of patients, respectively). In the discovery dataset this association was not significant ($p = 0.377$ and $p = 0.214$). Whereas the metaanalysis using BreastMark algorithm showed no significant difference in patients' overall survival for patients with higher or lower mRNA levels in ERBB2 overexpressing breast cancer subtype (as classified by PAM50), the disease-free survival in the patients with higher ERBB2 mRNA levels was decreased, however, this effect did not reach statistical significance ($p = 0.0569$) (Figure 13e).

Altogether, this and the previous analyses show that ERBB2 levels vary greatly in ERBB2-overexpressing patients at DNA, mRNA and protein levels. Additionally, data obtained from the METABRIC study show that, within IHC3+ classified patients, further quantitative stratification of the patients according to their ERBB2 expression levels may have additional predictive value - better survival for the patients with moderate ERBB2 levels and worse survival for the patients with high/very high ERBB2 levels.

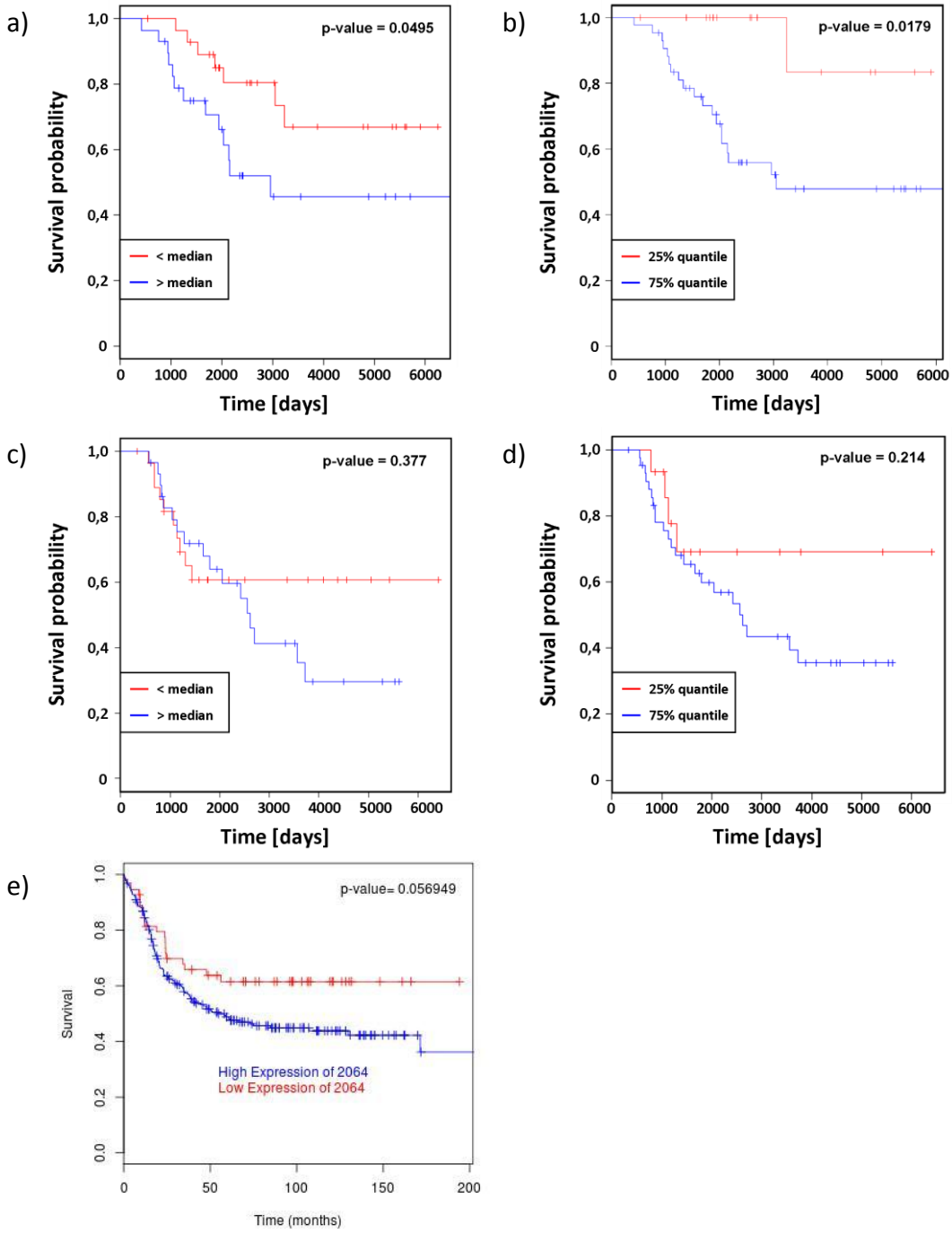

Figure 13

Kaplan-Meier curves showing overall survival probability of only ERBB2-positive patients (determined by IHC3+ status), depending on their ERBB2 mRNA expression levels in validation dataset, n=58 (a, b), or discovery dataset, n=63 (c, d) in METABRIC study. Patients were divided into two groups based on their ERBB2 mRNA expression level – higher or lower than median (a, c) or belonging to 25% or 75% quantiles (b, d). e) Disease-free survival of patients with higher or lower than median ERBB2 mRNA levels in ERBB2-overexpressing breast cancer subtype (determined by PAM50 classification), using BreastMark algorithm.[332] *n= 275, number of events=135.*

6.1.2 Construction of ERBB2-overexpressing cell line pools

To investigate how different ERBB2 levels affect cellular phenotypes, I derived four stable cell line pools from the stably transfected MCF10A cell line expressing different levels of ERBB2 receptor (for details see chapter 5.1 in "Methods"). MCF10A cell line is a non-transformed, immortalized epithelial breast cell line, which expresses low EGFR and ERBB3 levels, and no ERBB2 or ERBB4.[333] It is therefore suitable for ERBB2 overexpression studies as the basal level of ERBB-family signaling in this cell line is relatively low. Moreover, the MCF10A cell line has been shown to form hollow, acinus-like structures when grown in 3D cultures, resembling the formation of a duct in the normal breast. This particular feature of this cell line had been extensively exploited by several researchers in the past and several systems for growing MCF10A in 3D cultures have since been developed.

I designed the system in such a way that all ERBB2-overexpressing stable cell line pools expressed, apart from the ERBB2 receptor, also the enhanced green fluorescent protein (EGFP) as a non-fusion protein. EGFP was encoded by the same construct that carried ERBB2-coding sequence and thus the integration of both genes into the MCF10A genome occurred simultaneously. This allowed me to separate pools of cells with different ERBB2 levels via detection of green fluorescence during FACS sorting (Figure 14a). The choice of the EGFP intensity thresholds for selection of different ERBB2-overexpressing pools was arbitrary. A control cell line pool expressed just EGFP. The cell line pools which I obtained and expanded are listed below:

Control cell line pool:

MCF10A-EGFP (further called "CTRL")

ERBB2-overexpressing pools:

MCF10A-ERBB2-EGFP-A (further called "ERBB2-A")
MCF10A-ERBB2-EGFP-B (further called "ERBB2-B")
MCF10A-ERBB2-EGFP-C (further called "ERBB2-C")

EGFP level
ERBB2 level

In the next step, I checked if the ERBB2 protein is indeed expressed at increasing levels in these pools using enzyme-linked immunosorbent assay (Figure 14b). The ERBB2 levels increased in the following manner: CTRL-A < ERBB2-A < ERBB2-B <= ERBB2–C and did not change substantially during the culturing of cells for up to at least 8 passages (data not

shown). ERBB2 localized to the cell membrane in case of all ERBB2-overexpressing cell line pools (Figure 14c). Interestingly, basal ERBB2 levels were also detectable in the cytoplasmic compartment of two cell line pools with higher ERBB2 levels. This could be due to the increased endosomal-driven receptor internalization/recycling.[81] Since ERBB2-B and ERBB2-C cell line pools had similar, but not identical ERBB2 protein levels, they were further considered as non-perfect biological cell line pool replicates, bearing very high ERBB2 levels.

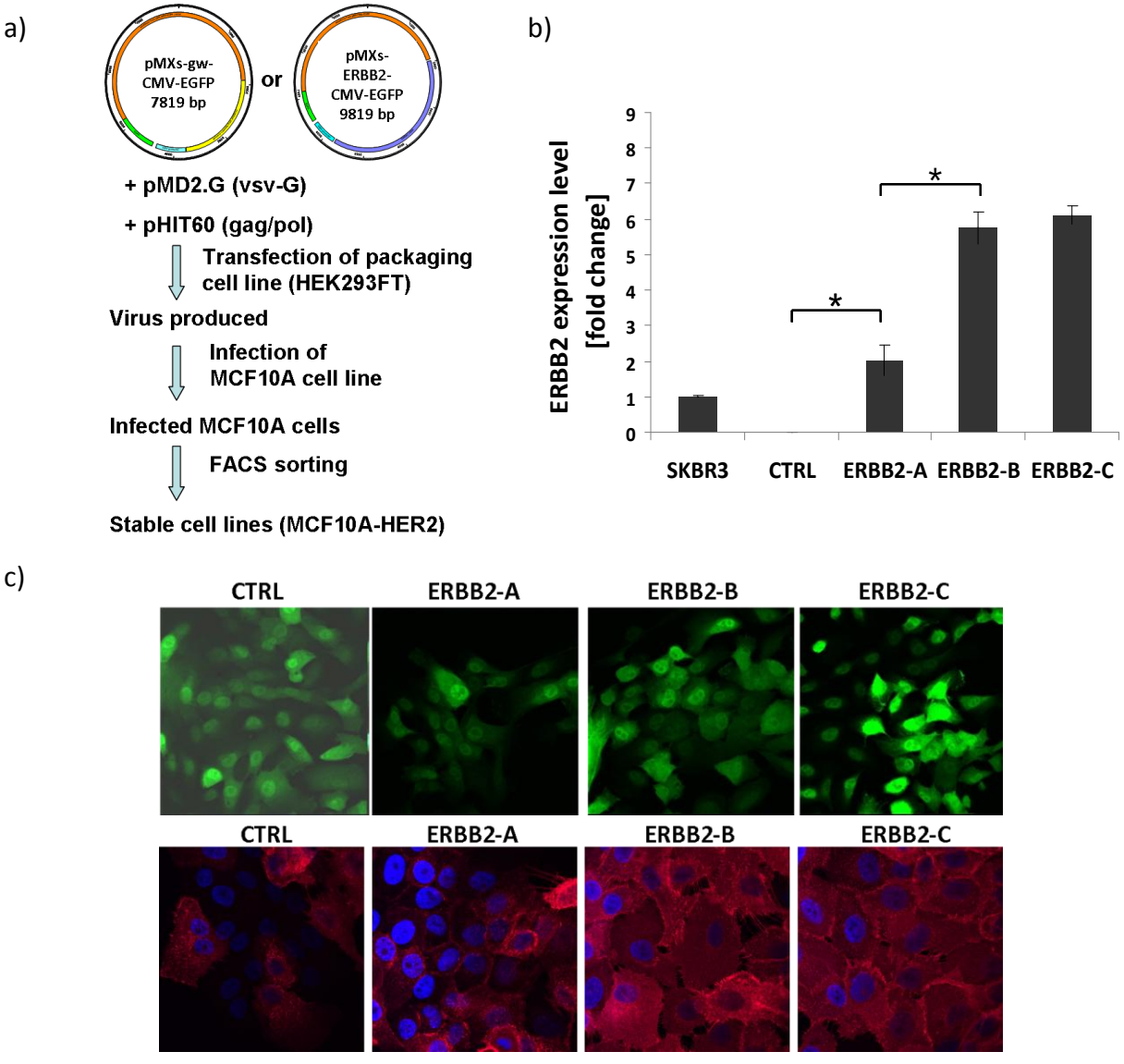

Figure 14

*Construction of stable cell line pools. a) Stable pools production outline. b) ERBB2 protein levels in CTRL, ERBB2-A, -B and -C cell line pools were determined by ELISA and normalized to ERBB2 level in SKBR3 cell line. Two biological replicates were used. *p<0.05. c) ERBB2-overexpressing cell pools were grown on glas slides for 2 days and then stained for ERBB2 as described in Methods (chapter 5.6). Note, that increasing intensity of EGFP corresponds to increasing ERBB2 protein level. CTRL cell line pool is shown as an ERBB2-negative control.*

To assess the relative ERBB2 overexpression levels in the ERBB2-A, ERBB2-B and ERBB2-C cell line pools, I quantified ERBB2 protein levels with ELISA taking the well-characterized ERBB2-overexpressing cell line SKBR3, carrying ~10^6 receptor molecules per cell, as a reference (Figure 14b).[334] ERBB2-A showed ~2 fold and ERBB2-B/ERBB2-C cell line pools 5-6 fold higher receptor expression level than the SKBR3 cell line, which would be then estimated to a number of 2x10^6 and 5-6x10^6 receptor molecules per cell, respectively. SKBR3 had also previously been shown to carry 10-fold more ERBB2 gene copies than MCF7 (carrying two ERBB2 copies)[335], whereas the cell line with one of the highest ERBB2 copy number, HCC1954, have been shown to carry ~55-80 fold more copy numbers (number depended on whether sequencing method or RT-PCR had been used for quantification) than control cells[336, 337]. Taking to account that ERBB2 protein levels correlate quite well with ERBB2 copy numbers in breast tumors (r= 0.52)[338], the levels found in ERBB2-B and -C cell line pools are expected to be in the range found in established breast cancer cell lines.

To relate the ERBB2 levels in constructed cell line pools to the levels detected in patients, the total ERBB2 protein level in each cell line pool and in 5 ERBB2-overexpressing patients was measured using reverse phase protein arrays (RPPA). Tumors from patients 1, 2, 3 and 5 showed in the routine clinical ERBB2 tests the strong positive staining for ERBB2 (IHC3+) whereas tumor from patient 4 showed moderate (IHC2+) staining and FISH-positivity. The majority of breast tumor specimen staining IHC3+ express more than 10^6 receptor molecules per cell.[334]

RPPA is a method which allows relative measurement of a given protein amount across larger sample sets in a quantitative manner. ERBB2 levels detected in the samples were normalized to the total protein amounts spotted on the array (for details see “Methods”, chapter 5.14). To be able to compare ERBB2 levels between the samples, a serial dilution of protein lysates from ERBB2-C cell line pool was spotted on the protein array as well. As ERBB2 gave a signal that was near-linear (with the lowest dilution giving signal close to 0; Supplementary Figure 1), the differences between ERBB2 signal for the inspected samples could be understood as expression fold changes, i.e. in a sample with a signal of 6000 there would be 10 times more ERBB2 than with sample of signal 600.

RPPA readout indicated ERBB2 levels in patients 2, 3 and 4 similar to those found in the CTRL cell line, and in patients 1 and 5 similar to those in ERBB2-A (Figure 15). The true ERBB2 levels in the tumors examined are usually, however, substantially higher than detected by

RPPA, which can explain the apparent low ERBB2 levels in patients 2, 3 and 4. Given that up to 30% of protein lysates from patients' samples originate from the surrounding stroma and that tumors were classified as ERBB2-positive if at least 30% of the cells in the invasive part of the tumor expressed ERBB2, the actual ERBB2 levels in the ERBB2-postitive cells could be in fact even up to ~5 times higher than detected (21% of protein lysate). I concluded therefore that ERBB2 protein levels found in all cell line pools are likely to be in the physiological range.

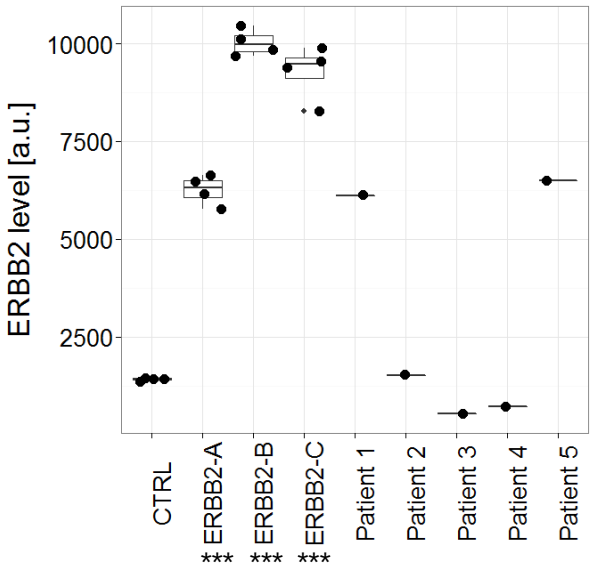

Figure 15
Comparison of ERBB2 protein levels in four MCF10A-derived cell line pools and in five samples from ERBB2-overexpressing breast cancer patients. For each cell line pool 4 biological and 3 technical and for patients' samples 3 technical replicates were used. Means for each technical replicate are shown as black dots, and the horizontal bars represent the means of all biological replicates.The y-axes shows the RPPA intensity measured in arbitrary units.

6.1.3 Characterization of ERBB2-overexpressing cell line pools in 2D culture

To characterize obtained CTRL and ERBB2-overexpressing cell line pools, I first examined cellular morphology, proliferation, viability, and signaling activation in 2D culture. I observed that, whereas MCF10A and CTRL cell line pool formed clearly visible cell clusters when grown on plastic dishes in full growth medium, all three ERBB2-overexpressing cell line pools did not (Figure 16a). In ERBB2-expressing pools, cell-cell connections were weaker than in CTRL cells, which lead to cell scattering. When the cells were grown in steady state (full growth

medium, containing EGF), phosphorylation of major autophosphorylation sites of ERBB2 (Y1248)[339] and EGFR (Y1068)[340] was ERBB2-level dependent, which indicates co-activation of both receptors resulting from ERBB2 overexpression. Total EGFR receptor levels were also increased, confirming previously reported ERBB2 stabilization effects on EGFR (Figure 16b).[341] Cell viability, although not strongly affected, increased steadily and significantly in ERBB2-dependent manner as well (Figure 16c).

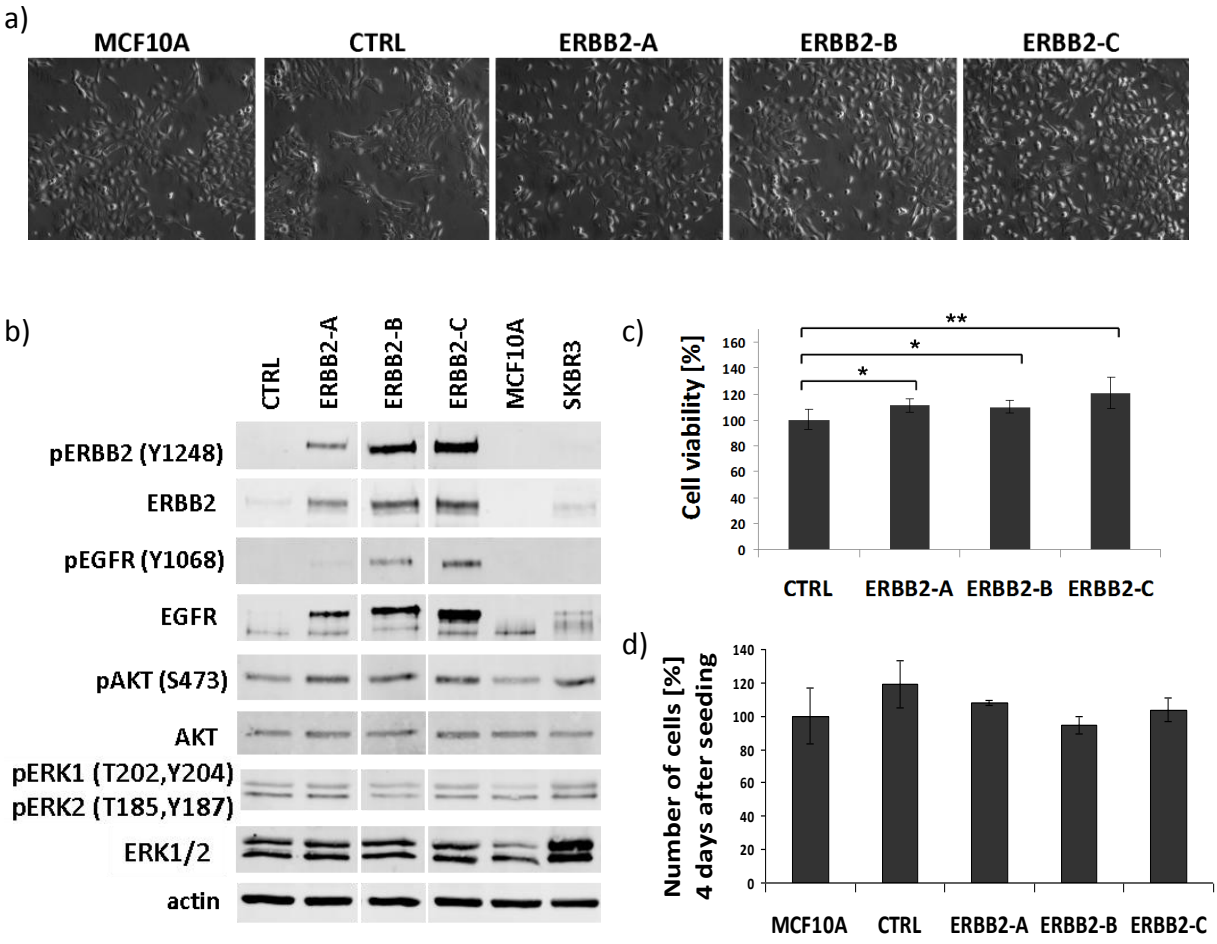

Figure 16

Characterization of stable cell line pools (2D culture). a) Morphology of cell line pools grown on plastic culture dishes in MCF10A full growth medium. Note that clusters of cells are present in normal MCF10A and CTRL but not in ERBB2-overexpressing cell line pools. b) Western blot analysis of cell line pools in comparison to MCF10A and SKBR3 cell lines. The names of cell lines and detected (phospho-) proteins are indicated. Note that protein lysates from all the cell lines were run on the same gel and the order of samples was rearranged post-detection for the figure clarity. c) Cell viability was measured 2 days after cell seeding as an absorbance of formazan in a colorimetric assay 2.5 hours after WST1 addition to all cell line pools and compared to CTRL cells. One asterisk (*) denotes a p-value of <0.05, two (**) denote p<0.01, and three (***) denote p<0.001, determined by a two-sided t-test. d) Direct cell counting analysis of cell proliferation in stable cell line pools after 4 days since equal number of cells were seeded. MCF10A served as a reference.

While the activating phosphorylation of AKT kinase at serine S473 was moderately elevated in ERBB2-overexpressing cell line pools, phosphorylation of ERK1 (T202/Y204) & ERK2 (T185/Y187) was similar to CTRL. This was reflected by a lack of significant changes in cell proliferation in two-dimensional cell culture (Figure 16d). In comparison with the SKBR3 cell line, ERBB2 and EGFR activation was higher in all ERBB2-overexpressing pools, however pAKT and pERK1/2 levels were comparable (Figure 16b).

Similar to proliferation, migration abilities of the ERBB2-overexpressing cells did not change in the absence of EGF as measured by wound-healing assay in assay medium containing reduced serum levels (2%) and no EGF (Figure 17a and 17b). Slight reduction in migration rates were even observed for the cell line pool with the highest ERBB2 level when migration was measured using real time cell analyzer (see "Methods", chapter 5.8) in the same medium but with 5% serum used as a chemoattractant (Figure 17c). As EGF enhances the migration of normal MCF10A cells, depletion of EGF from the medium assured me that the potentially observed changes in migration rate would have been induced by ERBB2 itself and not by EGF-EGFR/ERBB2 axes.

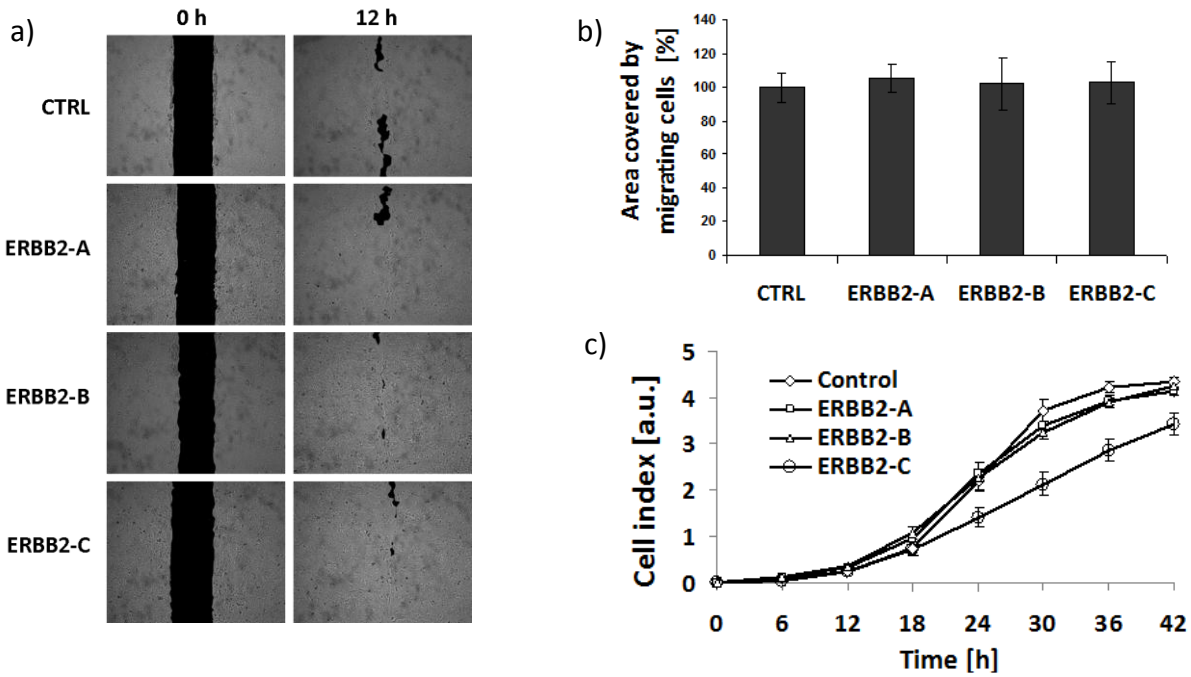

Figure 17

Migration of stable cell line pools. a) Wound healing assay in MCF10A assay medium. Representative pictures of 6 biological replicates are shown at 0 h and 12 h time points. b) Quantification of area covered by migrating cells in wound healing assay (a). c) Cell migration index was measured using RTCA. 5% serum was used as a chemoattractant. 4 biological replicates were used.

6.1.4 ERBB2 overexpression causes a dose-dependent invasive phenotype in cell line pools grown in 3D culture

To determine whether the three-dimensional context is required for ERBB2-driven cell proliferation and invasion observed in patients and having been reported in previous studies, I grew the four stable cell line pools in Matrigel for 9 days with four different EGF concentrations: 0, 1, 5 and 20 ng/ml (see "Methods", chapter 5.2). This concentration range was chosen based on the observation that growth of normal MCF10A in Matrigel is strictly dependent on EGF within this range and that 5 ng/ml EGF had proven to be the optimal growth condition for obtaining acinis with hollow lumen. While extra addition of EGF to the medium resulted in partially filled acini structures and slight increase in their volume, further EGF supplementation beyond 10 ng/ml did not have additional effect on spheroid sizes or lumen filling (Figure 18a). To ensure that saturation had been reached for the growth in Matrigel, I thus used 20 ng/ml EGF as the highest EGF concentration instead of 10 ng/ml.

Whereas all ERBB2-cell line pools showed much higher proliferation rates in 3D culture than CTRL cells, ERBB2-B and -C expressing very high ERBB2 levels formed much bigger and less acini-like structures than the one expressing moderate ERBB2 levels (ERBB2-A) (Figure 18b). These phenotypes were observed even in the absence of EGF which is normally required for growth of MCF10A cells. Additionally, the ERBB2-A cell line pool seemed much more responsive to EGF concentrations than the ERBB2-B and -C pools. Quantification of the structure sizes at close-to-normal (5 ng/ml) EGF concentration showed that all control spheroids were up to 100 µm in diameter with an average of 65.7 µm. ERBB2-A structures were on average 92.4 µm big and 66.3% of them had a diameter of between 100 µm and 200 µm. ERBB2-B/C structures were largest with 20% of the structures reaching sizes over 200 µm (Figure 18c).

To see whethere there are any additional morphological differences between cell line pools with different ERBB2 levels, like e.g. the presence or absence of hollow lumens within the structures, I observed the individual structures using confocal microscopy. As anticipated, in the control spheroids the expected lumens formed when cells were grown with 5 or 20 ng/ml of EGF. Similar to normal MCF10A (Figure 18a), EGF concentrations lower than 5 ng/ml EGF did not allow the control cells to form spheroids as cell proliferation was very low and the structures consisted of maximally 1-10 cells.

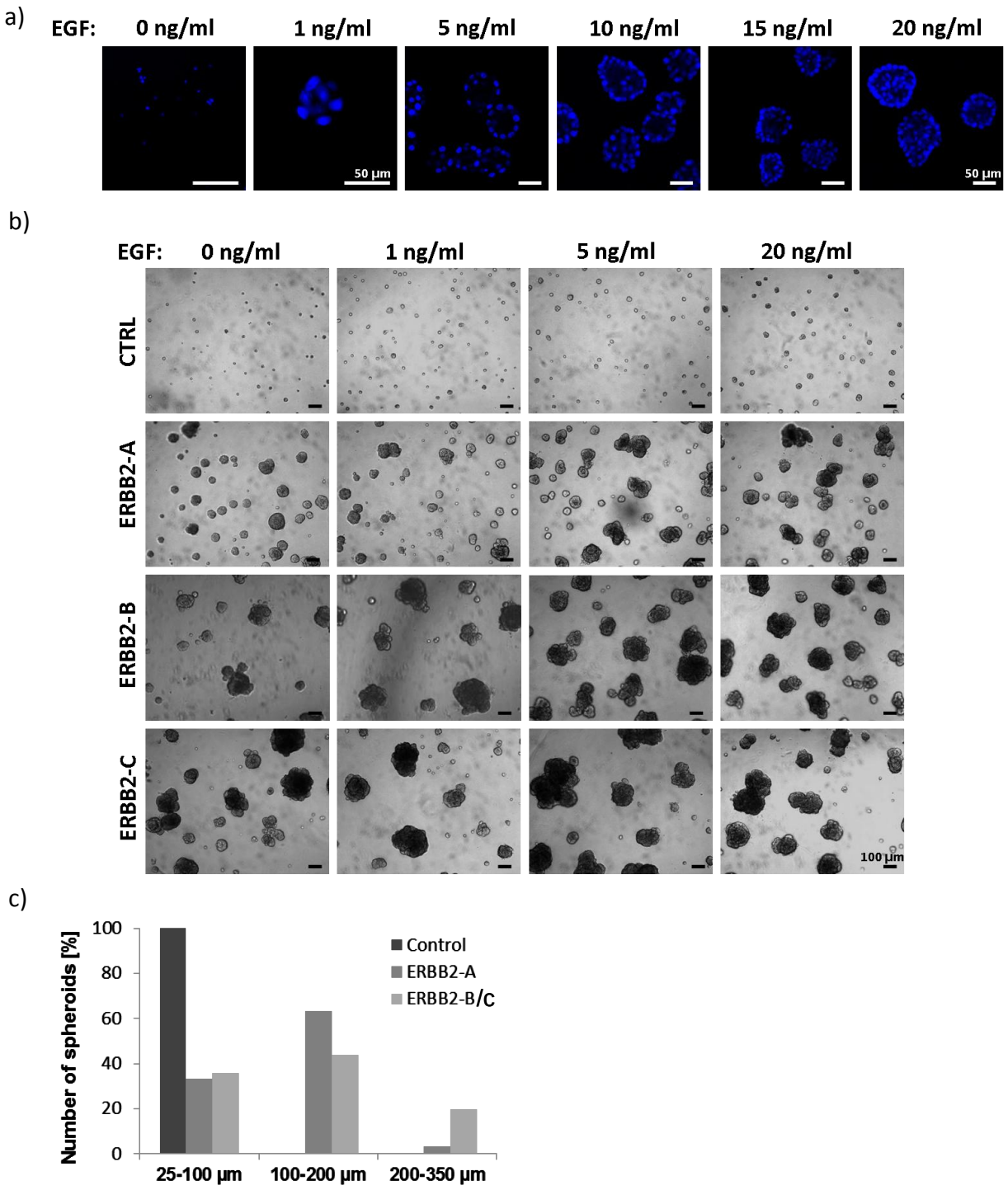

Figure 18

The growth of stable cell line pools, seeded as a single cell suspension in three-dimensional culture. a) MCF10A cells were grown for 9 days in Matrigel in assay mediumwith indicated concentrations of EGF and then the nuclei were stained with DAPI. Scale bars represent 50 µm. b) CTRL, ERBB2-A, -B and -C cell line pools were grown for 9 days in Matrigel in assay medium with indicated concentrations of EGF. Photographs were taken with a white-field microscope. Scale bars represent 100 µm. c) The sizes of 25-37 structures for each stable cell line pool were measured and the % of them falling into indicated size categories are shown. ERBB2-B and -C due to the smaller amount of structures were counted together.

In contrast, ERBB2-overexpressing cell line pools formed large multicellular clumps of cells that did not contain hollow lumens, irrespective of the presence or absence of EGF (Figure 19). Interestingly, structures formed by ERBB2-B and -C cells were not only much larger than those formed by ERBB2-A but also their surface was much more rough and irregular. As ERBB2-positive patients with very high ERBB2 levels are associated with worse overall survival, I hypothesized that the rough surface could be the sign of increased invasive properties of these cells.

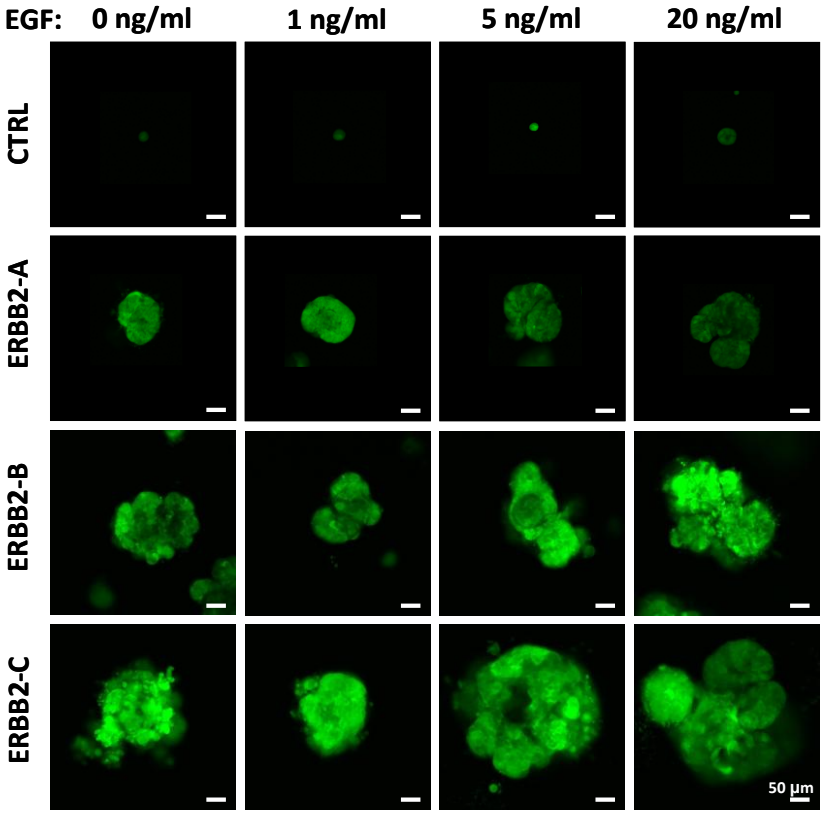

Figure 19
Stable cell line pools overexpressing increasing ERBB2 levels (Control-A < ERBB2-A < ERBB2-B < ERBB2-C) were grown in 3D culture for 9 days in the assay medium containing different amounts of EGF: 0, 1, 5, 20 ng/ml. Pictures were made using confocal microscope. Scale bar represents 50 µm.

The invasive properties of the cell line pools were confirmed in two independent assays. First I performed an invasion assay using matrigel-covered Boyden chambers which allow the measurement of the number of invaded cells at the chosen end time point – here 72 hours (Figures 20a and b). I could confirm that cell invasion was strictly ERBB2-level dependent and that the cell line pool expressing ERBB2 at the highest level had also the strongest invasive

properties (Figure 20a). Recently, it has been shown that overexpression of ERBB2 alone is not sufficient to trigger cell invasion and that additional presence of EGF or overexpression of ERBB3 is required.[342, 343] Indeed, the ERBB2-A cell line pool displayed increased invasiveness in an EGF-dependent manner. However, the ERBB2-B and -C cells were not much responsive to EGF presence and intrinsicly showed higher invasion levels.

In a second approach to study cell invasion I used a real time cell analyzer (RTCA), which allows the measurement of cell invasion in real time (see "Methods", chapter 5.9). As a chemoattractant either EGF (Figure 20c) or serum (Figure 20d) was used. In both cases I could show that two cell line pools expressing higher ERBB2 levels are much more invasive in comparison to cell line pool expressing moderate ERBB2 levels and control. They were also more invasive in the presence of serum than in the presence of EGF. I speculated that, on the one hand, this could be due to the fact that ERBB-signaling in these cell line pools is constitutively activated and addition of EGF does not cause further increase in signaling. On the other hand, serum can activate cell invasion through other pathways and therefore show an additional effect on already invasive ERBB2-B and -C cell line pools.

It is known, that ERBB2 exerts its function mostly via two signaling pathways, AKT and MAPK. As the cells composing the inner part of acini structures in 3D culture have reduced access to nutrients, like serum and EGF, I wanted to better understand what happens to these signaling pathways in starvation/EGF-stimulation conditions in cell line pools overexpressing different ERBB2 levels. To this end, I starved the cells for 24 in complete starvation medium (without any additives) in 2D culture and then stimulated them for 0, 15, 45, 75 and 105 minutes with 20 ng/ml EGF. I observed that AKT and ERK phoshorylation was increased even in starvation conditions when the ERBB2 level was very high, however, EGF stimulation could still cause a slight induction of AKT phosphorylation, but not of ERK whose phosphorylation was saturated (Figure 21a).

To check which of these two pathways has a stronger effect on invasive properties of cells, I incubated ERBB2-C cells with either U0126 or LY294002 inhibitors which block MEK and PI3K, respectively, in 3D culture starting from the second day on. Both inhibitors as well as lapatinib, which was used as a positive control blocking the tyrosine kinase domains of ERBB2 and EGFR, completely abrogated the growth of cells in 3D culture (Figure 21b).

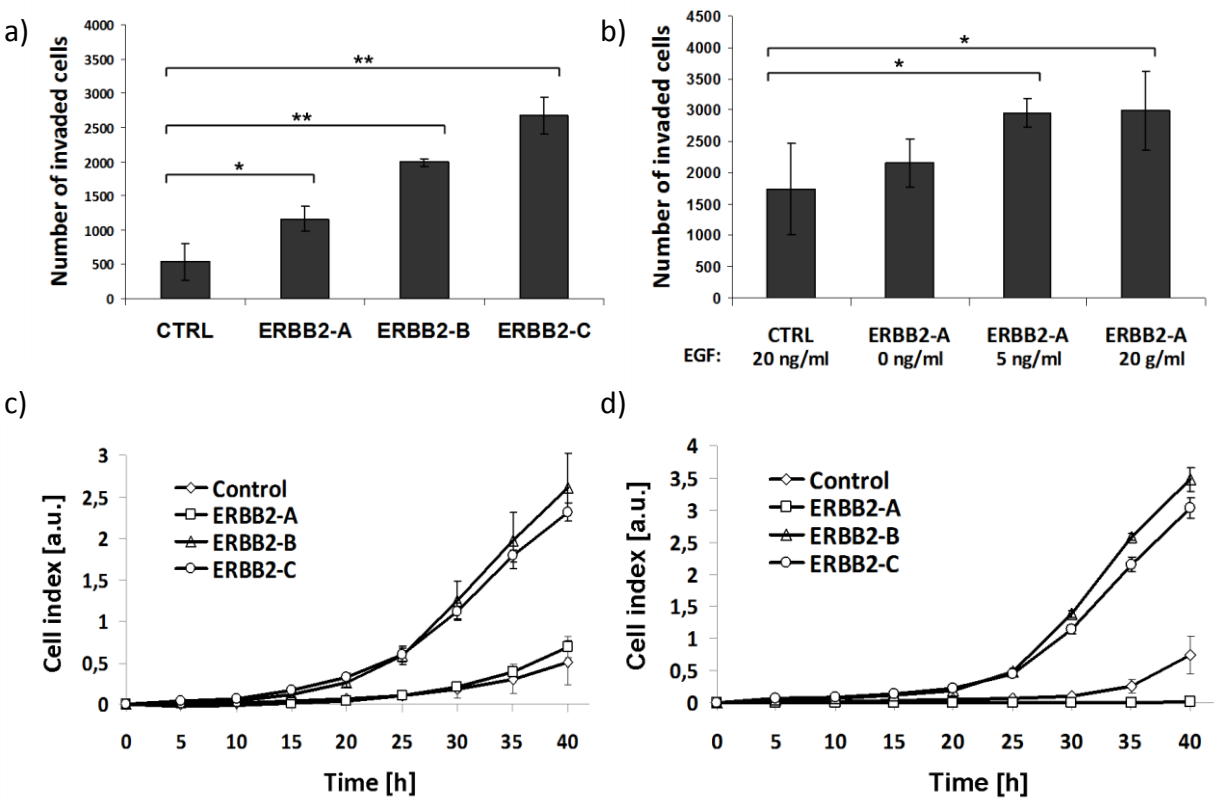

Figure 20

Stable cell line pools overexpressing increasing ERBB2 levels (CTRL < ERBB2-A < ERBB2-B <= ERBB2-C) were analyzed for their invasive potential after overnight incubation in the assay medium depleted of EGF and with reduced horse serum (2%). a, b) The number of invaded cells was measured 72 hours after seeding cells in the upper chambers. 5% horse serum (a) or indicated EGF concentrations (b) were used as chemoattractants. One asterisk (*) denotes a p-value of <0.05, two (**) denote p<0.01, determined by a two-sided t-test. c, d) Cell invasion was analyzed using real time cell analyzer (RTCA) for 42 hours. In the lower chambers either 20 ng/ml EGF (c) or 5% horse serum (d) was used as a chemoattractant.

At this point I concluded that ERBB2 overexpression does neither have to be accompanied by EGFR or ERBB3 overexpression, nor would EGF need to be present to trigger ERBB2-dependent invasion in the non-malignant breast cancer cell line MCF10A. I could show that, although for moderate ERBB2 levels the previous observations hold true, very high ERBB2 levels appear to overcome EGF-dependence and are sufficient to induce invasive properties of these cells. I speculated that the extent to which the MAPK and AKT pathways are activated plays a more critical role in driving the invasive phenotype of MCF10A cells rather than does the way how these pathways are activated.

a)

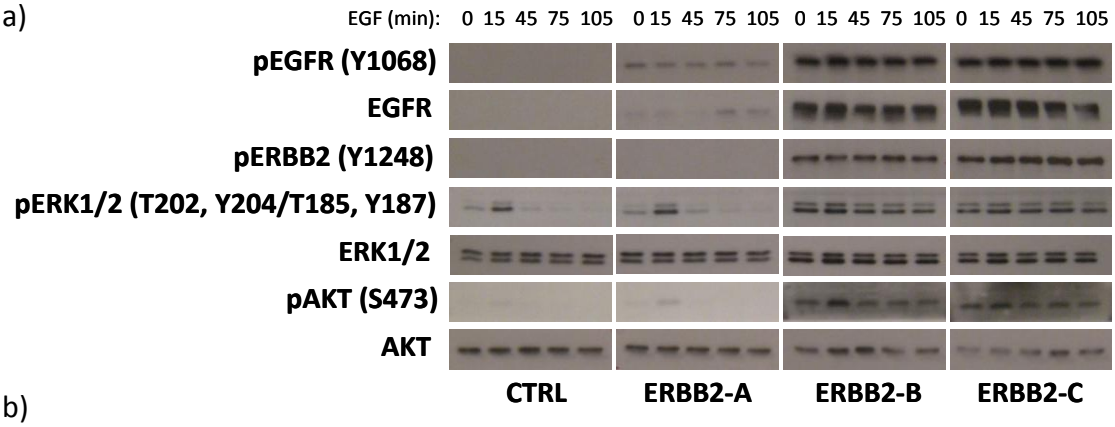

b)

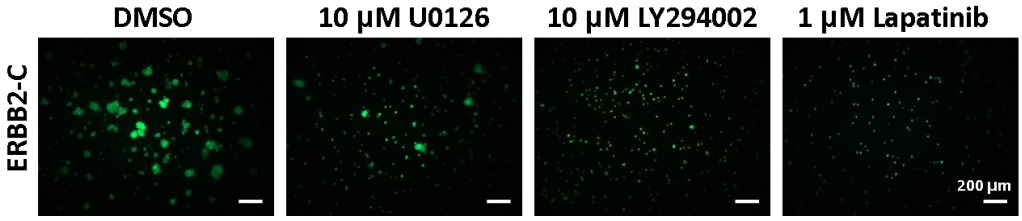

Figure 21

AKT and ERK activation play critical role in ERBB2-driven cell invasion. a) Western blot analysis of EGFR, Akt and ERK phosphorylation upon stimulation of stable cell line pools (CTRL-A, ERBB2-A, ERBB2-B and ERBB2-C) expressing different ERBB2 levels with 20 ng/ml EGF for 0, 15, 45, 75 and 105 minutes (from left to right). Before stimulation cells were starved overnight with the basic F12/DMEM medium containing no additives. b) ERBB2-C cells were grown in 3D culture for 9 days in assay medium containing 5 ng/ml EGF, in the presence of MEK inhibitor (U0126), PI3K inhibitor (LY294002) or EGFR/ERBB2 tyrosine kinase inhibitor (lapatinib). DMSO was used as a control. Scale bar represents 200 µm.

6.1.5 Epithelial-mesenchymal transition is triggered by ERBB2 in dose-dependent manner

As mentioned before, the cell line pool expressing moderate ERBB2 levels formed structures in 3D culture which were characterized by smooth edges, whereas those cell line pools expressing very high ERBB2 levels did not. I hypothesized that cellular polarity should be disrupted in the latter ones. Indeed, structures formed by ERBB2-B and ERBB2-C cells in 3D culture showed unorganized GM130 (Golgin A2, a Golgi marker) staining, whereas in acini structures formed by ERBB2-A and CTRL cells the Golgi apparatus was invariably directed towards the lumen, similarly as in the lobules in normal breast (Figure 22a). Moreover, E-cadherin staining, indicative of cell-cell connections, confirmed well organized acini structures formed by CTRL and ERBB2-A cells and disorganized structures arising from ERBB2-B and ERBB2-C cells (Figure 22b). Of note, the total levels of E-cadherin appeared to

be unaffected by the ERBB2 expression level in the respective cell line pools. In contrast, levels of filamentous actin (F-actin) which is often associated with invasive phenotype of cancerous cells and invadopodia formation, was considerably higher in ERBB2-B and -C cells in comparison to CTRL and ERBB2-A. (Figure 22c).

a)

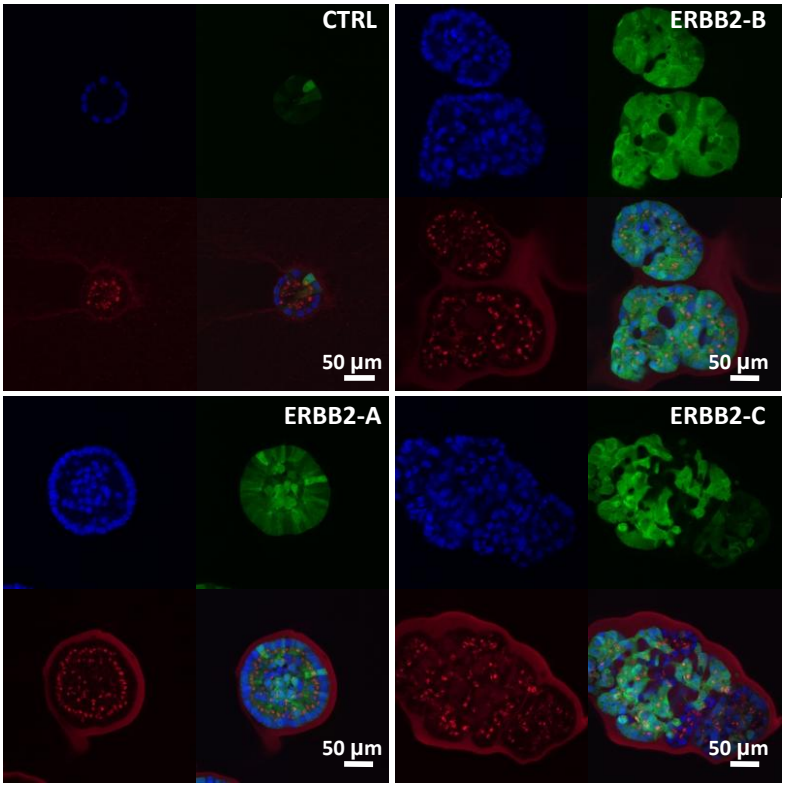

b)

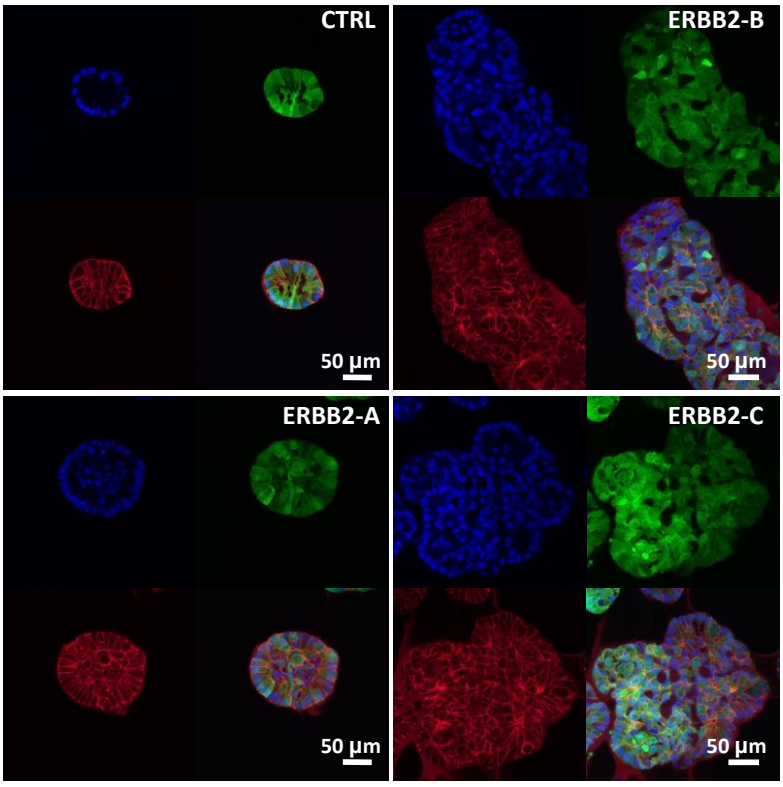

c)

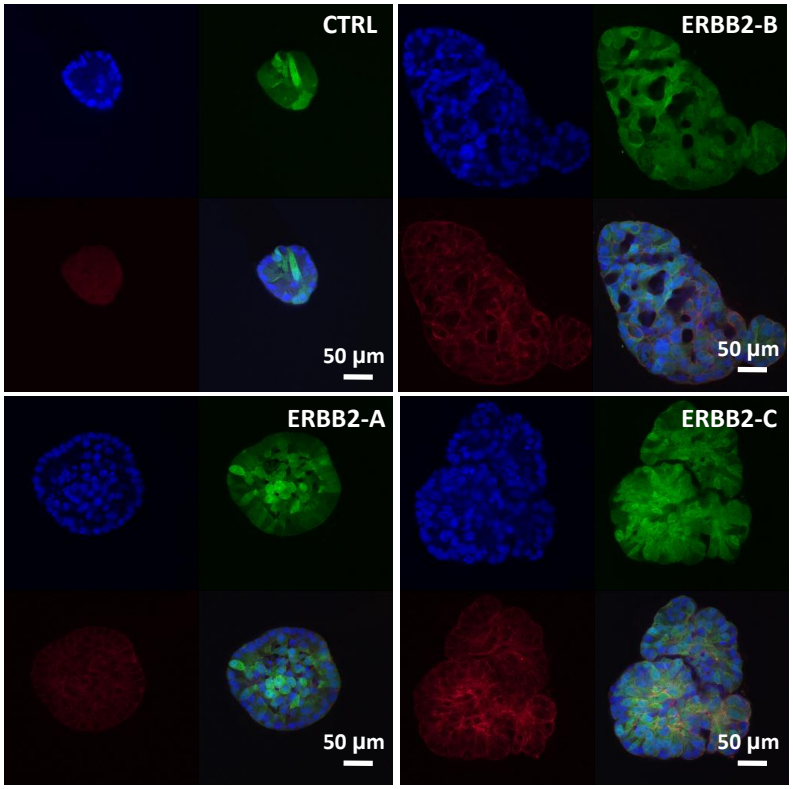

Figure 22
Stable cell line pools overexpressing different ERBB2 levels were grown in 3D culture for 9 days in assay medium containing 5 ng/ml EGF with medium change every 3-4 days. They were then fixed and stained (in red) for Golgi marker GM130 (a), E-cadherin (b) or F-actin (c). Note the position of Golgi apparatus at the inner side of the single cell outside layer of the acini structures (a); the regular cell-cell connections (b); and the absence of F-actin (c) for CTRL and ERBB2-A but not for ERBB2-B and -C celll lines. Nuclei were stained with DAPI (blue); EGFP, which was used as a control when obtaining stable cell line pools, is also shown (green). Scale bar represents 50 µm.

ERBB2 is involved in regulation of epithelial-mesenchymal transition (EMT) in mammary epithelial cells[344,345] and increase in F-actin levels is an indication of this process.[346,347] F-actin is also often associated with enhanced matrix degradation via metalloproteinases (MMPs) activity at the sites of invadopodia formation. I wanted therefore to check if the expression of EMT markers and MMPs could be responsible for the observed invasive phenotypes of ERBB2-B and -C. I could show that, in 2D culture, mRNA expression of the epithelial marker E-cadherin (CDH1) was downregulated, whereas mRNA expression of mesenchymal markers: N-cadherin (CDH2), ZEB1 and fibronectin (FN1) was upregulated in an ERBB2-dose dependent manner. However, higher ERBB2 levels were not associated with expression changes of two other markers: zonula occludens-1 (ZO-1) and SNAI2, which are epithelial

and mesenchymal markers, respectively. Expression of caveolin-1 (CAV1), which has been reported to be responsible for maintaining the hollow lumen in acini structures in normal breast, was also not affected (Figure 23).[348]

Interestingly, when I checked if the mRNA levels of EMT markers that are indeed affected in 2D would also change in 3D culture, only the expression level of N-cadherin was ERBB2-dependent (Figure 24). Similarly, MMP9 and MMP2 mRNA expression levels were ERBB2-dependent in 2D but not in 3D (Figures 23 and 24). One potential explanation for this observation could be the heterogeneity of the cells in 3D culture. In 2D culture the cells are grown in monolayers, and therefore the expression levels throughout the cell population is homogenous and the mRNA levels add up. However, in 3D culture the cells of the outer layer of acini-like structures are better exposed to nutrients and directly interact with proteins in Matrigel, which drive changes in gene expression levels. On the other hand, cells which reside in the inner parts of the structures have reduced access to growth factors (like EGF) and some of them undergo apoptosis. Measured gene expression levels in 3D cultures are therefore the resultant ensemble averages of the inner and outer cell layers. If the changes in expression levels happen in only one of the layers then only substantial changes in expression of these genes can shift the average enough to be detected by qRT-PCR. It could be, thus, that most of the EMT markers' expression is restricted within the acini-like structures only to one of the layers and N-cadherin changes occur either in both, or the levels are high enough in one of the layers to be detected.

Despite the lack of expression changes in 3D cell culture for a few EMT markes that were affected by ERBB2 in 2D culture, ERBB2 did induce EMT process in 3D culture. According to the recently proposed ways of studying EMT in 3D cell cultures, the ability of the cells to invade through extracellular matrix and disruption of cell polarity, which I have previously observed, are commonly accepted as markers of the ongoing EMT process.[346]

As epithelial-mesenchymal transition is often associated with gain of anchorage independent growth,[349] I next seeded CTRL, ERBB2-A, -B and -C cells on polyHema (poly(2-hydroxyethyl methacrylate))-coverd plates and measured their viability after 4 days. I observed that the more ERBB2 a cell line pool expressed, the more scattered and viable the cells were on the hydrogel surface (Figure 25a and b).

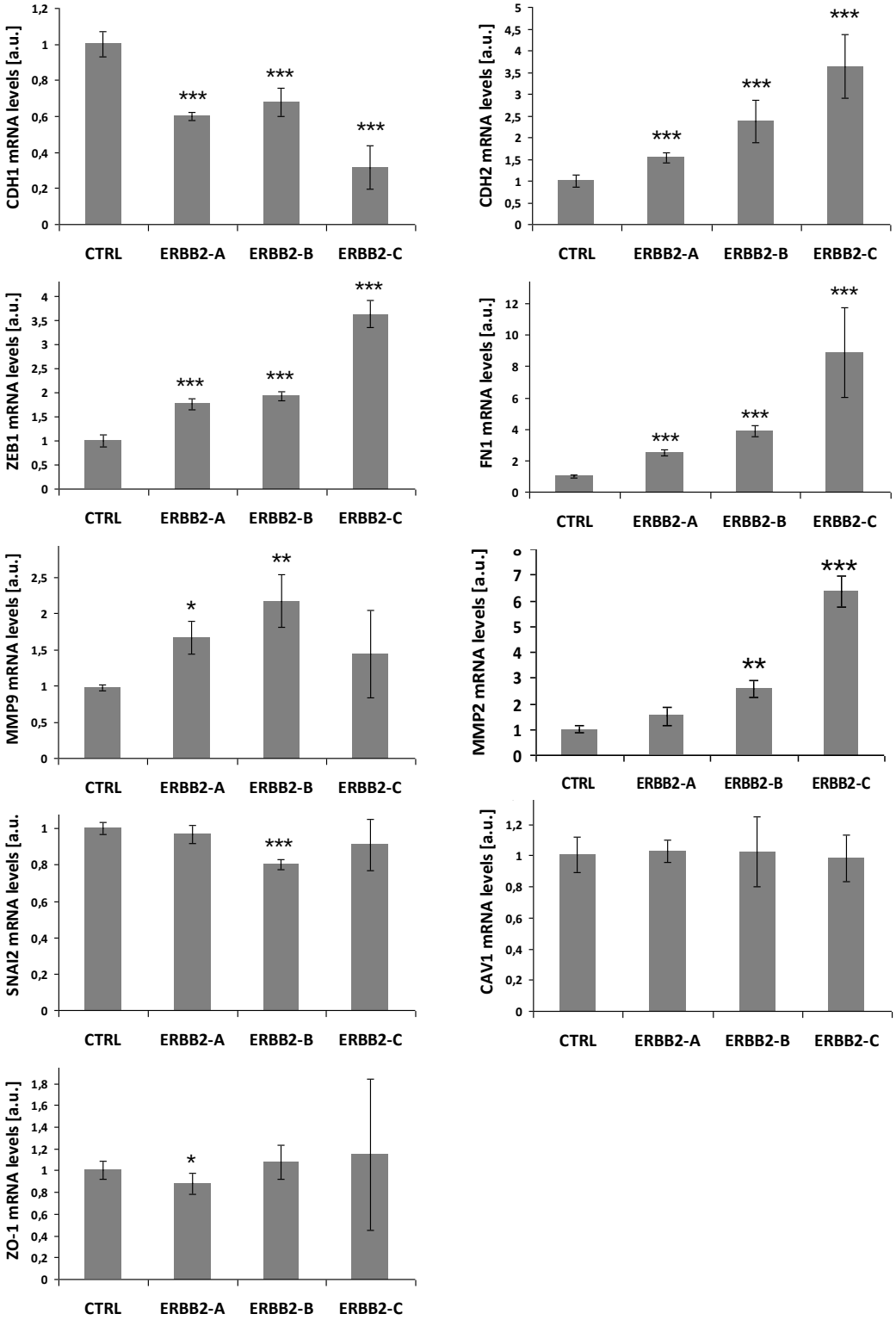

Figure 23

*RT-PCR (TaqMan) analysis of mRNA expression of 6 EMT markers (CDH1, CDH2, ZEB1, FN1, SNAI2 and ZO-1) and 2 metalloproteinases (MMP9 and MMP2) and CAV1 in **2D culture**. Stable cell line pools overexpressing different ERBB2 levels were grown in 2D culture for 3 days in full growth medium before RNA isolation. mRNA levels were normalized to combined expression levels of TFRC, GAPDH and HPRT and shown relative to control cells (CTRL). 2 biological and 3 technical replicates were used. Significance was measured using student's t-test. *p-value<0.05, **p-value<0.01, ***p-value<0.001*

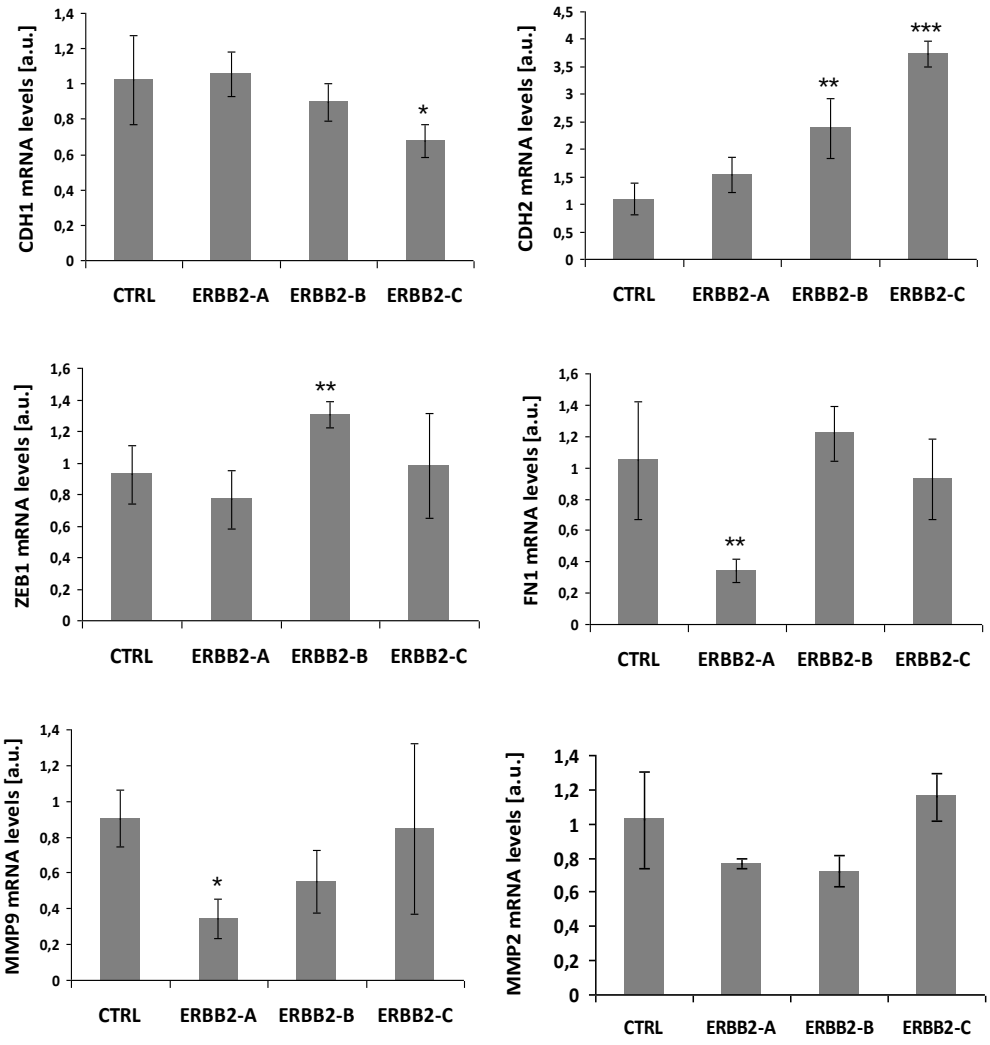

Figure 24

*RT-PCR (TaqMan) analysis of mRNA expression in **3D culture** of 4 EMT markers (CDH1, CDH2, ZEB1, FN1) and 2 metalloproteinases (MMP9 and MMP2), whose expression was changed in 2D culture. Stable cell line pools overexpressing different ERBB2 levels were grown in 3D culture for 9 days in assay medium with 5 ng/ml EGF before RNA isolation. mRNA levels were normalized to combined expression levels of TFRC, GAPDH and HPRT and shown relative to control cells (CTRL). 2 biological and 3 technical replicates were used. Significance was measured using student's t-test. *p-value<0.05, **p-value<0.01, ***p-value<0.001*

CTRL cells, which do not overexpress ERBB2, formed tightly packed structures indicating that these normal epithelial cells need cell-cell interactions to survive in the anchorage-independent conditions and very easily establish cell-cell contacts. Similar phenotypes of the cell line pools were observed when the cells were seeded on low attachment plates (Figure 25c).

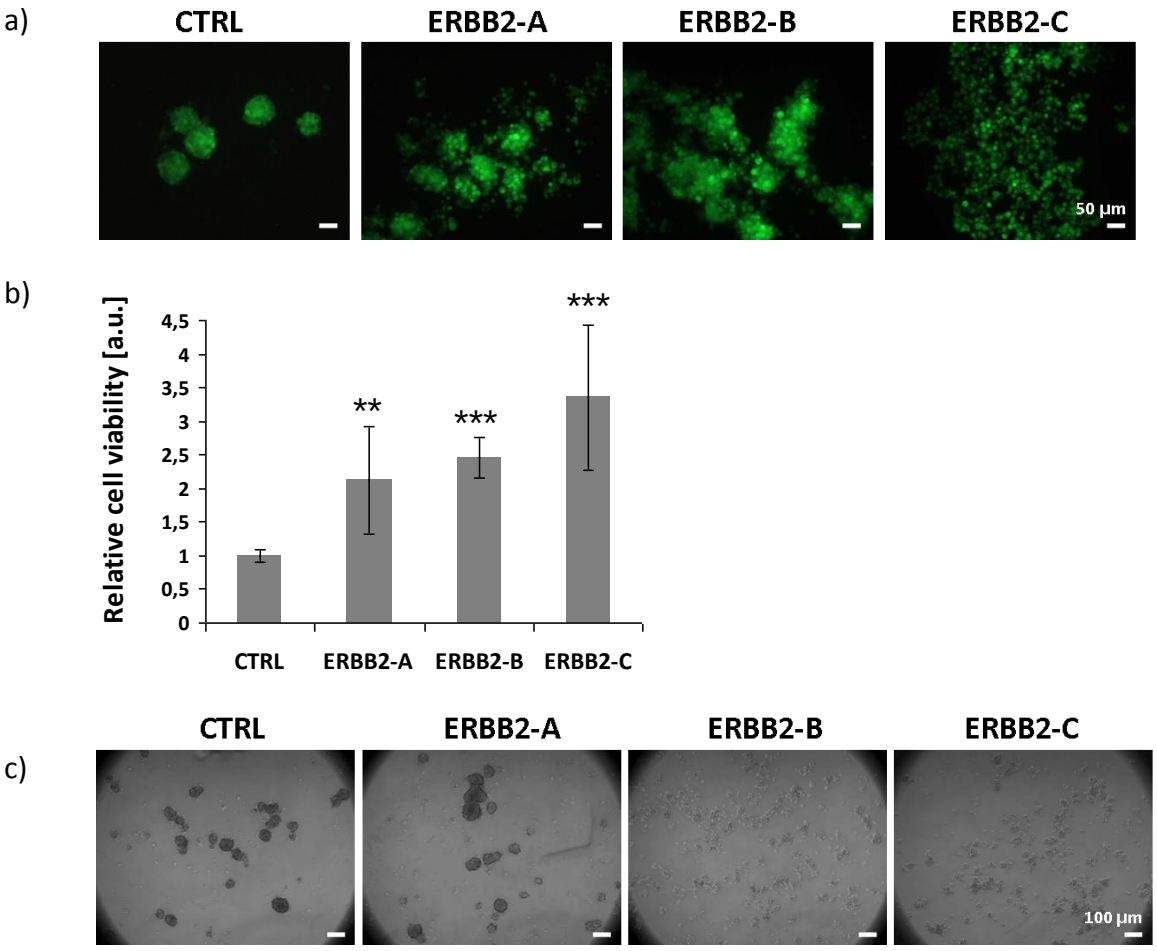

Figure 25

*High ERBB2 levels induce anchorage independent growth. a) Stable cell line pools were seeded on polyHema in full medium and pictures were taken using fluorescent microscope after 3 days. EGFP expressed by cell pools is visible in green. Scale bar represents 50 µm. b) Cell viability was measured 4 days after cell seeding on polyHema as an absorbance of formazan in a colorimetric assay 2 hours after WST1 addition to the cells. The cell viability is shown relative to CTRL cell line pool. **p-value<0.01, **p-value<0.001, determined by a two-sided t-test. c) Cells were seeded on ultra low attachment plates and grown in full growth medium for 72 hours before the pictures were taken using white-field microscope. Scale bar represents 100 µm.*

6.1.6 ERBB2 overexpression co-activates other tyrosine kinases and regulates expression of cytoskeleton-modulating genes.

To gain deeper insights into which proteins drive ERBB2-dependent invasion in MCF10A cells and if they are also regulated in a gradual manner (in contrary to an also possible on/off switch), I decided to check the expression and activation status of several migration-related proteins using reverse phase protein arrays (with a help of Dr. Johanna Sonntag).

69 antibodies recognizing signaling-related and cytoskeleton-regulating (phospho-) proteins, which had previously been validated in our laboratory for the use in RPPA, were incubated with lysates from MCF10A-derived stable cell line pools spotted on RPPA slides and then quantified (for the list of the antibodies used see "Materials", chapter 4.11.1). Four biological replicates of cells grown in full growth medium in standard cell culture dishes were used. Since RPPA requires a high protein concentration I could not use protein lysates from cells grown in matrigel and the following RPPA results were obtained from 2D culture.

The clustering presented in Figure 26 shows only those (phospho-) proteins for which the RPPA signal significantly correlated with ERBB2 expression.

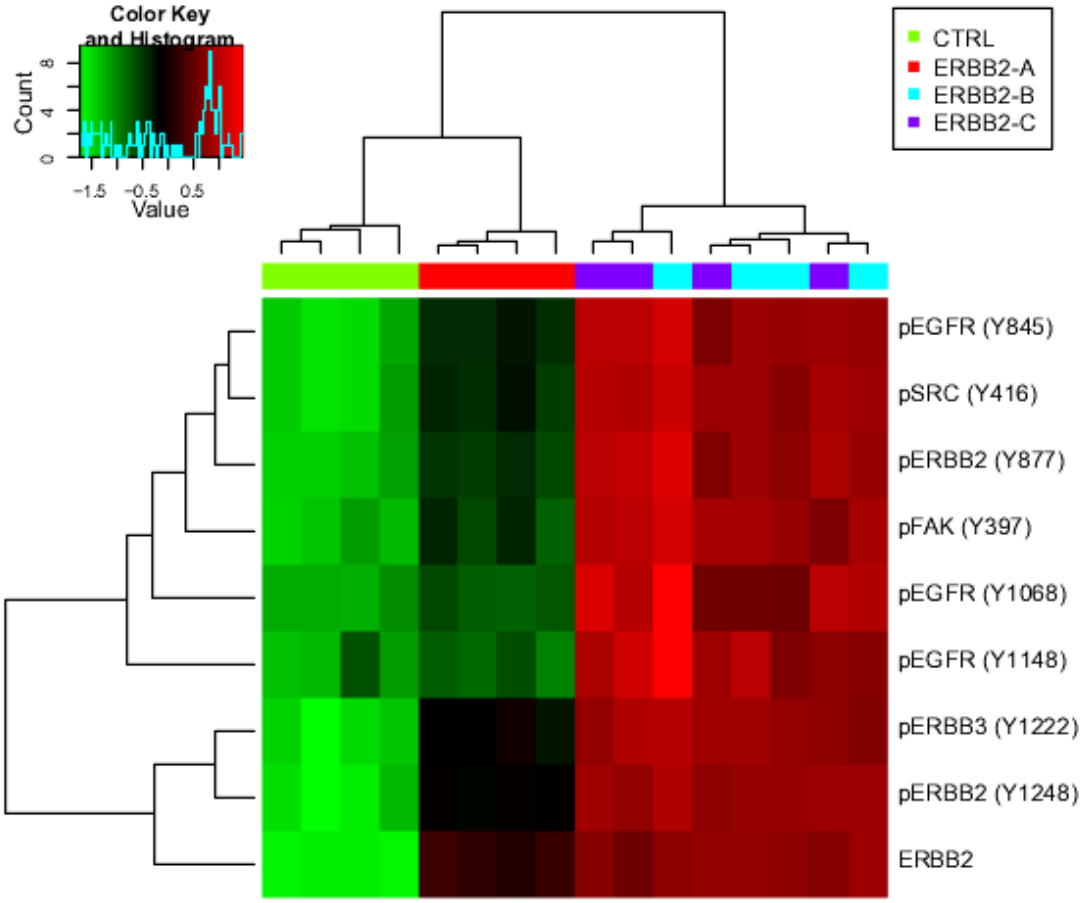

Figure 26

ERBB2 overexpression correlates with its own (Y877, Y1248), EGFR (Y845, Y1068, Y1148) and ERBB3 (Y1222) phosphorylation status, as well as with phosphorylation of two protein tyrosine kinases: Src (Y416) and Fak (Y397). Expression of 69 different phospho- and non-phospho- proteins involved in migration/invasion was investigated using reverse phase protein arrays (RPPA). Four independent biological replicates of each cell line pool were used. Cells were grown in full growth medium in 2D culture for 3 days before protein isolation. For the heatmap only targets with IQR > 0.5 on log2 scale were selected.

I could show that the gradual increase in ERBB2 levels is associated with a gradual increase in phosphorylation of ERBB-family receptors, i.e. EGFR (Y845, Y1068, Y1148), ERBB2 (Y877, Y1248), and ERBB3 (Y1222). ERBB2 levels also had a dose dependent effect on phosphorylation of SRC (Y416) and FAK (Y397), two other tyrosine kinases involved in migration/invasion regulation. ERBB2-B and ERBB2-C for which Western Blot analysis showed similar ERBB2 levels also presented comparable ERBB2 levels on RPPA.

Several other proteins showed slightly weaker, but still significant ERBB2-dependency, including upregulation of Vimentin, Cortactin, pCortactin (Y421), N-cadherin, metadherin (MTDH), RhoA, pPTEN (T366/S370 – inhibitory site), PI3K (p110), PI3K (p85), ERK1/ERK2, PKA; and downregulation of basal marker cytokeratins 5/6 (Figure 27a and 27b).[350,351] The expression of all above mentioned proteins/phospho-proteins was gradually changing with increasing ERBB2 levels (CTRL < ERBB2-A < ERBB2-B or ERBB2-C) rather than just showing on/off states.

Phosphorylated ERBB2 (Y1248) levels correlated also very well with total receptor levels (r=0.8894, p=1.81e-138) in breast cancer patients from TCGA RPPA dataset (Figure 28a). The correlation coefficient was even higher when only ERBB2-positive patients were considered (r=0.9578, p=2.2e-16; Figure 28b). Interestingly, a few patients with high pERBB2/ERBB2 levels were not classified as ERBB2-overexpressing based on immunohistochemistry or *in situ* hybridization performed at the time of diagnosis and, on the other hand, several patients with low pERBB2/ERBB2 levels were classified as ERBB2-positive. This discrepancy results most probably from the fact that for RPPA analysis the protein is isolated from the bigger portions of tumors and can include up to 30% of stromal cells, while ERBB2 receptor levels are detected using IHC in the invasive part of the tumor only.

Thus, on the one hand, if 10% (or previously 30%) of cells in the invasive part stain strongly for ERBB2 but the rest of the tumor does not stain for ERBB2 at all, then the detected by RPPA ERBB2 levels can be low despite tumor's ERBB2-positive status. On the other hand, if the whole tumor stains weakly for ERBB2 (ERBB2-negative status), the detected on RPPA ERBB2 levels can be high as the signals from individual cells add up.

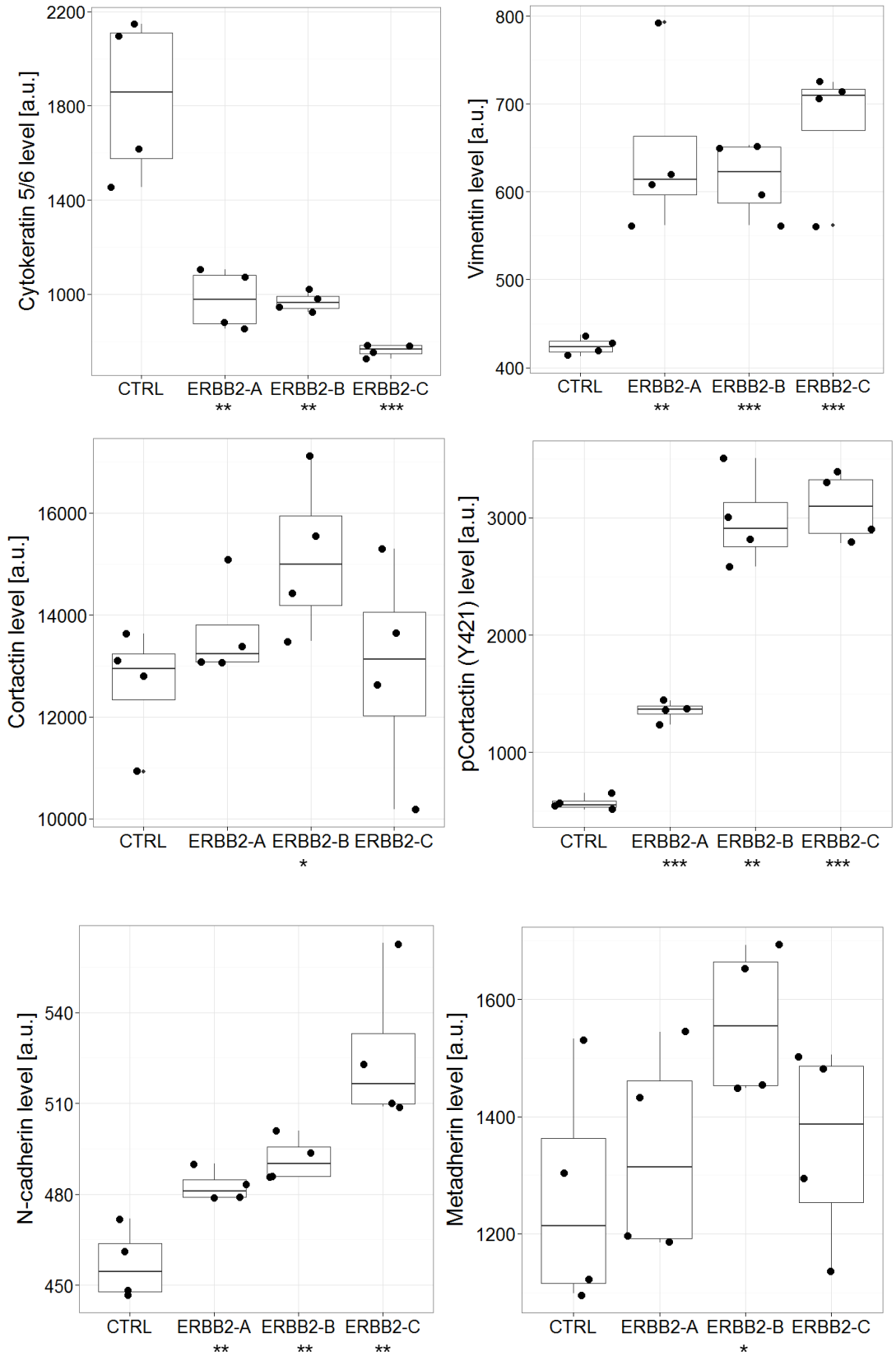

Figure 27a

Description under figure 27b.

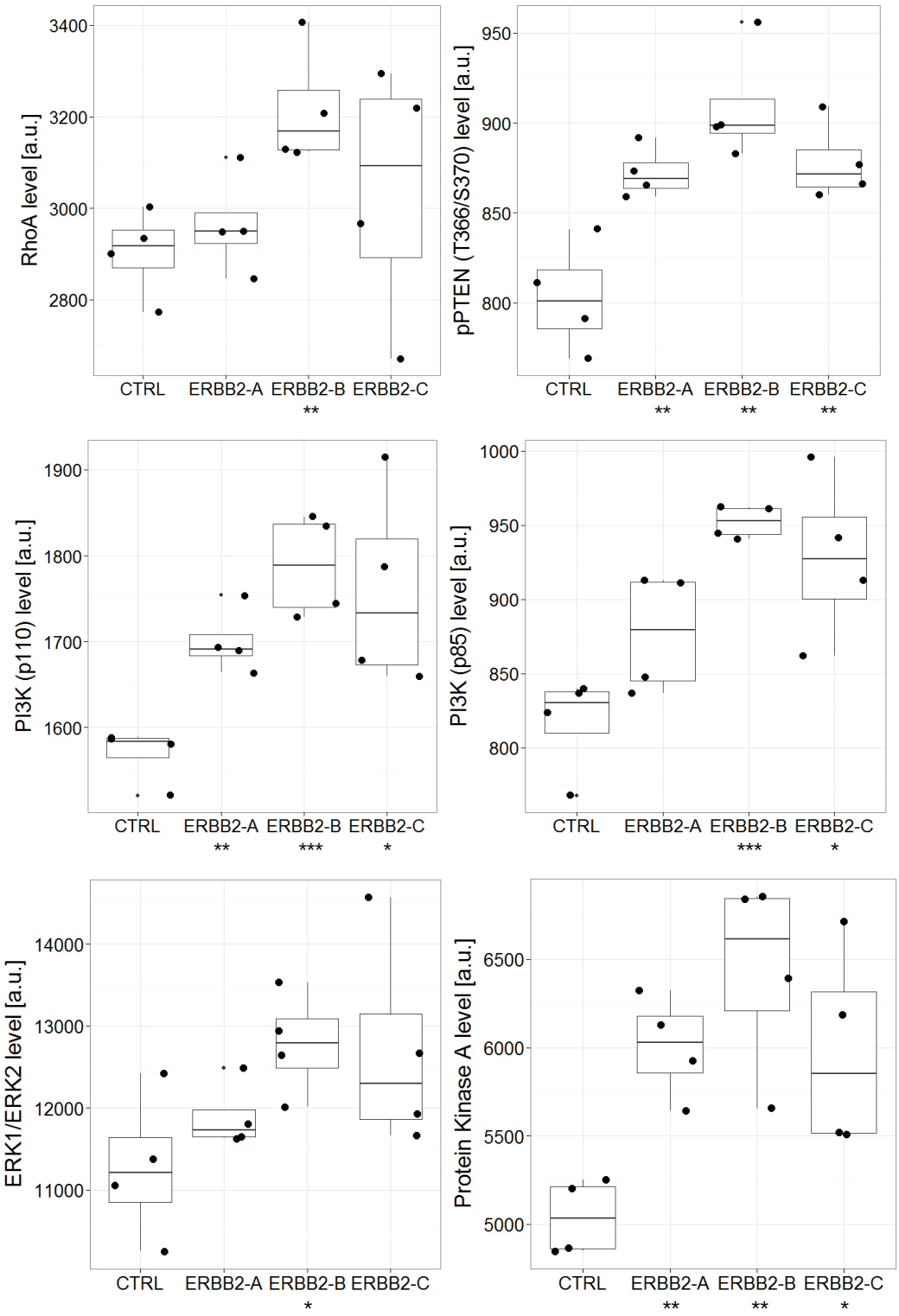

Figure 27b

Expression of 69 different phospho- and non-phospho- proteins involved in migration/invasion was investigated using reverse phase protein arrays (RPPA). Box plots indicating expression levels of those strongly correlating with ERBB2 are shown. Y-axes shows RPPA signal in arbitrary units. Four independent biological replicates of each cell pool were used (black dots). Cells were grown in full growth medium in 2D culture for 3 days before protein isolation. One asterisk (*) denotes a p-value of <0.05, two (**) denote p<0.01, and three (***) denote p<0.001, determined by a two-sided t-test and CTRL as reference.

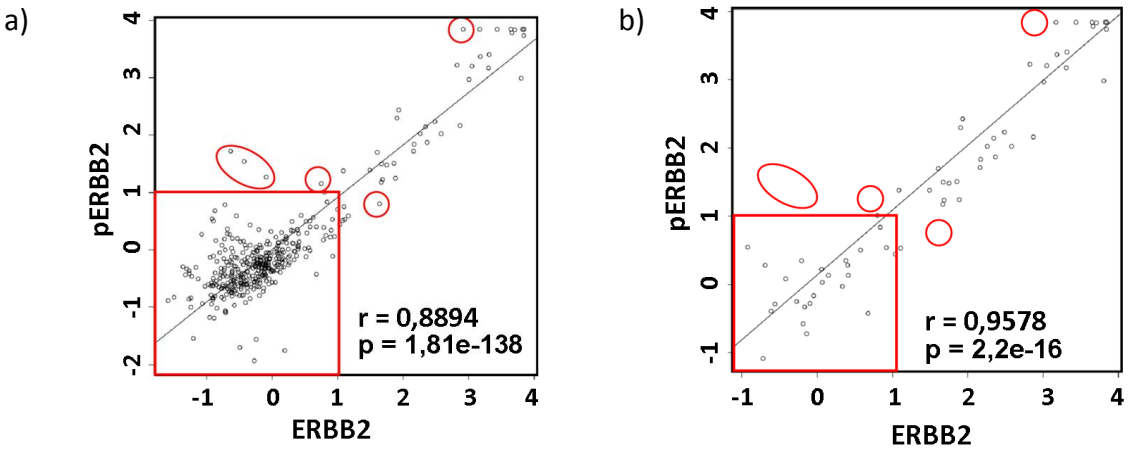

Figure 28

Correlation of ERBB2 with pERBB2 (Y1248) protein levels (log_2 scale) in breast cancer patients from TCGA RPPA dataset.[14] *a) ERBB2 and pERBB2 levels are shown in all patients independent of ERBB2 IHC status. b) Only patients with ERBB2 IHC status 3+ are shown. r - Pearson correlation coefficient. Note that a few patients (red circled) with high ERBB2 and/or pERBB2 protein levels were not detected as ERBB2-positive by IHC staining and several patients with low ERBB2 and pERBB2 protein levels (red square) were classified as ERBB2-positive.*

6.1.7 Identification of genes differentially regulated by ERBB2 in 3D culture

To determine whether migration/invasion-regulating genes are also induced by ERBB2 in 3D cell culture and to identify possible novel genes deregulated by ERBB2 but not described yet in 2D cultures, I have performed genome-wide mRNA expression profiling using Illumina micorarrays (for details see "Methods" chapter 5.16). Prior to RNA isolation, MCF10A-derived cell line pools expressing different ERBB2 levels were grown in Matrigel for 9 days in the MCF10A assay medium containing 5 ng/ml EGF – the optimal concentration at which normal MCF10A cell line forms hollow acini structures. Array hybridization, raw data analysis, including normalization using *variance stabilization transformation* algorithm (Bioconductor *vsn* package) and differential expression analysis (Bioconductor *limma* package) of all detected genes between each two cell line pools has been done by the Genomics and Proteomics Core Facility at DKFZ. Each three biological replicates of MCF10A-derived cell line pools expressing different ERBB2 levels clustered together, indicating high reproducibility of the experiment (Figure 29).

43 genes (Supplementary Table 1) were identified whose expression was both significantly downregulated in the direct comparison of ERBB2-A vs CTRL cell line pools (arbitrary cut-off: fold change=0.66, Benjamini-Hochberg adjusted p-value <0.05) and significantly downregulated in the direct comparison of ERBB2-B vs ERBB2-A (arbitrary cut-off: fold

change=0.75, Benjamini-Hochberg adjusted p-value <0.05) for at least one detection probe on the array. On the other hand, 41 genes (Supplementary Table 2) were upregulated in both comparisons with arbitrary cut-offs: fold change=1.5 and fold change=1.35, respectively (Figure 30).

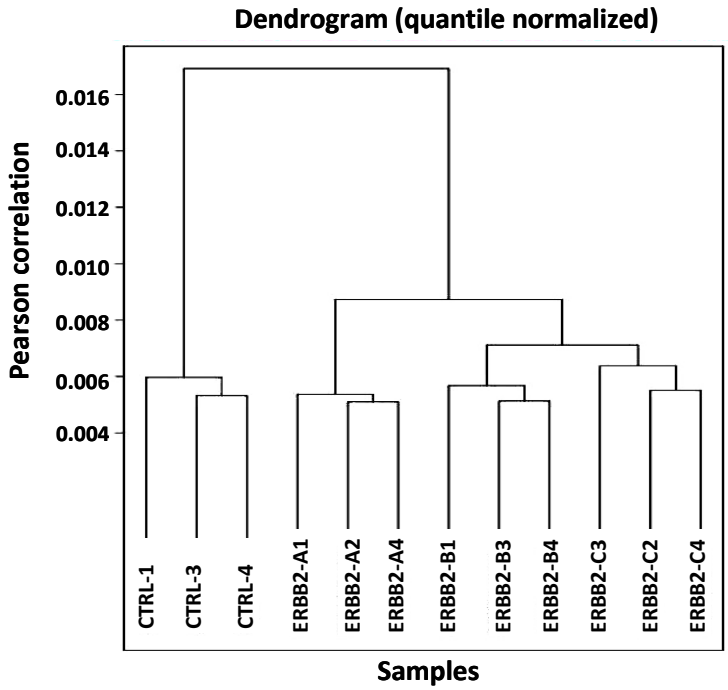

Figure 29
Whole genome expression profiling of CTRL, ERBB2-A, -B and -C cell line pools was done using Illumina's Sentrix HumanHT-12 v4 microarray. 3 replicates of each cell line pool were used and as a part of data quality check the dendrogram of quantile normalized data was plotted to see if the replicates cluster together. Note that ERBB2-B and -C cell line pools are more similar to each other than any of them to ERBB2-A and differ even more from CTRL cells.

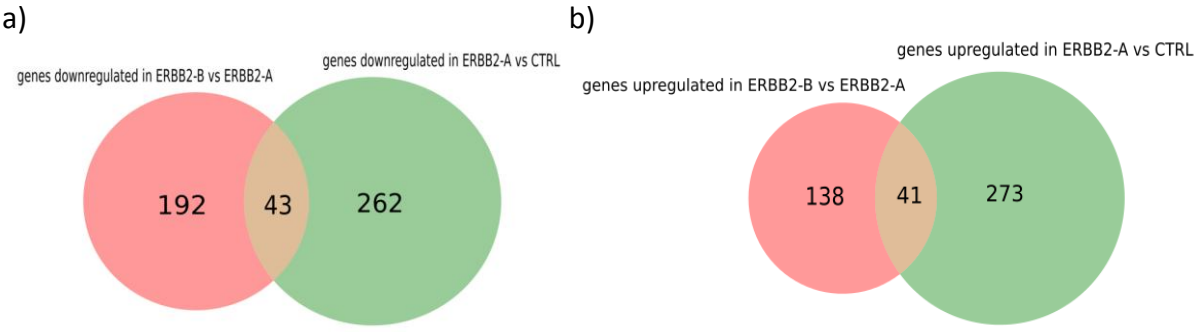

Figure 30
The numbers of differentialy expressed genes between ERBB2-A and CTRL as well as ERBB2-B and ERBB2-A in 3D cell culture are shown for: a) downregulated genes; b) upregulated genes.

As observed expression range of several genes was restricted only to the ERBB2 level range between CTRL and ERBB2-B cells, as had previously been observed for some proteins on RPPA, ERBB2-C was not included in this analysis (when ERBB2-C was also taken into account (arbitrary cut-offs: fold change=0.84 and fold change=1.1905) only keratin 16 (KRT16) and keratin 17 pseudogene 3 (KRT17P3; LOC650517) were negatively downregulated and stanniocalcin 1 (STC1) was upregulated).

Next, I used the functional annotation tool, DAVID 6.7 (Database for Annotation, Visualization and Integrated Discovery)[352,353], using Kyoto Encyclopedia of Genes and Genomes (KEGG)[354] annotation category "KEGG_PATHWAY", to perform gene annotation and molecular pathway enrichment analysis on the lists of 41 upregulated and 43 downregulated genes.

Table 1

The list of KEGG pathways enriched in genes deregulated in ERBB2-level dependent manner in 3D culture. Analysis were done using DAVID functional annotation tool. Note that both: cell cycle and oocyte meiosis pathways shared the same enriched genes.

Genes downregulated		
KEGG pathway	**Gene symbol**	**Gene name**
Metabolism of xenobiotics by cytochrome P450	UGT1A6	UDP glucuronosyltransferase 1 family, polypeptide A1, A3, A4, A5, A6, A7, A8, A9, A10
	ALDH3A1	aldehyde dehydrogenase 3 family, memberA1
	AKR1C4	aldo-keto reductase family 1, member C4 (chlordecone reductase; 3-alpha hydroxysteroid dehydrogenase, type I; dihydrodiol dehydrogenase 4)
Cell cycle - - - - - - - - - - - - - Oocyte meiosis	MAD2L1	MAD2 mitotic arrest deficient-like 1 (yeast)
	CDC20	cell division cycle 20 homolog (S. cerevisiae)
	CCNB2	cyclin B2
Genes upregulated		
KEGG pathway	**Gene symbol**	**Gene name**
Hematopoietic cell lineage	CD14	CD14 molecule
	IL1A	interleukin 1, alpha
	IL1B	interleukin 1, beta
Aminoacyl-tRNA biosynthesis	CARS	cysteinyl-tRNA synthetase
	GARS	glycyl-tRNA synthetase
	SARS	seryl-tRNA synthetase
	WARS	tryptophanyl-tRNA synthetase
	YARS	tyrosyl-tRNA synthetase
Cytokine-cytokine receptor interaction	CCL20	chemokine (C-C motif) ligand 20
	INHBE	inhibin, beta E
	IL1A	interleukin 1, alpha
	IL1B	interleukin 1, beta
	VEGFA	vascular endothelial growth factor A

The only significantly enriched pathway was the aminoacyl-tRNA biosynthesis pathway (B-H adjusted p-value=0.0011) with five genes being upregulated by ERBB2. Table 1 lists these genes as well as the genes in the pathways for which at least 3 genes were up- or downregulated by ERBB2. Interestingly, the third most strongly upregulated gene by ERBB2 was an asparagine synthetase (ASNS; see Supplementary table 2), which similarly to aa-tRNA synthetases also plays a role in protein production.

6.1.8 ERBB2 upregulates HBEGF expression

HBEGF was one of the most significantly upregulated genes within the set of 41 genes upregulated by ERBB2 in 3D cell culture, having an expression fold change of 1.82 (Benjamini-Hochberg adjusted p-value=8.54E-39) between ERBB2-A and CTRL, and with fold change of 1.61 (Benjamini-Hochberg adjusted p-value p=2.79E-41) between ERBB2-B and ERBB2-A. The upregulation was verified by RT-PCR (TaqMan). Interestingly, HBEGF upregulation was much stronger in 3D culture (up to 3.5 fold) than in 2D culture (max. 1.4 fold) (Figure 31). This gene encodes an EGFR ligand and it was therefore interesting to see that ERBB2 overexpression induces its expression. As mentioned before, other reports had shown before that ERBB2 alone does not induce MCF10A cell invasion and that additional presence of either EGF or ERBB3 is required to this end. I observed that, even in the absence of EGF, cells expressing very high ERBB2 levels are invasive. The observation that those cells can produce another EGFR ligand - HBEGF - themselves could explain how they escape the requirement of EGF (or ERBB3) to induce invasion. As HBEGF is a secreted protein and its expression was induced mainly in 3D culture, I attempted to measure its levels in the supernatant of MCF10A stable cell line pools grown in Matrigel using ELISA, but I was not successful. This could be possibly due to not sufficient sensitivity of antibody recognizing HBEGF for measurement of small amounts of HBEGF. Detection of this EGFR ligand would thus require either large-scale 3D cell cultures or a more sensitive method that both are considered for the follow-up of my project.

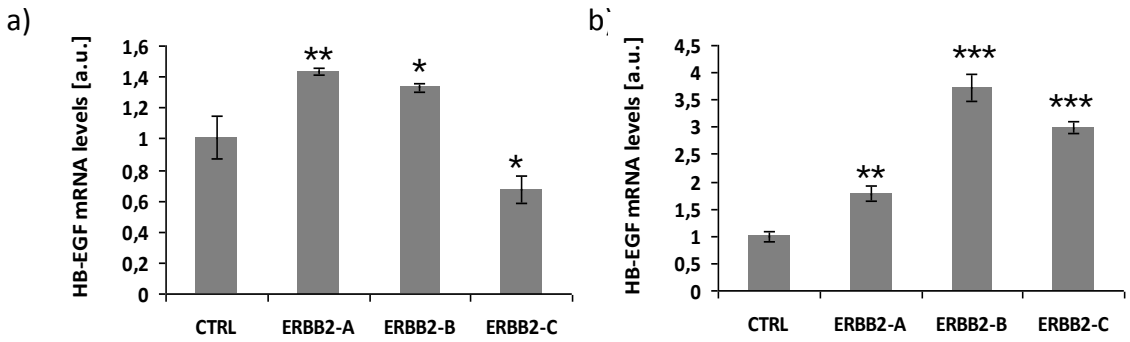

Figure 31

*RT-PCR (TaqMan) analysis of mRNA expression of HB-EGF in 2D (left panel) and 3D (right panel) culture. Stable cell line pools overexpressing different ERBB2 levels were grown in 2D culture for 3 days in full growth medium or in 3D culture for 9 days in assay medium containing 5 ng/ml EGF before RNA isolation. The expression levels are shown relative to control cell line pool (CTRL). *p-value<0.05. **p-value<0.01, ***p-value<0.001, as determined by two-sided t-test.*

6.1.9 MCF10A-derived ERBB2-overexpressing cell line pools are not more sensitive to drug treatment than control cells

To test whether overexpression of ERBB2 to different extents had an impact on drug sensitivity, MCF10A-derived cell line pools were grown in 2D culture and treated for 72 hours with increasing concentrations of doxorubicin, paclitaxel, or trastuzumab and followed by measurement of cell viability. Whereas higher concentrations of doxorubicin and paclitaxel decreased viability of all four cell line pools, trastuzumab treatment did not have an effect on any (Figure 32). The lack of sensitivity to trastuzumab, ERBB2-targeting humanized monoclonal antibody, is in line with the fact that in the developed stable cell line pools ERBB2 did not induce cell proliferation, nor had a direct impact on cell viability (measured by ATP levels) when cells were grown in 2D culture. Thus ERBB2 blocking by trastuzumab in 2D culture could not revert the non-present induction and did not cause any further drop in ATP levels.

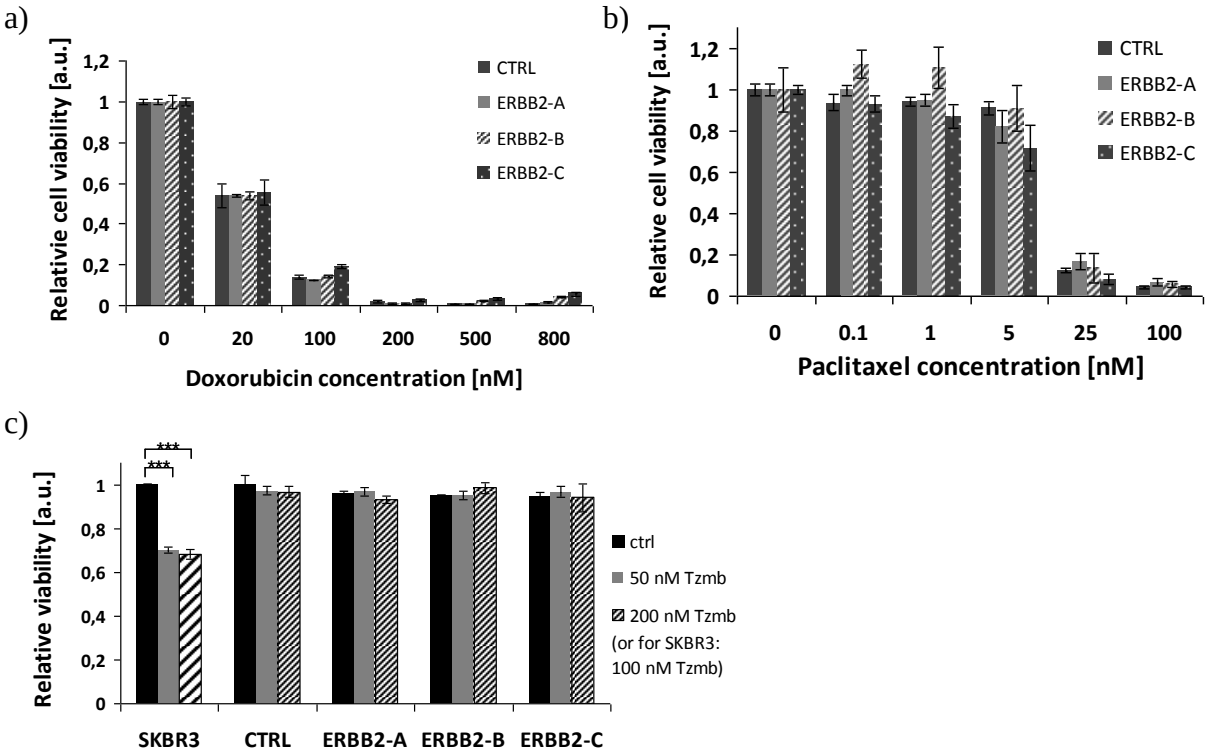

Figure 32

Viability was measured using Cell Titer Glo assay for CTRL, ERBB2-A, ERBB2-B and ERBB2-C cell line pools after incubation for 72 hours with increasing concentrations of a) doxorubicin, b) paclitaxel or c) trastuzumab. Concentrations of these drugs are indicated in the respective graphs. SKBR3, which is a trastuzumab sensitive cell line, was used as control. Concentrations of trastuzumab used to treat it were 0, 50 and 100 nM (for other cel lines the highest concentration used was 200 nM).

6.1.10 ERBB2-overexpressing MCF10A cell line pools do not induce tumor formation *in vivo*

The observation that cell invasion is induced by very high ERBB2 levels in MCF10A cells but not by moderate ERBB2 levels and that this effect is accompanied by EMT induction and anchorage-independent cell growth in the very high ERBB2 expressing cell line pools provided well founded motivation to test whether similar phenotype can be observed also *in vivo*. For this purpose 32 NSG mice were injected subcutaneously with 5 million cells each (CTRL, ERBB2-A, –B, or –C) into both flanks (for details see "Materials" chapter 4.12 and "Methods" chapter 5.19). The mice were inspected for tumor presence every week. As ERBB2 overexpression has been reported to be responsible for induction of tumors with a delayed onset (~7-8 months) in a few other model systems[355], including transgenic mice expressing ERBB2 under mammary specific (MMTV) promoter, the mice were kept for up to

9-10 months before they were sacrificed. At that time no tumors in mice have been found. Also no dormant cell (negative result for detection of GAPDH, HPRT, TFRC and ERBB2 on RT-PCR) or nodules have been detected in mice lungs. This leads to the conclusion that ERBB2-overexpression (even to a very high extent) is not sufficient to transform close to normal mammary epithelial cells MCF10A into tumorigenic cells, despite its clear effect observed in 3D culture. That stresses the importance of microenvironment in the regulation of cell survival and proliferation which extends beyond Matrigel components.

6.2 Part II: ERBB2 as an important regulator of oncogenic miRNA expression in breast cancer

6.2.1 miRNA sequencing and differential expression analysis reveal a subset of ERBB2-deregulated miRNAs

Recently miRNAs have been shown to be involved in EMT regulation as well as trastuzumab resistance.[356,305] ERBB2 has itself been reported to be targeted at mRNA level by several miRNAs and further to also regulate expression of miRNAs (see "Introduction", chapters 3.4.2 and 3.4.3). These studies however were all done in 2D cell culture growth conditions and until now there has been no study showing global miRNA changes upon ERBB2 overexpression using a three-dimensional culturing system. Since I had seen quite many molecular and phenotypic differences between cells grown in 2D vs 3D (see part I), I decided to perform short RNA sequencing (<50 bp) using RNA isolated from 3D culture of the cell line pools expressing different ERBB2 levels. The same RNA samples were also submitted for genome-wide mRNA profiling described in chapter 6.1.7, hence the same three biological replicates were used (Figure 33).

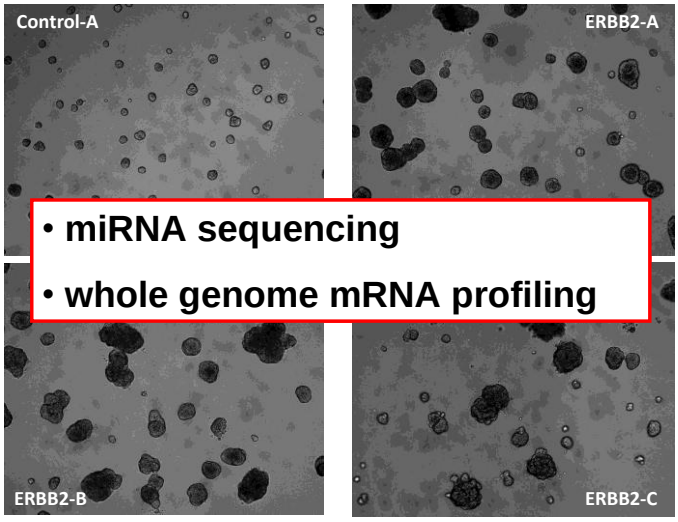

Figure 33
CTRL, ERBB2-A, -B and –C cell line pools were grown for 9 days in Matrigel in MCF10A assay medium in the presence of 5 ng/ml EGF (medium change every 3-4 days). Total RNA was isolated with miRNeasy Kit from Qiagen and samples were prepared for miRNA sequencing and whole genome expression profiling as described in "Methods" chapter 5.16.

Raw sequencing data was processed as described in "Methods" chapter 5.16, to find differentially expressed miRNAs between each two MCF10A-derived stable cell line pools. Thirty-six miRNAs showed significant deregulation (p-value <0.01 and fold change ≤0.5 or ≥2) by ERBB2 in at least one of the direct comparisons between the cell line pools. In Figure 34 the clustering of $\log_2$(fold change) values for those miRNAs is shown.

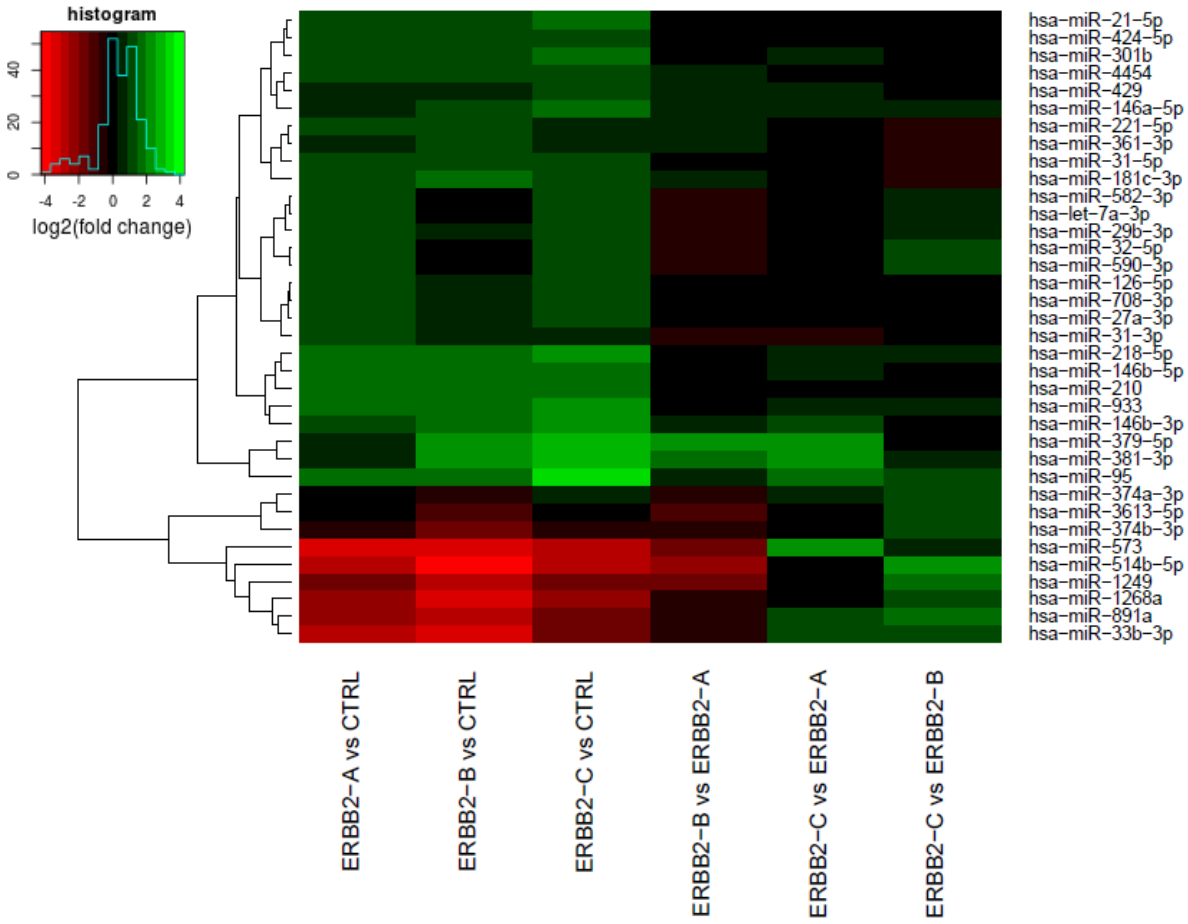

Figure 34
Heatmap presenting log2(fold change) values for differentially expressed (p-value <0.01, fold change ≤0.5 or ≥2) miRNAs between at least two different cell line pools grown in 3D culture. Red colour indicates decrease in miRNA expression with higher ERBB2 level of the indicated cell pool, green – increase (see the colour code in the upper left corner).

The oncogenic miR-21-5p, which had been previously shown to be upregulated by ERBB2 and linked to trastuzumab resistance was found among the top upregulated miRNAs.[314] Similarly, two other well studied oncogenic miRNAs in breast cancer were identified within this group: miR-221 and miR-210 (oncogenic miRNAs linked to trastuzumab resistance)[306,357,303]. A few other miRNAs from this group (like e.g. miR-146a-5p, miR-146b-

5p, miR-31-5p and miR-31-3p) have also been linked to breast cancer, but their general role is not yet fully understood as they bear both oncogenic and tumor suppressor properties depending on the context or the cancer subtype studied.

6.2.2 ERBB2-dependent miRNAs: miR-301b, miR-146a-5p and miR-210 are expressed at higher levels in breast tumors and associated with shorter overall survival

The miRNAs which I had identified by next generation sequencing to be ERBB2-dependent were next checked for their expression levels in breast tumors in comparison to normal tissue using patient data from The Cancer Genome Atlas (TCGA) dataset. If the difference between tumor and normal tissue was significant ($p<0.05$) for a certain miRNA, the miRNA received the score of +1 if the expression was higher in tumors than in normal tissues or -1 if it was lower. Similar scoring was applied when a given miRNA was higher expressed in HER2-positive than in HER2-negative tumors (+1) or vice versa (-1) as well as when a miRNA correlated negatively (+1) or positively (-1) with patient survival in the METABRIC dataset. These datasets contain a big number of patients and hence the use of them to obtain significant information was the best possible option (Table 2). Two miRNAs, that were differentially regulated by ERBB2 in 3D culture, were absent in TCGA dataset and eight were absent in METABRIC dataset.

Three highest scoring miRNAs: miR-301b, miR-146a-5p and miR-210 were ERBB2-dependent in the clinical datasets in the similar manner as in the ERBB2-overexpressing cell line pools in 3D culture (upregulated by ERBB2) and all three showed higher levels in breast tumors than in normal tissue. Moreover, patients with higher levels of these miRNAs showed shorter overall survival than those with lower miRNA levels (Table 2). Thus, since these three miRNAs showed association with clinical features alike ERBB2, they qualified as the most interesting candidates for the follow-up functional studies in relation to ERBB2 and breast cancer. Nevertheless, for the purpose of this thesis I decided to choose only one from the list and characterize it in more detail.

Table 2

Differential expression of miRNA candidates in tumor vs. normal tissue (TCGA database), in HER2-positive and -negative tumors as well as their correlation with patients' survival. The individual scores mean: "-1" if higher level of miRNA: is observed in normal tissue than in tumor; is observed in HER2-negative tumors; or is associated with better overall survival. "0" if there is no statistically significant correlation present. "1" if higher level of miRNA: is observed in tumor tissue than in normal; is observed in HER2-positive tumors; or is associated with worse overall survival. The brackets [] indicate that p-value was close to 0.05 and a score given was (+/-) 0.5 instead of (+/-)1.

miRBase ID	miRNA name	TCGA (T vs N)	p value	METABRIC (HER2+ vs HER2-)	p value	METABRIC (survival-median)	p value	final score
MIMAT0000076	hsa-miR-21-5p	1	4,59E-26	1	2,02E-06	0	0,721	2
MIMAT0001341	hsa-miR-424-5p	0	1,09E-01	1	8,02E-03	0	0,202	1
MIMAT0004958	**hsa-miR-301b**	**1**	**5,99E-05**	**1**	**4,04E-02**	**1**	**7,35E-03**	**3**
MIMAT0018976	hsa-miR-4454	N/A	N/A	N/A	N/A	N/A	N/A	N/A
MIMAT0001536	hsa-miR-429	1	4,25E-12	-1	1,52E-02	0	0,371	0
MIMAT0000449	**hsa-miR-146a-5p**	**[1]**	**0,054**	**1**	**4,79E-02**	**1**	**4,08E-02**	**2,5**
MIMAT0004568	hsa-miR-221-5p	0	0,611	0	0,594	0	0,277	0
MIMAT0004682	hsa-miR-361-3p	0	0,407	0	0,119	0	0,173	0
MIMAT0000089	hsa-miR-31-5p	0	0,459	0	0,724	0	0,632	0
MIMAT0004559	hsa-miR-181c-3p	1	9,89E-03	-1	2,87E-07	-1	1,07E-02	-1
MIMAT0004797	hsa-miR-582-3p	1	3,30E-02	0	0,425	0	2,84E-01	1
MIMAT0004481	hsa-let-7a-3p	1	7,95E-07	-1	3,16E-05	0	2,17E-01	0
MIMAT0000100	hsa-miR-29b-3p	1	1,58E-07	-1	2,14E-02	-1	4,21E-03	-1
MIMAT0000090	hsa-miR-32-5p	1	1,94E-07	0	0,226	[-1]	8,32E-02	0
MIMAT0004801	hsa-miR-590-3p	1	1,13E-08	N/A	N/A	N/A	N/A	N/A
MIMAT0000444	hsa-miR-126-5p	-1	2,24E-07	0	0,843	0	0,669	-1
MIMAT0004927	hsa-miR-708-3p	1	1,71E-06	0	0,873	0	0,303	1
MIMAT0000084	hsa-miR-27a-3p	1	4,25E-04	0	0,389	0	0,999	1
MIMAT0004504	hsa-miR-31-3p	0	0,567	0	0,45	0	0,339	0
MIMAT0000275	hsa-miR-218-5p	-1	1,00E-09	0	0,722	-1	4,37E-03	-2
MIMAT0002809	hsa-miR-146b-5p	1	7,99E-03	1	6,95E-03	0	7,88E-01	2
MIMAT0000267	**hsa-miR-210**	**1**	**1,35E-06**	**1**	**1,73E-02**	**1**	**4,58E-02**	**3**
MIMAT0004976	hsa-miR-933	0	0,145	0	0,79	0	0,649	0
MIMAT0004766	hsa-miR-146b-3p	-1	5,23E-03	N/A	N/A	N/A	N/A	N/A
MIMAT0000733	hsa-miR-379-5p	-1	4,73E-12	0	0,734	[-1]	0,0557	-1,5
MIMAT0000736	hsa-miR-381-3p	-1	3,21E-18	0	0,887	[-1]	0,051	-1,5
MIMAT0000094	hsa-miR-95	0	0,385	0	0,098	-1	1,41E-03	-1
MIMAT0004688	hsa-miR-374a-3p	1	3,48E-03	N/A	N/A	N/A	N/A	N/A
MIMAT0017990	hsa-miR-3613-5p	1	1,79E-13	N/A	N/A	N/A	N/A	N/A
MIMAT0004956	hsa-miR-374b-3p	1	7,17E-05	0	0,904	0	0,732	1
MIMAT0003238	hsa-miR-573	1	4,75E-02	N/A	N/A	N/A	N/A	N/A
MIMAT0015087	hsa-miR-514b-5p	0	0,803	0	0,11	1	4,34E-03	1
MIMAT0005901	hsa-miR-1249	0	0,252	0	0,536	[1]	0,0721	0,5
MIMAT0005922	hsa-miR-1268a	N/A	N/A	N/A	N/A	N/A	N/A	N/A
MIMAT0004902	hsa-miR-891a	-1	5,00E-03	N/A	N/A	N/A	N/A	N/A
MIMAT0004811	hsa-miR-33b-3p	1	1,42E-05	0	0,114	0	5,39E-01	1

To choose the most relevant miRNA candidate out of the three miRNAs, I used two publically available independent patient datasets - GSE22220 and GSE19783 and correlated ERBB2 mRNA expression with the expression of all miRNAs in those datasets (see "Methods" chapter 5.18). All miRNAs were first correlated with each ERBB2 probe and in this way four correlation lists were generated (as GSE22220 had only one probe for ERBB2 while GSE19783 had three). I took then top 100 miRNAs either positively or negatively correlating with ERBB2 from each list and looked for the overlapping miRNAs. There were 7 miRNAs found among first hundred positively correlating miRNAs with ERBB2 expression level in all four lists. These are (starting from the most positively correlating): miR-425, miR-181b, miR-331-3p, miR-301a, miR-629*, miR-183 and miR-429. On the other hand there were only 2 miRNAs negatively correlating with ERBB2 level: miR-483-3p and miR-328. As both these datasets are smaller than METABRIC only few miRNAs showed significant correlation with ERBB2 level in terms of p-value. Nevertheless, the above mentioned miRNAs showed the strongest correlations with ERBB2 from all miRNAs detected in these datasets.

As I was interested in particular in the three miRNAs differentially regulated by ERBB2 in my model system and showing similarity to ERBB2 in clinical setting (Table 2), I checked the correlation values for miR-301b, miR-146a-5p and miR-210 with each ERBB2 probe in both these datasets (Table 3). Based on these values I decided not to focus on miR-146a-5p during my further functional studies as it was a miRNA candidate that, unlike two other miRNAs, was not consistently associated with ERBB2 expression across all datasets (METABRIC vs GSE22220 vs GSE19783).

While both miR-210 and miR-301b seemed to be promising candidates for further investigation in relation to ERBB2, for miR-210 the association with breast cancer and trastuzumab resistance has already been documented. For miR-301b, however, no connection to breast cancer or ERBB2 has been established yet. Moreover, the related miR-301a ranked as one of the top ERBB2-dependent miRNAs in GSE22220 and GSE19783 datasets. These two miRNAs differ only in two nucleotide positions (two nucleotides are inverted, see Table 5) and share the same seed sequence. miR-301a (referred to also as miR-301) has been also previously reported to affect proliferation and invasion in breast cancer.[358] Interestingly, another miRNA, miR-130b, which belongs to the same miRNA family as miR-301b and miR-301a correlated positively with ERBB2 in three out of four correlation lists as well (with one ERBB2 probe in GSE22220 and two probes in GSE19783), which placed

it just below the seven miRNAs that were best positively correlating with ERBB2 on the rank list. Table 4 shows correlation coefficients for miR-301b, miR-301a and miR-130b with respective p-values for each probe.

Table 3

Correlation coefficients and p-values for miR-301b, miR-210 and miR-146a-5p expression levels with ERBB2 levels for the indicated ERBB2 probes in GSE22220 and GSE19783 datasets.

Dataset	ERBB2 probe ID	miRNA	correlation	p-value
GSE22220	"0002350129"	hsa-miR-301b	N/A	N/A
GSE22220	"0002350129"	hsa-miR-210	0,20200509	0,003433
GSE22220	"0002350129"	hsa-miR-146a-5p	-0,02421192	0,728489
GSE19783	A_23_P89249	hsa-miR-301b	0,08507969	0,395205
GSE19783	A_23_P89249	hsa-miR-210	-0,03807148	0,704018
GSE19783	A_23_P89249	hsa-miR-146a-5p	-0,09181444	0,358727
GSE19783	A_24_P284420	hsa-miR-301b	0,16263052	0,10244
GSE19783	A_24_P284420	hsa-miR-210	0,07445997	0,457013
GSE19783	A_24_P284420	hsa-miR-146a-5p	0,06214888	0,534904
GSE19783	A_24_P933108	hsa-miR-301b	0,19045924	0,055184
GSE19783	A_24_P933108	hsa-miR-210	0,17344868	0,081264
GSE19783	A_24_P933108	hsa-miR-146a-5p	0,02259732	0,821639

Table 4

Correlation coefficients and p-values for miR-301a, miR-301b and miR-130b expression levels with ERBB2 levels for the indicated ERBB2 probes in GSE22220 and GSE19783 datasets.

Dataset	ERBB2 probe ID	miRNA	correlation	p-value
GSE22220	"0002350129"	hsa-miR-301a	0,12585566	0,070081
GSE22220	"0002350129"	hsa-miR-301b	N/A	N/A
GSE22220	"0002350129"	hsa-miR-130b	0,13162956	0,058066
GSE19783	A_23_P89249	hsa-miR-301a	0,18149986	0,067901
GSE19783	A_23_P89249	hsa-miR-301b	0,08507969	0,395205
GSE19783	A_23_P89249	hsa-miR-130b	0,03687372	0,712917
GSE19783	A_24_P284420	hsa-miR-301a	0,16349652	0,1006
GSE19783	A_24_P284420	hsa-miR-301b	0,16263052	0,10244
GSE19783	A_24_P284420	hsa-miR-130b	0,15049611	0,13109
GSE19783	A_24_P933108	hsa-miR-301a	0,23225221	0,018827
GSE19783	A_24_P933108	hsa-miR-301b	0,19045924	0,055184
GSE19783	A_24_P933108	hsa-miR-130b	0,2073989	0,036473

The hypothesis that not a single miRNA but a few miRNAs belonging to the same miRNA family could be ERBB2-dependent eventually led me to choose miR-301b over miR-210 for further functional studies. The inclusion of miR-301a and miR-130b in my studies was a direct consequence of choosing miR-301b as a most prominent miRNA candidate. On the one hand, I wanted to directly compare the functions of miR-301b and breast cancer related

miR-301a in my model system. On the other hand, although miR-130b was not one of the top miRNAs deregulated by ERBB2, its levels steadily increased with ERBB2 expression in 3D cell culture as well. If it had been included in the scoring analysis presented in Table 2, miR-130b would have also received a high score of 2.5. Moreover, miR-130b is encoded by MIR130B gene located on chromosome 22, around 300 bp downstream from MIR301B gene, suggesting its possible co-regulation with miR-301b by ERBB2. Finally, similar to miR-301b, miR-130b has neither been reported to be involved in breast cancer nor has its relation to ERBB2 been investigated before.

6.2.3 ERBB2-dependent miR-301b and miR-130b as well as related miR-301a are associate with clinico-pathological features in breast cancer

To better understand the relation of miR-301b, miR-130b and miR-301a with ERBB2 I used the METABRIC study to establish direct correlation of miRNA expression with ERBB2 mRNA levels. Here, only miR-301a and miR-130b showed significant correlation (Figure 35a). When tumors were divided into ERBB2-positive and -negative based on immunohistochemistry, only miR-301b showed significant association with ERBB2-positivity (Figure 35b). All miRNAs, however, showed significant association with ERBB2 when tumors were divided according to their increasing ERBB2 IHC status (Figure 35c). This result was in line with my previous observation that miR-301b and miR-130b levels increase gradually with ERBB2 protein level in ERBB2-overexpressing cell line pools grown in 3D culture.

While all three miRNAs had higher expression in breast cancer than in normal tissue in the TCGA patient dataset (Figure 36a), only miR-301b and miR-130b were higher expressed in ER-negative than in ER-positive tumors in the METABRIC dataset (Figure 36b). In contrast, in TCGA dataset all three miRNAs were significantly higher expressed in ER-negative tumors (Supplementary Figure 2). ERBB2-overexpressing breast cancers rarely (in ~10% of the cases) express ER receptor and thus, if most of the ERBB2-overexpressing tumors fall into ER-negative group, then this association could have been anticipated. Similarly, ERBB2-enriched breast cancers are often (in ~72% of the cases) associated with p53 mutations. Figure 36c shows that miR-301b and miR-130b are indeed higher expressed in p53-mutated tumors than in those expressing wild-type p53. miR-301a, although not significantly associated with p53-mutated status, shows a similar trend.

To check whether chosen miRNAs can be linked to patients' prognosis, Kaplan-Meier survival curves were drawn to find the miRNAs' relation to disease-specific patient survival. Again, only high expression of miR-301b and miR-130b significantly correlated with shortened survival while miR-301a showed a similar trend (Figure 36d).

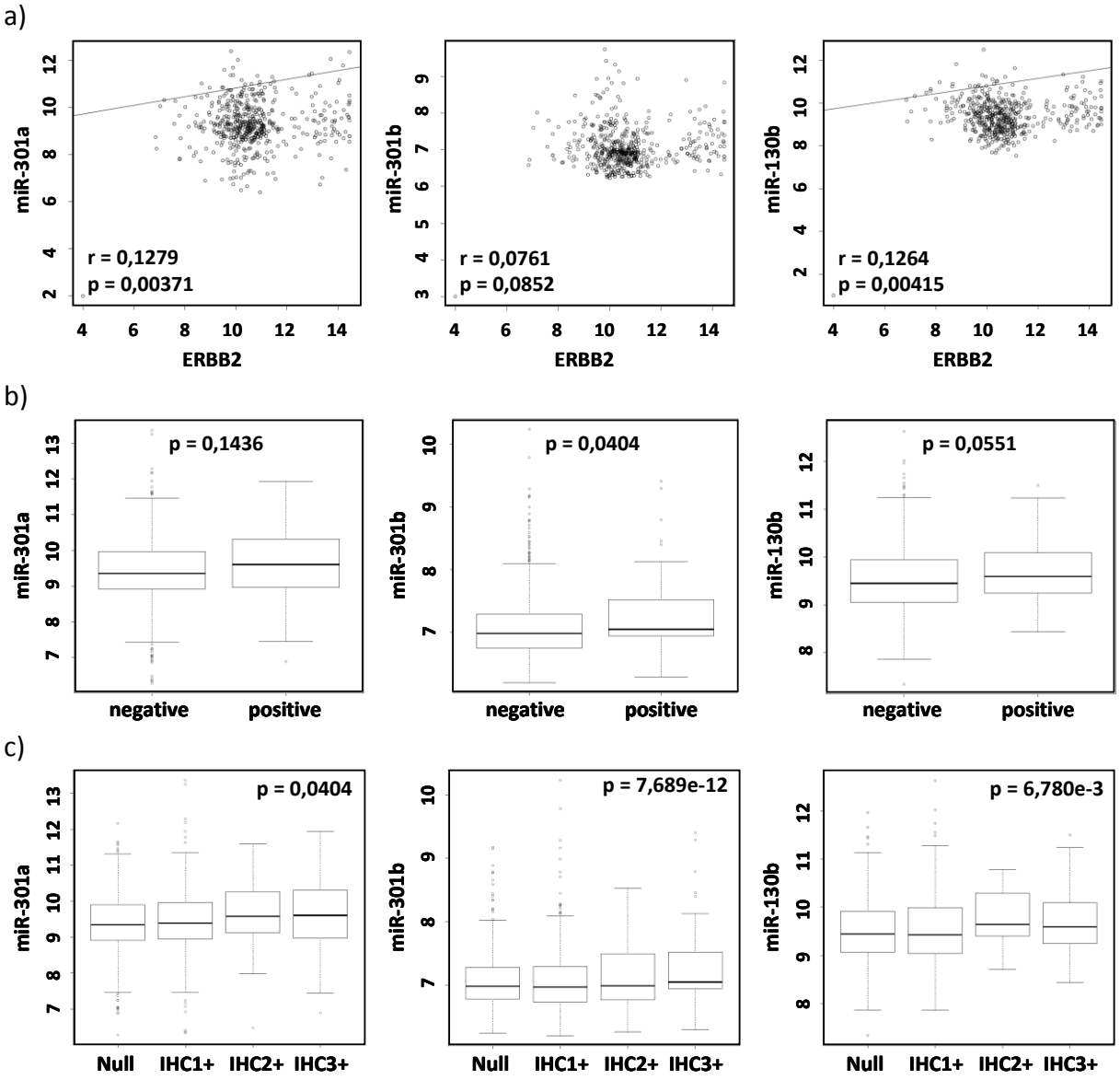

Figure 35

Relation of miR-301a, miR-301b and miR-130b with ERBB2 in METABRIC dataset. a) Correlation of miRNAs' expression level with ERBB2 mRNA level; b) miRNAs' expression levels in ERBB2-negative (IHC0, 1+ and 2+) vs ERBB2–positive (IHC3+) breast tumorss; c) miRNAs' expression levels in tumors with IHC0, IHC1+, IHC2+ and IHC3+ statuses. p-values are indicated.

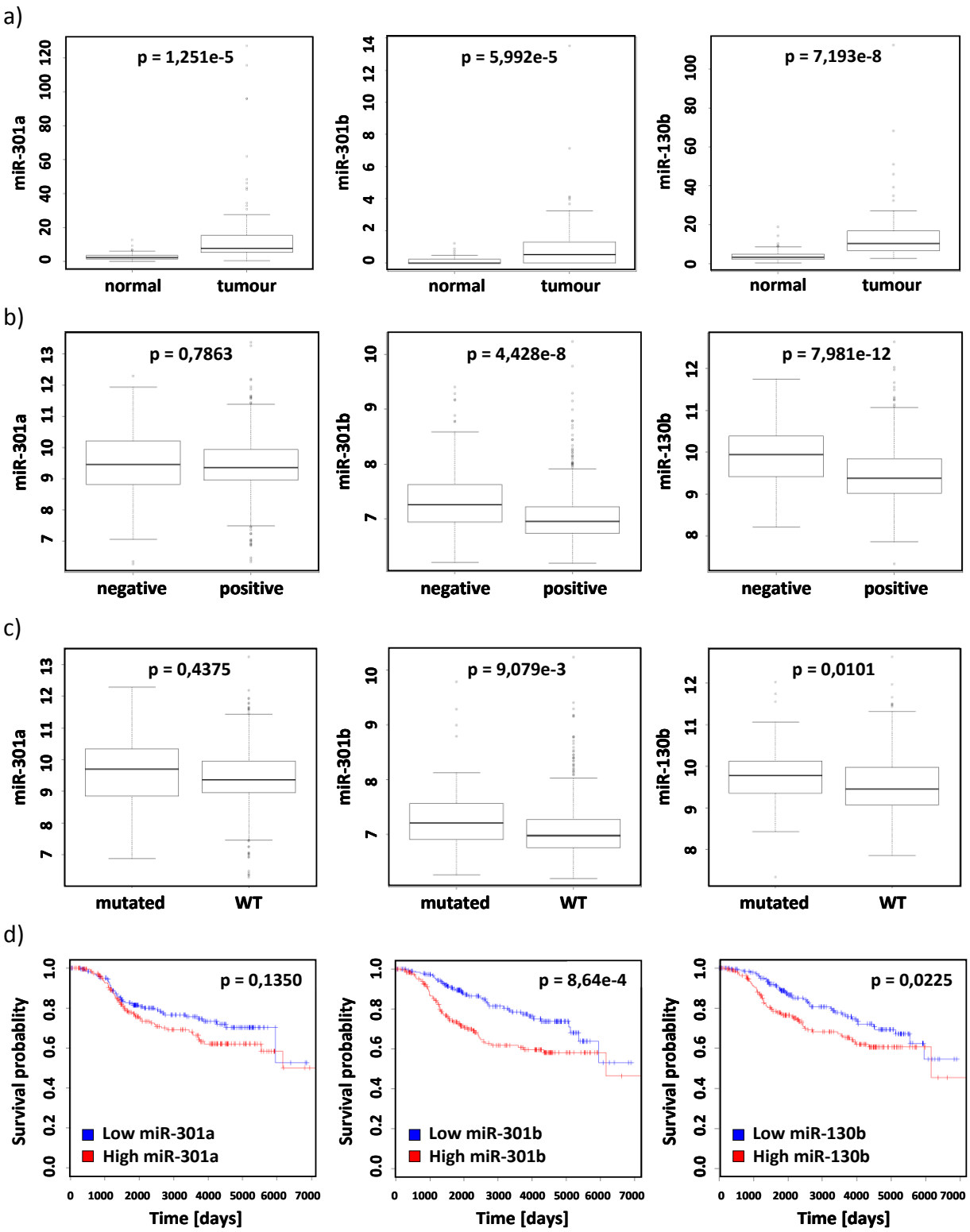

Figure 36

Mean expression levels of miR-301a, miR-301b and miR-130b were compared in a) normal tissue vs tumor in TCGA dataset; b) ER-negative vs ER-positive tumors in dataset from METABRIC study; c) p53-mutated and p53 wild-type tumors in dataset from METABRIC study. d) Kaplan-Meier curves were drawn for patients' disease-specific survival from METABRIC study for patients with either low or high miRNAs' levels (divided by quantiles - lower than Q1 or higher than Q3).

6.2.4 Expression of miR-301b and miR-130b is ERBB2-dependent in 3D cell culture but not in 2D culture.

Being reassured that miR-301b and miR-130b should be good candidates for further functional studies, I first validated their expression levels (along with miR-301a) using qRT-PCR in MCF10A-derived ERBB2-expressing cell line pools grown in 3D culture for 9 days in the presence of 5 ng/ml EGF. Similar to the results obtained from next generation sequencing, miR-301b and miR-130b but not miR-301a levels were higher in ERBB2-overexpressing cell pools than in control (Figures 37a, 37c and 37e). Moreover, their expression increased with increasing ERBB2 levels (better observed for miR-130b) and the maximum fold change was detected in ERBB2-C when compared to the CTRL cell pool. miR-301b expression fold change reached in this pool 2.08 (p-value=0.0029) compared to control, explaining the presence of miR-301b in the list of those miRNAs most prominently deregulated by ERBB2 (fold change <0.5 or >2) shown in Figure 34 and Table 2. For miR-130b the fold change threshold (=2) was not achieved to be listed among the top deregulated miRNAs, however, the upregulation was still significant (fold change=1.78, p-value=0.0394).

While miR-301b and miR-130b levels were ERBB2-level dependent in 3D culture, they did not show any association with ERBB2 levels when their expression was checked in the same cell line pools grown in 2D culture. This observation stresses the impact the cell environment has on miRNA expression in the context of ERBB2 upregulation.

Expression levels measured by qRT-PCR for all three miRNAs in RNA samples correlated well with the read counts obtained from sequencing data. To prove specificity of the qRT-PCR assays, I performed a control experiment in which I overexpressed separately either of the miRNA mimics - miR-301a, miR-301b or miR-130b, in normal MCF10A cells and detected all three miRNAs in each transfected condition using qRT-PCR. miR-301a and miR-130b measurement was very specific, i.e. miR-301a was detected only in miR-301a mimic transfected cells and miR-130b only in miR-130b mimic transfected cells (Figure 38a and 38c). miR-301b detection was however slightly less specific as it recognized also, yet to a much smaller extent, miR-301a (Figure 38b). The relative expression levels between the two miRNAs detected by miR-301b primer in miR-301b and miR-301a transfected cells differed by over 600-fold. I assumed therefore, that although the miR-301b assay was not 100% specific, it was still giving acceptable results.

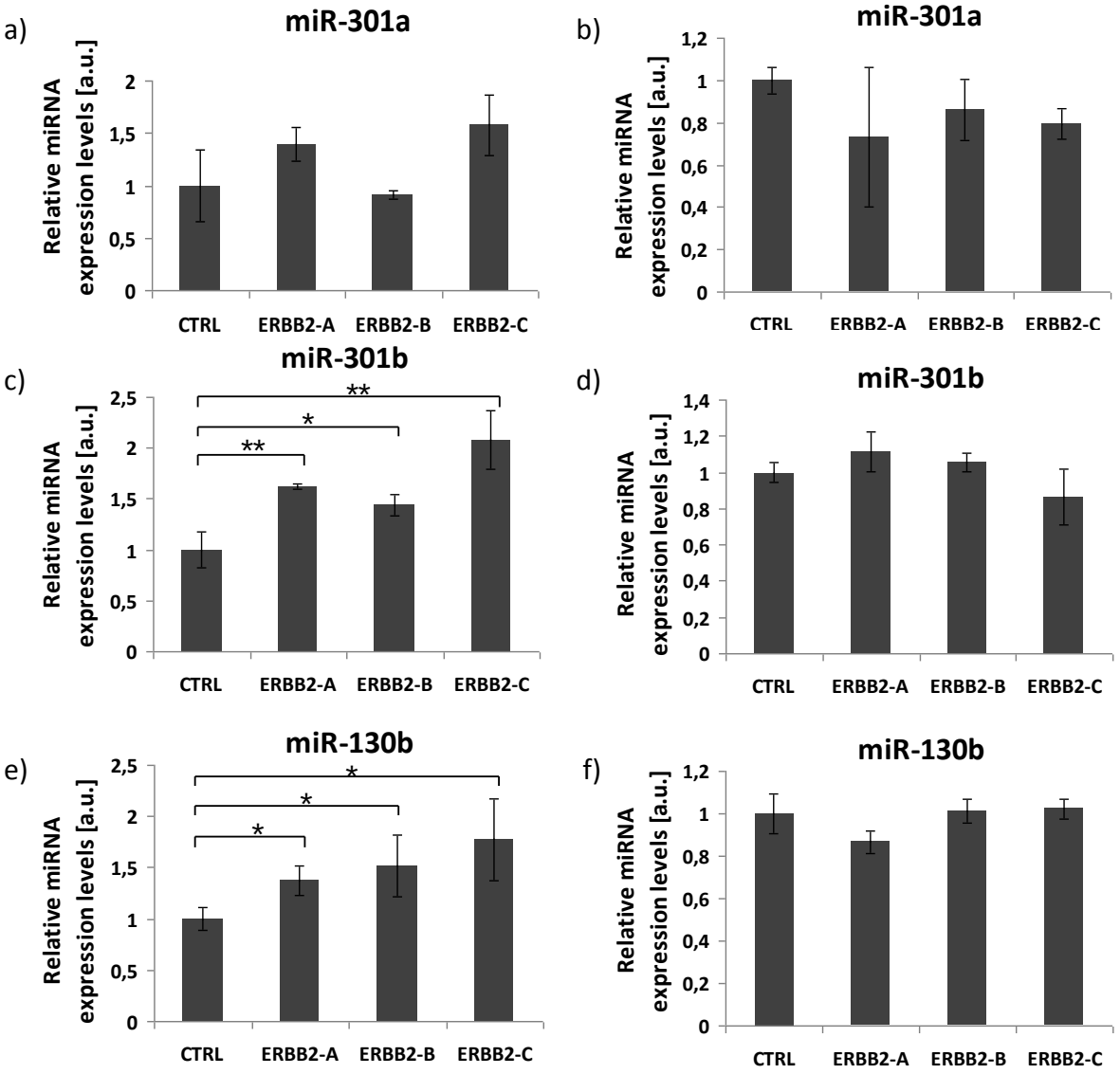

Figure 37

*Relative expression levels of miR-301a (a, b), miR-301b (c, d) and miR-130b (e, f) in CTRL, ERBB2-A, -B and –C cell line pools grown in either 3D culture (a, c, e) or in 2D culture (b, d, f), measured by qRT-PCR. Expression levels are represented as fold changes with CTRL cell pool as a reference. 4 biological and 3 technical replicates were used for 3D culture and 3 biological and 3 technical replicates were used for 2D culture. Statistical significance was tested using student's t-test. *p-value<0.05, **p-value<0.01*

Next, I wanted to check whether miR-301a, miR-301b and miR-130b expression is deregulated in breast cancer cell lines expressing different ERBB2 levels. For this purpose I used T47D, BT474, SKBR3 and UACC-812 cell lines which express ERBB2 at various levels (T47D < BT474 < SKBR3 < UACC-812, based on a report by Neve et al.)[333] and MCF10A cells as a negative control. Both miR-301b and miR-130b showed the highest expression levels in

the cell line expressing also the highest ERBB2 levels, UACC-812, and then gradually lower levels in SKBR3, BT474 and MCF10A (UACC-812 > SKBR3 > BT474 ≥ MCF10A), perfectly matching the levels of ERBB2 in these cell lines. That effect was not observed for miR-301a which showed the highest expression level in BT474 (Figure 39). For miR-301b and miR-130b, the T47D cell line did not follow this trend, as high expression level of miR-301b and moderate of miR-130b were detected there. As T47D expresses high levels of IGF1R and ERBB3 as well as above average expression levels of ERBB4 among other breast cancer cell lines, I speculate that these RTKs could activate similar signaling pathways leading to miR-301b induction. Another explanation could be that the RNA used for qRT-PCR was isolated from cell lines grown in 2D and not in 3D culture. As previously observed, the three-dimensional context was required for miR-301b and miR-130b induction by ERBB2 in MCF10A-derived stable cell line pools.

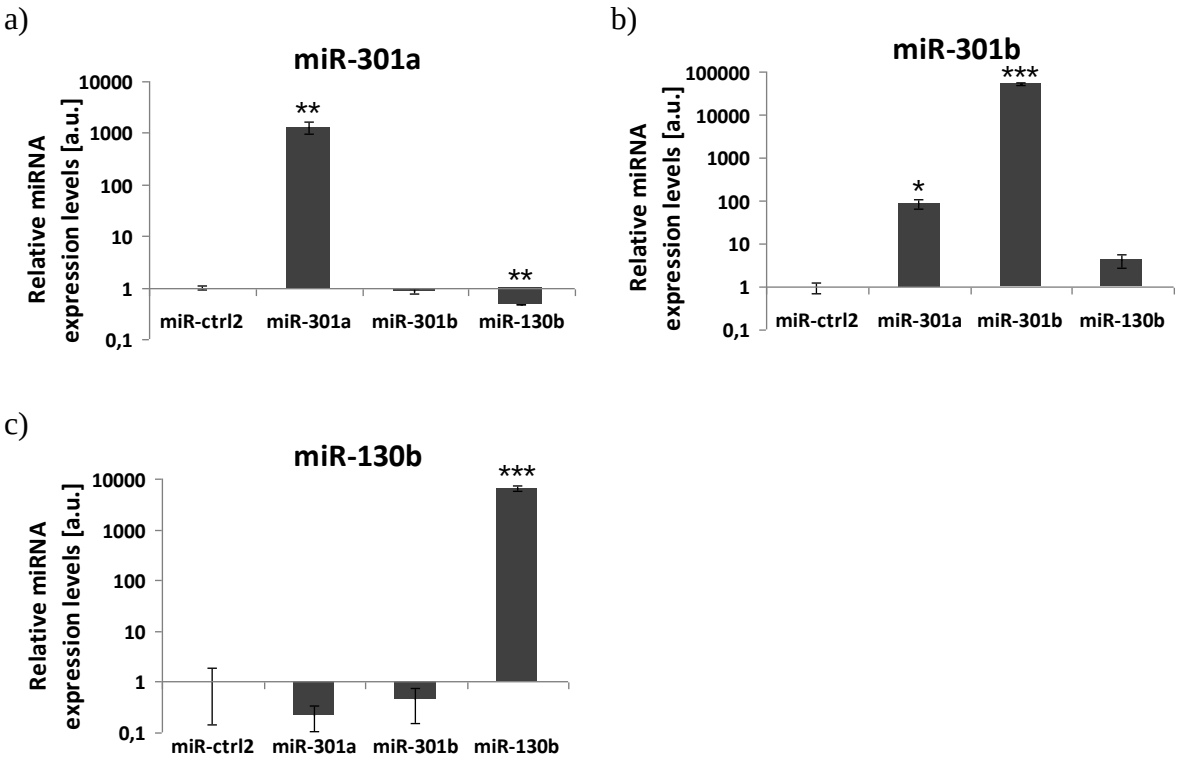

Figure 38

*Relative expression levels of miR-301a (a), miR-301b (b) and miR-130b (c) in miR-ctrl2, miR-301a, miR-301b and miR-130b transfected MCF10A cells, grown in 2D culture, measured by qRT-PCR. Expression levels are represented as fold changes with miR-ctrl2 transfected MCF10A cells as a reference. Note that logarithmic scale was used to better visualize miR-301a detection by miR-301b primer. 3 biological and 3 technical replicates were used. Statistical significance was tested using student's t-test. *p-value<0.05, **p-value<0.01, ***p-value<0.001*

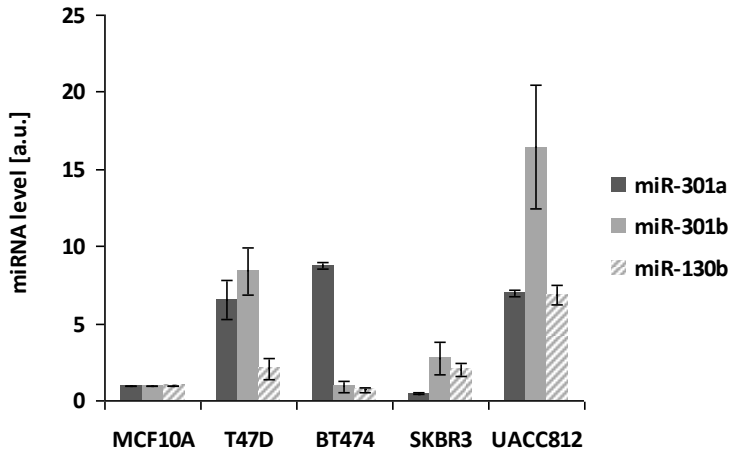

Figure 39

Relative expression levels of miR-301a, miR-301b and miR-130b in MCF10A, T47D, BT474, SKBR3 and UACC-812 cell lines grown in 2D culture, measured by qRT-PCR. Expression levels are represented as fold changes with MCF10A cell line as a reference. 3 technical replicates were used.

In parallel to my studies on miRNAs upregulated by ERBB2, in the collaborating group of Prof. Dr. Yosef Yarden at the Weizmann Institute of Science, several miRNAs were identified that are upregulated by EGF stimulation in MCF10A cells using miRNA microarrays. In the group of delayed upregulated miRNAs, miR-130b was found to be induced after 120 minutes of MCF10A incubation with EGF (Dr. Roi Avraham/Dr. Merav Kedmi, Figure 40a). Also, acetylation of histone 3 at lysine residue H3K27, an active chromatin mark, was elevated at the promoter located proximal to sequences coding for miR-301b and miR-130b at 60, 120 and 240 minutes time points following EGF stimulation (Dr. Yehoshua Enuka, Figure 40b). Since these observations suggested a link to exist between EGFR and ERBB2 in miR-301b and miR-130b induction, I wanted to validate this result in my system. qRT-PCR results showed, however, only slight elevation in the miR-130b expression level at 480 minutes after EGF stimulation, which was also not statistically significant (Figure 40c).

However, apart from miR-130b also three other oncogenic miRNAs from the list of ERBB2-dependent miRNAs presented in Table 2 were also found by colleagues at Weizmann Institute to be induced by EGF and classified as delayed upregulated miRNAs with ~120 minutes induction time point. This indicates that EGFR and ERBB2 might, nevertheless, drive expression of the similar pool of oncogenic miRNAs.

As mentioned before, miR-301b and miR-130b map to the same locus in the human genome, chr22q11.21 (chr22:22,007,270-22,007,347 and 22,007,593-22,007,674), and are likely

regulated by the same promoter. Around 100 transcription factor binding sites have been found upstream from the two genes by CHIP-seq by the ENCODE project (Figure 41).[359] Several of them bind transcription factors associated with the regulation of cell proliferation, survival and migration, including e.g.: MYC, YY1, RELA, EGR1, ETS1, FOS, FOSL1, JUNB, JUND, SP1, SP2 and ELF1. In particular, both MYC and YY1 overexpression in MCF10A had previously been shown to disrupt the regularity of acini structures formed by MCF10A cell line grown in Matrigel.[360,361] As most of these factors are downstream from MAPK and PI3K signaling, it is possible that expression of miR-301b and miR-130b could be cooperatively activated by ERBB-receptors. This, however, requires further investigation.

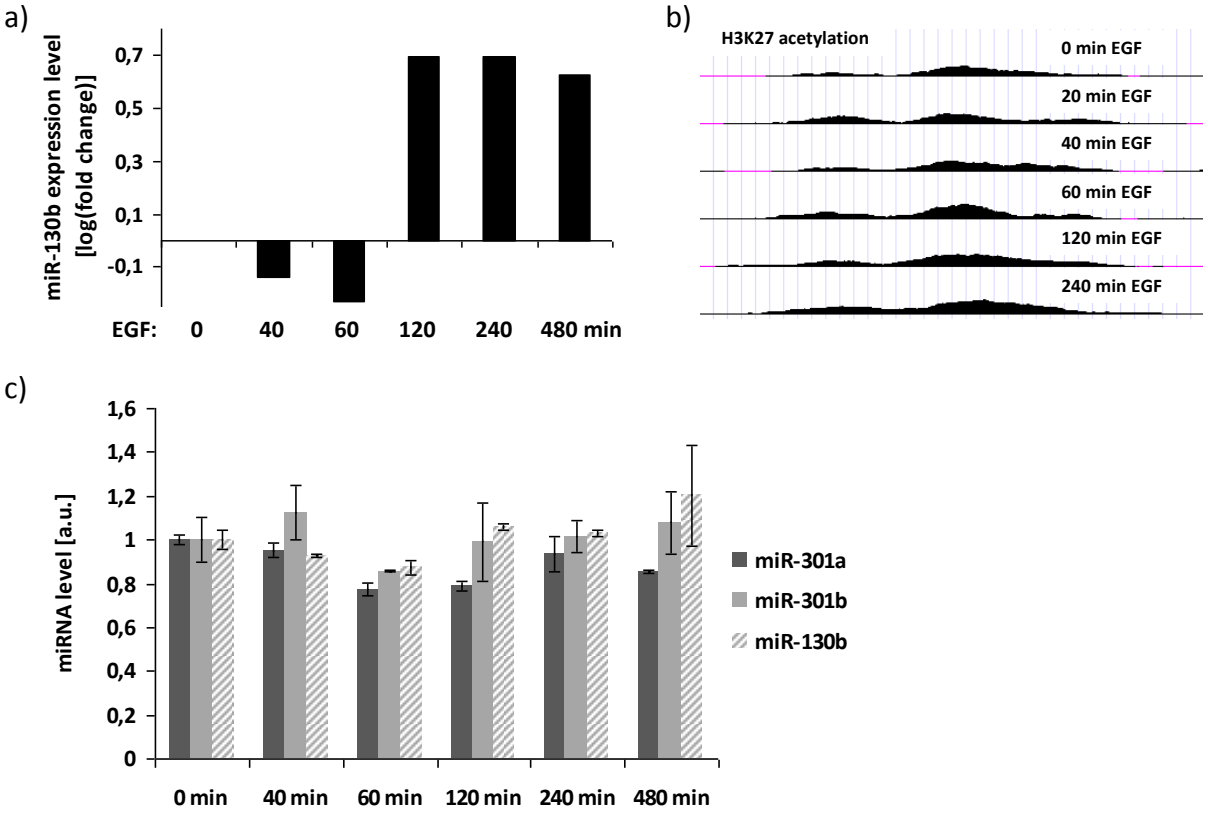

Figure 40

Expression levels of miR-301a (c), miR-301b (c) and miR-130b (a, c) after EGF stimulation detected on microarray (a) and validated using qRT-PCR (c), expressed as log(fold change) (a) or fold change (c) compared to 0 min time point. b) Relative H3K27 acetylation of common miR-301b and miR-130b promoter upon EGF treatment. Cells were starved with DMEM/F12 medium without additives for 20-24 hours prior to stimulations with 20 ng/ml EGF. Data kindly provided by Dr. Roi Avraham/Dr. Merav Kedmi (a) and Dr. Yehoshua Enuka (b).

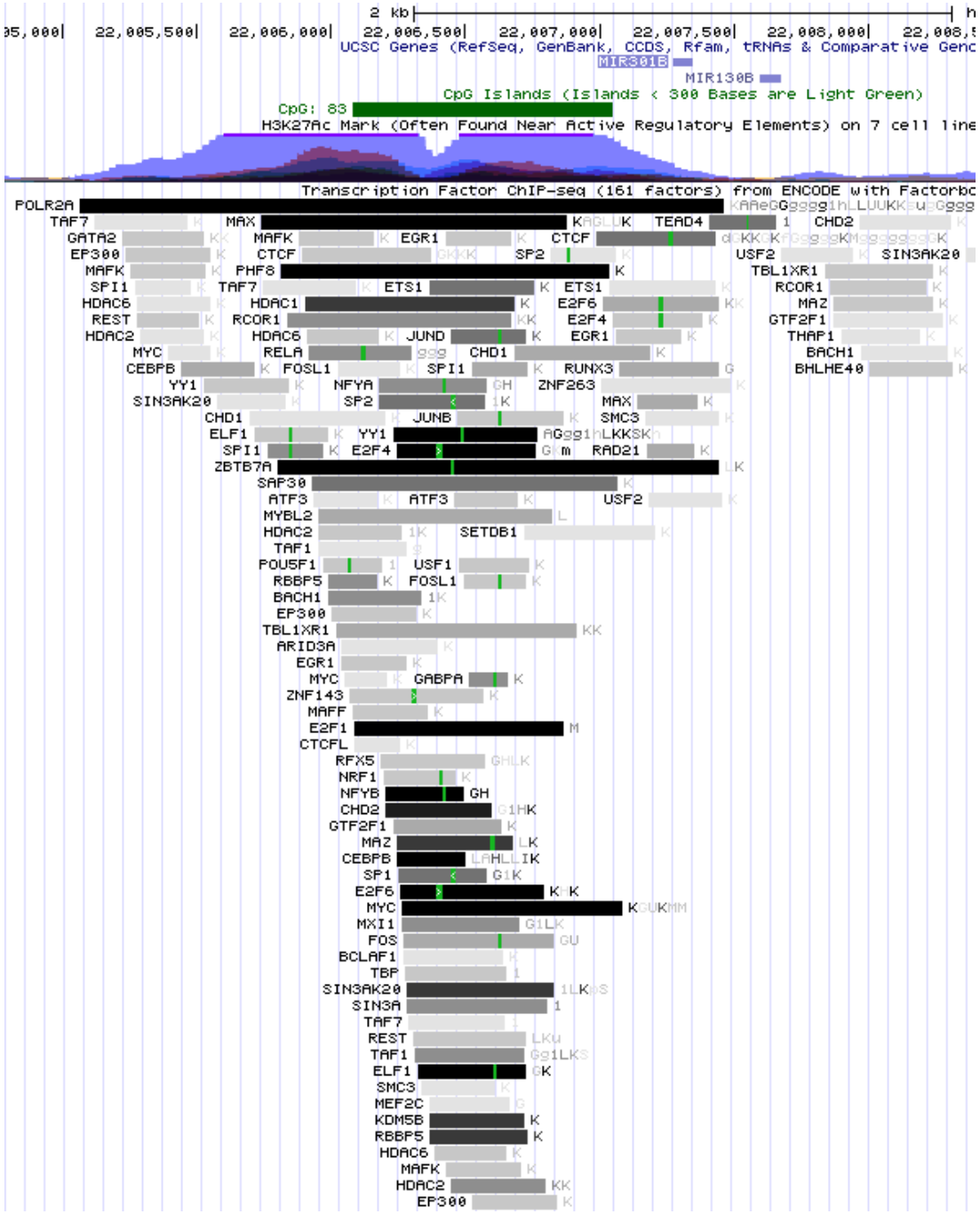

Figure 41

MIR301B and MIR130B genomic neighbourhood ecompassing promoter region and miRNA encoding genes (chr22:22005000-22008500). The image was taken from the UCSC Genome Browser and shows the genomic locus of miR-301b and miR-130b, as well as an upstream CpG island, active H3K27 acetylation marks and transcription factor bindind sites (TFBSs). TFBSs were detected by CHIP-seq in the ENCODE project.[359]

6.2.5 miR-301a, miR-301b and miR-130b increase cell proliferation, migration and invasion

To characterize the effects of miR-301b and miR-130b on cell viability, proliferation and migration, the respective miRNA mimics as well as miR-301a mimic were individually overexpressed in MCF10A cells. Viability was measured 72 hours after cell transfection, using either WST1 or Cell Titer Glo assays (see "Methods" chapter 5.5), in 2D culture. In both assays all three miRNAs significantly increased cell viability (by 20-50%, $p<0.001$), though to different extents (Figure 42a and 42b). The effect on cell viability was also measured 48 h or 72 h post-transfection with each of three miRNAs in two independent cell lines expressing little or no ERBB2 – MCF7 and MDA-MB-231.[333] In MCF7 all three miRNAs significantly increased cell viability (Figure 42c), while in MDA-MB-231 only miR-301b and miR-130b did (Figure 42d). This data shows that the miRNA effects on viability are not restricted to MCF10A.

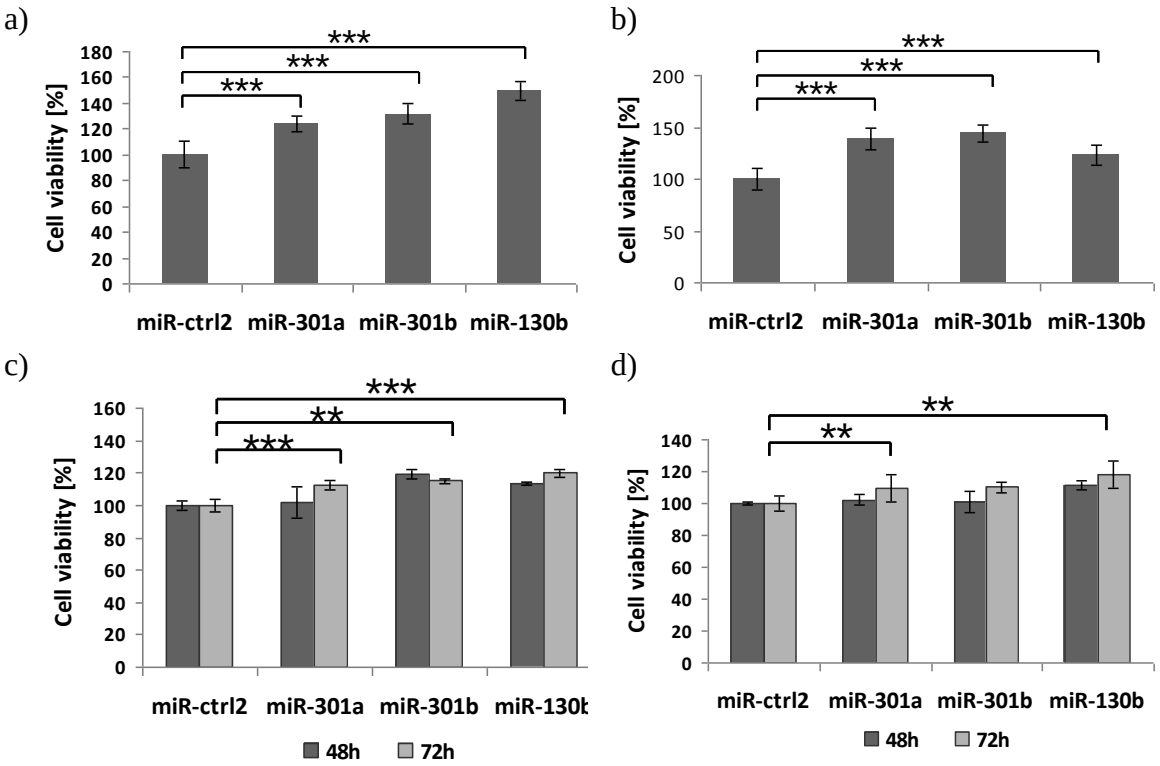

Figure 42

*Cell viability was measured 48 hours (a, b) or 48 and 72 hours (c, d) in MCF10A (a, b), MCF7 (c) and MDA-MB-231 (d) cell lines following miR-ctrl2, miR-301a, miR-301b and miR-130b transfection. Viability was measured either using CellTiterGlo assay (a, c, d) or WST1 assay (b), and compared to miR-ctrl2 transfected cells (shown in %). 5-6 biological replicates were used. Statistical significance was tested using student's t-test for 48h (a, b) or 72h (c, d) time point. **p-value<0.01, ***p-value<0.001*

Next, I investigated whether the observed changes in cell viability were also reflected by an induction of cell proliferation in MCF10A cells. To this end, equal numbers of cells were transfected with miR-ctrl2, miR-301a, miR-301b, or miR-130b, and cells were kept for 72 hours in MCF10A assay medium (containing reduced serum levels of 2% to avoid serum induction of cell proliferation)[362] in the presence or absence of EGF. The condition in which EGF is absent resembles more the situation found within the tumor mass, where growth factors penetrate less effectively than to its outer rim. In general, cell proliferation was higher in the presence of EGF. miR-301a and miR-301b increased cell proliferation irrespective of presence or absence of EGF, while miR-130b increased it only in the absence of EGF (Figure 43). miR-301a was the strongest activator of cell proliferation. The effect of this miRNA on cell proliferation had been previously shown by Shi and colleagues in MCF7 and T47D cells.[358] Here, I report it additionally in MCF10A cells.

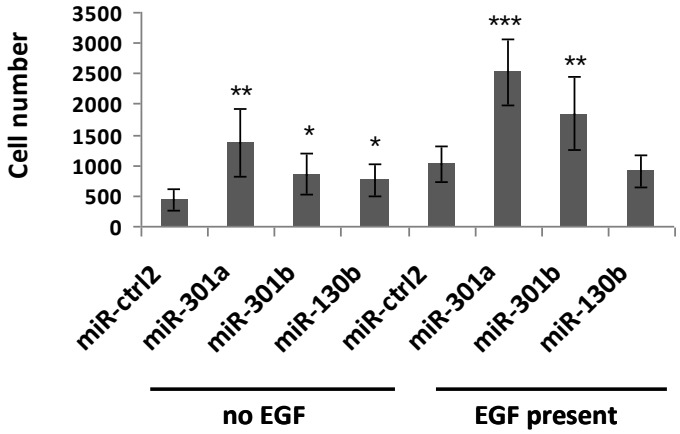

Figure 43
*Cell proliferation in MCF10A was measured 72 hours after transfection with miR-ctrl2, miR-301a, miR-301b and miR-130b. Cells were incubated either in the absence or presence of 5 ng/ml EGF in the medium containing reduced horse serum level (2%) for 48 hours prior to cell counting. The nuclei were stained with DAPI and then counted using Olympus scanning microscope. *p-value<0.05, **p-value<0.01, ***p-value<0.001*

As ERBB2 exerts its oncogenic properties via inducing cell proliferation and invasion, I next wanted to see if also miR-301b and miR-130b would affect cell migration and invasion in MCF10A. To this end, I performed two different types of migration assays – a wound healing assay and a Boyden chamber-based migration assay using the RTCA machine, as well as an invasion assay also using RTCA (Figure 44). In each case, after cell transfection with miRNAs,

cells were kept for 24 hours in assay medium (supplemented with 0.9% horse serum, no EGF) before the migration/invasion assay was started.

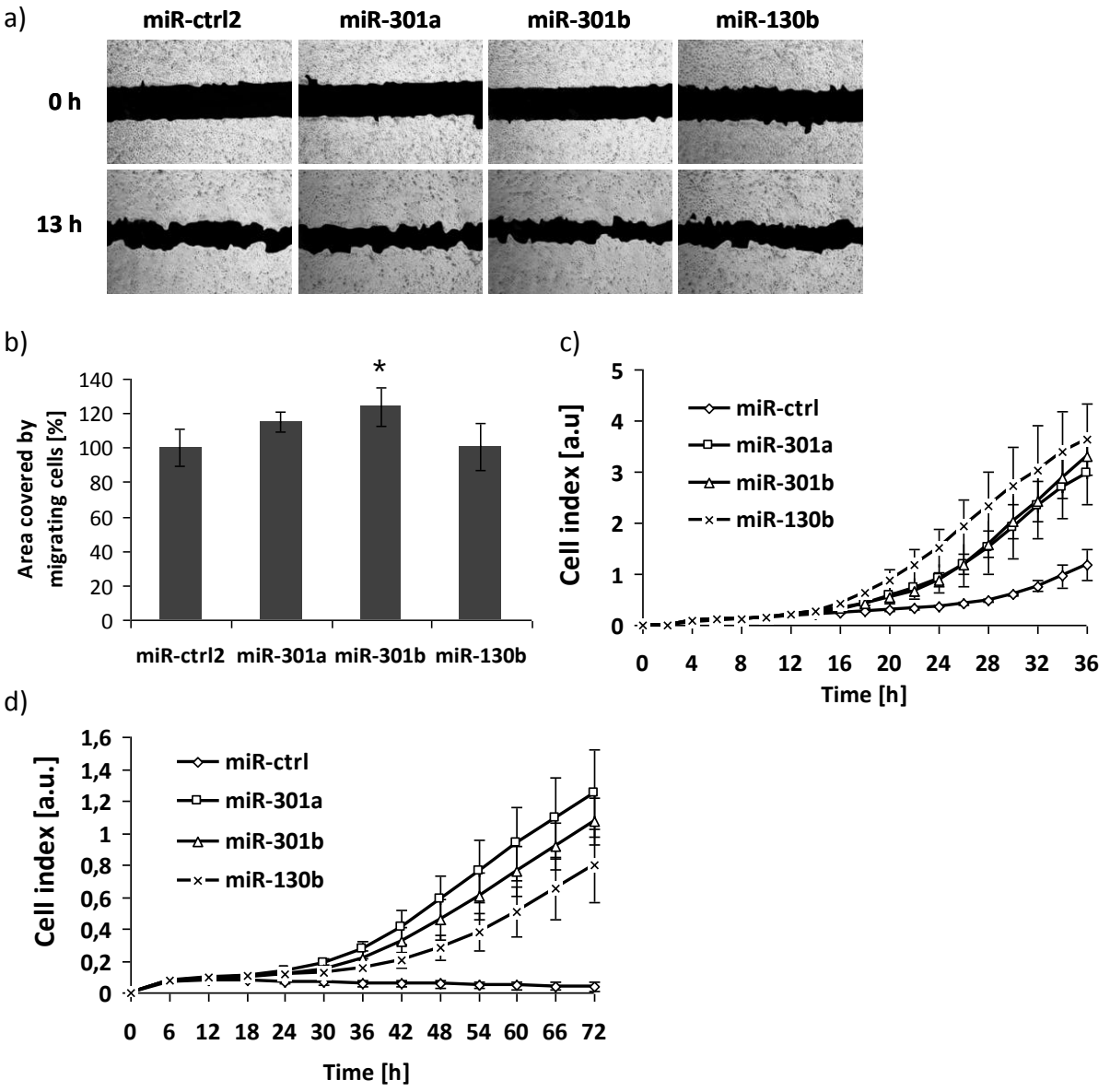

Figure 44

miR-301a, miR-301b and miR-130b increase cell migration and invasion in MCF10A cells. a) Cells transfected with miRNA mimics were kept in assay medium (0.9% horse serum, no EGF) for 24 hours before cells were allowed to migrate into the wound in the presence of 5% serum. Pictures were made at 0 and 13 hours time points. b) Quantification of the area covered by migrating cells are shown compared to miR-ctrl2 transfected cells. c, d) Cells transfected with miRNA mimics were kept in assay medium for 24 hours before the migration (c) or invasion through matrigel (d) was allowed. 5% horse serum was added to lower chambers of the CIM plates as chemoattractant. Cell index is shown for every 2 hours. Significance was measured using student's t-test at the 36 hours time point for migration assay (miR-301a: p= 0.0075; miR-301b: p= 0.00068; miR-130b: p = 0.0036) and 72 hours for invasion assay (miR-301a: p= 0.0011; miR-301b: p= 5.59E-05; miR-130b: p-value= 0.0019).

For analysis of the wound healing assay pictures were taken at 0h and 13h time points (Figure 44a). The area covered by migrating cells was then quantified, showing significant increase in migration for miR-301b transfected cells, but not for the other two miRNAs (Figure 44b). In the migration assay using RTCA, 5% serum was added as chemoattractant to the lower chambers of CIM plates. All three miRNAs induced increased migration rates towards higher serum concentration compared to the miR-ctrl2 (Figure 44c). The generally higher migration rates observed for miRNA-transfected cells in the RTCA assay may be due to the fact that cell migration measured by RTCA is induced towards the serum, and therefore is more directional, while there is no serum gradient in the wound-healing assay.

For the invasion assay the membranes in CIM plate upper chambers were covered with a thin layer of matrigel prior to cell seeding. Like in migration assay, 5% serum was used as chemoattractant in the lower chamber. miR-301b and miR-130b, along with miR-301a, increased significantly cell invasion (Figure 44d), mimicking the effect exerted by very high ERBB2 levels. While the connection between miR-301b and cell invasion discovered in this experiment is completely novel, miR-130b had been previously shown to modulate cell invasion either as an inducer or suppressor in other types of cancer. Here I show that in a semi-normal epithelial cell line it acts as an invasion inducer. The observation that miR-301a is involved in cell migration and invasion is in line with a previous report that this miRNA regulates cell migration in MCF7 and MDA-MB-231 and cell invasion in MDA-MB-231.[358]

6.2.6 miR-301a, miR-301b and miR-130b induce epithelial-mesenchymal transition of MCF10A cells grown in 2D cell culture

While all three miRNAs mimicked the ERBB2 effect on cell viability, proliferation and invasion, I wanted to see whether they also induce epithelial-mesenchymal transition. For this purpose, I overexpressed each of the miRNAs in MCF10A and examined the levels of modulated by ERBB2 EMT markers, i.e. E-cadherin, N-cadherin, ZEB1, fibronectin, the metalloproteinases MMP9 and MMP2, and of HB-EGF (Figure 45), which were all upregulated by ERBB2-overexpression in 2D cell culture. All three miRNAs influenced expression of only one of the four EMT markers tested, fibronectin, whose level was elevated.

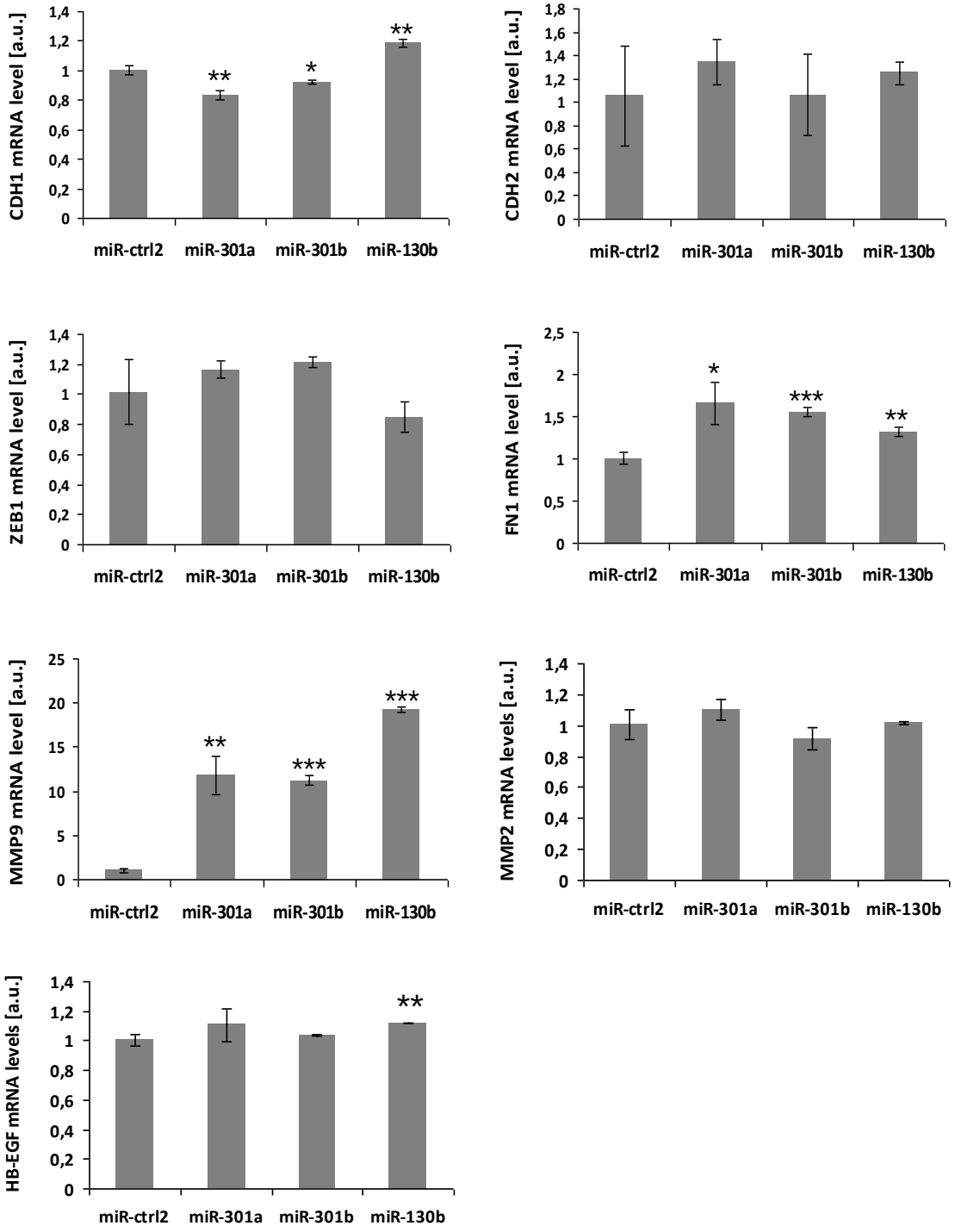

Figure 45

*RT-PCR (TaqMan) analysis of mRNA expression of four EMT markers (CDH1, CDH2, ZEB1, FN1), two metalloproteinases (MMP9 and MMP2) and HB-EG. MCF10A cells were transfected with miR-ctrl2, miR-301a, miR-301b and miR-130b and grown in 2D culture in full growth medium for 2 days before RNA was isolated. Y-axes represents fold changes in respect to miR-ctrl2 transfected cells. 3 technical replicates were used. Significance was measured using student's t-test. *p-value<0.05, **p-value<0.01, ***p-value<0.001*

E-cadherin levels were significantly (although not strongly) reduced by miR-301a and miR-301b but not by miR-130b which instead increased CDH1 levels. ZEB1, a negative regulator of E-cadherin, showed an inverse trend – its levels were slightly increased by miR-301a and miR-301b and decreased by miR-130b. Similar effects of miR-130b on the ZEB1/E-cadherin axes had been previously shown in two endometrial cancer cell lines, where miR-130b directly targeted ZEB1.[363] Its effect on E-cadherin is however inconclusive in endometrial cancer as miR-130b had been reported to induce EMT (and to downregulate E-cadherin level) in two other endometric cancer cell lines by directly targeting DICER1 and to play a rather oncogenic role.[364] Here I show that in MCF10A cells grown in 2D culture miR130b slightly increases E-cadherin mRNA levels.

While none of three miRNAs mimicked the ERBB2 effect on N-cadherin, MMP2 and HB-EGF (apart from a slight induction by miR-130b), MMP9 was very potently induced by each miRNA with the strongest effect observed for miR-130b. miR-130b has been recently shown to act as a powerful oncogenic miRNA and invasion inducer in colorectal cancer and miR-301a in breast cancer.[365,366,358] The observation that these miRNAs along with miR-301b are the novel, strong regulators of MMP9 further supports their oncogenic function in breast cancer and can explain the induction of cell invasion reported in the previous chapter.

6.2.7 miR-301a and miR-301b target similar subsets of genes, several of which are also targeted by miR-130b

To identify targets of miR-301a, miR-301b and miR-130b in a comprehensive manner the respective miRNA mimics along with miR-ctrl2 were overexpressed individually in the MCF10A cell line, in 3 biological replicates. Two days post-transfection, RNA was isolated and samples prepared for genome-wide mRNA profiling using microarrays (see “Methods”, chapter 5.16). Prior to sample submission, RNA quality was checked and miRNA overexpression was confirmed (Figure 46). Differential gene expression analysis between each of three miRNAs and miR-ctrl2 revealed 96 genes that were significantly ($p<0.05$) downregulated by at least 30% by miR-301a, 84 genes by miR-301b and 357 genes by miR-130b. The lists of these genes can be found in Supplementary Tables 3-5. While differential gene expression analysis cannot identify those miRNA targets whose expression is affected by translational repression and is limited to pointing out the genes whose mRNA

is degraded upon miRNA binding, it is currently the most feasible high throughput technique to find potential miRNA targets.

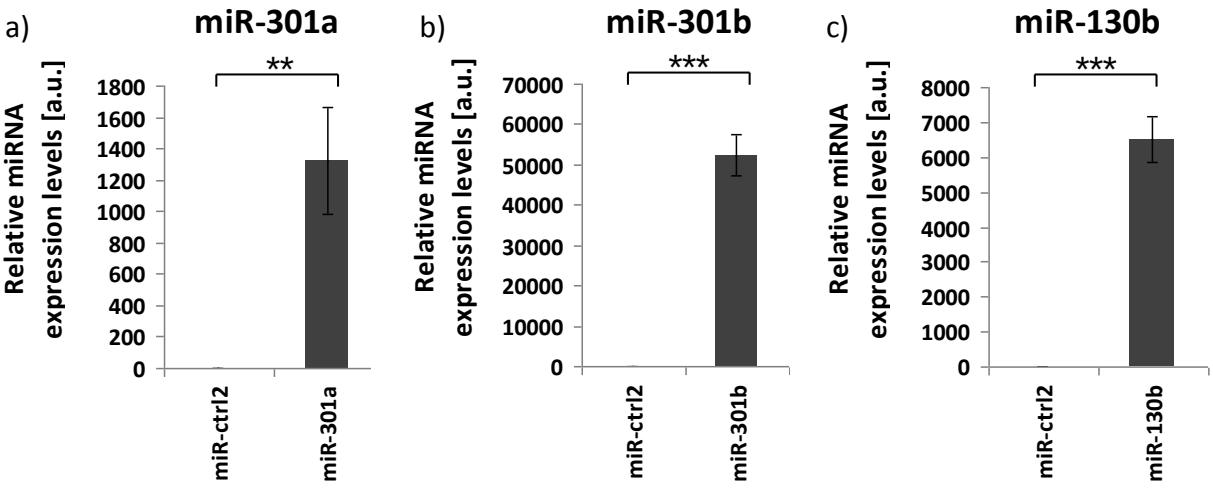

Figure 46

*RT-PCR (TaqMan) analysis of miRNA expression in miR-301a, miR-301b and miR-130b transfected MCF10A cells grown in full growth medium in 2D culture. RNA was isolated 2 days post-transfection. Y-axes represents fold changes in respect to miR-ctrl2 transfected cells. 3 biological and 3 technical replicates were used. Significance was measured using student's t-test. **p-value<0.01, ***p-value<0.001*

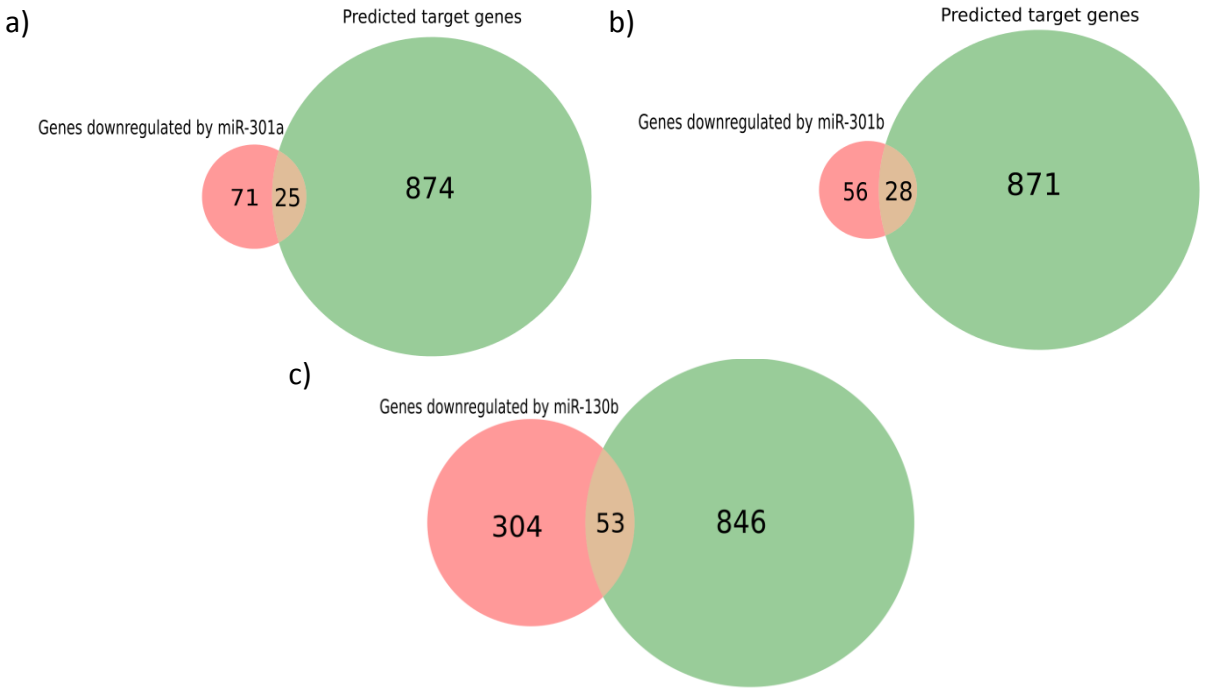

Figure 47

Genes whose expression was detected to be downregulated by at least 30% by miR-301a (a), miR-301b (b) and miR-130b (c) using whole genome expression profiling, were overlapped with pools of genes predicted by TargetScan 6.2 to be direct targets of each of three respective miRNAs. The numbers shown indicate how many genes belong to either only downregulated pool of genes, only predicted pool of genes, or to both (overlap).

Figure 47 shows how many of these genes are predicted by a miRNA target prediction tool - TargetScan 6.2 - to be direct targets of the respective miRNAs. Although several other prediction tools have been developed up to date, TargetScan was selected here as it takes evolutionary conservation and the context of predicted sites into account. This tool had been also reported to perform very well in detection of functional sites in comparison to other miRNA target prediction tools.[280]

Table 5

The sequences and seed sequences of miR-301a, miR-301b and miR-130b (upper panel) as well as miR-519a (lower panel). Notice that miR-301a and miR-301b differ only by two nucleotides (highlighted in bold) and that the seed sequence of miR-519a is shifted by just one base as compared to those of miR-301a, miR-301b and miR-130b.

microRNA	sequence	seed sequence
hsa-miR-301a	cagugcaau**ag**uauugucaaagc	agugca
hsa-miR-301b	cagugcaau**ga**uauugucaaagc	agugca
hsa-miR-130b	cagugcaaugaugaaagggcau	agugca
hsa-miR-519a	aa**agugca**uccuuuuagagugu	aagugc

Since miR-301a, miR-301b and miR-130b share the same seed sequences (Table 5) and showed similar effects on cell proliferation, migration and invasion, I hypothesized that some genes should be downregulated in common by all three miRNAs. Indeed, 53 genes (Supplementary Table 6) were downregulated by at least 30% (for at least one probe found on microarray) by each of three miRNAs and 19 of them, listed in Figure 48, were also predicted as direct targets by TargetScan.

From the list of 19 genes only 9 genes were downregulated by more than 15% for at least one probe present on the microarray in the whole-genome mRNA profiling in very high ERBB2 expressing cells (ERBB2-B or ERBB2-C) compared to CTRL cells - both grown in 3D cell culture (Table 6). These are: C9ORF69 (chromosome 9 open reading frame 69), CDS1 (CDP-diacylglycerol synthase 1), IMPDH1 (inosine 5'-monophosphate dehydrogenase 1), SLC44A1 (solute carrier family 44 member 1), VPS24 (CHMP3; charged multivesicular body protein 3), ZAK (sterile alpha motif and leucine zipper containing kinase AZK), ZMAT3 (Wig-1; zinc finger, matrin-type 3), CLIP1 (CAP-GLY domain containing linker protein 1) and PMEPA1 (prostate transmembrane protein, androgen induced 1). However, the last two did not show the

decrease for the majority of the probes present on the microarray. Remarkably, in this list a negative regulator of EGFR trafficking and degradation was found - VPS24[367,368], as well as two pro-apoptotic proteins – ZAK and ZMAT3. ZAK inhibits cell proliferation in lung cancer[369], while ZMAT3 regulates apoptosis by binding to and stabilizing the 3'UTR of p53.

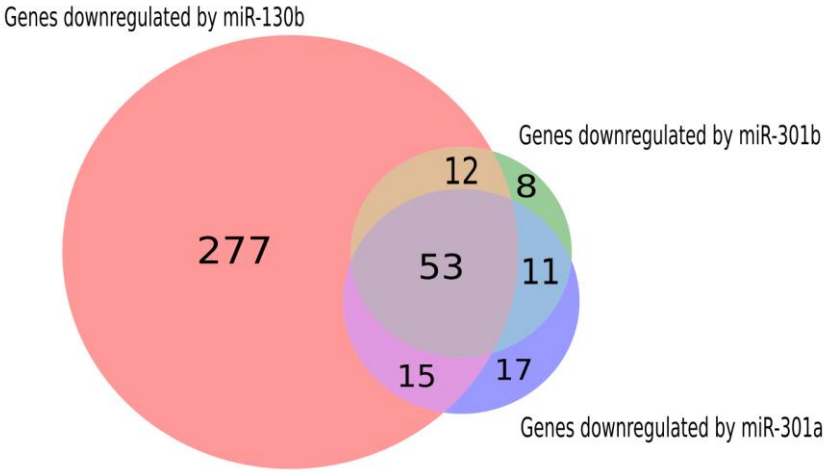

Downregulated by 3 miRNAs and predicted by TargetScan
ACVR1
C9orf69
CDS1
CLIP1
HPRT1
IMPDH1
MTMR9
PMEPA1
PSAP
RPS6KA2
RTCD1
SKP1
SLC44A1
STX6
TMEM9B
VPS24
VPS37A
ZAK
ZMAT3

Figure 48

Venn diagram showing genes whose expression was detected to be downregulated by at least 30% by miR-301a (a), miR-301b (b) and miR-130b (c) using genome-wide mRNA expression profiling. The numbers shown indicate how many genes were downregulated by the respective miRNAs, each pair of two miRNAs, or all three miRNAs in common. Genes downregulated by at least 30% by all three miRNAs and predicted to be direct targets by TargetScan are listed in alphabetical order in the table.

Table 6

*List of genes that were: 1) downregulated by miR-301a, miR-301b and miR130b by at least 30% for at least one probe present on the microarray as detected using whole genome mRNA profiling; 2) predicted as direct targets of miR-301a, miR-301b and miR130b by TargetScan; 3) downregulated in ERBB2-B or -C cell line pools by at least 15% for at least one probe present on the microarray compared to CTRL pool in 3D cell culture as detected in whole genome mRNA profiling; Levels of downregulation are indicated; *up - upregulation*

	ERBB2-B vs CTRL				ERBB2-C vs CTRL			
Gene	**Probe 1**	**Probe 2**	**Probe 3**	**Probe 4**	**Probe 1**	**Probe 2**	**Probe 3**	**Probe 4**
C9ORF69	11%	-	-	-	21%	-	-	-
CDS1	18%	-	-	-	19%	-	-	-
IMPDH1	26%	14%	10%	7%	31%	10%	6%	14%
SLC44A1	27%	17%	-	-	28%	10%	-	-
VPS24	33%	25%	2% up*	-	26%	19%	1%	-
ZAK	34%	18%	15%	-	26%	23%	15%	-
ZMAT3	18%	13%	-	-	17%	28%	-	-
CLIP1	23%	5%	8% up*	-	14%	3% up*	9% up*	-
PMEPA1	21%	18%	4%	1% up*	28%	29%	2%	3%

6.2.8 miR-301b and miR-130b target similar subset of genes as miR-519a

As shown in Table 5, the seed sequences of miR-301b and miR-130b are shifted by just one nucleotide compared to miR-519a - a miRNA recently reported in our research group to target a network of negative cell cycle regulators: p15 (CDKN2B), PTEN and p21 (CDKN1A), as well as estrogen receptor 1 (ESR1), and to drive tamoxifen resistance.[370] I hypothesized that the ERBB2-induced miRNAs could also affect expression of those genes. Hence, I transfected MCF7 cells with psiCheck2 reporter vectors expressing luciferase under the control of 3'UTR sequences from either of four genes (ESR1, p15, PTEN and p21) along with one of three miRNA mimics: miR-ctrl2, miR-301b or miR-130b (for details see "Methods", chapter 5.11.1). MCF7 cell line was used as the transfection efficiency of MCF10A with bigger plasmids like psiCheck2 is very low, irrespective of the transfection reagent used. I wanted also to be able to directly compare results which had previously been obtained for miR-519a in MCF7 with those obtained for these two miRNAs. Upon overexpression of miR-301b or miR-130b the luciferase signal decreased significantly for three out of four genes tested: ESR1, PTEN and p21, with the strongest signal reduction observed for ESR1, indicating that these miRNAs target important cell cycle regulators in the same manner as miR-519a (Figure 49). Only the

p15 3'UTR was not targeted by miR-301b and miR-130b. This is in line with miRNA target predictions by TargetScan algorithm, which indicated ESR1, PTEN and p21, but not p15, as potential miR-301a/301b/130b target genes.

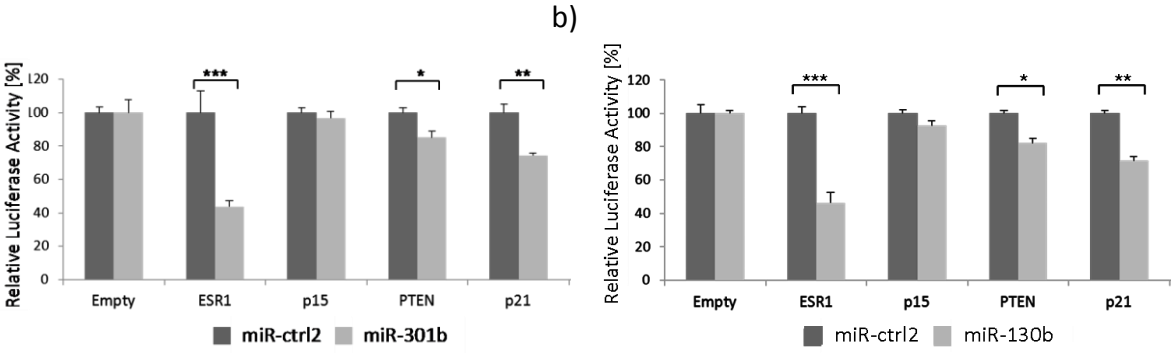

Figure 49

*ESR1, PTEN and p21 3'UTRs are targeted by miR-301b and miR-130b. miR-ctrl2 (a, b), miR-301b (a) and miR-130b (b) were overexpressed in the MCF7 cell line along with either empty psiCheck2 Renilla luciferase reporter vector or the same vector containing the 3'UTR of either estrogen receptor 1 (ESR1), p15, PTEN or p21. The Renilla luciferase signal was double normalized – first to the Firefly luciferase signal (cell number normalization) and then to the signal obtained from cells transfected with empty vector (to exclude the effect of 3'UTR-independent luciferase targeting by miRNA). Values are shown as % of the signal obtained for miR-ctrl2 transfected cells for each 3'UTR. Five biological replicates were used. Significance was measured using student's t-test. *p-value<0.05, **p-value<0.01, ***p-value<0.001*

However, in the data obtained from whole-genome mRNA profiling of MCF10A cell line, only CDKN1A was downregulated by each of the three miRNAs (by ~30% compared to control). As this suggested possible differences in miRNA function between normal (MCF10A) and cancer (MCF7) cell lines, I wanted to see whether targeting of ESR1, PTEN and p21 might also occur in breast cancer. To this end I correlated expression levels of miR-301b and miR-130b with mRNA expression levels of those genes. Since no data was available for miR-301b in the GSE22220 dataset, I correlated the expression levels of miR-301a, having a target spectrum very similar to that of miR-301b (see chapter 6.2.7) as well as of miR-130b with ESR1 expression. Inverse correlations were observed for both miRNAs (Figure 50a and b). Both miRNAs were also inversely correlated with PTEN (Figure 50c and d) but not p21 mRNA levels.

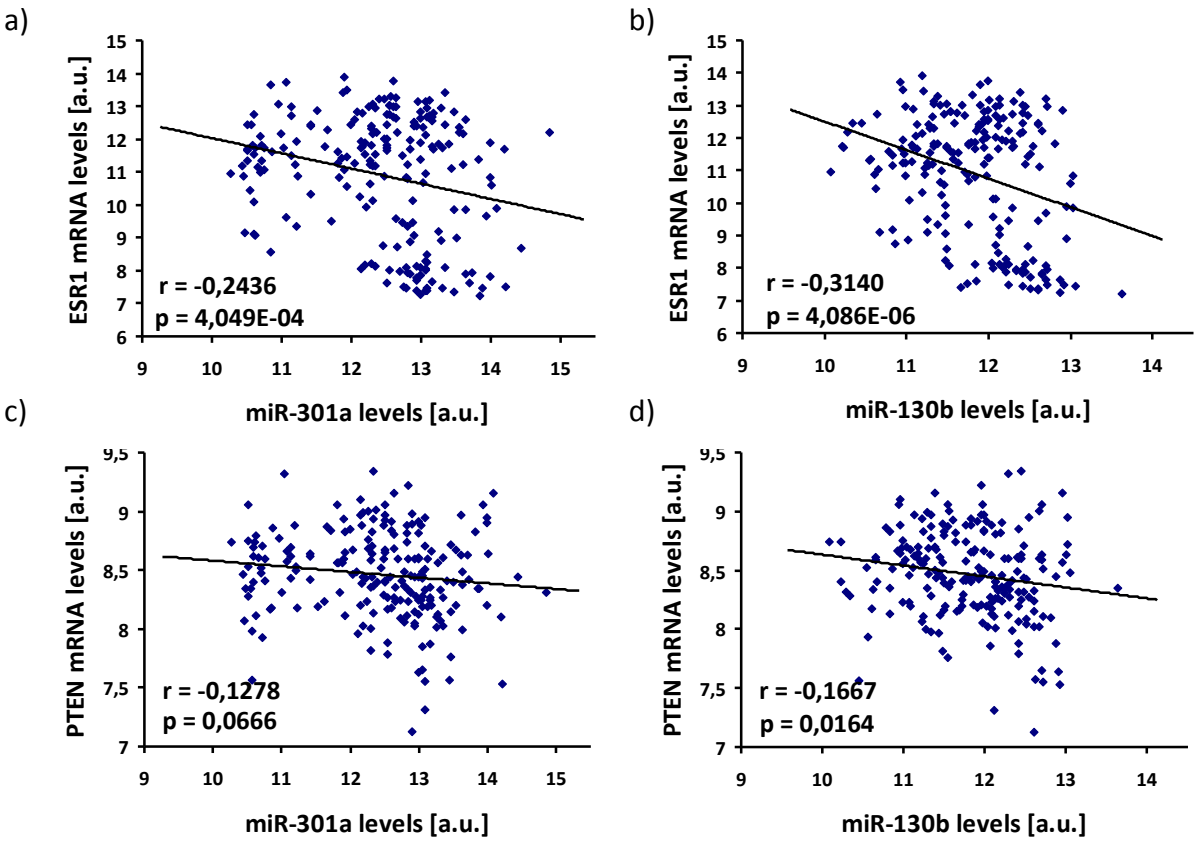

Figure 50

Correlations of miR-301a and miR-130b expression levels with ESR1 (a) or PTEN (b) mRNA expression levels in tumors from GEO22220 patient dataset. Correlation coefficients and p-values for ESR1 and PTEN are indicated in the graphs. For p21 correlations were not significant - probe 1: r = -0.0357, p = 0.6082; probe 2: r = 0.0680, p = 0.3292 for miR-301a; and probe 1: r = 0.0443, p = 0.5252; probe 2: r = 0.0783, p = 0.2611 for miR-130b.

I had previously seen a weak downregulating effect of miR-519a on ERBB2IP (whole-genome mRNA profiling data in SKBR3 cell line, not validated) - a negative regulator of ERBB2, whose downregulation had been reported to be associated with trastuzumab resistance in ERBB2-positive breast cancer and cell migration.[371] While ERBB2IP is also predicted by TargetScan and miRanda to be a target gene of the three miRNAs, I overexpressed miR-301a, miR-301b and miR-130b in MCF10A cell line and checked ERBB2IP levels by qRT-PCR.[372] All three miRNAs decreased ERBB2IP on mRNA level (Figure 51a). Moreover, ERBB2IP expression was also decreased in ERBB2-overexpressing stable cell line pools grown in 3D culture but not in 2D (Figures 51b and 51c), which supports the hypothesis that ERBB2 downregulates ERBB2IP via upregulation of miR-301b and miR-130b as they are only induced in 3D culture.

Consequently, knowing that ERBB2-regulated miRNAs downregulate both: ERBB2IP and PTEN (also very thoroughly studied in the context of trastuzumab resistance), I checked if

these miRNAs could induce trastuzumab resistance. To this end each of three miRNAs was overexpressed in trastuzumab sensitive SKBR3 cell line and 24 hours after transfection cells were treated with 50 nM or 200 nM trastuzumab or left untreated. 3 days later cell viability was measured to assess sensitivities to the drug treatment. As negative control, miR-ctrl2 transfected cells were used. However, none of the miRNAs showed an effect on trastuzumab sensitivity (Figure 52) suggesting that the tested miRNAs do not directly induce trastuzumab resistance in SKBR3.

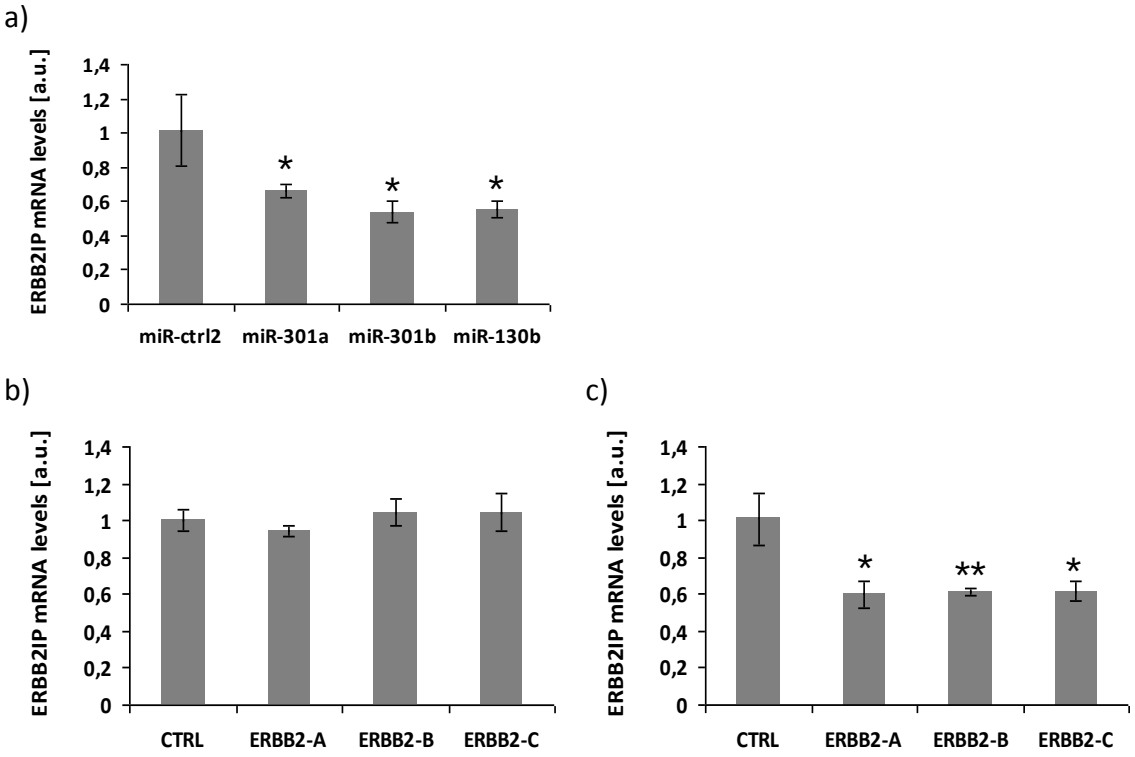

Figure 51

*RT-PCR (TaqMan) analysis of ERBB2IP mRNA expression in miR-ctrl, miR-301a, miR-301b and miR-130b transfected MCF10A cells (a) as well as in CTRL, ERBB2-A, ERBB2-B and ERBB2-C stable cell lines grown in 2D (b) or 3D (c) cell culture. Cells were grown in 2D culture for 3 days in full growth medium and in 3D culture for 9 days in assay medium containing 5 ng/ml EGF before RNA isolation. The expression levels are shown as fold changes relative to control cell pool (CTRL). 2 biological and 3 technical replicates were used. Significance was measured using student's t-test. *p-value<0.05, **p-value<0.01*

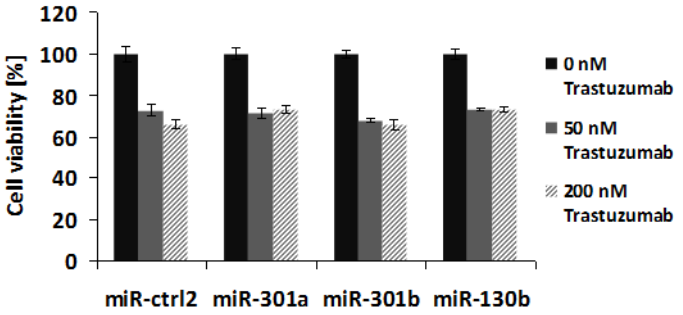

Figure 52

Trastuzumab sensitivity was measured in SKBR3 cell line. Cells were transfected with either miR-ctrl2, miR-301a, miR-301b or miR-130b and after 24 hours the medium was supplied with either 0, 50 or 200 nM of trastuzumab. Cell viability was measured 72 hours later using CellTiter Glo assay and is shown as % of viability measured for the cells untreated with trastuzumab. Significance was measured using student's t-test.

7. Discussion

Currently the type of treatment for ERBB2-positive breast cancer patients does not depend on whether ERBB2 is expressed at moderate, high or very high levels. As long as the tumor stains IHC3+ and/or is FISH-positive for ERBB2, the doctors in care of a patient will decide whether or not to treat the patient in adjuvant or neo-adjuvant setting with one of a few possible HER2-targeted therapies (described extensively in chapter 3.2.5). These can be administred in combination with chemotherapy, or as a monotherapy. Patients can be additionally or alternatively treated with ER-targeted drugs (for ER-positive tumors) and radiation therapy (if the tumor has metastasized). All these treatmens would usually be given at the set dosage for a particular drug or drug combinations, with only few exceptions, and the dose would not depend on ERBB2 levels found in the tumor.

My study, however, shows that patients not treated with an anti-HER2 therapy, who express very high ERBB2 levels, are associated with worse prognosis than those with moderate ERBB2 levels. It also indicates that cellular phenotype of ERBB2-overexpressing cells strictly depends on the receptor level. I report that the semi-normal epithelial breast cells (MCF10A) ectopically expressing very high ERBB2 levels are much more invasive when grown in 3D culture than cells expressing moderate ERBB2 levels and ERBB2-negative cells. Furthermore, I show that ERBB2 has a dose-dependent effect on induction of epithelial-to-mesynchymal transition (EMT), activation of migration/invasion-regulating genes and miRNA expression. These observations lead, thus, to the question whether or not further stratification of ERBB2-overexpressing patients according to their ERBB2 receptor level as well as following studies aimed at optimization of their treatment should be considered. The development of a more quantitative method to detect ERBB2 overexpression in clinics, ideally being able to detect the presence of subpopulations of cells within a tumor with very high receptor levels could help answer this question.

My study, apart from explaining ERBB2-dose dependent effects, shows that gene expression regulation by ERBB2 differs between 2D and 3D cell culture. In particular, I show that on one hand a few EMT markers are induced by ERBB2 in 2D but not in 3D environment and on the other hand, that two newly identified ERBB2-depenent miRNAs – miR-301b and miR-130b are induced by ERBB2 in 3D but not in 2D cell culture. These findings stress the importance

of cellular environment in regulation of gene expression. Researchers studying RNA/protein function *in vitro* still often limit their studies to 2D cell culture conditions which neglect the influence of three-dimensional environment on RNA/protein activity. They also rarely investigate the effects exerted by different levels of their molecules of interest, often overexpressing them at (and/or inhibiting them to) only one level. Importantly, this study suggests that such an approach might lead to an incomplete understanding of the function of a given RNA/protein.

Stratification of ERBB2-positive breast cancer patients

The current guideline of the American Society of Clinical Oncology and the College of American Pathologists (ASCO-CAP)[21] states that for the diagnosis of ERBB2-positive breast cancer at least 10% of tumor cells in the invasive part of the tumor should stain homogenously for the ERBB2 protein (IHC staining). The cut-off had been 30% before, also set by ASCO-CAP[179], and both METABRIC and TCGA dataset that I reanalyzed for the result part of this thesis are associated with this cut-off. While ERBB2-targeted therapies proved to be beneficial for the patients with lower ERBB2 staining (10-30% of invasive part of the tumor)[373], little is known about the differences in patients' responses to the drugs between those with tumors expressing very high ERBB2 levels in comparison to other ERBB2-positive tumors. According to a study published by Monogram Biosciences, the total level of detected ERBB2 in breast cancer by their novel quantitative VeraTag technique (described in the "Introduction") varied by 1808-fold in all tumors and by 69-fold in only ERBB2-positive patients (defined by immunohistochemistry).[200] The same group suggests that tumors with the highest ERBB2 levels (~13% of ERBB2-positive tumors) might be insensitive to trastuzumab.[194] While the study itself is rather preliminary, it introduces an idea that ERBB2-positive patients can be further stratified and should be potentially also differently treated.

In my study I have shown that cells expressing very high ERBB2 protein levels are more invasive than those with moderate ERBB2 levels and that patients with tumors expressing very high ERBB2 mRNA levels are characterized by shorter disease-specific survival than those with intermediate mRNA levels. Similarly, in 2010, J. Staaf et al. showed that ERBB2-positive patients could be also stratified according to their ERBB2 copy number into three groups with different time of overall survival. In that study the patients were first sorted according to their ERBB2 copy number and then divided into three groups: lower 15% of all

ERBB2-positive patients (with lowest ERBB2 copy number), intermediate (with medium copy number) and top 15% (with highest copy number). Such division of breast cancer patients could better stratify them into better and worse survivers than dividing them with cut-offs of: lower 25%, intermediate and top 25%.[175] Recently also E. Fuchs et al. showed that high-level amplification of ERBB2 leads to shorter time to metastasis, yet, it is associated with better response to trastuzumab treatment.[374] Other attempts of ERBB2-positive breast cancer patients' stratification included stratification into two groups by TOP2A (topoisomerase DNA II alpha) expression, where patients with TOP2A-positive tumors were better survivers than TOP2A-negative, or by LOXL2, were patients with higher LOXL2 expression were worse survivers than those with low LOXL2 levels.[175,375]

Detection of ERBB2 at mRNA and protein levels

As far as the quantification of ERBB2 receptor levels is concerned, the current breast cancer treatment guideline indicates the need of ERBB2 testing at DNA and/or protein level to decide wether or not to subject a patient for ERBB2-targeted therapy. However, recently emerging breast cancer signatures tend to detect expression levels rather of groups of genes at mRNA level. In one of the studies it has been therefore investigated whether the mRNA expression levels of ER/PR/ERBB2 could equally well predict the patients' outcome as ER/PR/ERBB2 protein levels determined by IHC. The authors state that in fact the mRNA levels could even better stratify the patients into better and worse survivers.[330] Considering results presented in this thesis, this maybe partly due to better quantification of ERBB2 receptor expression using RNA rather than poorly quantitative IHC.

However, some of the well-established breast cancer signatures, like e.g. Mammaprint do not test ERBB2 mRNA expression due to its lower predictive value of recurrence risk than a 70-gene signature.[376] It could be therefore more informative to detect ERBB2 expression, nevertheless at the protein level but using a more quantitative method than standard IHC. While in breast cancer ERBB2 protein and mRNA levels correlate relatively well, it has to be pointed out that in other tumor types, e.g. soft tissue sarcomas, mRNA and protein levels of ERBB2 have inverse prognostic values with high mRNA levels being associated with better overall survival and higher protein levels with poorer recurrence-free survival.[377] Developing a quantitative tool for ERBB2 protein measurement could thus serve beyond breast cancer.

The Reverse Phase Protein Array technology, which I also used in the course of my project, might be a useful technology along these lines.

Induction of cell invasion by very high ERBB2 levels versus double-hit models

In the "Results" part of this thesis I focused on the impact ERBB2 protein levels have on the induction of cell invasion, using stable cell line pools. While cell pools with different receptor levels were obtained via FACS sorting of cells infected with retroviral vectors, I decided to use two pools with very high ERBB2 levels (ERBB2-B and ERBB2-C) to ensure that observed phenotypes are not cell pool-dependent. While in most of the functional experiments the ERBB2-C cell pool showed slightly stronger phenotypes than ERBB2-B, in experiments involving RPPA and mRNA profiling this balance was reverted. That could be due to potential small differences in cell passage number accompanied by preferential proliferation of some cellular clones within both cell line pools within few passages. Nevertheless, ERBB2-B and ERBB2-C behaved similarly to each other and I argue that they should be considered as two independent very high ERBB2 expressing cell line pools, for which the statement, that ERBB2 protein level in ERBB2-B is higher than in ERBB2-A and level in ERBB2-C is higher than in ERBB2-A, is correct.

Enhanced invasion of ERBB2-B and -C cell line pools was accompanied by their grape-like phenotype of acini-like structures when grown in 3D cultures. This phenotype has been previously shown to be characteristic of cancer cell lines overexpressing ERBB2 (AU565, MCA-MB-361, MDA-MB-453, SKBR3 or UACC-812) in contrary to round, mass and stellate phenotypes in cell lines not overexpressing this RTK.[259] While ERBB2 might not be the sole factor responsible for the grape-like phenotype in these cell lines due to a presence of several other accompanying mutations, my observation that ERBB2 alone is capable of inducing a grape-like phenotype in 3D culture in a semi-normal epithelial cell line, indicates that this phenotype is indeed a direct consequence of ERBB2 overexpression.

Although my study shows that ERBB2 overexpression is a sufficient factor needed to induce invasion of normal epithelial MCF10A cell line, two recent reports claimed that it is required but does not suffice. One of them, published by Pradeep Chaluvally-Raghavan et al. (Oncogene, 2012) presented the requirement for at least one additional factor – namely epidermal growth factor (EGF) - apart from ERBB2 to transform normal epithelial MCF10A into an invasive cell line.[342] Another study, published by Nicola Aceto et al. (Breast Cancer

Research, 2012) similarly showed that overexpression of ERBB2 alone was incapable of inducing invasion of MCF10A cells, however, when ERBB2 was overexpressed together with ERBB3, it triggered cell invasion and a grape-like phenotype in 3D culture.[343] While both these studies seem at first sight contradictory to results presented in this thesis, this is not necessarily the case.

Interestingly, in both reports (especially in the one by Aceto et al.) the acini-like structures formed by ERBB2 overexpressing MCF10A cells resemble those formed by the ERBB2-A cell line pool expressing just moderate ERBB2 levels. As I have shown in my study, very high ERBB2 levels induce constitutive activation of downstream signaling pathways – MAPK/ERK and PI3K/AKT. I argue therefore that while suggested by Chaluvally-Raghavan and Aceto double-hit models hold true for moderate ERBB2 levels, high-level overexpression of ERBB2 overcomes the need for additional ERBB-family receptors' overexpression or exogenous EGF presence for activation of MAPK and PI3K/AKT signaling.

Potential contribution of ERBB2-containing homo- and heterodimers to invasiveness

The MCF10A cell line intrinsically expresses low levels of EGFR and very basal levels of ERBB3. Hence, the question which remains to be investigated as a continuation of my work is whether the observed induction of invasion by very high ERBB2 levels is indeed mediated by ERBB2 homodimers, or rather by EGFR-ERBB2 or ERBB2-ERBB3 heterodimers. High levels of ERBB2 in ERBB2-B and -C cell line pools should in principle favour formation of ERBB2 homodimers which have previously been shown to induce multiacinar structures lacking empty lumen. However, these cells did not display any invasive properties and did also not show anchorage independent growth (even at higher homodimer levels).[378]

As ERBB2 is a preferential dimerization partner for other ERBB-family receptors, it is highly possible that in the ERBB2-B and ERBB2-C cell line pools characterized in this thesis ERBB2 does not only form homodimers but also EGFR-ERBB2 heterodimers as very high ERBB2 abundance substantially increases the probability of their formation, even without presence of exogenous EGF. In this thesis I show that in 3D culture very high ERBB2 levels induce production of another EGFR ligand, HB-EGF, and that additionally, in 2D culture, the stability of EGFR is ERBB2 level-dependent. Since I also detected several tyrosine residues on C-termini of EGFR to be phosphorylated (Y845, Y1068, Y1148) in an ERBB2 dose-dependent

manner, heterodimerization of EGFR and ERBB2 seem to be a likely mechanism of invasion induction and anchorage-independent growth in these cells.

In fact, the researchers studying the function of artificially induced ERBB2 homodimers or EGFR-ERBB2 heterodimers in nontumorigenic breast epithelial cell line MCF10A suggested a similar mechanism. Whereas both kinds of receptor complexes were equally potent in activating the RAS-MAPK signaling, heterodimers much stronger induced activation of PI3K and phospholipase C1 (PLC1) pathways.[235] When they tested the ability of hetero- and homodimers to promote cell invasion through extracellular matrix, only heterodimers were capable of doing that, although both types of complexes induced disruption of three-dimensional acini-like structures. It was shown that invasion of MCF10A cells requires the activity of EGFR-ERBB2 heterodimers and stimulation of all three signaling pathways.[235] In this study, however, again, similar to the study on ERBB2-homodimers mentioned above, the accurate extent to which ERBB2 receptor was overexpressed is not known as it had not been compared to the levels of established ERBB2-positive cell lines. This makes it more difficult to compare with current results.

Whole genome expression profiling analysis of ERBB2-overexpressing cell line pools helped me to identify HB-EGF as one of the top upregulated genes in cell line pools higly expressing ERBB2 in 3D culture but not to such high extent in 2D. This finding stresses the importance and adds additional value to the study of F. Yotsumoto and colleagues, who recently showed that both EGFR and ERBB2 independently can increase secretion of HB-EGF into culture media by a few different breast cancer cell lines.[379]

Here, I additionally show, that HB-EGF induction is even higher in the 3D context and its level is strictly ERBB2-dose dependent. Yotsumoto and others show also that HB-EGF is the most highly expressed EGFR ligand out of four measured (HB-EGF, AR, TGFa and EGF) and the most deregulated one between normal and malignant tissue in breast cancer patients. Moreover, they show that patients with high HB-EGF levels are associated with shorter overall survival.[379] Interestingly, using BreastMark algorithm for metaanalysis of breast cancer patients' data, I discovered that HB-EGF expression is also capable of stratifying ERBB2-positive patients (according to PAM50 classification, but not IHC status) into better survivers with lower HB-EGF levels and worse survivers with high HB-EGF levels ($p=0.047$) (Figure 53).

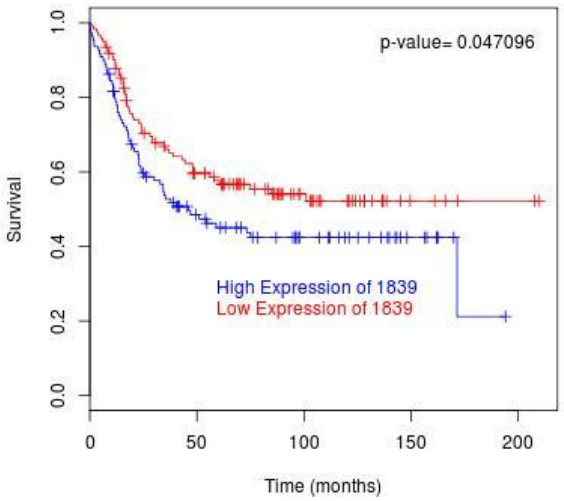

Figure 53

ERBB2-positive patients can be stratified into groups of better (low HB-EGF levels) and worse (high HB-EGF levels) survival. Analysis was done using BreastMark algorithm (http://glados.ucd.ie/BreastMark/index.html).[332] *Median HB-EGF mRNA expression level was used as cut-off. Data is included for only those patients who were classified by PAM50 into ERBB2-positive subtype.*

While EGFR-ERBB2 heterodimers might play important roles in the formation of invasive structures in 3D cultures of stable MCF10A cell line pools, ERBB3 is present in relatively low amount in MCF10A cells and its levels do not change significantly upon ERBB2 overexpression (see Figure 26).[333] Despite this fact, RPPA analysis of stable cell pools showed, apart from increased phosphorylation of several residues on EGFR receptor, also increased phosphorylation of ERBB3 (Y1222). Thus, while these basal levels of ERBB3 are less likely to drive the observed invasive phenotype, ERBB3 might still form dimers with ERBB2. Up to date, ERBB2/ERBB3 dimers are considered to be the most potent with regard to strength of interaction, ligand-induced tyrosine phosphorylation and downstream signaling among all dimers formed within ERBB-family of receptors.[71,380] Recently they had been also shown to induce expression of ZEB1, a transcription factor capable of driving an epithelial-mesenchymal transition.[381]

The absolute number of ERBB2 receptors needed to be present at breast cancer cell surface in order to induce cell transformation via enhanced homo- and heterodimer formation might be therefore difficult to specify as the levels of other ERBB-family receptors and corresponding growth factors may vary between individuals and affect this number.[382] However, rough estimation could be done. For example, it is known that most tumor samples staining IHC3+ express ERBB2 at levels $\geq 10^6$ receptor molecules per cell while

normal cells, including MCF10A, express ~2x10^4 receptors.[334] Also, breast cancer cell lines BT474 and SKBR3 had been shown to express ERBB2 in this range with BT474 expressing ~5x10^5-1,2x10^6 and SKBR3 expressing ~10^6 receptors per cell (both classified as IHC3+).[194,383,334] ERBB2-B and -C cell pools in my study expressed 5-6 fold higher amount of the receptor than SKBR3 as measured by ELISA, which would be estimated then to ~5-6x10^6 receptors per cell. Yet, SKBR3 and BT474 express much higher EGFR and ERBB3 levels than MCF10A cells and thus ERBB2 levels required for heterodimer formation and induction of cell invasion might be already reached at much lower levels in direct comparison of these cell lines.[333]

Dose-dependent EMT induction by ERBB2

In this thesis I report a disruption of cell polarity in acini-like structures and an increase in abundance of filamentous actin in 3D cell culture of cell line pools expressing very high ERBB2 levels. Both enhance the ability of cells to move. In growth-arrested acini structures, the Golgi apparatus is oriented towards the lumen and indicates an established cell polarity. However, this orientation was disrupted in ERBB2-B and ERBB2-C cell pools. In a migrating cell, the Golgi apparatus is located proximal to the nucleus towards the direction of migration.[225] Hence, disruption of polarity in acini may be linked to enhanced cell invasiveness. Previously disruption of cell polarity by ERBB2 has been shown in 3D cultures only in two type of cases – either in breast cancer cell lines which already bear several critical mutations or in normal epithelial cell lines (mainly MCF10A and HMEC) that required additionally a "second hit" apart from ERBB2 overexpression.[250] While overexpression of ERBB3 or presence of EGF had an effect on downstream signal activation, other "second hits" - TGFβ stimulation, 14-3-3ζ and LXB1 overexpression, which all have been reported to enhance cell mobility and invasion of ERBB2 overexpressing cells, induced epithelial-to-mesenchymal transition in those cells.[384,385,386] Here on the contrary I show that ERBB2 can drive EMT process in a dose-dependent manner without further requirement for those factors in 3D culture.

In the presence of EGF, the gradual regulation of E-cadherin, ZEB1, N-cadherin, fibronectin, MMP9 and MMP2 gene expression was, in my study, clearly ERBB2-dependent in MCF10A-derived cell line pools grown in 2D culture. Snail 2, ZO-1 and caveolin-1 expression levels were not affected. E-cadherin downregulation as well as vimentin, N-cadherin and

fibronectin upregulation by ERBB2 had been previously reported by Jenndahl and colleagues (2005). However, their model system was highly artificial as overexpressed ERBB2 molecules contained extracellular domain from the trkA nerve growth factor receptor which allowed NGF-regulated ERBB2 homodimer formation.[344] In my study, on the other hand, ERBB2 was neither mutated nor engineered but expressed as native protein.

Interestingly, although Snail 2 transcription factor upregulation by ERBB2 had been previously shown in ovarian cancer cell lines[387], in the semi-normal epithelial cell line system I did not observe its dependency on ERBB2, even at very high ERBB2 levels and additional EGF presence. Similarly, Jing Lu and colleagues (2009) had shown no association between ERBB2 and Snail 1, which is related to Snail 2, in the MCF10A cell line cultured in 2D.[385] On the other hand, here I show that E-cadherin and ZEB1 transcription factor are inversely expressed suggesting that E-cadherin regulation by ERBB2 might be achieved mainly via ZEB1 upregulation and not via Snail transcription factors in MCF10A. Moreover, ZEB1 had been reported to be upregulated in ERBB2 and ERBB3-overexpressing MCF10A via the ERBB2/ERBB3-SHP2 axis.[381] In my study ZEB1 upregulation was induced in ERBB2-dose dependent manner even in the absence of ERBB3 overexpression (yet in the presence of EGF).

The observed increased expression of metalloproteinases MMP9 and MMP2 is in line with previous studies that had shown their dependence on ERBB2 in MDA-MB-435 cell line (with stronger MMP2 upregulation by ERBB2) and in MCF10A in the presence of EGF (with stronger MMP9 upregulation).[388,389] Additionally MMP9 (along with MMP1) had been shown to be upregulated by ERBB2 in MCF7 cells in the presence of HRG.[390] On top of those discoveries my study shows that this control appears to be strictly regulated by ERBB2 as expression of those two MMPs increased gradually with ERBB2 level.

In the current literature the EMT process has been studied mostly in 2D cultures and focused on an analysis of expression of molecular markers, cellular phenotype (round vs elongated shape), character of cellular growth (tightly packed vs scattered cells), and anchorage independent growth abilities as well as their induction by gene expression changes coordinated by EMT-specific transcription factors. ERBB2-B and -C cell line pools expressing very high ERBB2 levels did not show the characteristics of elongated shape when grown on plastic dishes, indicating that even high ERBB2 expression is not capable on its own to induce a spindle-like shape in normal epithelial cells. The two cell pools were, however, much more

loosely adhering to each other and could grow on PolyHema without the need of cell-cell contacts or anchorage to a solid surface.

On the other hand, in 3D cell culture - the growth condition that more closely resembles situation *in vivo* than 2D culture - EMT has in general been less thoroughly studied. Its induction has been associated with phenotype changes (apico-basal polarity disruption and invasiveness) rather than with expression of EMT-related molecular markers or transcription factors. My study suggests that the differences in expression of EMT markers can be large between 2D and 3D cell culture conditions, and that observations true in 2D might need to be verified in a three-dimensional culture system or *in vivo*. One study, which did compare expression of a few EMT markers upon overexpression of ERBB2 in MCF10A grown in either 2D or 3D, reported little or no change in expression of E-cadherin, β-catenin, α-catenin, p120-catenin and N-cadherin at protein level in both conditions.[385] In cells highly expressing ERBB2 grown in 3D culture, however, I report a slight decrease in E-cadherin and a very strong, ERBB2-dose dependent, increase in N-cadherin at the mRNA level. While E-cadherin deregulation had been previously reported not to be required for ERBB2-induced EMT, a recent report points out the critical role of N-cadherin in metastasis induction in ERBB2-overexpressing mouse tumors via EMT and the regulation of stem/progenitor-like cell properties.[345,391] In that study, mice overexpressing ERBB2 showed significantly fewer metastases than those additionally overexpressing N-cadherin. It states also that this cell adhesion protein is often co-expressed with ERBB2 in invasive breast carcinomas. Here I show that ERBB2 itself is capable of N-cadherin induction – both in 2D and in 3D cell culture – and that from the EMT markers tested in MCF10A-derived stable cell line pools overexpressing ERBB2 it was the only one showing clear ERBB2-dependency in laminin-rich Matrigel.

Cytoskeleton rearrangement by ERBB2

Epithelial-mesenchymal transition is a complex process in which cytoskeleton rearrangement plays an essential role. Here I show that two tyrosine kinases important for cytoskeleton regulation, namely FAK and SRC, are activated by ERBB2 in a dose-dependent manner in 2D culture in the presence of EGF. Interestingly, ERBB2 had been previously reported to be found in ERBB2-FAK-SRC-p130Cas complexes which regulate Rac1 activation and MMP9 secretion leading to an invasive phenotype.[392] The interaction of FAK with

activated integrins leads to FAK autophosphorylation at tyrosine 397 and the subsequent recruitment of SRC, PI3K, PLCγ and GRB7 to focal adhesions and to their activation.[393] This in turn regulates integrins' attachment to ECM and modulates cell adhesion and the ability to move. FAK associated with integrins binds also ERBB2 and in this way triggers ERBB2 clustering in close vicinity to integrins. ERBB2 can then further influence integrins' function.[394] Here I show that ERBB2 upregulation affects FAK phosphorylation at Y397 without prior integrin activity and level modulation (control and ERBB2 overexpressing cells were grown in the same conditions and on the same type of surface). Previously it had been shown that treatment of ERBB2 overexpressing cells (MDA-MB-231-ERBB2 and SKBR3) with trastuzumab reduced FAK phosphorylation at two other tyrosine residues: Y861 - the major Src phosphorylation site of FAK and Y925 - which permits an SH2-mediated association with Grb2, but did not affect phosphorylation of Y397.[395,396] In my study I show that this FAK main autophosphorylation site is in fact affected by ERBB2 in a level-dependent manner. This is in line with another study which showed that silencing of ERBB2 decreased phosphorylation of Y397 of FAK in an ovarian cancer cell line.[397]

ERBB2 levels in MCF10A-derived cell line pools correlated very well with SRC phosphorylation at Y416. This is a main phosphorylation site on SRC kinase that is associated with catalytic activity. Once activated, SRC phosphorylates EGFR at Y845 - a site which is necessary for mitogenic function of the receptor and downstream signaling.[398] The significant clustering between SRC Y416 and EGFR Y845 which I report here hence further confirms their relation and stresses their activation dependence on the ERBB2 level. Apart from Y845, ERBB2 levels correlated significantly also with phosphorylation at two other major EGFR autophosphorylation sites tested: Y1068 and Y1148, which recruit GRB2 and Shc scaffold proteins, respectively, coupling EGFR with MAP kinase signaling.[399]

Beside tyrosine kinases activation, ERBB2 induced cytoskeleton rearrangement by regulating expression of other cytoskeleton-related proteins in a dose-dependent manner. Vimentin, an intermediate filament protein and EMT marker, had previously been shown to be induced by ERBB2 overexpression in MCF10A.[389] Similarly, cortactin, a cytoskeleton-binding protein was reported to be phosphorylated in response to overexpression of C-terminal ERBB2 fragment (611-CTF) and to be a critical protein involved in 611-CTF-induced cell migration.[400] The present study shows that also the full length receptor has a positive effect on both - total and phosphorylated form of this protein. Cortactin inhibits ligand-induced endocytosis

of EGFR and the present results therefore suggest that ERBB2 has a stabilization effect on EGFR and that this might be, at least partially, mediated by cortactin, although this has not been tested in my experimental system.[401]

RhoA and its downstream effectors ROCK1 and ROCK2 are important regulators of stress fiber formation. Activation of these proteins by ERBB2 has been well documented, yet, the effect of ERBB2 on total RhoA protein levels has not been extensively investigated.[402] As RhoA protein expression and activity is directly linked to cortactin's activity, it cannot be excluded that the effect of ERBB2 on RhoA that I have shown in this thesis is indeed exerted via cortactin. However, in a study reported previously, knockdown of only cortactin reduced RhoA levels and cortactin overexpression did not show increases in RhoA protein levels like in my study.[403] This could be, though, due to the different model systems and different RhoA basal levels in the studied cells.

Metadherin (MTDH), a protein that is associated with tight junction complexes in polarized epithelial cells, was the next protein whose expression I found to be ERBB2-level dependent.[404] Although MTDH is overexpressed in more than 40% of breast cancers, its relation to ERBB2 has not been well studied.[404,405] One research group detected ERBB2 level association with metadherin levels in a proteomic approach, while another showed that overexpression of MTDH causes an increase in ERBB2 at the protein level.[406,407] Importantly MTDH was also highly elevated at mRNA levels in Neu (i.e., the rat ortholog of ERBB2) overexpressing tumors in mice.[408] My study confirms that the relation between these two molecules exists. Further functional analysis would be required to answer how these two proteins interact or regulate with each other.

From over 30 cytoskeleton-related proteins whose levels where tested by RPPA only cytokeratins 5/6 were significantly downregulated by ERBB2 in a dose-dependent manner. The expression of these intermediate filament proteins is associated with the basal subtype of breast cancer comprising largely of triple negative breast cancers (ER-, PR-, ERBB2-negative). CK5 is also used as a marker for basal cancer.[409] Here I show that CK5/6 expression is strongly and inversely correlated with ERBB2 expression in MCF10A cells that are negative for ER, PR and ERBB2-expression in the native state. The absence of CK5/6 in the ERBB2 overexpressing breast cancer subtype might be similarly regulated.

PTEN is destabilized by phosphorylation at threonine 366 and serine 370 via glycogen synthase kinase 3β (GSK3β) and casein kinase 2 (CK2), respectively.[410,411] Whereas both of

these kinases are downstream of ERBB2 in the signaling pathway the effect of ERBB2 overexpression or the inhibition of phosphorylation at T366/S370 has not yet been shown. This is, thus, the first report of an ERBB2 dose-dependent upregulation of PTEN phosphorylation at T366/S370 residues. The observed negative regulation of PTEN by ERBB2 was accompanied by a dose-dependent upregulation of total PI3K levels (p110 and p85) which both facilitate PI3K/AKT signaling. The MAP kinase signaling pathway, similar to PI3K/AKT, was not only activated by ERBB2, but also the total ERK1/ERK2 levels were dependent on ERBB2 expression. Additionally, the total level of protein kinase A (PKA) was affected by ERBB2 in a level-dependent manner. ERBB2, thus enhances downstream signaling not only by its activation but also by the increase in the abundance of signaling components.

As in 2D culture I did not see the changes in cell migration upon ERBB2 overexpression, I speculate that the changes in expression of migration-related proteins detected using RPPA merely prime the cells towards an invasive phenotype which, however, only occurs and can be detected when ERBB2-overexpressing cells are confined to a three-dimensional environment. β4 integrin, for example had been shown to be critical for the onset of ERBB2-overexpressing tumors and for invasive growth, and also β1-integrin has been documented to play a crucial role in the process of tumor metastasis.[412,413]

ERBB2-dose dependent gene expression at mRNA in 3D culture

In the three-dimensional context, ERBB2 regulated the expression of several genes in a dose-dependent manner. I intentionally focused on identifying specifically such genes whose expression was dependent on different ERBB2 expression levels (i.e. their expression gradually increased or discreased with ERBB2 levels), while I disregarded e.g. those genes that were differentially expressed in the ERBB2-expressing vs. CTRL cell line pools.

Expression and function of KRT16 as well as KRT17P3 in breast cancer or their relation with ERBB2 has not been yet well studied. One of two existing reports regarding KRT16 in breast cancer showed that its high level is associated with worse patient survival and the second that the use of EGFR and ERBB2 inhibitiors, but not of an EGFR inhibitor alone, decreased KRT16 expression in the dermis of cancer patients.[414,415] This cytokeratin has been also implicated in induction of wound healing where it participates in reorganization of keratin

filaments.[416] It is thus, interesting that in my study KRT16 was the most ERBB2-level dependent, downregulated by ERBB2 gene in MCF10A-derived cell pools in 3D cell culture.

The two other cytokeratins, KRT14 and KRT5 (also detected to be downregulated on protein level) were also very strongly downregulated by ERBB2 when the gene expression comparison has been done between CTRL, ERBB2-A and ERBB2-B cell pools. Mutations or alternatively lack of expression of cytokeratins 5 and 14 are directly implicated in the development of an epidermolysis bullosa simplex – a disease characterized by impaired cell-cell adhesion resulting in widespread blisters, erosions, chronic wounds, and succeptibility to development of squamous cell carcinoma.[417] Reduction of the cell-cell attachement abilities, observed for the ERBB2-expressing cells in PolyHema assay, could, hence, result from the strong decrease of KRT14 and KRT5 expression levels in those cells detected in 3D cell culture.

Stanniocalcin 1 (STC1) along with STC2 were the most prominently upregulated genes by ERBB2 in a dose-dependent manner. These are closely related secreted glycoproteins and STC1 has been recently shown to have a very strong and positive effect on tumor progression as well as metastasis in breast cancer.[418] STC2 on the other hand has been shown to be capable of prediction tumor progression in gastric cancer.[419] Their regulation by ERBB2 reported in this thesis is the first indicating that stanniocalcins might play an important role in ERBB2-driven breast cancer. As stanniocalcins are secreted proteins and can act similarly to hormones (first identified and described in bony fish)[420], they seem to be promising therapeutic targets.

In MCF10A-derived stable cell line pools expressing ERBB2 grown in Matrigel the most enriched KEGG pathways (taking into account only ERBB2-dose dependent genes) were “aminoacyl-tRNA biosynthesis” - the only one significantly enriched, and “cytokine-cytokine receptor interaction”. In “cytokine signature” induced by ERBB2 in the luminal A MCF7 cell line it has been previously reported that IL-6, CXCL8 (IL-8), CXCL1 and IL-1α are top upregulated cytokines by ERBB2.[421,422] However, Vazquez-Martin et al. and Hartman et al. performed their studies using 2D cell cultures. In my study, on the other hand, I show the soluble factors that are highly upregulated by ERBB2 in the more informative three-dimensional context. These are: IL1A, IL1B, CCL20, VEGFA and INHBE. As ERBB2 is known to induce cannonical NFkB signaling, the inflammatory response induced by ERBB2 could be NFkB-dependent.[421,423] This might explain IL1A, IL1B, CCL20 and VEGF upreglation which are

all NFkB targets.[424,425,426,423,427] It also suggests that NFkB is likely to be activated by ERBB2 also in 3D cell culture. The way in which inhibin beta E becomes upregulated by ERBB2 remains yet to be identified. Prolonged induction of inflammatory response had been shown to promote tumorigenesis by increasing tumor infiltration by immunocompetent cells. These cells contribute further to the acquisition of the hallmarks of cancer by the tumor, including tumor angiogenesis, proliferation, tissue invasion, and initiation of metastasis.[223]

Aminoacyl-tRNA synthetases (AARSs) transfer specific aminoacids on the appropriate tRNAs, which are then further used as substrates for protein production during translation. In cancer, in which cell proliferation is increased, the requirement for protein production is higher and hence the need for enzymes involved in protein synthesis is increased. To date, deregulation of AARSs has been reported in a few cancers including colon and lung cancers, chronic myeloid leukemia and papillary thyroid carcinoma.[428] In this thesis I show that ERBB2 regulates very strongly and in a dose-dependent manner 5 aminoacyl-tRNA synthetases: CARS, GARS, SARS, WARS and YARS. This is one of the first two reports of ERBB2 being involved in AARSs regulation.

Recently Pincini and colleagues identified 91 genes that were upregulated by p130Cas overexpression in ERBB2-expressing MCF10A cell grown in 3D culture. They have shown that p130Cas overexpression can, similarly to other genes mentioned before, function as a "second hit" to induce cell invasion in ERBB2-overexpressing otherwise non-invasive cells. Three of the identified genes induced by p130Cas were GARS, YARS and WARS.[429] Additionally, Pincini showed that ERBB2 overexpression in p130Cas-overexpressing cells induced expression of GARS, MARS, WARS, TARS, AARS and YARS.[429] Together, my and Pincini's reports identify 8 AARSs to be regulated by ERBB2 with 5 of them being regulated by ERBB2 in the absence of p130Cas.

In the above mentioned study, PHGDH expression was elevated in response to increased p130Cas levels in ERBB2-overexpressing MCF10A cells and PHGDH and ASNS in response to increased ERBB2 levels in p130Cas-overexpressing MCF10A. PHGDH is involved in serine biosynthesis and contributes to insuline-independence triggered by ERBB2 in MCF10A cells (also observed in my study (data not shown)), whereas ASNS is an asparagine synthetase.[430] Interestingly, both these genes were also top genes induced in my study by ERBB2 in a dose-dependent manner, indicating that the presence of p130Cas is dispensable for their induction. These two studies hence, not only show similar (yet not identical) effect of ERBB2

on gene expression but also present a rather cohesive picture of ERBB2 function in protein synthesis despite the completely different nature of ERBB2 overexpression in MCF10A cells (full length unmodified receptor in my study vs chimeric ERBB2 containing extracellular and transmembrane domain from nerve growth factor receptor – p75NGFR).

Drug sensitivity of ERBB2-overexpressing cell line pools

Although MCF10A-derived cell line pools overexpressed full length native ERBB2 receptor without any tag, they were not sensitive to trastuzumab in the tested conditions. 2D culture of those pools has been used for the drug sensitivity assays due to technical difficulties associated with possible cell viability readouts in 3D cultures. There, the main challenge would have been normalization of readouts to the cell number, as in Matrigel ERBB2-overexpressing cell line pools had different proliferation rates, unlike in 2D culture. Currently new commercial assays are being developed to overcome this and other challenges related to 3D culture conditions.

Pick and colleagues had shown in 2009 that in SKBR cells substantially more ERBB2/ERBB3 and EGFR/ERBB2 heterodimers formed when grown in 2D culture compared to 3D culture conditions. In three-dimensional conditions the amount of heterodimers was strongly decreased while an increase in ERBB2 homodimers was observed.[431] Trastuzumab has been reported in this (SKBR3) and in MCF10A cell line overexpressing ERBB2 to preferentially bind and inactivate ERBB2 homodimers.[431,201] In MCF10A it has been shown on artificially induced homodimers of ERBB2 chimeras, containing full-length ERBB2 receptor fused to ligand binding domain of FKBP, and activated by syntetic FKBP ligand, AP1510.[201] In the study performed in MCF10A cells overexpressing ERBB2, trastuzumab was ineffective even in 3D culture conditions when either heregulin or EGF were present in the medium.[201] These observations could explain why also in my drug treatment experiment, which was limited to 2D culture and in which EGF was present in the medium, trastuzumab did not reduce cell viability. Moreover, MCF10A express relatively high IGFR levels which has been reported to contribute to trastuzumab resistance.[432]

In my study I also did not observe an effect of ERBB2 overexpression on doxorubicin or taxol sensitivity. This result was not anticipated as previously Yu et al. have reported a panel of 5 ERBB2 overexpressing breast cancer cell lines which clearly showed increased Taxol and Taxotere resistance compared to 3 controls not expressing ERBB2.[433] Yet, that study

compared the sensitivity to taxanes of cell lines with different genetic background, which cannot show the direct effect of ERBB2 on drug response. In the study reported by Pegram et al., on the other hand, the direct effect of ERBB2 was tested by overexpression of full length receptor in 4 different cell lines and comparison of drug sensitivity was done directly between ERBB2-overexpressing cell line and the appropriate cell line of origin. The cell lines developed for this study were obtained in a similar way as in my study (as cell line pools by FACS sorting). The results reported by Pegram and colleagues indicated no induction of resistance to doxorubicin or taxol treatment by ERBB2 across all four cell lines. In two out of four cell lines ERBB2 overexpression in fact increased taxol sensitivity.[434]

The report by Ciardiello and colleagues, which is presumably the closest related to the one presented here, has shown increased Taxol and Taxotere resistance and increased Doxorubicin sensitivity in ERBB2-overexpressing MCF10A cells. This has been shown in both: monolayer and in soft agar growth, with stronger effects observed in cell monolayers.[435] As I did not observe similar result, I searched for potential differences in the two experimental setups and found that Ciardiello et al. used additionally glutamine in the cell culture medium. Interestingly, in a very recent report it has been shown that Taxol increases the glutamine uptake and that Taxol-resistant cells metabolize glutamine at higher rate due to Taxol-induced glutaminase upregulation.[436] The potential effect of glutamine on Doxorubicin sensitivity, however, has not been yet well tested.

Lack of tumorigenesis in mice injected with MCF10A-derived cell line pools expressing ERBB2 at low, medium and high levels

In the animal experiment presented in this thesis, severely immunocompromised NSG mice were used. They are characterized by an impaired innate immune system, lack of mature T and B cells, lack of expression of several receptors for cytokines (including IL-2 receptor), and not functional NK cells. Hence, the main regulatory mechanisms responsible for clearing the injected MCF10A-derived stable cell line pools overexpressing ERBB2 observed in my study must have been related to the remaining immune cells which are neutrophils, monocytes as well as defective (although still present) dendritic cells and macrophages.

While several research groups worked with the MCF10A cell line in two- or three-dimensional cell cultures, only few have reported a study *in vivo*. One of the first reports showed that although MCF10A cells do not survive in immunodeficient mice, T24 HRAS

overexpressing MCF10A injected subcutaneously into nude/beige mice form small nodules which persist for at least 1 year and sporadically develop into carcinoma. Serial transplants of the cells derived from nodules caused a vast increase in nodule frequency from 23% (in first generation) to 56% (in the fourth generation). Interestingly, the lesions removed between 13-48 weeks after implantation were very similar.[437,438] Thus this study proved that a single oncogene is capable of MCF10A cell line transformation.

Another older study in which MCF10A were overexpressing ERBB2, HRAS or both, although performed mainly in vitro, showed that injected into nude mice transformed cells (all three transformants types) unlike untransformed MCF10A can halt after 48h post-injection mainly in lungs, indicating the possibility of these cells to colonize this organ.[439] Yet, in my study I did not observe neither nodules' growth nor dormant cells present in lungs even 10 months after NSG mice injection with any of the three ERBB2-overexpressing cell line pools. The initial post-injection localization of ERBB2-overexpressing MCF10A cells in lungs may, thus, not be sufficient for their efficient colonization.

The most interesting *in vivo* experiment which is also most related to my study has been performed very recently (in parallel to my ongoing mice experiment) by Alajati and colleagues.[440] They used MCF10A and MCF7 cell lines to overexpress either full length ERBB2 or p95-ERBB2 (called further also Delta-ERBB2) lacking exon 16. p95-ERBB2 constitutes 2-9% of ERBB2 mRNA in breast carcinomas and causes mammary tumor growth and metastasis.[106] Alajatali et al. showed that ERBB2-overexpressing MCF10A cells orthotopically injected into SCID-beige mice did not form tumors - confirming my result obtained in NSG mice - whereas Delta-ERBB2 did. When MCF7 cells were used as a cell of origin, Delta-ERBB2 overexpressing cells induced tumors characterized by significantly higher volume than cells overexpressing full length ERBB2 receptor. Moreover, 66% of mice with MCF10A-Delta-ERBB2 tumors developed lung metastasis, indicating that lungs are indeed a preferable organ of metastasis for this type of cells. Surprisingly, Alajatali and colleagues reported that tumors induced by these cells are trastzuzumab sensitive.[440]

Altogether my and previous reports indicate that ERBB2 alone is alone not capable of semi-normal epithelial MCF10A cell line transformation leading to tumorigenesis in immunocompromised mice. My study shows that this holds true even for very high ERBB2 levels in combination with severly immunocompromised animals. Hence, "second hit" which may be dispensable for induction of invasion in in-vitro cell culture conditions in the

presence of very high ERBB2 levels, may be still required for tumor formation and survival of transformed cells *in vivo*.

In contrary to mice injected with ERBB2-overexpressing MCF10A cells, mice expressing Neu (rat's ERBB2 homolog) under its endogenous promoter do develop mammary tumors. However, it has been reported that those tumors resemble in their character more ductal carcinoma in situ (DCIS) rather than metastatic breast cancer.[441,408] ERBB2 plays, thus, a role in the early stage of transformation process and expression of additional factors like e.g. previously mentioned 14-3-3ζ protein can facilitate progression of ERBB2-expressing DCIS into invasive breast carcinoma.[385]

Oncogenic potential of miRNA-301b and miR-130b induced by ERBB2

Since 2007 the number of publications regarding the role of miRNAs in human cancers has been steadily increasing and since then miRNAs have been shown to regulate several processes involved in tumorigenesis. In breast cancer miRNAs can act either like tumor suppressors by targeting proteins with established oncogenic functions or like oncogenes by targeting tumor suppressor genes. In our research group we have shown a few examples of such regulations. Firstly, we have shown that miRNA-200c can play a role of a tumor suppressor and function as an inhibitor of migration and invasion by directly targeting cytoskeleton-regulating genes: FHOD1 and PPM1F, as well as by inhibition of TGFβ-induced stress fibers formation.[442] The same miRNA has been previously reported to additionally suppress EMT by direct targeting of ZEB1/2. Secondly, we have shown that miR-375, another tumor suppressor miRNA, can sensitize tamoxifen resistant cells to tamoxifen treatment by partial reversion of EMT and targeting of MTDH, a resistance-associated gene.[443] On the other hand we have shown that miR-519a can induce tamoxifen resistance by targeting negative regulators of cell-cycle progression (CDKN1A and RB1) as well as targeting PI3K/AKT signaling inhibitor – PTEN.[370] Last but not least we have presented that miRNAs are capable of regulating intracellular signaling pathways involved in tumor progression, including NFkB (regulated by miR-30c-2-3p) and EGFR signaling pathways.[322]

One of few existing studies that have investigated miRNA expression in three-dimensional cell culture is a study by Pincini and colleagues (mentioned already before)[444], who identified 40 miRNAs that were differentially expressed between ERBB2/p130Cas-overexpressing MCF10A cells and ERBB2-overexpressing cells. Interestingly, the levels of 6 miRNAs were also

ERBB2-dose dependent with the same expression trend in my study. That suggests that combined overexpression of ERBB2 and p130Cas as well as overexpression of very high ERBB2 levels are capable of induction of a common miRNA subset, namely: miR-424-5p, miR-221-5p, miR-361-3p, miR-31-5p, miR-29b-3p (upregulated) and miR-33b-3b (downregulated). miR-301b and miR-130b have not been reported in that study.

In this thesis I show that ERBB2-overexpression in MCF10A cell line regulates expression of 36 miRNAs in a dose-dependent manner in a three-dimensional environment. Of these, miR-301b, miR-210 and miR-146-5p showed also higher expression in tumors compared to normal tissue as well as in ERBB2-positive patients compared to negative. Moreover, their high expression was also associated with worse clinical outcome. In my thesis I concentrated on functional analysis of miR-301b as well as miR-130b. The latter is likely regulated by the same promoter as miR-301b, it belongs to the same miRNA family and its expression level is also associated with patient outcome. Expression of these two miRNAs was ERBB2-dependent when cells were grown in 3D cell culture but not when they were grown in monolayer. Notably, miR-301b and miR-130b have not been identified to be differentially expressed between ERBB2-negative and ERBB2-positive breast cancer cells in 5 published datasets investigating miRNA expression in relation to ERBB2.[445] 2 of these datasets involved experiments in vitro in 2D cell culture conditions which could explain the lack of these miRNAs' upregulation by ERBB2 in that experimental setups.[446,447] The other 3 studies determined miRNAs' levels in patient specimen. However, they consisted only of 29, 93 and 20 breast cancer samples, respectively, which may not be representative for studying ERBB2-regulated processes including miRNA expression.[448,449,450] Remarkably, in the dataset consisting of 93 tumor specimen only 5 were classified as ERBB2-positive.

Scientific literature regarding miR-301b and miR-130b function in cancer is very limited with some reports on miR-130b contradicting one other, e.g. regarding its behaviour in EMT regulation in endometrial cancer.[363,364] Importantly, no reports about miR-301b and miR-130b function in breast or breast cancer have been published so far, and only one study has been done to find the role of a closely related miRNA, miR-301a, in breast cancer.[358] Here I show that expression of miR-301b and miR-130b is significantly associated with ERBB2 levels not only in MCF10A-derived stable cell line pools grown in 3D cell culture, but also in patients. miR-301a, a related miRNA belonging to the same miRNA family, which has been reported to play a role in breast cancer proliferation and invasion, was associated with

ERBB2 levels in clinical data as well.[358] A possible explanation for the lack of its association with ERBB2 detected in ERBB2-overexpressing cell line pools may be either that ERBB2 effects exerted on miR-301a expression are not direct (which is more probable), or, alternatively, that probes for miR-301a found on microarrays used for detection of miRNA levels in patients are not specific and cross-hybridize with miR-301b (differing only by two nucleotides), which would lead then to an artifact. Whether or not EGF can as well induce expression of the two miRNAs will need to be determined in a broader panel of breast cell lines. Besides, transcription factors activated by ERBB2 signaling that can directly bind to and activate miR-301b/miR-130b promoter remain yet to be identified.

All three miRNAs mentioned above had higher expression levels in tumor compared to respective normal tissues, but only miR-301b and miR-130b were expressed at higher levels in ER-negative or in p53-mutated tumors. This finding can be related to the fact that most of ERBB2-overexpressing breast cancers are ER-negative and that 72% of them bear mutations in TP53 gene.[14] It could however also mean that p53 (WT or mutated) may have a direct impact on expression of these two miRNAs. This requires, thus, additional investigation.

I have further reported here that high expression of miR-301b and miR-130b in breast tumors is significantly associated with worse overall survival of patients. For miR-301a this association was not significant but a similar trend was observed. All three miRNAs increased cell viability and proliferation (in the presence as well as in the absence of EGF), enhanced chemoattractant-induced cell migration, and induced cell invasion through Matrigel in MCF10A cells. Whereas miR-130b slightly enhanced E-cadherin expression, the other two studied miRNAs decreased its mRNA levels. Yet, all three miRNAs increased fibronectin expression and to a much greater extent expression of MMP9. Upregulation of MMP9 could, thus, be the main mechanism contributing to cell invasiveness induced by these miRNAs. Hence, miR-301b, miR-130b and miR-301a contribute at least partially to EMT process in MCF10A cell line.

Identification of critical miRNA targets constitutes one of the biggest challenges in the functional characterization of a given miRNA. While all three miRNAs described in this thesis share the same seed sequence, miR-301a and miR-301b do have many more common target genes (66) than either miR-301a and miR-130b or miR-301b and miR-130b. These two miRNAs differ only by 2 nucleotides outside of the seed sequence and it is thus not very surprising that they share common targets. It is, however, very interesting to see that while

miR-130b has the same seed sequence and a list of predicted target genes as miR-301a and miR-301b, it downregulates much broader pool of genes. This finding stresses the importance of the miRNA sequence outside the seed region in recognition of target genes. Remarkably, miR-130b downregulated more than 3 times more genes by at least 30% than the other two miRNAs. Moreover, 70% of genes targeted by miR-301a and 77% of genes targeted by miR-301b were also downregulated by miR-130b by at least 30%.

In the course of my study I identified 19 most promising target genes of the three miRNAs using rigorous selective criteria. These included 9 genes potentially relevant in the context of ERBB2-dose dependent upregulation of miRNAs in 3D cell culture. Interestingly, two of them have been previously implicated in apoptosis regulation (ZMAT3 and ZAK) indicating one other pathway how ERBB2 might affect programmed cell death. Another two genes - VPS24 and VPS37A - have been shown to play a role in EGFR trafficking and might possibly contribute to stabilization of EGFR by ERBB2 observed in MCF10A-derived stable cell line pools and reported by others. [341,78] Regulation of both of these pathways by miR-301b, miR-130b and miR-301a will be essential in the further development of this project.

miR-301a has been previously presented to target FOXF2, BBC3, PTEN, and COL2A1.[358] In the current study and in view of the similarity of seed sequence of the three miRNAs to miR-519a, I asked if these miRNAs might target similar sets of genes. Indeed, I found that the 3'UTRs of three direct targets of miR-519a, including the estrogen receptor, cell cycle inhibitor p21 and PI3K/AKT signaling suppressor PTEN were also targeted by miR-301b and miR-130b in a luciferase reporter assay. The strongest effect was observed on estrogen receptor expression, which showed also high negative correlation with miR-301a and miR-130b in breast cancer patients. As most of the ERBB2-positive tumors are ER-negative, it might be possible that in those tumors ERBB2-induced miR-301b and miR-130b contribute to estrogen receptor downregulation. Negative correlations of these two miRNAs were observed for PTEN as well, yet, despite PTEN's and ERBB2IP's established role in trastuzumab resistance, their targeting by overexpression of any of three miRNAs did not affect trastuzumab sensitivity in SKBR3 cells.[451,452]

To determine whether miRNAs: miR-301b, miR-130b and miR-301a play a critical role in ERBB2-driven invasion observed in 3D cell culture, or just an auxillary, the inhibition of the three miRNAs either each separately or in combinations in the MCF10A-derived cell line pools expressing very high ERBB2 level would be required. However, two technical

challenges need to be first overcome. Firstly, miRNA inhibitors are not very specific and inhibition of given miRNAs individually presents a big difficulty. Secondly, 3D cell culture requires stable cell line production. As MCF10A cell line can be cultured only for a few passages in a cell culture dish to avoid its abberant behaviour, and MCF10A-derived cell line pools had been already once retroviral-infected with ERBB2-overexpressing construct, further infection of the same cell line is not desirable. Developing of a similar ERBB2-overexpressing system in other cell line, which can be cultured for a longer time, could be therefore a solution.

The importance of miR-301b, miR-130b and miR-301a in cancer has been stressed in the recent paper by Hamilton and colleagues, who reported that 7 miRNA families, including miR-17, miR-19, miR-130, miR-93, miR-18, miR-455 and miR-210 families, co-target critical tumor suppressor genes via their central GUGC motif across many types of cancers. Significantly, from miR-130 family exactly these three miRNAs which were presented in this thesis were involved in tumor suppressors' regulation.[453]

In my PhD project I have identified also other miRNAs apart from miR-301b and miR-130b to be regulated by ERBB2. While I chose to functionally characterize these two, the other miRNAs from the list of 36 miRNAs might also play a role in ERBB2-driven invasion in breast cancer. In particular, miR-210 and miR-146-5p seem to be especially good candidates to study as a continuation of this project. Furthermore, miR-21 could serve as a good example of "false negative" miRNA, as it has been shown previously to be upregulated by ERBB2 and to have an established oncogenic function in different tumor types, yet was not significantly affecting patients' overall survival in METABRIC validation dataset.[314] Additionally, it must be mentioned that for a few miRNAs from the list clinical data was missing. These can be thus next "false negatives" as their expression in breast cancer and/or their effect on patients' survival remains to be determined.

Conclusion

In conclusion, I have shown that ERBB2 drives cell invasion in a dose-dependent manner by dose dependent: tyrosine kinases' activation (EGFR, ERBB3, FAK and SRC), EGFR ligand HB-EGF upregulation, EMT induction, cytoskeleton reorganization and miRNAs' expression deregulation. Importantly, I have reported that further increase of ERBB2 level in cells overexpressing ERBB2 at moderate/high level, and as a consequence further deregulation of all above mentioned factors, leads to progression from noninvasive to invasive cell behaviour. My study has stressed also the impact of three-dimensional cell environment on regulation of ERBB2 function and miRNA induction.

8. Own publications

1) **“miR-30c-2-3p negatively regulates NF-κB signaling and cell cycle through downregulation of TRADD and CCNE1 in breast cancer.”**; Shukla K, Sharma AK, Ward A, Hielscher T, Will R, **Balwierz A**, Breunig C, Münstermann A, König R, Keklikoglou I, Wiemann S; Mol Oncol. 2015 Jun; 9(6):1106-19
2) **“Combined DNA methylation and gene expression profiling in gastrointestinal stromal tumors (GISTs) reveals hypomethylation of *SPP1* as an independent prognostic factor”**; Haller F, Zhang JD, Moskalev EA, Braun A, Otto C, Geddert H, Riazalhosseini Y, Ward A, **Balwierz A**, Schaefer IM, Cameron S, Ghadimi BM, Agaimy A, Fletcher JA, Hoheisel J, Hartmann A, Werner M, Wiemann S, Şahin Ö; Int J Cancer. 2015 Mar 1; 136(5):1013-1023
3) “**MicroRNA-519a is a novel oncomir conferring tamoxifen resistance by targeting a network of tumor-suppressor genes in ER+ breast cancer.**”; Ward A, Shukla K, **Balwierz A**, Soons Z, König R, Sahin Ö, Wiemann S; J Pathol. 2014 Aug; 233(4):368-379
4) „**Re-expression of microRNA-375 reverses both tamoxifen resistance and accompanying EMT-like properties in breast cancer.**“; Ward A, **Balwierz A**, Zhang JD, Kublbeck M, Pawitan Y, Hielscher T, Wiemann S, Sahin Ö; Oncogene. 2013 Feb 28; 32(9):1173-1182.
5) “**EGF activates TTP expression by activation of ELK-1 and EGR-1 transcription factors.**“; Florkowska M, Tymoszuk P, **Balwierz A**, Skucha A, Kochan J, Wawro M, Stalinska K, Kasza A; BMC Mol Biol. 2012 Mar 20; 13:8
6) “**MicroRNA-200c represses migration and invasion of breast cancer cells by targeting actin regulatory proteins FHOD1 and PPM1F.**“; Jurmeister S, Baumann M, **Balwierz A**, Keklikoglou I, Ward A, Uhlmann S, Zhang JD, Wiemann S, Sahin Ö; Mol Cell Biol. 2012 Feb; 32(3):633-651.
7) “**Degradation of eukaryotic transcripts. Role and regulation of tristetraprolin activity.**” **Balwierz AK**, Tymoszuk P, Kasza A; Postepy Biochem. 2009; 55(3):290-8. Review. Polish.

9. References

1. Siegel, R., Naishadham, D. & Jemal, A. Cancer Statistics , 2013. 63, 11–30 (2013).

2. American Cancer Society. Cancer Facts & Figures 2013. Atlanta: American Cancer Society. (2013).

3. Ferlay, J. *et al.* Cancer Incidence and Mortality Worldwide: IARC CancerBase No.11 [Internet]. Lyon, France: International Agency for Research on Cancer; 2013. Available from: http://globocan.iarc.fr, accessed on 06/08/2014. *Eur. J. Cancer* 33, (2013).

4. Chen, X. *et al.* Poorer survival of male breast cancer compared with female breast cancer patients may be due to biological differences. *Jpn. J. Clin. Oncol.* 43, 954–63 (2013).

5. Contractor, K. B., Kaur, K., Rodrigues, G. S., Kulkarni, D. M. & Singhal, H. Male breast cancer: is the scenario changing. *World J. Surg. Oncol.* 6, 58 (2008).

6. Beatson, G. T. On the treatment of inoperable cases of carcinoma of the mamma: suggestions for a new method of treatment, with illustrative cases. *Lancet* 148, 104–107

7. Haddow, A., Watkinson, J. M., Paterson, E. & Koller, P. C. Influence of synthetic oestrogens upon advanced malignant disease. *Br. Med. J.* 393–398 (1944).

8. Lacassagne, A. The relation between hormones and cancer. *Can. Med. Assoc. J.* 112–117

9. Cole, M. P., Jones, C. T. A. & Todd, I. D. H. A new anti-oestrogenic agent in late breast cancer - an early clinical appraisal of ICI46474. *Br. J. Cancer* 270–275

10. Ward, H. W. Anti-oestrogen therapy for breast cancer: a trial of tamoxifen at two dose levels. *Br. Med. J.* 1, 13–14 (1973).

11. Nielsen, R., Paul, J. S., Albrechtsen, A. & Song, Y. S. Genotype and SNP calling from next-generation sequencing data. *Nat. Rev. Genet.* 12, 443–51 (2011).

12. Sotiriou, C. & Pusztai, L. Gene-expression signatures in breast cancer. *N. Engl. J. Med.* 360, 790–800 (2009).

13. Yu, X., Schneiderhan-Marra, N. & Joos, T. O. Protein microarrays for personalized medicine. *Clin. Chem.* 56, 376–87 (2010).

14. The Cancer Genome Atlas Network. Comprehensive molecular portraits of human breast tumors. *Nature* 490, 61–70 (2012).

15. Sørlie, T. *et al.* Gene expression patterns of breast carcinomas distinguish tumor subclasses with clinical implications. *Proc. Natl. Acad. Sci. U. S. A.* 98, 10869–74 (2001).

16. Sorlie, T. *et al.* Repeated observation of breast tumor subtypes in independent gene expression data sets. *Proc. Natl. Acad. Sci. U. S. A.* 100, 8418–23 (2003).

17. Goldhirsch, a *et al.* Strategies for subtypes--dealing with the diversity of breast cancer: highlights of the St. Gallen International Expert Consensus on the Primary Therapy of Early Breast Cancer 2011. *Ann. Oncol.* 22, 1736–47 (2011).

18. Parise, C. a & Caggiano, V. Breast Cancer Survival Defined by the ER/PR/HER2 Subtypes and a Surrogate Classification according to Tumor Grade and Immunohistochemical Biomarkers. *J. Cancer Epidemiol.* 2014, 469251 (2014).

19. Turner, N. C. & Reis-Filho, J. S. Basal-like breast cancer and the BRCA1 phenotype. *Oncogene* 25, 5846–53 (2006).

20. Slamon, D. J. *et al.* Studies of the HER2/neu proto-oncogene in human breast and ovarian cancer. *Science (80-.).* 244(4905), 707–712 (1989).

21. Wolff, A. C. *et al.* Recommendations for human epidermal growth factor receptor 2 testing in breast cancer: American Society of Clinical Oncology/College of American Pathologists clinical practice guideline update. *J. Clin. Oncol.* 31, 3997–4013 (2013).

22. Toikkanen, S., Helin, H., Isola, J. & Joensuu, H. Prognostic significance of HER-2 oncoprotein expression in breast cancer: a 30-year follow-up. *J. Clin. Oncol.* 10, 1044–8 (1992).

23. Charpin, C. *et al.* c-erbB-2 oncoprotein detected by automated quantitative immunocytochemistry in breast carcinomas correlates with patients' overall and disease-free survival. *Br. J. Cancer* 75, 1667–73 (1997).

24. Van de Vijver, M. J. *et al.* A gene-expression signature as a predictor of survival in breast cancer. *N. Engl. J. Med.* 347, 1999–2009 (2002).

25. Glas, A. M. *et al.* Converting a breast cancer microarray signature into a high-throughput diagnostic test. *BMC Genomics* 7, 278 (2006).

26. Drukker, C. a *et al.* A prospective evaluation of a breast cancer prognosis signature in the observational RASTER study. *Int. J. Cancer* 133, 929–36 (2013).

27. Drukker, C. a *et al.* Optimized outcome prediction in breast cancer by combining the 70-gene signature with clinical risk prediction algorithms. *Breast Cancer Res. Treat.* 145, 697–705 (2014).

28. Paik, S. *et al.* A multigene assay to predict recurrence of tamoxifen-treated, node-negative breast cancer. *N. Engl. J. Med.* 351, 2817–26 (2004).

29. Parker, J. S. *et al.* Supervised risk predictor of breast cancer based on intrinsic subtypes. *J. Clin. Oncol.* 27, 1160–7 (2009).

30. Krijgsman, O. *et al.* A diagnostic gene profile for molecular subtyping of breast cancer associated with treatment response. *Breast Cancer Res. Treat.* 133, 37–47 (2012).

31. Whitworth, P. *et al.* Chemosensitivity Predicted by BluePrint 80-Gene Functional Subtype and MammaPrint in the Prospective Neoadjuvant Breast Registry Symphony Trial (NBRST). *Ann. Surg. Oncol.* (2014). doi:10.1245/s10434-014-3908-y

32. Roepman, P. *et al.* Microarray-based determination of estrogen receptor, progesterone receptor, and HER2 receptor status in breast cancer. *Clin. Cancer Res.* 15, 7003–11 (2009).

33. Ma, X.-J. *et al.* A Five-Gene Molecular Grade Index and HOXB13:IL17BR Are Complementary Prognostic Factors in Early Stage Breast Cancer. *Clin. Cancer Res.* 14, 2601–2608 (2008).

34. Jerevall, P.-L. *et al.* Prognostic utility of HOXB13:IL17BR and molecular grade index in early-stage breast cancer patients from the Stockholm trial. *Br. J. Cancer* 104, 1762–9 (2011).

35. Jankowitz, R. C. *et al.* Prognostic utility of the breast cancer index and comparison to Adjuvant! Online in a clinical case series of early breast cancer. *Breast Cancer Res.* 13, R98 (2011).

36. Haibe-Kains, B. *et al.* A three-gene model to robustly identify breast cancer molecular subtypes. *J. Natl. Cancer Inst.* 104, 311–25 (2012).

37. Prat, a, Parker, J. S., Fan, C. & Perou, C. M. PAM50 assay and the three-gene model for identifying the major and clinically relevant molecular subtypes of breast cancer. *Breast Cancer Res. Treat.* 135, 301–6 (2012).

38. Cuzick, J. *et al.* Prognostic value of a combined estrogen receptor, progesterone receptor, Ki-67, and human epidermal growth factor receptor 2 immunohistochemical score and comparison with the Genomic Health recurrence score in early breast cancer. *J. Clin. Oncol.* 29, 4273–8 (2011).

39. Bartlett, J. M. S. *et al.* Mammostrat as a tool to stratify breast cancer patients at risk of recurrence during endocrine therapy. *Breast Cancer Res.* 12, R47 (2010).

40. Green, a R. *et al.* Identification of key clinical phenotypes of breast cancer using a reduced panel of protein biomarkers. *Br. J. Cancer* 109, 1886–94 (2013).

41. Rakha, E. a *et al.* Nottingham Prognostic Index Plus (NPI+): a modern clinical decision making tool in breast cancer. *Br. J. Cancer* 110, 1688–97 (2014).

42. Ward, S. *et al.* Gene expression profiling and expanded immunohistochemistry tests to guide the use of adjuvant chemotherapy in breast cancer management: a systematic review and cost-effectiveness analysis. *Health Technol. Assess.* 17, 1–302 (2013).

43. Metzger Filho, O., Ignatiadis, M. & Sotiriou, C. Genomic Grade Index: An important tool for assessing breast cancer tumor grade and prognosis. *Crit. Rev. Oncol. Hematol.* 77, 20–9 (2011).

44. Hallett, R. M., Dvorkin-Gheva, A., Bane, A. & Hassell, J. a. A gene signature for predicting outcome in patients with basal-like breast cancer. *Sci. Rep.* 2, 227 (2012).

45. Chang, H. Y. *et al.* Robustness, scalability, and integration of a wound-response gene expression signature in predicting breast cancer survival. *Proc. Natl. Acad. Sci. U. S. A.* 102, 3738–43 (2005).

46. Tutt, A. *et al.* Risk estimation of distant metastasis in node-negative, estrogen receptor-positive breast cancer patients using an RT-PCR based prognostic expression signature. *BMC Cancer* 8, 339 (2008).

47. Wang, Y. *et al.* Gene-expression profiles to predict distant metastasis of lymph-node-negative primary breast cancer. *Lancet* 365, 671–9 (2005).

48. Miller, L. D. *et al.* An expression signature for p53 status in human breast cancer predicts mutation status, transcriptional effects, and patient survival. *Proc. Natl. Acad. Sci. U. S. A.* 102, 13550–5 (2005).

49. Teschendorff, A. E. & Caldas, C. A robust classifier of high predictive value to identify good prognosis patients in ER-negative breast cancer. *Breast Cancer Res.* 10, R73 (2008).

50. Yau, C. *et al.* A multigene predictor of metastatic outcome in early stage hormone receptor-negative and triple-negative breast cancer. *Breast Cancer Res.* 12, R85 (2010).

51. Yau, C. *et al.* An optimized five-gene multi-platform predictor of hormone receptor negative and triple negative breast cancer metastatic risk. *Breast Cancer Res.* 15, R103 (2013).

52. Carter, P. *et al.* Humanization of an anti-p185HER2 antibody for human cancer therapy. *Proc. Natl. Acad. Sci. U. S. A.* 89, 4285–9 (1992).

53. Cobleigh, M. a *et al.* Multinational study of the efficacy and safety of humanized anti-HER2 monoclonal antibody in women who have HER2-overexpressing metastatic breast cancer that has progressed after chemotherapy for metastatic disease. *J. Clin. Oncol.* 17, 2639–48 (1999).

54. Slamon, D. J. *et al.* Use of chemotherapy plus a monoclonal antibody against HER2 for metastatic breast cancer that overexpresses HER2. *N. Engl. J. Med.* 344, 783–792 (2001).

55. Sauter, G., Lee, J., Bartlett, J. M. S., Slamon, D. J. & Press, M. F. Guidelines for human epidermal growth factor receptor 2 testing: biologic and methodologic considerations. *J. Clin. Oncol.* 27, 1323–33 (2009).

56. Hammond, M. E. H. *et al.* American Society of Clinical Oncology/College Of American Pathologists guideline recommendations for immunohistochemical testing of estrogen and progesterone receptors in breast cancer. *J. Clin. Oncol.* 28, 2784–95 (2010).

57. Burstein, H. J. *et al.* Adjuvant Endocrine Therapy for Women With Hormone Receptor-Positive Breast Cancer: American Society of Clinical Oncology Clinical Practice Guideline Focused Update. *J. Clin. Oncol.* 1–16 (2014). doi:10.1200/JCO.2013.54.2258

58. Goldhirsch, a *et al.* Personalizing the treatment of women with early breast cancer: highlights of the St Gallen International Expert Consensus on the Primary Therapy of Early Breast Cancer 2013. *Ann. Oncol.* 24, 2206–23 (2013).

59. Ishitobi, M. *et al.* Phase II study of neoadjuvant anastrozole and concurrent radiotherapy for postmenopausal breast cancer patients. *Breast Cancer* (2012). doi:10.1007/s12282-012-0426-2

60. Giordano, S. H. *et al.* Systemic therapy for patients with advanced human epidermal growth factor receptor 2-positive breast cancer: american society of clinical oncology clinical practice guideline. *J. Clin. Oncol.* 32, 2078–99 (2014).

61. Gianni, L. *et al.* Neoadjuvant chemotherapy with trastuzumab followed by adjuvant trastuzumab versus neoadjuvant chemotherapy alone, in patients with HER2-positive locally advanced breast cancer (the NOAH trial): a randomised controlled superiority trial with a parallel HER. *Lancet* 375, 377–84 (2010).

62. Arteaga, C. L. & Engelman, J. A. ERBB Receptors: From Oncogene Discovery to Basic Science to Mechanism-Based Cancer Therapeutics. *Cancer Cell* 25, 282–303 (2014).

63. Romond, E. H. *et al.* Trastuzumab plus adjuvant chemotherapy for operable HER2-positive breast cancer. *N. Engl. J. Med.* 353, 1673–84 (2005).

64. Bines, J. & Eniu, A. Effective but cost-prohibitive drugs in breast cancer treatment: a clinician's perspective. *Cancer* 113, 2353–8 (2008).

65. Gianni, L. *et al.* Efficacy and safety of neoadjuvant pertuzumab and trastuzumab in women with locally advanced, inflammatory, or early HER2-positive breast cancer (NeoSphere): a randomised multicentre, open-label, phase 2 trial. *Lancet Oncol.* 13, 25–32 (2012).

66. Citri, A. & Yarden, Y. EGF-ERBB signaling: towards the systems level. *Nat. Rev. Mol. Cell Biol.* 7, 505–16 (2006).

67. Olayioye, M. A., Neve, R. M., Lane, H. A. & Hynes, N. E. The ErbB signaling network: receptor heterodimerization in development and cancer. *EMBO J.* 19, 3159–3167 (2000).

68. Burgess, A. W. *et al.* An Open-and-Shut Case ? Recent Insights into the Activation of EGF / ErbB Receptors CSIRO Health Science and Nutrition. 12, 541–552 (2008).

69. Klapper, L. N. *et al.* The ErbB-2/HER2 oncoprotein of human carcinomas may function solely as a shared coreceptor for multiple stroma-derived growth factors. *Proc. Natl. Acad. Sci. U. S. A.* 96, 4995–5000 (1999).

70. Guy, P. M., Platko, J. V, Cantleyt, L. C., Cerione, R. A. & Iiitt, K. L. C. Insect cell-expressed p180/ERBB3 possesses an impaired tyrosine kinase activity. *Proc. Natl. Acad. Sci. U. S. A.* 91, 8132–8136 (1994).

71. Pinkas-Kramarski, R. *et al.* Diversification of Neu differentiation factor and epidermal growth factor signaling by combinatorial receptor interactions. *EMBO J.* 15, 2452–67 (1996).

72. Shi, F., Telesco, S. E., Liu, Y., Radhakrishnan, R. & Lemmon, M. a. ErbB3/HER3 intracellular domain is competent to bind ATP and catalyze autophosphorylation. *Proc. Natl. Acad. Sci. U. S. A.* 107, 7692–7 (2010).

73. Dawson, J. P. *et al.* Epidermal Growth Factor Receptor Dimerization and Activation Require Ligand-Induced Conformational Changes in the Dimer Interface. *Mol. Cell. Biol.* 25, 7734–7742 (2005).

74. Jura, N., Shan, Y., Cao, X., Shaw, D. E. & Kuriyan, J. Structural analysis of the catalytically inactive kinase domain of the human EGF receptor 3. *Proc. Natl. Acad. Sci. U. S. A.* 106, 21608–13 (2009).

75. Cho, H.-S. & Leahy, D. J. Structure of the extracellular region of HER3 reveals an interdomain tether. *Science* 297, 1330–3 (2002).

76. Garrett, T. P. J. *et al.* The Crystal Structure of a Truncated ErbB2 Ectodomain Reveals an Active Conformation , Poised to Interact with Other ErbB Receptors Cooperative Research Centre for Cellular Growth Factors CSIRO Health Sciences and Nutrition. 11, 495–505 (2008).

77. Wang, Z., Zhang, L., Yeung, T. K. & Chen, X. Endocytosis deficiency of epidermal growth factor (EGF) receptor-ErbB2 heterodimers in response to EGF stimulation. *Mol. Biol. Cell* 10, 1621–36 (1999).

78. Haslekås, C. *et al.* The Inhibitory Effect of ErbB2 on Epidermal Growth Factor-induced Formation of Clathrin-coated Pits Correlates with Retention of Epidermal Growth

Factor Receptor – ErbB2 Oligomeric Complexes at the Plasma Membrane. 16, 5832–5842 (2005).

79. Hendriks, B. S., Opresko, L. K., Wiley, H. S. & Lauffenburger, D. Quantitative analysis of HER2-mediated effects on HER2 and epidermal growth factor receptor endocytosis: distribution of homo- and heterodimers depends on relative HER2 levels. *J. Biol. Chem.* 278, 23343–51 (2003).

80. Karunagaran, D. *et al.* ErbB-2 is a common auxiliary subunit of NDF and EGF receptors: implications for breast cancer. *EMBO J.* 15, 254–64 (1996).

81. Harari, D. & Yarden, Y. Molecular mechanisms underlying ErbB2/HER2 action in breast cancer. *Oncogene* 19, 6102–14 (2000).

82. Ward, C. W. & Lawrence, M. C. Similar but different: ligand-induced activation of the insulin and epidermal growth factor receptor families. *Curr. Opin. Struct. Biol.* 22, 360–6 (2012).

83. Alvarado, D., Klein, D. E. & Lemmon, M. a. ErbB2 resembles an autoinhibited invertebrate epidermal growth factor receptor. *Nature* 461, 287–91 (2009).

84. Carraway, K. L. *et al.* An Intramembrane Modulator of the ErbB2 Receptor Tyrosine Kinase That Potentiates Neuregulin Signaling. *J. Biol. Chem.* 274, 5263–5266 (1999).

85. Ramsauer, V. P. *et al.* Muc4 – ErbB2 Complex Formation and Signaling in Polarized CACO-2 Epithelial Cells Indicate That Muc4 Acts as an Unorthodox Ligand for ErbB2. 17, 2931–2941 (2006).

86. Kozloski, G. a, Carraway, C. a C. & Carraway, K. L. Mechanistic and signaling analysis of Muc4-ErbB2 signaling module: new insights into the mechanism of ligand-independent ErbB2 activity. *J. Cell. Physiol.* 224, 649–57 (2010).

87. Burden, S. & Yarden, Y. Neuregulins and their receptors: a versatile signaling module in organogenesis and oncogenesis. *Neuron* 18, 847–55 (1997).

88. Elenius, K., Paul, S., Allison, G., Sun, J. & Klagsbrun, M. Activation of HER4 by heparin-binding EGF-like growth factor stimulates chemotaxis but not proliferation. *EMBO J.* 16, 1268–78 (1997).

89. Higashiyama, S., Abraham, J. a, Miller, J., Fiddes, J. C. & Klagsbrun, M. A heparin-binding growth factor secreted by macrophage-like cells that is related to EGF. *Science* 251, 936–9 (1991).

90. Wieduwilt, M. J. & Moasser, M. M. The epidermal growth factor receptor family: biology driving targeted therapeutics. *Cell. Mol. Life Sci.* 65, 1566–84 (2008).

91. Arteaga, C. L. *et al.* Treatment of HER2-positive breast cancer: current status and future perspectives. *Nat. Rev. Clin. Oncol.* 9, 16–32 (2012).

92. Chen, W. W. *et al.* Input-output behavior of ErbB signaling pathways as revealed by a mass action model trained against dynamic data. *Mol. Syst. Biol.* 5, 239 (2009).

93. Uchida, T. *et al.* A Novel Epidermal Growth Factor-like Molecule Containing Two Follistatin Modules Stimulates Tyrosine Phosphorylation of erbB-4 in MKN28 Gastric Cancer Cells. *Biochem. Biophys. Res. Commun.* 266, 593–602 (1999).

94. Kinugasa, Y. *et al.* Neuroglycan C, a novel member of the neuregulin family. *Biochem. Biophys. Res. Commun.* 321, 1045–9 (2004).

95. Hayes, N. V. L. & Gullick, W. J. The neuregulin family of genes and their multiple splice variants in breast cancer. *J. Mammary Gland Biol. Neoplasia* 13, 205–14 (2008).

96. Vermeer, P. D. *et al.* ErbB2, EphrinB1, Src Kinase and PTPN13 Signaling Complex Regulates MAP Kinase Signaling in Human Cancers. *PLoS One* 7, e30447 (2012).

97. Higashiyama, S. & Nanba, D. ADAM-mediated ectodomain shedding of HB-EGF in receptor cross-talk. *Biochim. Biophys. Acta* 1751, 110–7 (2005).

98. Steinthorsdottir, V. *et al.* Multiple novel transcription initiation sites for NRG1. *Gene* 342, 97–105 (2004).

99. Flicek, P. *et al.* Ensembl 2014. *Nucleic Acids Res.* 42, D749–55 (2014).

100. Wang, J. *et al.* Bringing cancer serological diagnosis to a new level: focusing on HER2, protein ectodomain shedding and neoepitope technology. *Futur. Oncol.* 9, 35–44 (2013).

101. Sasso, M., Bianchi, F., Ciravolo, V., Tagliabue, E. & Campiglio, M. HER2 splice variants and their relevance in breast cancer. *J. Nucleic Acids Investig.* 2, (2011).

102. Marchini, C. *et al.* The human splice variant Δ16HER2 induces rapid tumor onset in a reporter transgenic mouse. *PLoS One* 6, e18727 (2011).

103. Bertelsen, V. & Stang, E. The Mysterious Ways of ErbB2/HER2 Trafficking. *Membranes (Basel).* 4, 424–446 (2014).

104. Liu, P. C. C. *et al.* Identification of ADAM10 as a major source of HER2 ectodomain sheddase activity in HER2 overexpressing breast cancer cells. *Cancer Biol. Ther.* 5, 657–664 (2006).

105. Codony-servat, J., Albanell, J., Lopez-talavera, J. C. & Cells, C. Cleavage of the HER2 Ectodomain Is a Pervanadate-activable Process That Is Inhibited by the Tissue Inhibitor of Metalloproteases-1 in Breast Cancer Cells Advances in Brief Cleavage of the HER2 Ectodomain Is a Pervanadate-activable Process That Is Inhibite. 1196–1201 (1999).

106. Pedersen, K. *et al.* A naturally occurring HER2 carboxy-terminal fragment promotes mammary tumor growth and metastasis. *Mol. Cell. Biol.* 29, 3319–31 (2009).

107. García-Castillo, J. *et al.* HER2 carboxyl-terminal fragments regulate cell migration and cortactin phosphorylation. *J. Biol. Chem.* 284, 25302–13 (2009).

108. Piccione, E. C. *et al.* A novel epidermal growth factor receptor variant lacking multiple domains directly activates transcription and is overexpressed in tumors. *Oncogene* 31, 2953–67 (2012).

109. Andrique, L. *et al.* ErbB3(80 kDa), a nuclear variant of the ErbB3 receptor, binds to the Cyclin D1 promoter to activate cell proliferation but is negatively controlled by p14ARF. *Cell. Signal.* 24, 1074–85 (2012).

110. Williams, C. C. *et al.* The ERBB4/HER4 receptor tyrosine kinase regulates gene expression by functioning as a STAT5A nuclear chaperone. *J. Cell Biol.* 167, 469–78 (2004).

111. Wang, S.-C. & Hung, M.-C. Nuclear translocation of the epidermal growth factor receptor family membrane tyrosine kinase receptors. *Clin. Cancer Res.* 15, 6484–9 (2009).

112. Chandarlapaty, S. *et al.* Inhibitors of HSP90 block p95-HER2 signaling in Trastuzumab-resistant tumors and suppress their growth. *Oncogene* 29, 325–34 (2010).

113. Borg, J. P. *et al.* ERBIN: a basolateral PDZ protein that interacts with the mammalian ERBB2/HER2 receptor. *Nat. Cell Biol.* 2, 407–14 (2000).

114. Huang, Y. Z., Zang, M., Xiong, W. C., Luo, Z. & Mei, L. Erbin suppresses the MAP kinase pathway. *J. Biol. Chem.* 278, 1108–14 (2003).

115. Fiorentino, L. *et al.* Inhibition of ErbB-2 Mitogenic and Transforming Activity by RALT , a Mitogen-Induced Signal Transducer Which Binds to the ErbB-2 Kinase Domain Inhibition of ErbB-2 Mitogenic and Transforming Activity by RALT , a Mitogen-Induced Signal Transducer Which Bin. (2000). doi:10.1128/MCB.20.20.7735-7750.2000.Updated

116. Zrihan-Licht, S. Csk Homologous Kinase, a Novel Signaling Molecule, Directly Associates with the Activated ErbB-2 Receptor in Breast Cancer Cells and Inhibits Their Proliferation. *J. Biol. Chem.* 273, 4065–4072 (1998).

117. Kim, S. *et al.* Csk homologous kinase (CHK) and ErbB-2 interactions are directly coupled with CHK negative growth regulatory function in breast cancer. *J. Biol. Chem.* 277, 36465–70 (2002).

118. Jaulin-Bastard, F. *et al.* The ERBB2/HER2 receptor differentially interacts with ERBIN and PICK1 PSD-95/DLG/ZO-1 domain proteins. *J. Biol. Chem.* 276, 15256–63 (2001).

119. Nahta, R., Yuan, L. X. H., Zhang, B., Kobayashi, R. & Esteva, F. J. Insulin-like growth factor-I receptor/human epidermal growth factor receptor 2 heterodimerization

contributes to trastuzumab resistance of breast cancer cells. *Cancer Res.* 65, 11118–28 (2005).

120. Huang, X. *et al.* Heterotrimerization of the growth factor receptors erbB2, erbB3, and insulin-like growth factor-i receptor in breast cancer cells resistant to herceptin. *Cancer Res.* 70, 1204–14 (2010).

121. Zhang, S. *et al.* Combating trastuzumab resistance by targeting SRC, a common node downstream of multiple resistance pathways. *Nat. Med.* 17, 461–9 (2011).

122. Qiu, Y., Ravi, L. & Kung, H. J. Requirement of ErbB2 for signaling by interleukin-6 in prostate carcinoma cells. *Nature* 393, 83–5 (1998).

123. Schulze, W. X., Deng, L. & Mann, M. Phosphotyrosine interactome of the ErbB-receptor kinase family. *Mol. Syst. Biol.* 1, 2005.0008 (2005).

124. Saxena, R. & Dwivedi, A. ErbB Family Receptor Inhibitors as Therapeutic Agents in Breast Cancer : Current Status and Future Clinical Perspective. *Med. Res. Rev.* 32, 166–215 (2012).

125. Gale, N. W., Kaplan, S., Lowenstein, E. J., Schlessinger, J. & Bar-Sagi, D. GRB2 mediates the EGF-dependent activation of guanine nucleotide exchange on RAS. *Nature* 363, 88–92 (1993).

126. Yamasaki, S. *et al.* Gab1 is required for EGF receptor signaling and the transformation by activated ErbB2. *Oncogene* 22, 1546–56 (2003).

127. Bentires-Alj, M. *et al.* A role for the scaffolding adapter GAB2 in breast cancer. *Nat. Med.* 12, 114–21 (2006).

128. Lowenstein, E. J. *et al.* The SH2 and SH3 Domain-Containing Protein GRB2 Links Receptor Tyrosine Kinases to ras Signaling. *Cell* 70, 431–442 (1992).

129. Gureasko, J. *et al.* Membrane-dependent signal integration by the Ras activator Son of sevenless. *Nat. Struct. Mol. Biol.* 15, 452–61 (2008).

130. Jelinek, T., Dent, P., Sturgill, T. W. & Weber, M. J. Ras-induced activation of Raf-1 is dependent on tyrosine phosphorylation. *Mol. Cell. Biol.* 16, 1027–1034 (1996).

131. Kolch, W. Meaningful relationships : the regulation of the Ras/Raf/MEK/ERK pathway by protein interactions. *Biochem. J.* 351, 289–305 (2000).

132. Baselga, J. & Swain, S. M. Novel anticancer targets: revisiting ERBB2 and discovering ERBB3. *Nat. Rev. Cancer* 9, 463–75 (2009).

133. Irie, H. Y. *et al.* Distinct roles of Akt1 and Akt2 in regulating cell migration and epithelial-mesenchymal transition. *J. Cell Biol.* 171, 1023–34 (2005).

134. Castellano, E. & Downward, J. RAS Interaction with PI3K: More Than Just Another Effector Pathway. *Genes Cancer* 2, 261–74 (2011).

135. Maehama, T. & Dixon, J. E. The Tumor Suppressor, PTEN/MMAC1, Dephosphorylates the Lipid Second Messenger, Phosphatidylinositol 3,4,5-Trisphosphate. *J. Biol. Chem.* 273, 13375–13378 (1998).

136. Anderson, K. E., Coadwell, J., Stephens, L. R. & Hawkins, P. T. Translocation of PDK-1 to the plasma membrane is important in allowing PDK-1 to activate protein kinase B. *Curr. Biol.* 8, 684–91 (1998).

137. Sarbassov, D. D., Guertin, D. a, Ali, S. M. & Sabatini, D. M. Phosphorylation and regulation of Akt/PKB by the rictor-mTOR complex. *Science* 307, 1098–101 (2005).

138. Datta, S. R. *et al.* Akt phosphorylation of BAD couples survival signals to the cell-intrinsic death machinery. *Cell* 91, 231–41 (1997).

139. Gardai, S. J. *et al.* Phosphorylation of Bax Ser184 by Akt regulates its activity and apoptosis in neutrophils. *J. Biol. Chem.* 279, 21085–95 (2004).

140. Ogawara, Y. *et al.* Akt enhances Mdm2-mediated ubiquitination and degradation of p53. *J. Biol. Chem.* 277, 21843–50 (2002).

141. Dummler, B. *et al.* Life with a single isoform of Akt: mice lacking Akt2 and Akt3 are viable but display impaired glucose homeostasis and growth deficiencies. *Mol. Cell. Biol.* 26, 8042–51 (2006).

142. Hutchinson, J. N., Jin, J., Cardiff, R. D., Woodgett, J. R. & Muller, W. J. Activation of Akt-1 (PKB-α) Can Accelerate ErbB-2-Mediated Mammary Tumorigenesis but Suppresses Tumor Invasion. *Cancer Res.* 64, 3171–3178 (2004).

143. Arboleda, M. J. *et al.* Overexpression of AKT2/protein kinase Bbeta leads to up-regulation of beta1 integrins, increased invasion, and metastasis of human breast and ovarian cancer cells. *Cancer Res.* 63, 196–206 (2003).

144. Peles, E., Levy, R. Ben, Or, E., Ulirich, A. & Yarden, Y. Oncogenic forms of the neu/HER2 tyrosine kinase are permanently coupled to phospholipase Cgamma. *EMBO J.* 10, 2077–2086 (1991).

145. Berridge, M. J. & Irvine, R. F. Inositol phosphates and cell signaling. *Nature* 341, 197–205 (1989).

146. Tan, M., Li, P., Sun, M., Yin, G. & Yu, D. Upregulation and activation of PKC alpha by ErbB2 through Src promotes breast cancer cell invasion that can be blocked by combined treatment with PKC alpha and Src inhibitors. *Oncogene* 25, 3286–95 (2006).

147. Urtreger, A. J., Kazanietz, M. G. & Bal de Kier Joffé, E. D. Contribution of individual PKC isoforms to breast cancer progression. *IUBMB Life* 64, 18–26 (2012).

148. Liu, J. & Kern, J. a. Neuregulin-1 activates the JAK-STAT pathway and regulates lung epithelial cell proliferation. *Am. J. Respir. Cell Mol. Biol.* 27, 306–13 (2002).

149. Ren, Z. & Schaefer, T. S. ErbB-2 activates Stat3 alpha in a Src- and JAK2-dependent manner. *J. Biol. Chem.* 277, 38486–93 (2002).

150. Austin, C. D. *et al.* Endocytosis and Sorting of ErbB2 and the Site of Action of Cancer Therapeutics Trastuzumab and Geldanamycin. *Mol. Biol. Cell* 15, 5268–5282 (2004).

151. Cortese, K. *et al.* The HSP90 inhibitor geldanamycin perturbs endosomal structure and drives recycling ErbB2 and transferrin to modified MVBs/lysosomal compartments. *Mol. Biol. Cell* 24, 129–44 (2013).

152. Yuan, T., Wang, Y., Zhao, Z. J. & Gu, H. Protein-tyrosine phosphatase PTPN9 negatively regulates ErbB2 and epidermal growth factor receptor signaling in breast cancer cells. *J. Biol. Chem.* 285, 14861–70 (2010).

153. Zhu, J.-H. *et al.* Protein tyrosine phosphatase PTPN13 negatively regulates Her2/ErbB2 malignant signaling. *Oncogene* 27, 2525–31 (2008).

154. Rubin, C. *et al.* Sprouty fine-tunes EGF signaling through interlinked positive and negative feedback loops. *Curr. Biol.* 13, 297–307 (2003).

155. Marx, C., Held, J. M., Gibson, B. W. & Benz, C. C. ErbB2 trafficking and degradation associated with K48 and K63 polyubiquitination. *Cancer Res.* 70, 3709–17 (2010).

156. Levkowitz, G. *et al.* c-Cbl is a suppressor of the neu oncogene. *J. Biol. Chem.* 275, 35532–9 (2000).

157. Xu, W. *et al.* Chaperone-dependent E3 ubiquitin ligase CHIP mediates a degradative pathway for c-ErbB2/Neu. *Proc. Natl. Acad. Sci. U. S. A.* 99, 12847–52 (2002).

158. Laederich, M. B. *et al.* The leucine-rich repeat protein LRIG1 is a negative regulator of ErbB family receptor tyrosine kinases. *J. Biol. Chem.* 279, 47050–6 (2004).

159. Hens, J. R. & Wysolmerski, J. J. Key stages of mammary gland development: molecular mechanisms involved in the formation of the embryonic mammary gland. *Breast Cancer Res.* 7, 220–4 (2005).

160. Brisken, C. & O'Malley, B. Hormone action in the mammary gland. *Cold Spring Harb. Perspect. Biol.* 2, a003178 (2010).

161. Hynes, N. E. & Watson, C. J. Mammary gland growth factors: roles in normal development and in cancer. *Cold Spring Harb. Perspect. Biol.* 2, a003186 (2010).

162. Soloff, M. S. Oxytocin receptors and mammary myoepithelial cells. *J. Dairy Sci.* 65, 326–37 (1982).

163. Van Amerongen, R., Bowman, A. N. & Nusse, R. Developmental stage and time dictate the fate of Wnt/β-catenin-responsive stem cells in the mammary gland. *Cell Stem Cell* 11, 387–400 (2012).

164. Casalini, P., Iorio, M. V, Galmozzi, E. & Ménard, S. Role of HER receptors family in development and differentiation. *J. Cell. Physiol.* 200, 343–50 (2004).

165. Sebastian, J. *et al.* Activation and function of the epidermal growth factor receptor and ERBB2 during mammary gland morphogenesis. *Cell Growth Differ.* 9, 777–785 (1998).

166. Jackson-Fisher, A. J. *et al.* ErbB2 is required for ductal morphogenesis of the mammary gland. *Proc. Natl. Acad. Sci. U. S. A.* 101, 17138–43 (2004).

167. Andrechek, E. R., White, D. & Muller, W. J. Targeted disruption of ErbB2/Neu in the mammary epithelium results in impaired ductal outgrowth. *Oncogene* 24, 932–7 (2005).

168. Jackson-Fisher, A. J. *et al.* ErbB3 is required for ductal morphogenesis in the mouse mammary gland. *Breast Cancer Res.* 10, R96 (2008).

169. Tidcombe, H. *et al.* Neural and mammary gland defects in ErbB4 knockout mice genetically rescued from embryonic lethality. *Proc. Natl. Acad. Sci. U. S. A.* 100, 8281–6 (2003).

170. Arteaga, C. L. & Engelman, J. a. ERBB receptors: from oncogene discovery to basic science to mechanism-based cancer therapeutics. *Cancer Cell* 25, 282–303 (2014).

171. Park, H. S. *et al.* High EGFR gene copy number predicts poor outcome in triple-negative breast cancer. *Mod. Pathol.* 27, 1212–1222 (2014).

172. Arteaga, C. L. Epidermal Growth Factor Receptor Dependence in Human Tumors: More Than Just Expression? *Oncologist* 7, 31–39 (2002).

173. Pietras, R. J. *et al.* Monoclonal Antibody to HER-2/neu Receptor Modulates Repair of Radiation-induced DNA Damage and Enhances Radiosensitivity of Human Breast Cancer Cells Overexpressing This Oncogene. *Cancer Res.* 59, 1347–1355 (1999).

174. Slamon, D. J. *et al.* Human breast cancer: Correlation of relapse and survival with amplification of the HER-2/neu oncogene. *Science (80-.).* 235, 177–182 (1987).

175. Staaf, J. *et al.* High-resolution genomic and expression analyses of copy number alterations in HER2-amplified breast cancer. *Breast Cancer Res.* 12, R25 (2010).

176. Bai, T. & Luoh, S.-W. GRB-7 facilitates HER-2/Neu-mediated signal transduction and tumor formation. *Carcinogenesis* 29, 473–9 (2008).

177. Han, D. C., Shen, T. L. & Guan, J. L. Role of Grb7 targeting to focal contacts and its phosphorylation by focal adhesion kinase in regulation of cell migration. *J. Biol. Chem.* 275, 28911–7 (2000).

178. Katz, E. *et al.* A gene on the HER2 amplicon, C35, is an oncogene in breast cancer whose actions are prevented by inhibition of Syk. *Br. J. Cancer* 103, 401–10 (2010).

179. Wolff, A. C. *et al.* American Society of Clinical Oncology/College of American Pathologists guideline recommendations for human epidermal growth factor receptor 2 testing in breast cancer. *J. Clin. Oncol.* 25, 118–45 (2007).

180. Rakha, E. a, Starczynski, J., Lee, A. H. S. & Ellis, I. O. The updated ASCO/CAP guideline recommendations for HER2 testing in the management of invasive breast cancer: a critical review of their implications for routine practice. *Histopathology* 64, 609–15 (2014).

181. Vergara-Lluri, M. E., Moatamed, N. a, Hong, E. & Apple, S. K. High concordance between HercepTest immunohistochemistry and ERBB2 fluorescence in situ hybridization before and after implementation of American Society of Clinical Oncology/College of American Pathology 2007 guidelines. *Mod. Pathol.* 25, 1326–32 (2012).

182. Allison, M. The HER2 testing conundrum. *Nat. Biotechnol.* 28, 117–9 (2010).

183. DeFazio-Eli, L. *et al.* Quantitative assays for the measurement of HER1-HER2 heterodimerization and phosphorylation in cell lines and breast tumors: applications for diagnostics and targeted drug mechanism of action. *Breast Cancer Res.* 13, R44 (2011).

184. Sperinde, J. *et al.* Quantitation of p95HER2 in paraffin sections by using a p95-specific antibody and correlation with outcome in a cohort of trastuzumab-treated breast cancer patients. *Clin. Cancer Res.* 16, 4226–35 (2010).

185. Lipton, A. *et al.* HER3, p95HER2, and HER2 protein expression levels define multiple subtypes of HER2-positive metastatic breast cancer. *Breast Cancer Res. Treat.* 141, 43–53 (2013).

186. Huang, W. *et al.* Comparison of central HER2 testing with quantitative total HER2 expression and HER2 homodimer measurements using a novel proximity-based assay. *Am. J. Clin. Pathol.* 134, 303–11 (2010).

187. Spears, M. *et al.* In situ detection of HER2:HER2 and HER2:HER3 protein-protein interactions demonstrates prognostic significance in early breast cancer. *Breast Cancer Res. Treat.* 132, 463–70 (2012).

188. Tabatabaei-Panah, A.-S. *et al.* Accurate sensitivity of quantum dots for detection of HER2 expression in breast cancer cells and tissues. *J. Fluoresc.* 23, 293–302 (2013).

189. Wulfkuhle, J. D. *et al.* Molecular analysis of HER2 signaling in human breast cancer by functional protein pathway activation mapping. *Clin. Cancer Res.* 18, 6426–35 (2012).

190. Gujral, T. S. *et al.* Profiling phospho-signaling networks in breast cancer using reverse-phase protein arrays. *Oncogene* 32, 3470–6 (2013).

191. Frogne, T., Laenkholm, A.-V., Lyng, M. B., Henriksen, K. L. & Lykkesfeldt, A. E. Determination of HER2 phosphorylation at tyrosine 1221/1222 improves prediction of poor survival for breast cancer patients with hormone receptor-positive tumors. *Breast Cancer Res.* 11, R11 (2009).

192. Thor, A. D. *et al.* Activation (tyrosine phosphorylation) of ErbB-2 (HER-2/neu): A Study of Incidence and Correlation With Outcome in Breast Cancer. *J. Clin. Oncol.* 18, 3230–3239 (2000).

193. Atlas, E., Cardillo, M., Mehmi, I., Zahedkargaran, H. & Tang, C. Heregulin Is Sufficient for the Promotion of Tumorigenicity and Metastasis of Breast Cancer Cells in Vivo 1 1 NIH , Contract No . DK49049 (R . L .); Department of Energy under Contract No . DE-AC03 76SF00098 (R . L .); and National Cancer Institute of C. 49049, (2003).

194. Bates, M. *et al.* Identification of a subpopulation of metastatic breast cancer patients with very high HER2 expression levels and possible resistance to trastuzumab. *Ann. Oncol.* 22, 2014–20 (2011).

195. Arnould, L. *et al.* Pathologic complete response to trastuzumab-based neoadjuvant therapy is related to the level of HER-2 amplification. *Clin. Cancer Res.* 13, 6404–9 (2007).

196. Toi, M. *et al.* Differential survival following trastuzumab treatment based on quantitative HER2 expression and HER2 homodimers in a clinic-based cohort of patients with metastatic breast cancer. *BMC Cancer* 10, 56 (2010).

197. Isola, J. *et al.* Genetic Alterations in ERBB2 -amplified Breast Carcinomas. *Clin. Cancer Res.* 5, 4140–4145 (1999).

198. Kallioniemi, O.-P. *et al.* ERBB2 amplification in breast cancer analyzed by fluorescence in situ hybridization. *Proc. Natl. Acad. Sci.* 89, 5321–5325 (1992).

199. Szöllösi, J., Balázs, M., Feuerstein, B. G., Benz, C. & Waldman, M. ERBB-2 (HER2 / neu) Gene Copy Number , p185 HER-2 Overexpression , and Intratumor Heterogeneity in Human Breast Cancer Heterogeneity in Human Breast Cancer ’. 2, 5400–5407 (1995).

200. Joensuu, H. *et al.* Very high quantitative tumor HER2 content and outcome in early breast cancer. *Ann. Oncol.* 22, 2007–13 (2011).

201. Ghosh, R. *et al.* Trastuzumab has preferential activity against breast cancers driven by HER2 homodimers. *Cancer Res.* 71, 1871–82 (2011).

202. Hervent, A.-S. & De Keulenaer, G. W. Molecular mechanisms of cardiotoxicity induced by ErbB receptor inhibitor cancer therapeutics. *Int. J. Mol. Sci.* 13, 12268–86 (2012).

203. Nahta, R. & Esteva, F. J. HER2 therapy: molecular mechanisms of trastuzumab resistance. *Breast Cancer Res.* 8, 215 (2006).

204. Franklin, M. C. *et al.* Insights into ErbB signaling from the structure of the ErbB2-pertuzumab complex. *Cancer Cell* 5, 317–28 (2004).

205. Mukohara, T. Mechanisms of resistance to anti-human epidermal growth factor receptor 2 agents in breast cancer. *Cancer Sci.* 102, 1–8 (2011).

206. Cortés, J. *et al.* Pertuzumab monotherapy after trastuzumab-based treatment and subsequent reintroduction of trastuzumab: activity and tolerability in patients with advanced human epidermal growth factor receptor 2-positive breast cancer. *J. Clin. Oncol.* 30, 1594–600 (2012).

207. Amos, L. a & Löwe, J. How Taxol stabilises microtubule structure. *Chem. Biol.* 6, R65–9 (1999).

208. Valent, A., Penault-Llorca, F., Cayre, A. & Kroemer, G. Change in HER2 (ERBB2) gene status after taxane-based chemotherapy for breast cancer: polyploidization can lead to diagnostic pitfalls with potential impact for clinical management. *Cancer Genet.* 206, 37–41 (2013).

209. Blackwell, K. L. *et al.* Randomized study of Lapatinib alone or in combination with trastuzumab in women with ErbB2-positive, trastuzumab-refractory metastatic breast cancer. *J. Clin. Oncol.* 28, 1124–30 (2010).

210. Blackwell, K. L. *et al.* Overall survival benefit with lapatinib in combination with trastuzumab for patients with human epidermal growth factor receptor 2-positive metastatic breast cancer: final results from the EGF104900 Study. *J. Clin. Oncol.* 30, 2585–92 (2012).

211. Konecny, G. E. *et al.* Activity of the dual kinase inhibitor lapatinib (GW572016) against HER-2-overexpressing and trastuzumab-treated breast cancer cells. *Cancer Res.* 66, 1630–9 (2006).

212. Junttila, T. T., Li, G., Parsons, K., Phillips, G. L. & Sliwkowski, M. X. Trastuzumab-DM1 (T-DM1) retains all the mechanisms of action of trastuzumab and efficiently inhibits growth of lapatinib insensitive breast cancer. *Breast Cancer Res. Treat.* 128, 347–56 (2011).

213. Hurvitz, S. a *et al.* Phase II randomized study of trastuzumab emtansine versus trastuzumab plus docetaxel in patients with human epidermal growth factor receptor 2-positive metastatic breast cancer. *J. Clin. Oncol.* 31, 1157–63 (2013).

214. Lewis Phillips, G. D. *et al.* Targeting HER2-positive breast cancer with trastuzumab-DM1, an antibody-cytotoxic drug conjugate. *Cancer Res.* 68, 9280–90 (2008).

215. Barok, M., Tanner, M., Köninki, K. & Isola, J. Trastuzumab-DM1 causes tumor growth inhibition by mitotic catastrophe in trastuzumab-resistant breast cancer cells in vivo. *Breast Cancer Res.* 13, R46 (2011).

216. Loi, S. *et al.* Gene expression profiling identifies activated growth factor signaling in poor prognosis (Luminal-B) estrogen receptor positive breast cancer. *BMC Med. Genomics* 2, 37 (2009).

217. Gjorevski, N. & Nelson, C. M. Integrated morphodynamic signaling of the mammary gland. *Nat. Rev. Mol. Cell Biol.* 12, 581–93 (2011).

218. Horwitz, R. & Webb, D. Cell migration. *Curr. Biol.* 13, R756–9 (2003).

219. Baranwal, S. & Alahari, S. K. miRNA control of tumor cell invasion and metastasis. *Int. J. Cancer* 126, 1283–90 (2010).

220. Matsui, J., Wakabayashi, T., Asada, M., Yoshimatsu, K. & Okada, M. Stem cell factor/c-kit signaling promotes the survival, migration, and capillary tube formation of human umbilical vein endothelial cells. *J. Biol. Chem.* 279, 18600–7 (2004).

221. Muggerud, A. A. *et al.* Molecular diversity in ductal carcinoma in situ (DCIS) and early invasive breast cancer. *Mol. Oncol.* 4, 357–68 (2010).

222. Collins, L. C. *et al.* Outcome of patients with ductal carcinoma in situ untreated after diagnostic biopsy: results from the Nurses' Health Study. *Cancer* 103, 1778–84 (2005).

223. Hanahan, D. & Weinberg, R. a. Hallmarks of cancer: the next generation. *Cell* 144, 646–74 (2011).

224. Friedl, P., Locker, J., Sahai, E. & Segall, J. E. Classifying collective cancer cell invasion. *Nat. Cell Biol.* 14, 777–83 (2012).

225. Ridley, A. J. *et al.* Cell migration: integrating signals from front to back. *Science* 302, 1704–9 (2003).

226. Ridley, A. J. Pulling back to move forward. *Cell* 116, 357–8 (2004).

227. Lauffenburger, D. a & Horwitz, a F. Cell migration: a physically integrated molecular process. *Cell* 84, 359–69 (1996).

228. Mimeault, M. & Batra, S. K. Interplay of distinct growth factors during epithelial mesenchymal transition of cancer progenitor cells and molecular targeting as novel cancer therapies. *Ann. Oncol.* 18, 1605–19 (2007).

229. Siesser, P. M. F. & Hanks, S. K. The signaling and biological implications of FAK overexpression in cancer. *Clin. Cancer Res.* 12, 3233–7 (2006).

230. Shien, T. *et al.* PLC and PI3K Pathways are Important in the Inhibition of EGF-Induced Cell Migration by Gefitinib (' Iressa ', ZD 1839). *Breast cancer* 11, 367–373 (2004).

231. Meier, F. *et al.* Combined targeting of MAPK and AKT signaling pathways is a promising strategy for melanoma treatment. *Br. J. Dermatol.* 156, 1204–13 (2007).

232. Kumar, N., Afeyan, R., Kim, H. & Lauffenburger, D. A. Multipathway Model Enables Prediction of Kinase Inhibitor Cross-Talk Effects on Migration of Her2-Overexpressing Mammary Epithelial Cells □. 1668–1678 (2008). doi:10.1124/mol.107.043794.

233. Simpson, K. J. *et al.* Identification of genes that regulate epithelial cell migration using an siRNA screening approach. *Nat. Cell Biol.* 10, 1027–38 (2008).

234. Balz, L. M. *et al.* The interplay of HER2/HER3/PI3K and EGFR/HER2/PLC-γ1 signaling in breast cancer cell migration and dissemination. *J. Pathol.* 227, 234–44 (2012).

235. Zhan, L., Xiang, B. & Muthuswamy, S. K. Controlled activation of ErbB1/ErbB2 heterodimers promote invasion of three-dimensional organized epithelia in an ErbB1-dependent manner: implications for progression of ErbB2-overexpressing tumors. *Cancer Res.* 66, 5201–8 (2006).

236. Huang, Y. E. *et al.* Receptor-mediated Regulation of PI3Ks Confines PI (3 , 4 , 5) P 3 to the Leading Edge of Chemotaxing Cells. 14, 1913–1922 (2003).

237. Kurokawa, K. *et al.* Coactivation of Rac1 and Cdc42 at Lamellipodia and Membrane Ruffles Induced by Epidermal Growth Factor. *Mol. Biol. Cell* 15, 1003–1010 (2004).

238. Burridge, K. & Doughman, R. Front and back by Rho and Rac. *Nat. Cell Biol.* 8, 781–2 (2006).

239. Sander, E. E., ten Klooster, J. P., van Delft, S., van der Kammen, R. a & Collard, J. G. Rac downregulates Rho activity: reciprocal balance between both GTPases determines cellular morphology and migratory behavior. *J. Cell Biol.* 147, 1009–22 (1999).

240. Weaver, A. M. *et al.* Cortactin promotes and stabilizes Arp2/3-induced actin filament network formation. *Curr. Biol.* 11, 370–4 (2001).

241. Kirkbride, K. C., Sung, B. H., Sinha, S. & Weaver, A. M. Cortactin: A multifunctional regulator of cellular invasiveness. *Cell Adh. Migr.* 5, 187–198 (2011).

242. Lee, C.-H., Hung, H.-W., Hung, P.-H. & Shieh, Y.-S. Epidermal growth factor receptor regulates beta-catenin location, stability, and transcriptional activity in oral cancer. *Mol. Cancer* 9, 64 (2010).

243. Brembeck, F. H., Rosário, M. & Birchmeier, W. Balancing cell adhesion and Wnt signaling, the key role of beta-catenin. *Curr. Opin. Genet. Dev.* 16, 51–9 (2006).

244. Li, X.-Q. *et al.* Nuclear β-catenin accumulation is associated with increased expression of Nanog protein and predicts poor prognosis of non-small cell lung cancer. *J. Transl. Med.* 11, 114 (2013).

245. Guarino, M. Epithelial-mesenchymal transition and tumor invasion. *Int. J. Biochem. Cell Biol.* 39, 2153–60 (2007).

246. Lamouille, S., Xu, J. & Derynck, R. Molecular mechanisms of epithelial-mesenchymal transition. *Nat. Rev. Mol. Cell Biol.* 15, 178–96 (2014).

247. Lee, J. M., Dedhar, S., Kalluri, R. & Thompson, E. W. The epithelial-mesenchymal transition: new insights in signaling, development, and disease. *J. Cell Biol.* 172, 973–81 (2006).

248. Dave, B., Mittal, V., Tan, N. M. & Chang, J. C. Epithelial-mesenchymal transition, cancer stem cells and treatment resistance. *Breast Cancer Res.* 14, 202 (2012).

249. Chung, S. S., Giehl, N., Wu, Y. & Vadgama, J. V. STAT3 activation in HER2-overexpressing breast cancer promotes epithelial-mesenchymal transition and cancer stem cell traits. *Int. J. Oncol.* 44, 403–11 (2014).

250. Ortega-Cava, C. F. *et al.* Continuous requirement of ErbB2 kinase activity for loss of cell polarity and lumen formation in a novel ErbB2/Neu-driven murine cell line model of metastatic breast cancer. *J. Carcinog.* 10, 29 (2011).

251. Gupta, P. & Srivastava, S. K. HER2 mediated de novo production of TGFβ leads to SNAIL driven epithelial-to-mesenchymal transition and metastasis of breast cancer. *Mol. Oncol.* 2–4 (2014). doi:10.1016/j.molonc.2014.06.006

252. Giordano, A. *et al.* Epithelial-mesenchymal transition and stem cell markers in patients with HER2-positive metastatic breast cancer. *Mol. Cancer Ther.* 11, 2526–34 (2012).

253. Lesniak, D. *et al.* Spontaneous epithelial-mesenchymal transition and resistance to HER-2-targeted therapies in HER-2-positive luminal breast cancer. *PLoS One* 8, e71987 (2013).

254. Oliveras-Ferraros, C. *et al.* Epithelial-to-mesenchymal transition (EMT) confers primary resistance to trastuzumab (Herceptin). *Cell Cycle* 11, 4020–32 (2012).

255. Bissell, M. J., Hall, H. G. & Parry, G. How does the extracellular matrix direct gene expression? *J. Theor. Biol.* 99, 31–68 (1982).

256. Nyga, A., Cheema, U. & Loizidou, M. 3D tumor models: novel in vitro approaches to cancer studies. *J. Cell Commun. Signal.* 5, 239–48 (2011).

257. Hughes, C. S., Postovit, L. M. & Lajoie, G. a. Matrigel: a complex protein mixture required for optimal growth of cell culture. *Proteomics* 10, 1886–90 (2010).

258. Pampaloni, F., Reynaud, E. G. & Stelzer, E. H. K. The third dimension bridges the gap between cell culture and live tissue. *Nat. Rev. Mol. Cell Biol.* 8, 839–45 (2007).

259. Kenny, P. a *et al.* The morphologies of breast cancer cell lines in three-dimensional assays correlate with their profiles of gene expression. *Mol. Oncol.* 1, 84–96 (2007).

260. Wang, F. *et al.* Reciprocal interactions between beta1-integrin and epidermal growth factor receptor in three-dimensional basement membrane breast cultures : A different perspective in epithelial biology. *Proc. Natl. Acad. Sci. U. S. A.* 95, 14821–14826 (1998).

261. Wang, F. *et al.* Phenotypic reversion or death of cancer cells by altering signaling pathways in three-dimensional contexts. *J. Natl. Cancer Inst.* 94, 1494–503 (2002).

262. Bissell, M. J., Rizki, A. & Mian, I. S. Tissue architecture: the ultimate regulator of breast epithelial function. *Curr. Opin. Cell Biol.* 15, 753–762 (2003).

263. Herr, R., Wöhrle, F. U., Danke, C., Berens, C. & Brummer, T. A novel MCF-10A line allowing conditional oncogene expression in 3D culture. *Cell Commun. Signal.* 9, 17 (2011).

264. Debnath, J. & Brugge, J. S. Modelling glandular epithelial cancers in three-dimensional cultures. *Nat. Rev. Cancer* 5, 675–88 (2005).

265. Debnath, J., Muthuswamy, S. K. & Brugge, J. S. Morphogenesis and oncogenesis of MCF-10A mammary epithelial acini grown in three-dimensional basement membrane cultures. *Methods* 30, 256–268 (2003).

266. Petersen, O. W., Rønnov-Jessen, L., Howlett, a R. & Bissell, M. J. Interaction with basement membrane serves to rapidly distinguish growth and differentiation pattern of normal and malignant human breast epithelial cells. *Proc. Natl. Acad. Sci. U. S. A.* 89, 9064–8 (1992).

267. Hackenberg, M., Rodríguez-Ezpeleta, N. & Aransay, A. M. miRanalyzer: an update on the detection and analysis of microRNAs in high-throughput sequencing experiments. *Nucleic Acids Res.* 39, W132–8 (2011).

268. Kozomara, A. & Griffiths-Jones, S. miRBase: annotating high confidence microRNAs using deep sequencing data. *Nucleic Acids Res.* 42, D68–73 (2014).

269. Lee, Y. *et al.* MicroRNA genes are transcribed by RNA polymerase II. *EMBO J.* 23, 4051–60 (2004).

270. Monteys, A. M. *et al.* Structure and activity of putative intronic miRNA promoters. *RNA* 16, 495–505 (2010).

271. Bracht, J., Hunter, S., Eachus, R., Weeks, P. & Pasquinelli, A. M. Y. E. Trans -splicing and polyadenylation of let-7 microRNA primary transcripts. 1586–1594 (2004). doi:10.1261/rna.7122604.the

272. Hayashita, Y. *et al.* A polycistronic microRNA cluster, miR-17-92, is overexpressed in human lung cancers and enhances cell proliferation. *Cancer Res.* 65, 9628–32 (2005).

273. Lee, Y. *et al.* The nuclear RNase III Drosha initiates microRNA processing. *Nature* 425, 415–9 (2003).

274. Han, J. *et al.* The Drosha-DGCR8 complex in primary microRNA processing. *Genes Dev.* 18, 3016–27 (2004).

275. Bohnsack, M. T., Czaplinski, K. & Go, D. Exportin 5 is a RanGTP-dependent dsRNA-binding protein that mediates nuclear export of pre-miRNAs. 185–191 (2004). doi:10.1261/rna.5167604.Most

276. Flores-Jasso, C. F. *et al.* First step in pre-miRNAs processing by human Dicer. *Acta Pharmacol. Sin.* 30, 1177–85 (2009).

277. Lima, W. F. *et al.* Binding and cleavage specificities of human Argonaute2. *J. Biol. Chem.* 284, 26017–28 (2009).

278. Gregory, R. I., Chendrimada, T. P., Cooch, N. & Shiekhattar, R. Human RISC couples microRNA biogenesis and posttranscriptional gene silencing. *Cell* 123, 631–40 (2005).

279. Khvorova, A., Reynolds, A. & Jayasena, S. D. Functional siRNAs and miRNAs exhibit strand bias. *Cell* 115, 209–16 (2003).

280. Khorshid, M., Hausser, J., Zavolan, M. & van Nimwegen, E. A biophysical miRNA-mRNA interaction model infers canonical and noncanonical targets. *Nat. Methods* 10, 253–5 (2013).

281. Zeng, Y., Yi, R. & Cullen, B. R. MicroRNAs and small interfering RNAs can inhibit mRNA expression by similar mechanisms. *Proc. Natl. Acad. Sci. U. S. A.* 100, 9779–84 (2003).

282. Hutvágner, G. & Zamore, P. D. A microRNA in a multiple-turnover RNAi enzyme complex. *Science* 297, 2056–60 (2002).

283. Takahashi, R.-U., Miyazaki, H. & Ochiya, T. The role of microRNAs in the regulation of cancer stem cells. *Front. Genet.* 4, 295 (2014).

284. Saraiya, A. a, Li, W. & Wang, C. C. Transition of a microRNA from repressing to activating translation depending on the extent of base pairing with the target. *PLoS One* 8, e55672 (2013).

285. Baek, D. *et al.* The impact of microRNAs on protein output. *Nature* 455, 64–71 (2008).

286. Hausser, J., Syed, A. P., Bilen, B. & Zavolan, M. Analysis of CDS-located miRNA target sites suggests that they can effectively inhibit translation. *Genome Res.* 23, 604–615 (2013).

287. Grimson, A. *et al.* MicroRNA targeting specificity in mammals: determinants beyond seed pairing. *Mol. Cell* 27, 91–105 (2007).

288. Balaji, S., Iyer, L. M., Babu, M. M. & Aravind, L. Comparison of transcription regulatory interactions inferred from high-throughput methods: what do they reveal? *Trends Genet.* 24, 319–23 (2008).

289. Calin, G. a & Croce, C. M. MicroRNA signatures in human cancers. *Nat. Rev. Cancer* 6, 857–66 (2006).

290. Enerly, E. *et al.* miRNA-mRNA integrated analysis reveals roles for miRNAs in primary breast tumors. *PLoS One* 6, e16915 (2011).

291. Lewis, B. P., Burge, C. B. & Bartel, D. P. Conserved seed pairing, often flanked by adenosines, indicates that thousands of human genes are microRNA targets. *Cell* 120, 15–20 (2005).

292. Betel, D., Koppal, A., Agius, P., Sander, C. & Leslie, C. Comprehensive modeling of microRNA targets predicts functional non-conserved and non-canonical sites. *Genome Biol.* 11, R90 (2010).

293. Gaidatzis, D., van Nimwegen, E., Hausser, J. & Zavolan, M. Inference of miRNA targets using evolutionary conservation and pathway analysis. *BMC Bioinformatics* 8, 69 (2007).

294. Dweep, H., Sticht, C., Pandey, P. & Gretz, N. miRWalk--database: prediction of possible miRNA binding sites by “walking” the genes of three genomes. *J. Biomed. Inform.* 44, 839–47 (2011).

295. Paraskevopoulou, M. D. *et al.* DIANA-microT web server v5.0: service integration into miRNA functional analysis workflows. *Nucleic Acids Res.* 41, W169–73 (2013).

296. Kertesz, M., Iovino, N., Unnerstall, U., Gaul, U. & Segal, E. The role of site accessibility in microRNA target recognition. *Nat. Genet.* 39, 1278–84 (2007).

297. O’Day, E. & Lal, A. MicroRNAs and their target gene networks in breast cancer. *Breast Cancer Res.* 12, 201 (2010).

298. Findlay, V. J. MicroRNAs and Breast Cancer. *Open Cancer J.* 3, 55–61 (2010).

299. Ling, H., Fabbri, M. & Calin, G. a. MicroRNAs and other non-coding RNAs as targets for anticancer drug development. *Nat. Rev. Drug Discov.* 12, 847–65 (2013).

300. Wang, C., Bian, Z., Wei, D. & Zhang, J. miR-29b regulates migration of human breast cancer cells. *Mol. Cell. Biochem.* 352, 197–207 (2011).

301. Janssen, H. L. a *et al.* Treatment of HCV infection by targeting microRNA. *N. Engl. J. Med.* 368, 1685–94 (2013).

302. Heneghan, H. M., Miller, N., Lowery, a J., Sweeney, K. J. & Kerin, M. J. MicroRNAs as Novel Biomarkers for Breast Cancer. *J. Oncol.* 2009, 950201 (2009).

303. Jung, E.-J. *et al.* Plasma microRNA 210 levels correlate with sensitivity to trastuzumab and tumor presence in breast cancer patients. *Cancer* 118, 2603–14 (2012).

304. Ye, X.-M. *et al.* Epigenetic silencing of miR-375 induces trastuzumab resistance in HER2-positive breast cancer by targeting IGF1R. *BMC Cancer* 14, 134 (2014).

305. Gong, C. *et al.* Up-regulation of miR-21 mediates resistance to trastuzumab therapy for breast cancer. *J. Biol. Chem.* 286, 19127–37 (2011).

306. Ye, X. *et al.* MiR-221 promotes trastuzumab-resistance and metastasis in HER2-positive breast cancers by targeting PTEN. *BMB Rep.* 47, 268–73 (2014).

307. Sochor, M. *et al.* Oncogenic microRNAs: miR-155, miR-19a, miR-181b, and miR-24 enable monitoring of early breast cancer in serum. *BMC Cancer* 14, 448 (2014).

308. Shen, J. *et al.* Circulating miR-148b and miR-133a as biomarkers for breast cancer detection. *Oncotarget* 5, 5284–94 (2014).

309. Obernosterer, G., Leuschner, P. J. F., Alenius, M. & Martinez, J. Post-transcriptional regulation of microRNA expression. *RNA* 12, 1161–1167 (2006).

310. Saunders, M. a, Liang, H. & Li, W.-H. Human polymorphism at microRNAs and microRNA target sites. *Proc. Natl. Acad. Sci. U. S. A.* 104, 3300–5 (2007).

311. Avraham, R. *et al.* EGF decreases the abundance of microRNAs that restrain oncogenic transcription factors. *Sci. Signal.* 3, ra43 (2010).

312. Si, M.-L. *et al.* miR-21-mediated tumor growth. *Oncogene* 26, 2799–803 (2007).

313. Zhu, S. *et al.* MicroRNA-21 targets tumor suppressor genes in invasion and metastasis. *Cell Res.* 18, 350–9 (2008).

314. Huang, T.-H. *et al.* Up-regulation of miR-21 by HER2/neu signaling promotes cell invasion. *J. Biol. Chem.* 284, 18515–24 (2009).

315. Gabriely, G. *et al.* MicroRNA 21 promotes glioma invasion by targeting matrix metalloproteinase regulators. *Mol. Cell. Biol.* 28, 5369–80 (2008).

316. Papagiannakopoulos, T. *et al.* Pro-neural miR-128 is a glioma tumor suppressor that targets mitogenic kinases. *Oncogene* 31, 1884–95 (2012).

317. Hurst, D. R. *et al.* Breast cancer metastasis suppressor 1 up-regulates miR-146, which suppresses breast cancer metastasis. *Cancer Res.* 69, 1279–83 (2009).

318. Scott, G. K. *et al.* Coordinate suppression of ERBB2 and ERBB3 by enforced expression of micro-RNA miR-125a or miR-125b. *J. Biol. Chem.* 282, 1479–86 (2007).

319. Iorio, M. V *et al.* microRNA-205 regulates HER3 in human breast cancer. *Cancer Res.* 69, 2195–200 (2009).

320. Uhlmann, S. *et al.* miR-200bc/429 cluster targets PLCgamma1 and differentially regulates proliferation and EGF-driven invasion than miR-200a/141 in breast cancer. *Oncogene* 29, 4297–306 (2010).

321. Inui, M., Martello, G. & Piccolo, S. MicroRNA control of signal transduction. *Nat. Rev. Mol. Cell Biol.* 11, 252–63 (2010).

322. Uhlmann, S. *et al.* Global microRNA level regulation of EGFR-driven cell-cycle protein network in breast cancer. *Mol. Syst. Biol.* 8, 570 (2012).

323. Henjes, F. *et al.* Strong EGFR signaling in cell line models of ERBB2-amplified breast cancer attenuates response towards ERBB2-targeting drugs. *Oncogenesis* 1, e16 (2012).

324. Mannsperger, H. a *et al.* RNAi-based validation of antibodies for reverse phase protein arrays. *Proteome Sci.* 8, 69 (2010).

325. Loebke, C. *et al.* Infrared-based protein detection arrays for quantitative proteomics. *Proteomics* 7, 558–64 (2007).

326. Mannsperger, H. a, Gade, S., Henjes, F., Beissbarth, T. & Korf, U. RPPanalyzer: Analysis of reverse-phase protein array data. *Bioinformatics* 26, 2202–3 (2010).

327. Curtis, C. *et al.* The genomic and transcriptomic architecture of 2,000 breast tumors reveals novel subgroups. *Nature* 486, 346–52 (2012).

328. Desmedt, C. *et al.* Strong time dependence of the 76-gene prognostic signature for node-negative breast cancer patients in the TRANSBIG multicenter independent validation series. *Clin. Cancer Res.* 13, 3207–14 (2007).

329. Pawitan, Y. *et al.* Gene expression profiling spares early breast cancer patients from adjuvant therapy: derived and validated in two population-based cohorts. *Breast Cancer Res.* 7, R953–64 (2005).

330. Du, X., Li, X.-Q., Li, L., Xu, Y.-Y. & Feng, Y.-M. The detection of ESR1/PGR/ERBB2 mRNA levels by RT-QPCR: a better approach for subtyping breast cancer and predicting prognosis. *Breast Cancer Res. Treat.* 138, 59–67 (2013).

331. Sircoulomb, F. *et al.* Genome profiling of ERBB2-amplified breast cancers. *BMC Cancer* 10, 539 (2010).

332. Madden, S. F. *et al.* BreastMark: an integrated approach to mining publicly available transcriptomic datasets relating to breast cancer outcome. *Breast Cancer Res.* 15, R52 (2013).

333. Neve, R. M. *et al.* A collection of breast cancer cell lines for the study of functionally distinct cancer subtypes. *Cancer Cell* 10, 515–27 (2006).

334. Beerli, R. R. *et al.* Neu Differentiation Factor Activation of ErbB-3 and ErbB-4 Is Cell Specific and Displays a Differential Requirement for ErbB-2. *Mol. Cell. Biol.* 15, 6496–6505 (1995).

335. Xiao, Y., Gao, X., Maragh, S., Telford, W. G. & Tona, A. Cell lines as candidate reference materials for quality control of ERBB2 amplification and expression assays in breast cancer. *Clin. Chem.* 55, 1307–15 (2009).

336. Kao, J. *et al.* Molecular profiling of breast cancer cell lines defines relevant tumor models and provides a resource for cancer gene discovery. *PLoS One* 4, e6146 (2009).

337. Chiang, D. Y. *et al.* High-resolution mapping of copy-number alterations with massively parallel sequencing. *Nat. metho* 6, 99–103 (2009).

338. Myhre, S. *et al.* Influence of DNA copy number and mRNA levels on the expression of breast cancer related proteins. *Mol. Oncol.* 7, 704–18 (2013).

339. Hazan, R. *et al.* Identification of Autophosphorylation Sites of HER2/neu. *Cell Growth Differ.* 1, 3–7 (1990).

340. Bishayee, A., Beguinot, L. & Bishayee, S. Phosphorylation of Tyrosine 992 , 1068 , and 1086 Is Required for Conformational Change of the Human Epidermal Growth Factor Receptor C-Terminal Tail. *Mol. Biol. Cell* 10, 525–536 (1999).

341. Grassian, A. R., Schafer, Z. T. & Brugge, J. S. ErbB2 stabilizes epidermal growth factor receptor (EGFR) expression via Erk and Sprouty2 in extracellular matrix-detached cells. *J. Biol. Chem.* 286, 79–90 (2011).

342. Pradeep, C.-R. *et al.* Modeling invasive breast cancer: growth factors propel progression of HER2-positive premalignant lesions. *Oncogene* 31, 3569–83 (2012).

343. Aceto, N. *et al.* Co-expression of HER2 and HER3 receptor tyrosine kinases enhances invasion of breast cells via stimulation of interleukin-8 autocrine secretion. *Breast Cancer Res.* 14, R131 (2012).

344. Jenndahl, L. E., Isakson, P. & Baeckström, D. c-erbB2-induced epithelial-mesenchymal transition in mammary epithelial cells is suppressed by cell-cell contact and initiated prior to E-cadherin downregulation. *Int. J. Oncol.* 27, 439–448 (2005).

345. Nilsson, G. M. a, Akhtar, N., Kannius-Janson, M. & Baeckström, D. Loss of E-cadherin expression is not a prerequisite for c-erbB2-induced epithelial-mesenchymal transition. *Int. J. Oncol.* 45, 82–94 (2014).

346. Moreno-Bueno, G. *et al.* The morphological and molecular features of the epithelial-to-mesenchymal transition. *Nat. Protoc.* 4, 1591–613 (2009).

347. Wu, T. *et al.* The F-actin and adherence-dependent mechanical differentiation of normal epithelial cells after TGF-β1-induced EMT (tEMT) using a microplate measurement system. *Biomed. Microdevices* 16, 465–478 (2014).

348. Sotgia, F. *et al.* Caveolin-1 deficiency (-/-) conveys premalignant alterations in mammary epithelia, with abnormal lumen formation, growth factor independence, and cell invasiveness. *Am. J. Pathol.* 168, 292–309 (2006).

349. Jenndahl, L. E., Taylor-Papadimitriou, J. & Baeckström, D. Characterization of Integrin and Anchorage Dependence in Mammary Epithelial Cells following c-erbB2-Induced Epithelial-Mesenchymal Transition. *Tumor Biol.* 27, 50–58 (2006).

350. Nielsen, T. O. *et al.* Immunohistochemical and Clinical Characterization of the Basal-Like Subtype of Invasive Breast Carcinoma. 10, 5367–5374 (2004).

351. Cheang, M. C. U. *et al.* Basal-like breast cancer defined by five biomarkers has superior prognostic value than triple-negative phenotype. *Clin. Cancer Res.* 14, 1368–76 (2008).

352. Huang, D. W., Sherman, B. T. & Lempicki, R. a. Bioinformatics enrichment tools: paths toward the comprehensive functional analysis of large gene lists. *Nucleic Acids Res.* 37, 1–13 (2009).

353. Huang, D. W., Sherman, B. T. & Lempicki, R. A. Systematic and integrative analysis of large gene lists using DAVID bioinformatics resources. *Nat. Protoc.* 4, 44–57 (2009).

354. Kanehisa, M. & Goto, S. KEGG : Kyoto Encyclopedia of Genes and Genomes. 28, 27–30 (2000).

355. Li, B., Rosen, J. M., McMenamin-Balano, J., Muller, W. J. & Perkins, A. S. Neu/ERBB2 cooperates with p53-172H during mammary tumorigenesis in transgenic mice. *Mol. Cell. Biol.* 17, 3155–3163 (1997).

356. Wright, J. A., Richer, J. K. & Goodall, G. J. microRNAs and EMT in mammary cells and breast cancer. *J. Mammary Gland Biol. Neoplasia* 15, 213–23 (2010).

357. Hong, L. *et al.* High expression of miR-210 predicts poor survival in patients with breast cancer: a meta-analysis. *Gene* 507, 135–8 (2012).

358. Shi, W. *et al.* MicroRNA-301 mediates proliferation and invasion in human breast cancer. *Cancer Res.* 71, 2926–37 (2011).

359. Wang, J. *et al.* Sequence features and chromatin structure around the genomic regions bound by 119 human transcription factors. 1798–1812 (2012). doi:10.1101/gr.139105.112.

360. Simpson, D. R. *et al.* Epithelial Cell Organization Suppresses Myc Function by Attenuating Myc Expression. 71, (2011).

361. Wan, M. *et al.* Yin Yang 1 plays an essential role in breast cancer and negatively regulates p27. *Am. J. Pathol.* 180, 2120–33 (2012).

362. Tarcic, G. *et al.* EGR1 and the ERK-ERF axis drive mammary cell migration in response to EGF. *FASEB J.* 26, 1582–92 (2012).

363. Dong, P. *et al.* Mutant p53 gain-of-function induces epithelial – mesenchymal transition through modulation of the miR-130b – ZEB1 axis. *Oncogene* 32, 3286–3295 (2013).

364. Li, B.-L. *et al.* miR-130b is an EMT-related microRNA that targets DICER1 for aggression in endometrial cancer. *Med. Oncol.* 30, 484 (2013).

365. Cancer, C. *et al.* MicroRNA-130b Promotes Tumor Development and Is Associated with Poor Prognosis in Colorectal Cancer. *Neoplasia* 15, 1086–1099 (2013).

366. Ma, F. *et al.* Upregulated microRNA-301a in breast cancer promotes tumor metastasis by targeting PTEN and activating Wnt / β -catenin signaling ☆. *Gene* 535, 191–197 (2014).

367. Yan, Q. *et al.* mVps24p functions in EGF receptor sorting/trafficking from the early endosome. *Exp. Cell Res.* 304, 265–73 (2005).

368. Bache, K. G. *et al.* The ESCRT-III Subunit hVps24 Is Required for Degradation but Not Silencing of the Epidermal Growth Factor Receptor. *Mol. Biol. Cell* 17, 2513–2523 (2006).

369. Yang, J. *et al.* ZAK inhibits human lung cancer cell growth via ERK and JNK activation in an AP-1-dependent manner. *Cancer Sci.* 101, 1374–1381 (2010).

370. Ward, A. *et al.* MicroRNA-519a is a novel oncomir conferring tamoxifen resistance by targeting a network of tumor-suppressor genes in ER+ breast cancer. *J. Pathol.* 233, 368–79 (2014).

371. Liu, D. *et al.* Downregulation of Erbin in Her2-overexpressing breast cancer cells promotes cell migration and induces trastuzumab resistance. *Mol. Immunol.* 56, 104–12 (2013).

372. Liu, D. *et al.* Downregulation of Erbin in Her2-overexpressing breast cancer cells promotes cell migration and induces trastuzumab resistance. *Mol. Immunol.* 56, 104–12 (2013).

373. Perez, E. a *et al.* Predictability of adjuvant trastuzumab benefit in N9831 patients using the ASCO/CAP HER2-positivity criteria. *J. Natl. Cancer Inst.* 104, 159–62 (2012).

374. Fuchs, E. *et al.* High-level ERBB2 gene amplification is associated with a particularly short time-to-metastasis, but results in a high rate of complete response once trastuzumab-based therapy is offered in the metastatic setting. *Int. J. cancer* 135, 224–31 (2014).

375. Chang, J. *et al.* LOXL2 induces aberrant acinar morphogenesis via ErbB2 signaling. *Breast Cancer Res.* 15, R67 (2013).

376. van't Veer, L. J. *et al.* Gene expression profiling predicts clinical outcome of breast cancer. *Nature* 415, 530–536 (2002).

377. Wichmann, H. *et al.* Inverse prognostic impact of ErbB2 mRNA and protein expression level in tumors of soft tissue sarcoma patients. *Strahlentherapie und Onkol.* 912–918 (2014). doi:10.1007/s00066-014-0655-8

378. Muthuswamy, S. K. *et al.* ERBB2, but not ERBB1, reinitiates proliferation and induces luminal repopulation in epithelial acini. *Nat. Cell Biol.* 3, (2001).

379. Yotsumoto, F. *et al.* HB-EGF orchestrates the complex signals involved in triple-negative and trastuzumab-resistant breast cancer. *Int. J. Cancer* 127, 2707–17 (2010).

380. Tzahar, E. *et al.* A Hierarchical Network of Interreceptor Interactions Determines Signal Transduction by Neu Differentiation Factor/Neuregulin and Epidermal Growth Factor. *Mol. Cell. Biol.* 16, 5276–5287 (1996).

381. Aceto, N. *et al.* Tyrosine phosphatase SHP2 promotes breast cancer progression and maintains tumor-initiating cells via activation of key transcription factors and a positive feedback signaling loop. *Nat. Med.* 18, 529–37 (2012).

382. Muller, W. J. *et al.* Synergistic Interaction of the Neu Proto-Oncogene Product and Transforming Growth Factor ␣ in the Mammary Epithelium of Transgenic Mice. 16, 5726–5736 (1996).

383. Ward, T. M. *et al.* Truncated p110 ERBB2 induces mammary epithelial cell migration, invasion and orthotopic xenograft formation, and is associated with loss of phosphorylated STAT5. *Oncogene* 32, 2463–74 (2013).

384. Ueda, Y. *et al.* Overexpression of HER2 (erbB2) in human breast epithelial cells unmasks transforming growth factor beta-induced cell motility. *J. Biol. Chem.* 279, 24505–13 (2004).

385. Lu, J. *et al.* 14-3-3zeta Cooperates with ErbB2 to promote ductal carcinoma in situ progression to invasive breast cancer by inducing epithelial-mesenchymal transition. *Cancer Cell* 16, 195–207 (2009).

386. Yu, M. *et al.* A developmentally regulated inducer of EMT , LBX1 , contributes to breast cancer progression. *Genes Dev.* 23, 1737–1742 (2009).

387. Cheng, J.-C., Qiu, X., Chang, H.-M. & Leung, P. C. K. HER2 mediates epidermal growth factor-induced down-regulation of E-cadherin in human ovarian cancer cells. *Biochem. Biophys. Res. Commun.* 434, 81–6 (2013).

388. Tan, M., Yao, J. & Yu, D. Overexpression of the c-erbB-2 Gene Enhanced Intrinsic Metastasis Potential in Human Breast Cancer Cells without Increasing Their Transformation Abilities. *Cancer Res.* 57, 1199–1205 (1997).

389. Kim, I.-Y., Yong, H.-Y., Kang, K. W. & Moon, A. Overexpression of ErbB2 induces invasion of MCF10A human breast epithelial cells via MMP-9. *Cancer Lett.* 275, 227–33 (2009).

390. Kim, S. *et al.* A functional comparison between the HER2(high)/HER3 and the HER2(low)/HER3 dimers on heregulin-β1-induced MMP-1 and MMP-9 expression in breast cancer cells. *Exp. Mol. Med.* 44, 473–82 (2012).

391. Qian, X. *et al.* N-cadherin/FGFR promotes metastasis through epithelial-to-mesenchymal transition and stem/progenitor cell-like properties. *Oncogene* 33, 3411–21 (2014).

392. Cabodi, S. *et al.* p130Cas is an essential transducer element in ErbB2 transformation. *FASEB J.* 24, 3796–808 (2010).

393. Reiske, H. R., Zhao, J., Han, D. C., Cooper, L. A. & Guan, J.-L. Analysis of FAK-associated signaling pathways in the regulation of cell cycle progression. *FEBS Lett.* 486, 275–280 (2000).

394. Wang, S. E. *et al.* Transforming growth factor beta induces clustering of HER2 and integrins by activating Src-focal adhesion kinase and receptor association to the cytoskeleton. *Cancer Res.* 69, 475–82 (2009).

395. Xu, Y., Benlimame, N., Su, J., He, Q. & Alaoui-Jamali, M. a. Regulation of focal adhesion turnover by ErbB signaling in invasive breast cancer cells. *Br. J. Cancer* 100, 633–43 (2009).

396. Calalb, M. B., Zhang, X., Polte, T. R. & Hanks, S. K. Focal Adhesion Kinase Tyrosine-861 Is a Major Site of Phosphorylation by Src. *Biochem Biophys Res Commun.* 228, 662–8 (1996).

397. Villa-Moruzzi, E. Tyrosine phosphatases in the HER2-directed motility of ovarian cancer cells: Involvement of PTPN12, ERK5 and FAK. *Anal. Cell. Pathol. (Amst).* 34, 101–12 (2011).

398. Biscardi, J. S. *et al.* c-Src-mediated Phosphorylation of the Epidermal Growth Factor Receptor on Tyr 845 and Tyr 1101 Is Associated with Modulation of Receptor Function. *J. Biol. Chem.* 274, 8335–8343 (1999).

399. Okutani, T. *et al.* Grb2/Ash Binds Directly to Tyrosines 1068 and 1086 and Indirectly to Tyrosine 1148 of Activated Human Epidermal Growth Factor Receptors in Intact Cells. *J. Biol. Chem.* 269, 31310–31314 (1994).

400. García-Castillo, J. *et al.* HER2 carboxyl-terminal fragments regulate cell migration and cortactin phosphorylation. *J. Biol. Chem.* 284, 25302–13 (2009).

401. Timpson, P., Lynch, D. K., Schramek, D., Walker, F. & Daly, R. J. Cortactin Overexpression Inhibits Ligand-Induced Down-regulation of the Epidermal Growth Factor Receptor. *Cancer Res.* 65, 3273–3280 (2005).

402. Akhtar, S. *et al.* Activation of ErbB2 and Downstream Signaling via Rho Kinases and ERK1/2 Contributes to Diabetes-Induced Vascular Dysfunction. *PLoS One* 8, e67813 (2013).

403. Croucher, D. R., Rickwood, D., Tactacan, C. M., Musgrove, E. a & Daly, R. J. Cortactin modulates RhoA activation and expression of Cip/Kip cyclin-dependent kinase inhibitors to promote cell cycle progression in 11q13-amplified head and neck squamous cell carcinoma cells. *Mol. Cell. Biol.* 30, 5057–70 (2010).

404. Britt, D. E. *et al.* Identification of a novel protein, LYRIC, localized to tight junctions of polarized epithelial cells. *Exp. Cell Res.* 300, 134–48 (2004).

405. Hu, G. *et al.* MTDH activation by 8q22 genomic gain promotes chemoresistance and metastasis of poor-prognosis breast cancer. *Cancer Cell* 15, 9–20 (2009).

406. Zhang, E. Y. *et al.* Genome Wide Proteomics of ERBB2 and EGFR and Other Oncogenic Pathways in Iflammatory Breast Cancer. *J. Proteome Res.* 12, 2805–2817 (2013).

407. Xin, Z., Ning, Z. & Mei-xin, Z. Astrocyte elevated gene-1 induces breast cancer proliferation and invasion through upregulating HER2/neu expression. *Chin. Med. J. (Engl).* 124, 3546–3550 (2011).

408. Andrechek, E. R. *et al.* Gene Expression Profiling of Neu-induced Mammary Tumors from Transgenic Mice Reveals Genetic and Morphological Similarities to ErbB2-expressing Human Breast Cancers. *Cancer Res.* 63, 4920–4926 (2003).

409. Bhargava, R., Beriwal, S., McManus, K. & Dabbs, D. J. CK5 is more sensitive than CK5/6 in identifying the “basal-like” phenotype of breast carcinoma. *Am. J. Clin. Pathol.* 130, 724–30 (2008).

410. Maccario, H., Perera, N. M., Davidson, L., Downes, C. P. & Leslie, N. R. PTEN is destabilized by phosphorylation on Thr366. *Biochem. J.* 405, 439–44 (2007).

411. Al-Khouri, A. M., Ma, Y., Togo, S. H., Williams, S. & Mustelin, T. Cooperative phosphorylation of the tumor suppressor phosphatase and tensin homologue (PTEN) by casein kinases and glycogen synthase kinase 3beta. *J. Biol. Chem.* 280, 35195–202 (2005).

412. Guo, W. *et al.* β4 Integrin Amplifies ErbB2 Signaling to Promote Mammary Tumorigenesis. *Cell* 126, 489–502 (2006).

413. Huck, L., Pontier, S. M., Zuo, D. M. & Muller, W. J. beta1-integrin is dispensable for the induction of ErbB2 mammary tumors but plays a critical role in the metastatic phase of tumor progression. *Proc. Natl. Acad. Sci. U. S. A.* 107, 15559–64 (2010).

414. Joosse, S. a *et al.* Changes in keratin expression during metastatic progression of breast cancer: impact on the detection of circulating tumor cells. *Clin. Cancer Res.* 18, 993–1003 (2012).

415. Nardone, B. *et al.* Histopathologic and immunohistochemical characterization of rash to human epidermal growth factor receptor 1 (HER1) and HER1/2 inhibitors in cancer patients. *Clin. Cancer Res.* 16, 4452–60 (2010).

416. Paladini, R. D., Takahashi, K., Bravo, N. S. & Coulombe, P. A. Onset of Re-epithelialization After Skin Injury Correlates with a Reorganization of Keratin Filaments in Wound Edge Keratinocytes: Defining a Potential Role for Keratin 16. *J. Cell Biol.* 132, 381–397 (1996).

417. Bolling, M., Lemmink, H., Jansen, G. & Jonkman, M. Mutations in KRT5 and KRT14 cause epidermolysis bullosa simplex in 75% of the patients. *Br. J. Dermatol.* 164, 637–644 (2011).

418. Chang, A. C.-M. *et al.* STC1 expression is associated with tumor growth and metastasis in breast cancer. *Clin. Exp. Metastasis* 32, 15–27 (2015).

419. Arigami, T. *et al.* Clinical significance of stanniocalcin 2 expression as a predictor of tumor progression in gastric cancer. *Oncol. Rep.* 30, 2838–44 (2013).

420. Chang, a C.-M., Jellinek, D. a & Reddel, R. R. Mammalian stanniocalcins and cancer. *Endocr. Relat. Cancer* 10, 359–73 (2003).

421. Hartman, Z. C. *et al.* HER2 overexpression elicits a proinflammatory IL-6 autocrine signaling loop that is critical for tumorigenesis. *Cancer Res.* 71, 4380–91 (2011).

422. Vazquez-Martin, A., Colomer, R. & Menendez, J. Protein array technology to detect HER2 (erbB-2)-induced “cytokine signature” in breast cancer. *Eur. J. Cancer* 43, 1117–1124 (2007).

423. Liu, M. *et al.* Nuclear factor-kappaB enhances ErbB2-induced mammary tumorigenesis and neoangiogenesis in vivo. *Am. J. Pathol.* 174, 1910–20 (2009).

424. Mori, B. N. & Prager, D. Transactivation of the Interleukin-1alpha Promoter by Human T-Cell Leukemia Virus Type I and Type II Tax Proteins. *Blood* 87, 3410–3417 (1996).

425. Hiscott, J. *et al.* Characterization of a Functional NFkB Site in the Human Interleukin 1bete Promoter : Evidence for a Positive Autoregulatory Loop. *Mol. Cell. Biol.* 13, 6231–6240 (1993).

426. Battaglia, F. *et al.* Hypoxia transcriptionally induces macrophage-inflammatory protein-3alpha/CCL-20 in primary human mononuclear phagocytes through nuclear factor (NF)-kappaB. *J. Leukoc. Biol.* 83, 648–62 (2008).

427. Adachi, R. *et al.* ErbB2 down-regulates microRNA-205 in breast cancer. *Biochem. Biophys. Res. Commun.* 411, 804–8 (2011).

428. Park, S. G., Schimmel, P. & Kim, S. Aminoacyl tRNA synthetases and their connections to disease. *PNAS* 105, 11043–11049 (2008).

429. Pincini, A. *et al.* Identification of p130Cas/ErbB2-dependent invasive signatures in transformed mammary epithelial cells. *Cell Cycle* 12, 2409–2422 (2013).

430. Bollig-Fischer, A., Dewey, T. G. & Ethier, S. P. Oncogene activation induces metabolic transformation resulting in insulin-independence in human breast cancer cells. *PLoS One* 6, e17959 (2011).

431. Pickl, M. & Ries, C. H. Comparison of 3D and 2D tumor models reveals enhanced HER2 activation in 3D associated with an increased response to trastuzumab. *Oncogene* 28, 461–8 (2009).

432. Gallardo, a *et al.* Increased signaling of EGFR and IGF1R, and deregulation of PTEN/PI3K/Akt pathway are related with trastuzumab resistance in HER2 breast carcinomas. *Br. J. Cancer* 106, 1367–73 (2012).

433. Yu, D. *et al.* Overexpression of both p185 c-erbB2 and p170 mdr-1 renders breast cancer cells highly resistant to taxol. *Oncogene* 16, 2087–2094 (1998).

434. Pegram, M. D. *et al.* The effect of HER-2/neu overexpression on chemotherapeutic drug sensitivity in human breast and ovarian cancer cells. *Oncogene* 15, 537–547 (1997).

435. Ciardiello, F. *et al.* Resistance to taxanes is induced by c-erbB-2 overexpression in human MCF-10A mammary epithelial cells and is blocked by combined treatment with an antisense oligonucleotide targeting type I protein kinase A. *Int. J. cancer* 85, 710–715 (2000).

436. Fu, A., Yu, Z., Song, Y. & Zhang, E. Silencing of glutaminase 1 resensitizes Taxol-resistant breast cancer cells to Taxol. *Mol. Med. reports reports* (2015). doi:10.1016/S0305-7372(03)00133-6

437. Dawson, P. J., Wolman, S. R., Tait, L., Heppner, G. H. & Miller, F. R. MCF10AT: a model for the evolution of cancer from proliferative breast disease. *Am. J. Pathol.* 148, 313–9 (1996).

438. Miller, F. R. *et al.* Xenograft Model of Progressive Human Proliferative Breast Disease. *J. Natl. Cancer Inst.* 85, 1725–1732 (1993).

439. Giunciuglio, D. *et al.* Invasive Phenotype of MCF10A Cells Overexpressing c-Ha-ras and c-erbB-2 Oncogenes. *Int. J. cancer* 63, 815–822 (1995).

440. Alajati, A. *et al.* Mammary tumor formation and metastasis evoked by a HER2 splice variant. *Cancer Res.* 73, 5320–7 (2013).

441. Latta, E. K., Tjan, S., Parkes, R. K. & O'Malley, F. P. The role of HER2/neu overexpression/amplification in the progression of ductal carcinoma in situ to invasive carcinoma of the breast. *Mod. Pathol.* 15, 1318–25 (2002).

442. Jurmeister, S. *et al.* MicroRNA-200c represses migration and invasion of breast cancer cells by targeting actin-regulatory proteins FHOD1 and PPM1F. *Mol. Cell. Biol.* 32, 633–51 (2012).

443. Ward, a *et al.* Re-expression of microRNA-375 reverses both tamoxifen resistance and accompanying EMT-like properties in breast cancer. *Oncogene* 1–10 (2012). doi:10.1038/onc.2012.128

444. Pincini, A. *et al.* Identification of p130Cas/ErbB2-dependent invasive signatures in transformed mammary epithelial cells. *Cell Cycle* 12, 2409–22 (2013).

445. Nie, W., Jin, L., Wang, Y., Wang, Z. & Guan, X. The bioinformatics analysis of miRNAs signatures differentially expressed in HER2(+) versus HER2(-) breast cancers. *Cancer Biother. Radiopharm.* 28, 71–6 (2013).

446. Ichikawa, T. *et al.* Trastuzumab produces therapeutic actions by upregulating miR-26a and miR-30b in breast cancer cells. *PLoS One* 7, e31422 (2012).

447. Mackiewicz, M. *et al.* Identification of the receptor tyrosine kinase AXL in breast cancer as a target for the human miR-34a microRNA. *Breast Cancer Res. Treat.* 130, 663–79 (2011).

448. Lowery, A. J. *et al.* MicroRNA signatures predict oestrogen receptor, progesterone receptor and HER2/neu receptor status in breast cancer. *Breast Cancer Res.* 11, R27 (2009).

449. Blenkiron, C. *et al.* MicroRNA expression profiling of human breast cancer identifies new markers of tumor subtype. *Genome Biol.* 8, R214 (2007).

450. Mattie, M. D. *et al.* Optimized high-throughput microRNA expression profiling provides novel biomarker assessment of clinical prostate and breast cancer biopsies. *Mol. Cancer* 5, 24 (2006).

451. Nagata, Y. *et al.* PTEN activation contributes to tumor inhibition by trastuzumab, and loss of PTEN predicts trastuzumab resistance in patients. *Cancer Cell* 6, 117–27 (2004).

452. Liu, D. *et al.* Downregulation of Erbin in Her2-overexpressing breast cancer cells promotes cell migration and induces trastuzumab resistance. *Mol. Immunol.* 56, 104–12 (2013).

453. Hamilton, M. P. *et al.* Identification of a pan-cancer oncogenic microRNA superfamily anchored by a central core seed motif. *Nat. Commun.* 4, 2730 (2013).

454. The Cancer Genome Atlas Network. Comprehensive molecular portraits of human breast tumors - The Cancer Genome Atlas Network. Supplementary information. *Nature* 490, 61–70 (2012).

11. Supplementary data

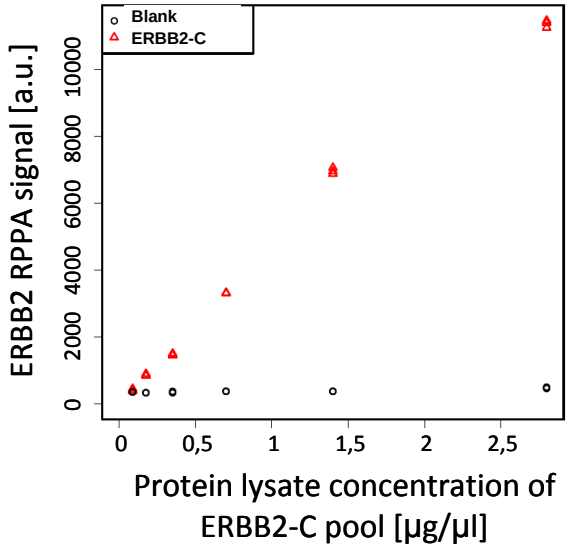

Supplementary Figure 1

*ERBB2 RPPA signal intensity detected for a serial dilution of protein lysate obtained from ERBB2-C cell line pool, grown on plastic dish in the presence of 10 ng/ml EGF. Antibody Ab-17 from NeoMarkes was used (*MS-730-P*) to detect ERBB2 on reverse phase protein array. The signal is expressed in arbitrary units [a.u.]. Blank – negative control.*

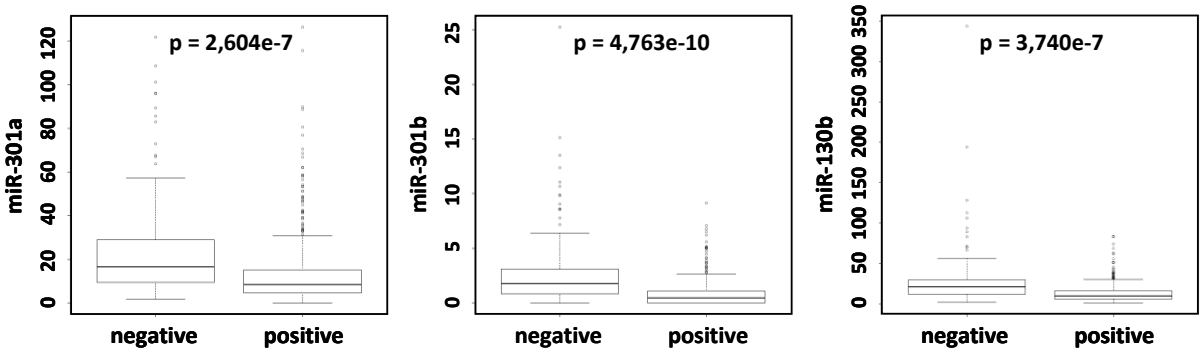

Supplementary Figure 2

Mean expression levels of miR-301a, miR-301b and miR-130b were compared in ER-negative vs ER-positive tumors in dataset from The Cancer Genome Atlas Network study.[454]

Supplementary Table 1

The list of transcripts downregulated in direct comparison of ERBB2-A and control (A vs R) as well as in direct comparison of ERBB2-B and ERBB2-A (B vs A) for at least one probe. The transcripts are sorted according to the fold change ERBB2-A vs CTRL; P-val (BH) – Benjamini Hochberg adjusted p-value, R – reference (CTRL cell line pool)

Probe ID	Gene symbol	Definition	Fold change A vs R	p-val (BH) A vs R	Fold change B vs A	p-val (BH) B vs A
5870653	LOC651397	PREDICTED: Homo sapiens misc_RNA (LOC651397), miscRNA.	0,13	7,32E-45	0,344	4,29E-39
4900458	KRT14	Homo sapiens keratin 14 (epidermolysis bullosa simplex, Dowling-Meara, Koebner) (KRT14), mRNA.	0,162	1,25E-63	0,273	5,12E-42
7650441	FGFBP1	Homo sapiens fibroblast growth factor binding protein 1 (FGFBP1), mRNA.	0,208	3,25E-39	0,612	1,18E-21
6130441	ASPM	Homo sapiens asp (abnormal spindle) homolog, microcephaly associated (Drosophila) (ASPM), mRNA.	0,388	7,13E-43	0,734	1,66E-10
1500010	CDC20	Homo sapiens cell division cycle 20 homolog (S. cerevisiae) (CDC20), mRNA.	0,392	3,41E-39	0,558	1,72E-46
7570324	ID3	Homo sapiens inhibitor of DNA binding 3, dominant negative helix-loop-helix protein (ID3), mRNA.	0,399	2,79E-29	0,622	2,34E-32
5960168	C10ORF58	Homo sapiens chromosome 10 open reading frame 58 (C10orf58), transcript variant 1, mRNA.	0,436	9,19E-25	0,619	7,01E-17
1050195	KIF20A	Homo sapiens kinesin family member 20A (KIF20A), mRNA.	0,451	2,62E-43	0,62	8,81E-29
6620392	LFNG	Homo sapiens LFNG O-fucosylpeptide 3-beta-N-acetylglucosaminyltransferase (LFNG), transcript variant 1, mRNA.	0,498	1,43E-39	0,706	3,25E-09
5310646	AKR1B10	Homo sapiens aldo-keto reductase family 1, member B10 (aldose reductase) (AKR1B10), mRNA.	0,504	4,39E-31	0,741	9,22E-12
5860289	KRT5	Homo sapiens keratin 5 (KRT5), mRNA.	0,515	1,9E-49	0,573	7,65E-37
5310471	UBE2C	Homo sapiens ubiquitin-conjugating enzyme E2C (UBE2C), transcript variant 6, mRNA.	0,528	2,27E-25	0,589	3,35E-24
4260368	UBE2C	Homo sapiens ubiquitin-conjugating enzyme E2C (UBE2C), transcript variant 3, mRNA.	0,533	1,38E-37	0,603	6,70E-30
5360070	CCNB2	Homo sapiens cyclin B2 (CCNB2), mRNA.	0,536	2,1E-35	0,674	1,16E-16
6770026	AURKB	Homo sapiens aurora kinase B (AURKB), mRNA.	0,539	1,59E-19	0,712	1,36E-17
4780187	HS.19339	Homo sapiens cDNA clone IMAGE:5263177	0,543	5,42E-28	0,732	2,10E-11
4180324	FAM46B	Homo sapiens family with sequence similarity 46, member B (FAM46B), mRNA.	0,549	9,94E-29	0,678	2,83E-24
1400673	CDCA5	Homo sapiens cell division cycle associated 5 (CDCA5), mRNA.	0,554	1,86E-37	0,681	4,17E-19
7330674	KIFC1	Homo sapiens kinesin family member C1 (KIFC1), mRNA.	0,557	5,5E-26	0,723	1,52E-12
3990619	TOP2A	Homo sapiens topoisomerase (DNA) II alpha 170kDa (TOP2A), mRNA.	0,559	4,18E-35	0,659	9,35E-25
150543	FAM83D	Homo sapiens family with sequence similarity 83, member D (FAM83D), mRNA.	0,56	1,12E-33	0,69	4,52E-17

3450735	UGT1A6	Homo sapiens UDP glucuronosyltransferase 1 family, polypeptide A6 (UGT1A6), transcript variant 2, mRNA.	0,562	7,43E-24	0,711	1,51E-15
7650296	DCN	Homo sapiens decorin (DCN), transcript variant C, mRNA.	0,563	3,23E-28	0,72	2,18E-16
5560369	ALDH3A1	Homo sapiens aldehyde dehydrogenase 3 family, memberA1 (ALDH3A1), mRNA.	0,576	1,94E-37	0,408	2,24E-62
4060064	HMMR	Homo sapiens hyaluronan-mediated motility receptor (RHAMM) (HMMR), transcript variant 2, mRNA.	0,586	1,19E-26	0,69	1,17E-14
2070494	PRC1	Homo sapiens protein regulator of cytokinesis 1 (PRC1), transcript variant 2, mRNA.	0,588	1,15E-33	0,714	1,44E-25
1410209	SGK1	Homo sapiens serum/glucocorticoid regulated kinase 1 (SGK1), transcript variant 1, mRNA.	0,589	1,53E-19	0,452	1,31E-35
2030324	SGK1	Homo sapiens serum/glucocorticoid regulated kinase 1 (SGK1), transcript variant 1, mRNA.	0,593	1,13E-28	0,455	2,50E-47
6370703	UGT1A6	Homo sapiens UDP glucuronosyltransferase 1 family, polypeptide A6 (UGT1A6), transcript variant 1, mRNA.	0,594	4,09E-21	0,741	5,42E-11
2120468	C10ORF58	Homo sapiens chromosome 10 open reading frame 58 (C10orf58), mRNA.	0,601	3,12E-27	0,745	1,11E-14
7050220	NMU	Homo sapiens neuromedin U (NMU), mRNA.	0,605	8,62E-18	0,722	5,29E-12
870546	MAD2L1	Homo sapiens MAD2 mitotic arrest deficient-like 1 (yeast) (MAD2L1), mRNA.	0,606	9,22E-24	0,739	3,30E-10
7570326	ADRB2	Homo sapiens adrenergic, beta-2-, receptor, surface (ADRB2), mRNA.	0,61	1,88E-28	0,745	2,75E-12
4390450	SGK	Homo sapiens serum/glucocorticoid regulated kinase (SGK), mRNA.	0,614	8,11E-34	0,426	4,35E-31
6900408	EFEMP1	Homo sapiens EGF-containing fibulin-like extracellular matrix protein 1 (EFEMP1), transcript variant 2, mRNA.	0,615	3,54E-25	0,731	1,71E-17
3360064	PLA2G4F	Homo sapiens phospholipase A2, group IVF (PLA2G4F), mRNA.	0,623	1,12E-23	0,71	3,56E-16
4590767	SPRR1B	Homo sapiens small proline-rich protein 1B (cornifin) (SPRR1B), mRNA.	0,627	2,72E-11	0,445	3,28E-22
4560497	ETNK2	Homo sapiens ethanolamine kinase 2 (ETNK2), mRNA.	0,63	2,34E-18	0,63	7,64E-14
1470441	LOC650517	PREDICTED: Homo sapiens hypothetical LOC650517 (LOC650517), mRNA.	0,639	6,35E-15	0,61	1,84E-13
1070279	DLK2	Homo sapiens delta-like 2 homolog (Drosophila) (DLK2), transcript variant 2, mRNA.	0,642	1,52E-28	0,575	5,53E-36
4540246	KRT16	Homo sapiens keratin 16 (focal non-epidermolytic palmoplantar keratoderma) (KRT16), mRNA.	0,644	1,6E-22	0,696	5,96E-15
5420368	ROS1	Homo sapiens c-ros oncogene 1, receptor tyrosine kinase (ROS1), mRNA.	0,648	1,44E-18	0,746	1,62E-10
4730196	TK1	Homo sapiens thymidine kinase 1, soluble (TK1), mRNA.	0,649	6,61E-21	0,709	2,22E-18
3120598	AKR1C4	Homo sapiens aldo-keto reductase family 1, member C4 (chlordecone reductase; 3-alpha hydroxysteroid dehydrogenase, type I; dihydrodiol dehydrogenase 4) (AKR1C4), mRNA.	0,65	8,26E-18	0,674	1,30E-15

5690408	IRX3	Homo sapiens iroquois homeobox 3 (IRX3), mRNA.	0,652	8,9E-24	0,595	9,33E-48
5420474	HSPBL2	Homo sapiens heat shock 27kDa protein-like 2 pseudogene (HSPBL2), non-coding RNA.	0,656	2E-17	0,732	7,66E-13
5260196	BCL7C	Homo sapiens B-cell CLL/lymphoma 7C (BCL7C), mRNA.	0,659	7,64E-17	0,725	5,57E-12

Supplementary Table 2

The list of transcripts upregulated in direct comparison of ERBB2-A and control (A vs R) as well as in direct comparison of ERBB2-B and ERBB2-A (B vs A) for at least one probe. The transcripts are sorted according to the fold change ERBB2-A vs CTRL; P-val (BH) – Benjamini Hochberg adjusted p-value, R – reference (CTRL cell line pool)

Probe ID	Gene symbol	Definition	Fold change A vs R	p-val (BH) A vs R	Fold change B vs A	p-val (BH) B vs A
1170170	STC2	Homo sapiens stanniocalcin 2 (STC2), mRNA.	5,523	1,61E-42	2,373	6,44E-33
240086	PHGDH	Homo sapiens phosphoglycerate dehydrogenase (PHGDH), mRNA.	4,437	4,08E-71	1,378	7,98E-26
1510296	ASNS	Homo sapiens asparagine synthetase (ASNS), transcript variant 1, mRNA.	4,415	7,38E-63	1,652	1,03E-39
1780446	PCK2	Homo sapiens phosphoenolpyruvate carboxykinase 2 (mitochondrial) (PCK2), nuclear gene encoding mitochondrial protein, transcript variant 1, mRNA.	3,091	7,94E-47	1,578	5,77E-36
6420168	DBNDD2	Homo sapiens dysbindin (dystrobrevin binding protein 1) domain containing 2 (DBNDD2), transcript variant 3, mRNA.	2,958	6,92E-63	1,419	1,80E-27
3450288	LOC100134134	PREDICTED: Homo sapiens similar to peroxidasin homolog (LOC100134134), mRNA.	2,86	2,76E-35	1,464	9,76E-25
4220246	CCL20	Homo sapiens chemokine (C-C motif) ligand 20 (CCL20), mRNA.	2,79	1,36E-46	1,709	2,26E-33
840685	IL1B	Homo sapiens interleukin 1, beta (IL1B), mRNA.	2,703	1,19E-53	2,482	1,49E-41
7560364	LOC729779	PREDICTED: Homo sapiens misc_RNA (LOC729779), miscRNA.	2,521	1,98E-46	1,454	3,77E-14
5960181	ASNS	Homo sapiens asparagine synthetase (ASNS), transcript variant 1, mRNA.	2,501	2,78E-27	1,543	1,10E-10
3390129	C9ORF103	Homo sapiens chromosome 9 open reading frame 103 (C9orf103), mRNA.	2,289	2,42E-48	1,365	2,93E-17
5090671	GDF15	Homo sapiens growth differentiation factor 15 (GDF15), mRNA.	2,134	8,48E-33	1,705	2,59E-27
830619	DDIT3	Homo sapiens DNA-damage-inducible transcript 3 (DDIT3), mRNA.	2,034	3,38E-32	1,912	6,42E-29
1510424	S100P	Homo sapiens S100 calcium binding protein P (S100P), mRNA.	2,011	4,67E-23	1,8	1,19E-34
1980672	IL1A	Homo sapiens interleukin 1, alpha (IL1A), mRNA.	2,009	4,76E-48	1,629	1,25E-19
5290148	GPT2	Homo sapiens glutamic pyruvate transaminase (alanine aminotransferase) 2 (GPT2), mRNA.	2,006	1,54E-26	1,494	4,28E-16

6620689	MTHFD2	Homo sapiens methylenetetrahydrofolate dehydrogenase (NADP+ dependent) 2, methenyltetrahydrofolate cyclohydrolase (MTHFD2), nuclear gene encoding mitochondrial protein, transcript variant 2, mRNA.	1,966	2E-50	1,532	7,39E-16
4830433	LARP6	Homo sapiens La ribonucleoprotein domain family, member 6 (LARP6), transcript variant 1, mRNA.	1,828	1,06E-38	1,508	1,61E-27
3890373	ITGB2	Homo sapiens integrin, beta 2 (complement component 3 receptor 3 and 4 subunit) (ITGB2), mRNA.	1,821	2,19E-45	1,368	4,91E-18
1820594	HBEGF	Homo sapiens heparin-binding EGF-like growth factor (HBEGF), mRNA.	1,819	8,54E-39	1,61	2,79E-41
3610626	ADM2	Homo sapiens adrenomedullin 2 (ADM2), mRNA.	1,813	2,09E-22	1,48	7,93E-15
6370369	CD14	Homo sapiens CD14 molecule (CD14), transcript variant 2, mRNA.	1,798	6,18E-29	1,562	7,66E-21
2510091	COL8A1	Homo sapiens collagen, type VIII, alpha 1 (COL8A1), transcript variant 2, mRNA.	1,758	1,12E-21	1,37	2,56E-11
1300706	MTHFD2	Homo sapiens methylenetetrahydrofolate dehydrogenase (NADP+ dependent) 2, methenyltetrahydrofolate cyclohydrolase (MTHFD2), nuclear gene encoding mitochondrial protein, transcript variant 1, mRNA.	1,742	1,9E-28	1,489	4,24E-18
7320370	STAT4	Homo sapiens signal transducer and activator of transcription 4 (STAT4), mRNA.	1,717	5,77E-16	1,442	8,89E-15
2640224	VEGFA	Homo sapiens vascular endothelial growth factor A (VEGFA), transcript variant 2, mRNA.	1,704	1,71E-18	1,461	1,76E-16
3190608	SLC6A9	Homo sapiens solute carrier family 6 (neurotransmitter transporter, glycine), member 9 (SLC6A9), transcript variant 3, mRNA.	1,686	8E-33	1,428	7,12E-16
240309	CTSB	Homo sapiens cathepsin B (CTSB), transcript variant 2, mRNA.	1,677	6,46E-30	1,398	9,56E-12
2650730	STC1	Homo sapiens stanniocalcin 1 (STC1), mRNA.	1,662	4,7E-17	1,52	6,43E-18
5700278	GARS	Homo sapiens glycyl-tRNA synthetase (GARS), mRNA.	1,642	1,27E-22	1,406	6,95E-20
510577	TRIML2	Homo sapiens tripartite motif family-like 2 (TRIML2), mRNA.	1,639	1,8E-29	1,591	4,93E-35
4860224	WARS	Homo sapiens tryptophanyl-tRNA synthetase (WARS), transcript variant 1, mRNA.	1,633	5,72E-27	1,552	1,87E-21
3800161	KRT7	Homo sapiens keratin 7 (KRT7), mRNA.	1,632	7,58E-23	1,611	6,66E-32
60121	CTSB	Homo sapiens cathepsin B (CTSB), transcript variant 1, mRNA.	1,625	6,89E-31	1,376	4,56E-18
270615	ABCC3	Homo sapiens ATP-binding cassette, sub-family C (CFTR/MRP), member 3 (ABCC3), mRNA.	1,62	2,53E-24	1,485	2,33E-30
7000682	CARS	Homo sapiens cysteinyl-tRNA synthetase (CARS), transcript variant 4, mRNA.	1,613	3,2E-26	1,541	8,80E-14
3710068	WARS	Homo sapiens tryptophanyl-tRNA synthetase (WARS), transcript variant 2, mRNA.	1,612	9,28E-24	1,637	5,21E-21
2100762	INHBE	Homo sapiens inhibin, beta E (INHBE), mRNA.	1,611	4,14E-19	1,685	9,19E-17

6020093	SARS	Homo sapiens seryl-tRNA synthetase (SARS), mRNA.	1,598	4,22E-24	1,429	1,31E-13
650554	LOC100132240	PREDICTED: Homo sapiens misc_RNA (LOC100132240), miscRNA.	1,597	1,73E-26	1,388	1,71E-15
1690553	EPCAM	Homo sapiens epithelial cell adhesion molecule (EPCAM), mRNA.	1,571	8,5E-17	1,424	5,70E-10
4070575	TACSTD1	Homo sapiens tumor-associated calcium signal transducer 1 (TACSTD1), mRNA.	1,571	3,43E-24	1,471	3,61E-23
3520040	YARS	Homo sapiens tyrosyl-tRNA synthetase (YARS), mRNA.	1,563	1,19E-27	1,364	8,89E-23
7000369	CD14	Homo sapiens CD14 molecule (CD14), transcript variant 1, mRNA.	1,557	6,74E-20	1,374	2,45E-12
2450156	XBP1	Homo sapiens X-box binding protein 1 (XBP1), transcript variant 2, mRNA.	1,55	1,23E-22	1,368	1,32E-13

Supplementary Table 3

The list of transcripts downregulated by at least 30% upon overexpression of miR-301a.

Probe ID	**Gene symbol**	**Definition**	**Fold change**	**p-value (BH)**
3990170	IFI27	Homo sapiens interferon, alpha-inducible protein 27 (IFI27), transcript variant 2, mRNA.	0,275	1,31E-27
7100193	RTCD1	Homo sapiens RNA terminal phosphate cyclase domain 1 (RTCD1), mRNA.	0,461	2,1E-25
6960014	MTMR9	Homo sapiens myotubularin related protein 9 (MTMR9), mRNA.	0,466	8,48E-45
5690687	CTGF	Homo sapiens connective tissue growth factor (CTGF), mRNA.	0,492	7,44E-18
5420326	RTCD1	Homo sapiens RNA terminal phosphate cyclase domain 1 (RTCD1), mRNA.	0,498	3,26E-28
5090215	IFI6	Homo sapiens interferon, alpha-inducible protein 6 (IFI6), transcript variant 3, mRNA.	0,501	4,62E-30
10079	F3	Homo sapiens coagulation factor III (thromboplastin, tissue factor) (F3), mRNA.	0,503	2,03E-17
3120138	F3	Homo sapiens coagulation factor III (thromboplastin, tissue factor) (F3), mRNA.	0,511	1,45E-18
770408	SERPINE1	Homo sapiens serpin peptidase inhibitor, clade E (nexin, plasminogen activator inhibitor type 1), member 1 (SERPINE1), mRNA.	0,523	2,2E-19
1010246	IFI6	Homo sapiens interferon, alpha-inducible protein 6 (IFI6), transcript variant 2, mRNA.	0,531	1,8E-20
2650598	CYP4V2	Homo sapiens cytochrome P450, family 4, subfamily V, polypeptide 2 (CYP4V2), mRNA.	0,542	4,11E-19
3840154	SPP1	Homo sapiens secreted phosphoprotein 1 (SPP1), transcript variant 1, mRNA.	0,55	5,16E-20
5570279	HIST1H1C	Homo sapiens histone cluster 1, H1c (HIST1H1C), mRNA.	0,552	7,01E-22
3140543	ZMAT3	Homo sapiens zinc finger, matrin type 3 (ZMAT3), transcript variant 2, mRNA.	0,556	2,35E-31
3930452	CDC2L6	Homo sapiens cell division cycle 2-like 6 (CDK8-like) (CDC2L6), mRNA.	0,565	3,47E-20
3460070	SPP1	Homo sapiens secreted phosphoprotein 1 (SPP1), transcript variant 2, mRNA.	0,578	4,81E-15
3450735	UGT1A6	Homo sapiens UDP glucuronosyltransferase 1 family, polypeptide A6 (UGT1A6), transcript variant 2, mRNA.	0,58	3,79E-14
650678	TAGLN	Homo sapiens transgelin (TAGLN), transcript variant 2, mRNA.	0,582	7,12E-30

2100196	ISG15	Homo sapiens ISG15 ubiquitin-like modifier (ISG15), mRNA.	0,585	3,34E-18
2470600	KATNAL1	Homo sapiens katanin p60 subunit A-like 1 (KATNAL1), transcript variant 2, mRNA.	0,585	9,99E-22
7610286	HPRT1	Homo sapiens hypoxanthine phosphoribosyltransferase 1 (Lesch-Nyhan syndrome) (HPRT1), mRNA.	0,586	3,15E-19
240400	PMEPA1	Homo sapiens prostate transmembrane protein, androgen induced 1 (PMEPA1), transcript variant 2, mRNA.	0,587	3,72E-18
5550431	MMD	Homo sapiens monocyte to macrophage differentiation-associated (MMD), mRNA.	0,588	5,69E-27
7650333	PSAP	Homo sapiens prosaposin (PSAP), transcript variant 2, mRNA.	0,589	5,67E-32
3780095	AOX1	Homo sapiens aldehyde oxidase 1 (AOX1), mRNA.	0,594	3,63E-18
2340626	TFB1M	Homo sapiens transcription factor B1, mitochondrial (TFB1M), mRNA.	0,599	2,16E-20
5860010	CDS1	Homo sapiens CDP-diacylglycerol synthase (phosphatidate cytidylyltransferase) 1 (CDS1), mRNA.	0,604	1,05E-17
4490010	DAAM1	Homo sapiens dishevelled associated activator of morphogenesis 1 (DAAM1), mRNA.	0,605	9,45E-14
5360424	RPS6KA2	Homo sapiens ribosomal protein S6 kinase, 90kDa, polypeptide 2 (RPS6KA2), transcript variant 2, mRNA.	0,606	8,54E-24
2970762	HCCS	Homo sapiens holocytochrome c synthase (cytochrome c heme-lyase) (HCCS), mRNA.	0,606	1,62E-14
6400270	HPRT1	Homo sapiens hypoxanthine phosphoribosyltransferase 1 (Lesch-Nyhan syndrome) (HPRT1), mRNA.	0,607	4,78E-20
6200086	PSAP	Homo sapiens prosaposin (PSAP), transcript variant 1, mRNA.	0,608	5,11E-29
2510091	COL8A1	Homo sapiens collagen, type VIII, alpha 1 (COL8A1), transcript variant 2, mRNA.	0,618	7,03E-31
4290088	MSRB3	Homo sapiens methionine sulfoxide reductase B3 (MSRB3), transcript variant 1, mRNA.	0,62	1,2E-17
4010086	OKL38	Homo sapiens pregnancy-induced growth inhibitor (OKL38), transcript variant 1, mRNA.	0,623	9,59E-20
3120431	IMPDH1	Homo sapiens IMP (inosine monophosphate) dehydrogenase 1 (IMPDH1), transcript variant 1, mRNA.	0,623	2,07E-36
2760452	RPS29	Homo sapiens ribosomal protein S29 (RPS29), transcript variant 2, mRNA.	0,625	1,27E-07
2260066	CLIP1	Homo sapiens CAP-GLY domain containing linker protein 1 (CLIP1), transcript variant 1, mRNA.	0,625	1,69E-22
2000546	C3orf10	Homo sapiens chromosome 3 open reading frame 10 (C3orf10), mRNA.	0,63	7,54E-17
6370703	UGT1A6	Homo sapiens UDP glucuronosyltransferase 1 family, polypeptide A6 (UGT1A6), transcript variant 1, mRNA.	0,631	3,16E-16
2940369	SKP1	Homo sapiens S-phase kinase-associated protein 1 (SKP1), transcript variant 1, mRNA.	0,632	8E-25
510577	TRIML2	Homo sapiens tripartite motif family-like 2 (TRIML2), mRNA.	0,632	1,9E-28
2140634	VPS24	Homo sapiens vacuolar protein sorting 24 homolog (S. cerevisiae) (VPS24), transcript variant 2, mRNA.	0,632	1,36E-24
730040	LAMB3	Homo sapiens laminin, beta 3 (LAMB3), transcript variant 1, mRNA.	0,635	4,14E-21
3940088	ZBED2	Homo sapiens zinc finger, BED-type containing 2 (ZBED2), mRNA.	0,635	4,94E-19
6400717	SFTA1P	Homo sapiens surfactant associated 1 (pseudogene) (SFTA1P), non-coding RNA.	0,637	1,88E-16
4880392	KIAA1539	Homo sapiens KIAA1539 (KIAA1539), mRNA.	0,637	1,25E-21
5260070	HES4	Homo sapiens hairy and enhancer of split 4 (Drosophila) (HES4), mRNA.	0,637	1,2E-20

510100	CBY1	Homo sapiens chibby homolog 1 (Drosophila) (CBY1), transcript variant 1, mRNA.	0,64	2,58E-20
5810685	THBS1	Homo sapiens thrombospondin 1 (THBS1), mRNA.	0,64	1,15E-19
4670059	ZAK	Homo sapiens sterile alpha motif and leucine zipper containing kinase AZK (ZAK), transcript variant 2, mRNA.	0,642	2,84E-21
4290148	HIST2H2AA4	Homo sapiens histone cluster 2, H2aa4 (HIST2H2AA4), mRNA.	0,643	3,76E-15
3140092	TRAK1	Homo sapiens trafficking protein, kinesin binding 1 (TRAK1), mRNA.	0,644	1,13E-20
380026	C1orf116	Homo sapiens chromosome 1 open reading frame 116 (C1orf116), mRNA.	0,645	3,34E-17
730491	C1orf116	Homo sapiens chromosome 1 open reading frame 116 (C1orf116), transcript variant 1, mRNA.	0,645	8,19E-23
6370133	SEC23B	Homo sapiens Sec23 homolog B (S. cerevisiae) (SEC23B), transcript variant 2, mRNA.	0,646	6,64E-21
3780053	PALLD	Homo sapiens palladin, cytoskeletal associated protein (PALLD), transcript variant 2, mRNA.	0,647	1,35E-26
3870338	IFI44L	Homo sapiens interferon-induced protein 44-like (IFI44L), mRNA.	0,647	4,98E-27
6940360	ACVR1	Homo sapiens activin A receptor, type I (ACVR1), mRNA.	0,647	9,34E-19
270615	ABCC3	Homo sapiens ATP-binding cassette, sub-family C (CFTR/MRP), member 3 (ABCC3), mRNA.	0,647	3,16E-28
2970730	MYADM	Homo sapiens myeloid-associated differentiation marker (MYADM), transcript variant 4, mRNA.	0,648	7,52E-22
7200156	ITGB2	Homo sapiens integrin, beta 2 (antigen CD18 (p95), lymphocyte function-associated antigen 1; macrophage antigen 1 (mac-1) beta subunit) (ITGB2), mRNA.	0,653	3,06E-23
110161	EFR3A	Homo sapiens EFR3 homolog A (S. cerevisiae) (EFR3A), mRNA.	0,653	3,22E-18
6580091	LOC339352	PREDICTED: Homo sapiens misc_RNA (LOC339352), miscRNA.	0,653	1,16E-15
1980209	SEC23B	Homo sapiens Sec23 homolog B (S. cerevisiae) (SEC23B), transcript variant 2, mRNA.	0,654	4,19E-16
990372	COL17A1	Homo sapiens collagen, type XVII, alpha 1 (COL17A1), mRNA.	0,655	3,87E-19
3610129	HSD17B1	Homo sapiens hydroxysteroid (17-beta) dehydrogenase 1 (HSD17B1), mRNA.	0,657	3,27E-21
1430673	SDCBP2	Homo sapiens syndecan binding protein (syntenin) 2 (SDCBP2), transcript variant 2, mRNA.	0,658	2,15E-18
2640324	SLC46A3	Homo sapiens solute carrier family 46, member 3 (SLC46A3), mRNA.	0,658	8,47E-15
4290605	SLC44A1	Homo sapiens solute carrier family 44, member 1 (SLC44A1), mRNA.	0,658	5,32E-21
3440224	YRDC	Homo sapiens yrdC domain containing (E. coli) (YRDC), nuclear gene encoding mitochondrial protein, mRNA.	0,662	2,14E-23
4050161	STX6	Homo sapiens syntaxin 6 (STX6), mRNA.	0,662	5,04E-18
240594	ANXA3	Homo sapiens annexin A3 (ANXA3), mRNA.	0,662	1,49E-20
6290592	LOC649821	PREDICTED: Homo sapiens similar to 60S ribosomal protein L14 (CAG-ISL 7), transcript variant 1 (LOC649821), mRNA.	0,663	5,11E-07
3930605	CYR61	Homo sapiens cysteine-rich, angiogenic inducer, 61 (CYR61), mRNA.	0,663	3,51E-19
1090221	VPS37A	Homo sapiens vacuolar protein sorting 37 homolog A (S. cerevisiae) (VPS37A), mRNA.	0,663	2,59E-15
3360452	COL8A1	Homo sapiens collagen, type VIII, alpha 1 (COL8A1), transcript variant 2, mRNA.	0,665	1,78E-14
2120270	COL17A1	Homo sapiens collagen, type XVII, alpha 1 (COL17A1), mRNA.	0,666	1,05E-14
7000086	KCTD20	Homo sapiens potassium channel tetramerisation domain containing 20 (KCTD20), mRNA.	0,666	4,62E-17

3290458	FEZ1	Homo sapiens fasciculation and elongation protein zeta 1 (zygin I) (FEZ1), transcript variant 1, mRNA.	0,666	1,45E-27
2480487	STX6	Homo sapiens syntaxin 6 (STX6), mRNA.	0,669	2,67E-25
4640066	VAMP3	Homo sapiens vesicle-associated membrane protein 3 (cellubrevin) (VAMP3), mRNA.	0,67	8,72E-15
1510091	VPS36	Homo sapiens vacuolar protein sorting 36 homolog (S. cerevisiae) (VPS36), mRNA.	0,673	5,2E-12
5690762	FAM18B	Homo sapiens family with sequence similarity 18, member B (FAM18B), mRNA.	0,675	3,85E-13
4610433	ANGPTL4	Homo sapiens angiopoietin-like 4 (ANGPTL4), transcript variant 1, mRNA.	0,675	3,05E-31
4570091	NDUFAF3	Homo sapiens NADH dehydrogenase (ubiquinone) 1 alpha subcomplex, assembly factor 3 (NDUFAF3), nuclear gene encoding mitochondrial protein, transcript variant 1, mRNA.	0,677	1,37E-36
1770402	PIR	Homo sapiens pirin (iron-binding nuclear protein) (PIR), transcript variant 2, mRNA.	0,677	2,99E-13
130360	IDS	Homo sapiens iduronate 2-sulfatase (Hunter syndrome) (IDS), transcript variant 1, mRNA.	0,677	1,75E-29
1820592	HIST2H2AA3	Homo sapiens histone cluster 2, H2aa3 (HIST2H2AA3), mRNA.	0,677	4,36E-06
830164	ZFP36L1	Homo sapiens zinc finger protein 36, C3H type-like 1 (ZFP36L1), mRNA.	0,679	3,81E-08
4010554	C13orf1	Homo sapiens chromosome 13 open reading frame 1 (C13orf1), mRNA.	0,68	3,24E-14
2480739	SKP1A	Homo sapiens S-phase kinase-associated protein 1A (p19A) (SKP1A), transcript variant 1, mRNA.	0,682	8,04E-19
2060440	MAFB	Homo sapiens v-maf musculoaponeurotic fibrosarcoma oncogene homolog B (avian) (MAFB), mRNA.	0,683	2,18E-20
5310168	HLA-B	Homo sapiens major histocompatibility complex, class I, B (HLA-B), mRNA.	0,684	2,28E-16
770672	THOP1	Homo sapiens thimet oligopeptidase 1 (THOP1), mRNA.	0,685	2,08E-20
6200332	VPS24	Homo sapiens vacuolar protein sorting 24 homolog (S. cerevisiae) (VPS24), transcript variant 2, mRNA.	0,686	2,73E-14
2640292	CTGF	Homo sapiens connective tissue growth factor (CTGF), mRNA.	0,686	1,46E-06
3170162	PRNP	Homo sapiens prion protein (PRNP), transcript variant 3, mRNA.	0,686	1,32E-20
5420025	UBE3B	Homo sapiens ubiquitin protein ligase E3B (UBE3B), transcript variant 1, mRNA.	0,687	3,78E-11
1230025	CYB5R1	Homo sapiens cytochrome b5 reductase 1 (CYB5R1), mRNA.	0,688	4,62E-17
4070427	TTLL11	Homo sapiens tubulin tyrosine ligase-like family, member 11 (TTLL11), mRNA.	0,691	5,47E-12
7160010	RNF19A	Homo sapiens ring finger protein 19A (RNF19A), transcript variant 2, mRNA.	0,693	2,22E-05
6220746	GLIPR1	Homo sapiens GLI pathogenesis-related 1 (GLIPR1), mRNA.	0,694	4,99E-17
7550608	TMEM9B	Homo sapiens TMEM9 domain family, member B (TMEM9B), mRNA.	0,694	1,16E-21
1690709	UBE3C	Homo sapiens ubiquitin protein ligase E3C (UBE3C), mRNA.	0,695	2,67E-18
5130091	DICER1	Homo sapiens Dicer1, Dcr-1 homolog (Drosophila) (DICER1), transcript variant 2, mRNA.	0,696	1,11E-11
2510220	IFI35	Homo sapiens interferon-induced protein 35 (IFI35), mRNA.	0,696	1,32E-13
2360326	TAGLN	Homo sapiens transgelin (TAGLN), transcript variant 2, mRNA.	0,697	3,11E-13
610451	HIST2H2AA3	Homo sapiens histone cluster 2, H2aa3 (HIST2H2AA3), mRNA.	0,698	3,97E-13
6130259	LOC402644	PREDICTED: Homo sapiens similar to peptidylprolyl isomerase A isoform 1 (LOC402644), mRNA.	0,698	0,000291
7380367	C9orf69	Homo sapiens chromosome 9 open reading frame 69 (C9orf69),	0,698	5,1E-16

		mRNA.		
5570427	GLS	Homo sapiens glutaminase (GLS), mRNA.	0,699	2,5E-07

Supplementary Table 4

The list of transcripts downregulated by at least 30% upon overexpression of miR-301b.

Probe ID	Gene symbol	Definition	Fold change	p-value (BH)
3990170	IFI27	Homo sapiens interferon, alpha-inducible protein 27 (IFI27), transcript variant 2, mRNA.	0,307	1,1E-26
6960014	MTMR9	Homo sapiens myotubularin related protein 9 (MTMR9), mRNA.	0,462	6,66E-44
7100193	RTCD1	Homo sapiens RNA terminal phosphate cyclase domain 1 (RTCD1), mRNA.	0,478	1,14E-24
5090215	IFI6	Homo sapiens interferon, alpha-inducible protein 6 (IFI6), transcript variant 3, mRNA.	0,483	2,76E-31
2760452	RPS29	Homo sapiens ribosomal protein S29 (RPS29), transcript variant 2, mRNA.	0,52	5,44E-11
6200086	PSAP	Homo sapiens prosaposin (PSAP), transcript variant 1, mRNA.	0,525	2,21E-33
5570279	HIST1H1C	Homo sapiens histone cluster 1, H1c (HIST1H1C), mRNA.	0,527	2,84E-23
1010246	IFI6	Homo sapiens interferon, alpha-inducible protein 6 (IFI6), transcript variant 2, mRNA.	0,529	9,38E-21
7650333	PSAP	Homo sapiens prosaposin (PSAP), transcript variant 2, mRNA.	0,536	1,78E-36
3930452	CDC2L6	Homo sapiens cell division cycle 2-like 6 (CDK8-like) (CDC2L6), mRNA.	0,554	8,48E-20
5860010	CDS1	Homo sapiens CDP-diacylglycerol synthase (phosphatidate cytidylyltransferase) 1 (CDS1), mRNA.	0,555	5,86E-21
2340626	TFB1M	Homo sapiens transcription factor B1, mitochondrial (TFB1M), mRNA.	0,562	1,37E-22
3140543	ZMAT3	Homo sapiens zinc finger, matrin type 3 (ZMAT3), transcript variant 2, mRNA.	0,562	2,87E-30
5360424	RPS6KA2	Homo sapiens ribosomal protein S6 kinase, 90kDa, polypeptide 2 (RPS6KA2), transcript variant 2, mRNA.	0,57	9,41E-26
5550431	MMD	Homo sapiens monocyte to macrophage differentiation-associated (MMD), mRNA.	0,571	2,39E-31
5420326	RTCD1	Homo sapiens RNA terminal phosphate cyclase domain 1 (RTCD1), mRNA.	0,572	3,95E-23
3460070	SPP1	Homo sapiens secreted phosphoprotein 1 (SPP1), transcript variant 2, mRNA.	0,577	2,43E-15
2510091	COL8A1	Homo sapiens collagen, type VIII, alpha 1 (COL8A1), transcript variant 2, mRNA.	0,579	8,43E-34
1090221	VPS37A	Homo sapiens vacuolar protein sorting 37 homolog A (S. cerevisiae) (VPS37A), mRNA.	0,581	1,88E-19
510100	CBY1	Homo sapiens chibby homolog 1 (Drosophila) (CBY1), transcript variant 1, mRNA.	0,584	4,98E-23
1820592	HIST2H2AA3	Homo sapiens histone cluster 2, H2aa3 (HIST2H2AA3), mRNA.	0,586	3,83E-09
6400270	HPRT1	Homo sapiens hypoxanthine phosphoribosyltransferase 1 (Lesch-Nyhan syndrome) (HPRT1), mRNA.	0,587	3,02E-21
2640324	SLC46A3	Homo sapiens solute carrier family 46, member 3 (SLC46A3), mRNA.	0,591	1,49E-20
3450735	UGT1A6	Homo sapiens UDP glucuronosyltransferase 1 family, polypeptide A6 (UGT1A6), transcript variant 2, mRNA.	0,592	1,91E-12
990372	COL17A1	Homo sapiens collagen, type XVII, alpha 1 (COL17A1), mRNA.	0,592	1,13E-22

3120431	IMPDH1	Homo sapiens IMP (inosine monophosphate) dehydrogenase 1 (IMPDH1), transcript variant 1, mRNA.	0,595	1,72E-39
2260066	CLIP1	Homo sapiens CAP-GLY domain containing linker protein 1 (CLIP1), transcript variant 1, mRNA.	0,6	3,26E-21
2000546	C3orf10	Homo sapiens chromosome 3 open reading frame 10 (C3orf10), mRNA.	0,601	2E-18
5570427	GLS	Homo sapiens glutaminase (GLS), mRNA.	0,602	1,15E-11
2100196	ISG15	Homo sapiens ISG15 ubiquitin-like modifier (ISG15), mRNA.	0,605	4,65E-17
2650598	CYP4V2	Homo sapiens cytochrome P450, family 4, subfamily V, polypeptide 2 (CYP4V2), mRNA.	0,606	4,13E-16
2060440	MAFB	Homo sapiens v-maf musculoaponeurotic fibrosarcoma oncogene homolog B (avian) (MAFB), mRNA.	0,606	9,29E-29
7610286	HPRT1	Homo sapiens hypoxanthine phosphoribosyltransferase 1 (Lesch-Nyhan syndrome) (HPRT1), mRNA.	0,608	3,24E-18
150474	CA12	Homo sapiens carbonic anhydrase XII (CA12), transcript variant 1, mRNA.	0,612	3,21E-30
7200156	ITGB2	Homo sapiens integrin, beta 2 (antigen CD18 (p95), lymphocyte function-associated antigen 1; macrophage antigen 1 (mac-1) beta subunit) (ITGB2), mRNA.	0,619	4,77E-27
3120138	F3	Homo sapiens coagulation factor III (thromboplastin, tissue factor) (F3), mRNA.	0,619	5,66E-13
770408	SERPINE1	Homo sapiens serpin peptidase inhibitor, clade E (nexin, plasminogen activator inhibitor type 1), member 1 (SERPINE1), mRNA.	0,62	2,3E-13
4290148	HIST2H2AA4	Homo sapiens histone cluster 2, H2aa4 (HIST2H2AA4), mRNA.	0,621	1,42E-17
2470600	KATNAL1	Homo sapiens katanin p60 subunit A-like 1 (KATNAL1), transcript variant 2, mRNA.	0,622	1,26E-18
4290605	SLC44A1	Homo sapiens solute carrier family 44, member 1 (SLC44A1), mRNA.	0,623	4,14E-23
2120270	COL17A1	Homo sapiens collagen, type XVII, alpha 1 (COL17A1), mRNA.	0,626	1,65E-22
3940088	ZBED2	Homo sapiens zinc finger, BED-type containing 2 (ZBED2), mRNA.	0,626	6,69E-20
1980209	SEC23B	Homo sapiens Sec23 homolog B (S. cerevisiae) (SEC23B), transcript variant 2, mRNA.	0,628	2,05E-19
2140634	VPS24	Homo sapiens vacuolar protein sorting 24 homolog (S. cerevisiae) (VPS24), transcript variant 2, mRNA.	0,63	1,72E-24
5130091	DICER1	Homo sapiens Dicer1, Dcr-1 homolog (Drosophila) (DICER1), transcript variant 2, mRNA.	0,63	3,99E-17
4050161	STX6	Homo sapiens syntaxin 6 (STX6), mRNA.	0,63	9,38E-21
610451	HIST2H2AA3	Homo sapiens histone cluster 2, H2aa3 (HIST2H2AA3), mRNA.	0,631	2,81E-18
3840154	SPP1	Homo sapiens secreted phosphoprotein 1 (SPP1), transcript variant 1, mRNA.	0,632	3,36E-15
3870338	IFI44L	Homo sapiens interferon-induced protein 44-like (IFI44L), mRNA.	0,634	2,25E-24
2970762	HCCS	Homo sapiens holocytochrome c synthase (cytochrome c heme-lyase) (HCCS), mRNA.	0,636	5,02E-13
6370133	SEC23B	Homo sapiens Sec23 homolog B (S. cerevisiae) (SEC23B), transcript variant 2, mRNA.	0,637	1,68E-19
2690411	GOLSYN	Homo sapiens Golgi-localized protein (GOLSYN), transcript variant 7, mRNA.	0,638	7,97E-22
6330377	ATP6V0D1	Homo sapiens ATPase, H+ transporting, lysosomal 38kDa, V0 subunit d1 (ATP6V0D1), mRNA.	0,646	7,47E-20
2480487	STX6	Homo sapiens syntaxin 6 (STX6), mRNA.	0,648	2,43E-25
7380367	C9orf69	Homo sapiens chromosome 9 open reading frame 69 (C9orf69), mRNA.	0,65	1,01E-19

3140092	TRAK1	Homo sapiens trafficking protein, kinesin binding 1 (TRAK1), mRNA.	0,652	1,1E-20
240400	PMEPA1	Homo sapiens prostate transmembrane protein, androgen induced 1 (PMEPA1), transcript variant 2, mRNA.	0,652	1,01E-13
3360452	COL8A1	Homo sapiens collagen, type VIII, alpha 1 (COL8A1), transcript variant 2, mRNA.	0,657	5,16E-13
730040	LAMB3	Homo sapiens laminin, beta 3 (LAMB3), transcript variant 1, mRNA.	0,658	1,63E-19
3890373	ITGB2	Homo sapiens integrin, beta 2 (complement component 3 receptor 3 and 4 subunit) (ITGB2), mRNA.	0,658	4,46E-26
4640066	VAMP3	Homo sapiens vesicle-associated membrane protein 3 (cellubrevin) (VAMP3), mRNA.	0,66	1,49E-14
6580091	LOC339352	PREDICTED: Homo sapiens misc_RNA (LOC339352), miscRNA.	0,661	4,01E-13
6940360	ACVR1	Homo sapiens activin A receptor, type I (ACVR1), mRNA.	0,661	1,94E-15
6100022	HIST2H2AC	Homo sapiens histone cluster 2, H2ac (HIST2H2AC), mRNA.	0,661	2,25E-27
110161	EFR3A	Homo sapiens EFR3 homolog A (S. cerevisiae) (EFR3A), mRNA.	0,662	3,2E-22
5220070	HLA-F	Homo sapiens major histocompatibility complex, class I, F (HLA-F), transcript variant 1, mRNA.	0,662	1,92E-10
770538	LYSMD2	Homo sapiens LysM, putative peptidoglycan-binding, domain containing 2 (LYSMD2), mRNA.	0,664	5,69E-17
2940369	SKP1	Homo sapiens S-phase kinase-associated protein 1 (SKP1), transcript variant 1, mRNA.	0,665	1,06E-19
4570091	NDUFAF3	Homo sapiens NADH dehydrogenase (ubiquinone) 1 alpha subcomplex, assembly factor 3 (NDUFAF3), nuclear gene encoding mitochondrial protein, transcript variant 1, mRNA.	0,665	1,03E-33
3610129	HSD17B1	Homo sapiens hydroxysteroid (17-beta) dehydrogenase 1 (HSD17B1), mRNA.	0,665	1,09E-19
1690446	PNPLA6	Homo sapiens patatin-like phospholipase domain containing 6 (PNPLA6), mRNA.	0,667	1,01E-15
6580553	ABCC5	Homo sapiens ATP-binding cassette, sub-family C (CFTR/MRP), member 5 (ABCC5), transcript variant 1, mRNA.	0,667	1,8E-13
5490626	SUMF1	Homo sapiens sulfatase modifying factor 1 (SUMF1), mRNA.	0,668	1,32E-25
4670059	ZAK	Homo sapiens sterile alpha motif and leucine zipper containing kinase AZK (ZAK), transcript variant 2, mRNA.	0,671	1,62E-18
6200332	VPS24	Homo sapiens vacuolar protein sorting 24 homolog (S. cerevisiae) (VPS24), transcript variant 2, mRNA.	0,673	6,11E-15
270615	ABCC3	Homo sapiens ATP-binding cassette, sub-family C (CFTR/MRP), member 3 (ABCC3), mRNA.	0,673	4,33E-24
2480440	C3orf64	Homo sapiens chromosome 3 open reading frame 64 (C3orf64), mRNA.	0,674	1,04E-12
2450725	SLC3A2	Homo sapiens solute carrier family 3 (activators of dibasic and neutral amino acid transport), member 2 (SLC3A2), transcript variant 6, mRNA.	0,675	1,73E-16
4880392	KIAA1539	Homo sapiens KIAA1539 (KIAA1539), mRNA.	0,677	1,02E-17
510577	TRIML2	Homo sapiens tripartite motif family-like 2 (TRIML2), mRNA.	0,678	3,83E-24
7550608	TMEM9B	Homo sapiens TMEM9 domain family, member B (TMEM9B), mRNA.	0,68	2,29E-22
2470762	SECISBP2L	Homo sapiens SECIS binding protein 2-like (SECISBP2L), mRNA.	0,68	2,43E-14
4490010	DAAM1	Homo sapiens dishevelled associated activator of morphogenesis 1 (DAAM1), mRNA.	0,681	4,37E-10
60324	OCRL	Homo sapiens oculocerebrorenal syndrome of Lowe (OCRL), transcript variant a, mRNA.	0,682	3,26E-22

5310168	HLA-B	Homo sapiens major histocompatibility complex, class I, B (HLA-B), mRNA.	0,682	1,97E-12
1430673	SDCBP2	Homo sapiens syndecan binding protein (syntenin) 2 (SDCBP2), transcript variant 2, mRNA.	0,684	7,55E-17
6250484	CFH	Homo sapiens complement factor H (CFH), transcript variant 2, mRNA.	0,687	9,43E-19
2900441	ZBTB4	Homo sapiens zinc finger and BTB domain containing 4 (ZBTB4), mRNA.	0,688	5,89E-16
6940356	PREP	Homo sapiens prolyl endopeptidase (PREP), mRNA.	0,689	8,33E-12
4010086	OKL38	Homo sapiens pregnancy-induced growth inhibitor (OKL38), transcript variant 1, mRNA.	0,69	2,34E-14
1240551	ACADVL	Homo sapiens acyl-Coenzyme A dehydrogenase, very long chain (ACADVL), nuclear gene encoding mitochondrial protein, transcript variant 1, mRNA.	0,691	1,37E-09
6370703	UGT1A6	Homo sapiens UDP glucuronosyltransferase 1 family, polypeptide A6 (UGT1A6), transcript variant 1, mRNA.	0,692	8,51E-13
4150193	CD47	Homo sapiens CD47 molecule (CD47), transcript variant 2, mRNA.	0,693	8,61E-12
6250553	ITFG3	Homo sapiens integrin alpha FG-GAP repeat containing 3 (ITFG3), mRNA.	0,699	2,02E-15
3360131	NAPRT1	Homo sapiens nicotinate phosphoribosyltransferase domain containing 1 (NAPRT1), mRNA.	0,7	5,25E-14
3780053	PALLD	Homo sapiens palladin, cytoskeletal associated protein (PALLD), transcript variant 2, mRNA.	0,7	2,07E-22
4290088	MSRB3	Homo sapiens methionine sulfoxide reductase B3 (MSRB3), transcript variant 1, mRNA.	0,7	2,19E-11

Supplementary Table 5

The list of transcripts downregulated by at least 30% upon overexpression of miR-130b.

Probe ID	Gene symbol	Definition	Fold change	p-value (BH)
510100	CBY1	Homo sapiens chibby homolog 1 (Drosophila) (CBY1), transcript variant 1, mRNA.	0,346	1,03E-32
6400270	HPRT1	Homo sapiens hypoxanthine phosphoribosyltransferase 1 (Lesch-Nyhan syndrome) (HPRT1), mRNA.	0,376	1,38E-32
3990170	IFI27	Homo sapiens interferon, alpha-inducible protein 27 (IFI27), transcript variant 2, mRNA.	0,398	6,34E-24
2230161	RTN4	Homo sapiens reticulon 4 (RTN4), transcript variant 3, mRNA.	0,4	3,93E-47
2340626	TFB1M	Homo sapiens transcription factor B1, mitochondrial (TFB1M), mRNA.	0,411	9,74E-29
780402	RTN4	Homo sapiens reticulon 4 (RTN4), transcript variant 1, mRNA.	0,424	1,63E-25
7610286	HPRT1	Homo sapiens hypoxanthine phosphoribosyltransferase 1 (Lesch-Nyhan syndrome) (HPRT1), mRNA.	0,433	4,44E-29
4180431	LOC205251	PREDICTED: Homo sapiens misc_RNA (LOC205251), miscRNA.	0,441	3,03E-28
4670059	ZAK	Homo sapiens sterile alpha motif and leucine zipper containing kinase AZK (ZAK), transcript variant 2, mRNA.	0,444	4,38E-34
1690709	UBE3C	Homo sapiens ubiquitin protein ligase E3C (UBE3C), mRNA.	0,453	6,89E-34
3120431	IMPDH1	Homo sapiens IMP (inosine monophosphate) dehydrogenase 1 (IMPDH1), transcript variant 1, mRNA.	0,453	2,28E-55
4570091	NDUFAF3	Homo sapiens NADH dehydrogenase (ubiquinone) 1 alpha subcomplex, assembly factor 3 (NDUFAF3), nuclear gene encoding mitochondrial protein, transcript variant 1, mRNA.	0,454	2,2E-59

650678	TAGLN	Homo sapiens transgelin (TAGLN), transcript variant 2, mRNA.	0,465	2,78E-38
7100193	RTCD1	Homo sapiens RNA terminal phosphate cyclase domain 1 (RTCD1), mRNA.	0,468	3,8E-26
6270437	FJX1	Homo sapiens four jointed box 1 (Drosophila) (FJX1), mRNA.	0,474	5,69E-45
6960014	MTMR9	Homo sapiens myotubularin related protein 9 (MTMR9), mRNA.	0,475	1,32E-44
3610129	HSD17B1	Homo sapiens hydroxysteroid (17-beta) dehydrogenase 1 (HSD17B1), mRNA.	0,475	9,39E-36
2970025	SEPW1	Homo sapiens selenoprotein W, 1 (SEPW1), mRNA.	0,477	1E-39
3120138	F3	Homo sapiens coagulation factor III (thromboplastin, tissue factor) (F3), mRNA.	0,481	7,65E-20
7380367	C9orf69	Homo sapiens chromosome 9 open reading frame 69 (C9orf69), mRNA.	0,484	4,53E-31
1090500	LOC645166	PREDICTED: Homo sapiens similar to lymphocyte-specific protein 1 (LOC645166), mRNA.	0,491	7,31E-34
60324	OCRL	Homo sapiens oculocerebrorenal syndrome of Lowe (OCRL), transcript variant a, mRNA.	0,492	1,65E-37
2480554	POP7	Homo sapiens processing of precursor 7, ribonuclease P/MRP subunit (S. cerevisiae) (POP7), mRNA.	0,497	7,95E-39
1230639	TRAPPC4	Homo sapiens trafficking protein particle complex 4 (TRAPPC4), mRNA.	0,503	3,2E-27
3930452	CDC2L6	Homo sapiens cell division cycle 2-like 6 (CDK8-like) (CDC2L6), mRNA.	0,504	1,57E-23
6560750	UBE3C	Homo sapiens ubiquitin protein ligase E3C (UBE3C), mRNA.	0,506	1,94E-26
2100196	ISG15	Homo sapiens ISG15 ubiquitin-like modifier (ISG15), mRNA.	0,508	2,17E-22
5420326	RTCD1	Homo sapiens RNA terminal phosphate cyclase domain 1 (RTCD1), mRNA.	0,51	1,49E-27
150474	CA12	Homo sapiens carbonic anhydrase XII (CA12), transcript variant 1, mRNA.	0,513	1,62E-39
2760452	RPS29	Homo sapiens ribosomal protein S29 (RPS29), transcript variant 2, mRNA.	0,513	5,99E-11
770408	SERPINE1	Homo sapiens serpin peptidase inhibitor, clade E (nexin, plasminogen activator inhibitor type 1), member 1 (SERPINE1), mRNA.	0,515	4,32E-20
5690687	CTGF	Homo sapiens connective tissue growth factor (CTGF), mRNA.	0,515	2,93E-17
770672	THOP1	Homo sapiens thimet oligopeptidase 1 (THOP1), mRNA.	0,516	9,42E-36
1010246	IFI6	Homo sapiens interferon, alpha-inducible protein 6 (IFI6), transcript variant 2, mRNA.	0,517	8,31E-22
5860050	LOC388564	PREDICTED: Homo sapiens hypothetical gene supported by BC052596 (LOC388564), mRNA.	0,519	8,52E-31
5570279	HIST1H1C	Homo sapiens histone cluster 1, H1c (HIST1H1C), mRNA.	0,521	2,66E-24
3140543	ZMAT3	Homo sapiens zinc finger, matrin type 3 (ZMAT3), transcript variant 2, mRNA.	0,523	4,36E-33
5260070	HES4	Homo sapiens hairy and enhancer of split 4 (Drosophila) (HES4), mRNA.	0,523	2,8E-28
6510377	TNFRSF12A	Homo sapiens tumor necrosis factor receptor superfamily, member 12A (TNFRSF12A), mRNA.	0,525	5,09E-20
6580091	LOC339352	PREDICTED: Homo sapiens misc_RNA (LOC339352), miscRNA.	0,525	7,69E-24
620615	NDUFA7	Homo sapiens NADH dehydrogenase (ubiquinone) 1 alpha subcomplex, 7, 14.5kDa (NDUFA7), mRNA.	0,528	1,53E-35
2000546	C3orf10	Homo sapiens chromosome 3 open reading frame 10 (C3orf10), mRNA.	0,528	4,07E-22
5090215	IFI6	Homo sapiens interferon, alpha-inducible protein 6 (IFI6), transcript variant 3, mRNA.	0,53	4,42E-29

4610433	ANGPTL4	Homo sapiens angiopoietin-like 4 (ANGPTL4), transcript variant 1, mRNA.	0,532	1,54E-44
6330377	ATP6V0D1	Homo sapiens ATPase, H+ transporting, lysosomal 38kDa, V0 subunit d1 (ATP6V0D1), mRNA.	0,532	9,43E-29
6250553	ITFG3	Homo sapiens integrin alpha FG-GAP repeat containing 3 (ITFG3), mRNA.	0,533	9,2E-28
2360326	TAGLN	Homo sapiens transgelin (TAGLN), transcript variant 2, mRNA.	0,537	2,87E-25
5390603	UPF2	Homo sapiens UPF2 regulator of nonsense transcripts homolog (yeast) (UPF2), transcript variant 2, mRNA.	0,539	2,61E-29
7650333	PSAP	Homo sapiens prosaposin (PSAP), transcript variant 2, mRNA.	0,539	1,32E-36
2340521	C17orf61	Homo sapiens chromosome 17 open reading frame 61 (C17orf61), mRNA.	0,542	6,1E-22
2100411	CDK2AP2	Homo sapiens cyclin-dependent kinase 2 associated protein 2 (CDK2AP2), mRNA.	0,542	5,68E-21
5900725	PHLDA1	Homo sapiens pleckstrin homology-like domain, family A, member 1 (PHLDA1), mRNA.	0,543	1,52E-31
7050180	SLC22A5	Homo sapiens solute carrier family 22 (organic cation transporter), member 5 (SLC22A5), mRNA.	0,543	4,39E-40
1510608		Homo sapiens cDNA clone IMAGE:5261213	0,544	5,24E-26
6480082	ARHGAP1	Homo sapiens Rho GTPase activating protein 1 (ARHGAP1), mRNA.	0,544	4,73E-33
6450424	NME3	Homo sapiens non-metastatic cells 3, protein expressed in (NME3), mRNA.	0,545	7,56E-33
4050161	STX6	Homo sapiens syntaxin 6 (STX6), mRNA.	0,55	6,88E-28
2480487	STX6	Homo sapiens syntaxin 6 (STX6), mRNA.	0,551	5,82E-35
7320435	DPM3	Homo sapiens dolichyl-phosphate mannosyltransferase polypeptide 3 (DPM3), transcript variant 2, mRNA.	0,551	1,17E-27
7210484	C6orf108	Homo sapiens chromosome 6 open reading frame 108 (C6orf108), transcript variant 2, mRNA.	0,553	1,53E-27
4060437	C11orf70	Homo sapiens chromosome 11 open reading frame 70 (C11orf70), mRNA.	0,554	5,27E-20
770538	LYSMD2	Homo sapiens LysM, putative peptidoglycan-binding, domain containing 2 (LYSMD2), mRNA.	0,555	2,49E-23
4200181	C19orf70	Homo sapiens chromosome 19 open reading frame 70 (C19orf70), mRNA.	0,556	3,11E-36
3610735	F12	Homo sapiens coagulation factor XII (Hageman factor) (F12), mRNA.	0,556	8,85E-27
6840246	CTSA	Homo sapiens cathepsin A (CTSA), transcript variant 1, mRNA.	0,556	6,21E-24
5960411	BCYRN1	Homo sapiens brain cytoplasmic RNA 1 (non-protein coding) (BCYRN1), non-coding RNA.	0,557	1,47E-17
4640066	VAMP3	Homo sapiens vesicle-associated membrane protein 3 (cellubrevin) (VAMP3), mRNA.	0,557	6,66E-21
6480184	LSMD1	Homo sapiens LSM domain containing 1 (LSMD1), mRNA.	0,559	1,83E-17
6380037	LOC100130516	PREDICTED: Homo sapiens hypothetical protein LOC100130516 (LOC100130516), mRNA.	0,559	8,03E-25
3800025	C2orf28	Homo sapiens chromosome 2 open reading frame 28 (C2orf28), transcript variant 2, mRNA.	0,559	5,9E-27
2470689	SPHK1	Homo sapiens sphingosine kinase 1 (SPHK1), transcript variant 1, mRNA.	0,562	2,96E-23
2850520	DPM3	Homo sapiens dolichyl-phosphate mannosyltransferase polypeptide 3 (DPM3), transcript variant 1, mRNA.	0,563	2,32E-20
2650598	CYP4V2	Homo sapiens cytochrome P450, family 4, subfamily V, polypeptide 2 (CYP4V2), mRNA.	0,564	3,41E-18

4480224	SRPRB	Homo sapiens signal recognition particle receptor, B subunit (SRPRB), mRNA.	0,564	3,85E-34
4150309	ZNHIT1	Homo sapiens zinc finger, HIT type 1 (ZNHIT1), mRNA.	0,565	2,01E-23
1980209	SEC23B	Homo sapiens Sec23 homolog B (S. cerevisiae) (SEC23B), transcript variant 2, mRNA.	0,566	6,17E-24
50240	NDUFA3	Homo sapiens NADH dehydrogenase (ubiquinone) 1 alpha subcomplex, 3, 9kDa (NDUFA3), mRNA.	0,566	3,99E-26
240400	PMEPA1	Homo sapiens prostate transmembrane protein, androgen induced 1 (PMEPA1), transcript variant 2, mRNA.	0,567	1,48E-19
3940088	ZBED2	Homo sapiens zinc finger, BED-type containing 2 (ZBED2), mRNA.	0,567	6,54E-23
730739	TCEAL3	Homo sapiens transcription elongation factor A (SII)-like 3 (TCEAL3), transcript variant 2, mRNA.	0,568	1,29E-22
10220	ANAPC11	Homo sapiens anaphase promoting complex subunit 11 (ANAPC11), transcript variant 4, mRNA.	0,568	1,42E-41
630470	C19orf33	Homo sapiens chromosome 19 open reading frame 33 (C19orf33), mRNA.	0,569	3,21E-24
6200086	PSAP	Homo sapiens prosaposin (PSAP), transcript variant 1, mRNA.	0,57	1,2E-32
4010270	LOC440731	PREDICTED: Homo sapiens hypothetical LOC440731, transcript variant 2 (LOC440731), mRNA.	0,57	1,3E-21
4010554	C13orf1	Homo sapiens chromosome 13 open reading frame 1 (C13orf1), mRNA.	0,57	1,57E-25
6370044	PTRH1	Homo sapiens peptidyl-tRNA hydrolase 1 homolog (S. cerevisiae) (PTRH1), mRNA.	0,572	1,54E-25
1690446	PNPLA6	Homo sapiens patatin-like phospholipase domain containing 6 (PNPLA6), mRNA.	0,573	1,68E-20
4290148	HIST2H2AA4	Homo sapiens histone cluster 2, H2aa4 (HIST2H2AA4), mRNA.	0,574	1,73E-19
2450592	ANGPTL4	Homo sapiens angiopoietin-like 4 (ANGPTL4), transcript variant 3, mRNA.	0,576	9,94E-13
5860010	CDS1	Homo sapiens CDP-diacylglycerol synthase (phosphatidate cytidylyltransferase) 1 (CDS1), mRNA.	0,577	2,64E-20
2340092	TCEB1	Homo sapiens transcription elongation factor B (SIII), polypeptide 1 (15kDa, elongin C) (TCEB1), mRNA.	0,577	1,2E-30
6370133	SEC23B	Homo sapiens Sec23 homolog B (S. cerevisiae) (SEC23B), transcript variant 2, mRNA.	0,578	2,01E-24
6290091	SNORD104	Homo sapiens small nucleolar RNA, C/D box 104 (SNORD104), small nucleolar RNA.	0,579	4,54E-18
5570110	TRIOBP	Homo sapiens TRIO and F-actin binding protein (TRIOBP), transcript variant 6, mRNA.	0,579	8,65E-37
7550608	TMEM9B	Homo sapiens TMEM9 domain family, member B (TMEM9B), mRNA.	0,58	2,33E-29
2680438	C2orf28	Homo sapiens chromosome 2 open reading frame 28 (C2orf28), transcript variant 2, mRNA.	0,58	2,13E-28
1240482	LAGE3	Homo sapiens L antigen family, member 3 (LAGE3), mRNA.	0,58	4,26E-22
6200332	VPS24	Homo sapiens vacuolar protein sorting 24 homolog (S. cerevisiae) (VPS24), transcript variant 2, mRNA.	0,581	7,3E-22
4040343	LOC100129673	PREDICTED: Homo sapiens similar to hCG2042915 (LOC100129673), mRNA.	0,581	1,21E-23
6400717	SFTA1P	Homo sapiens surfactant associated 1 (pseudogene) (SFTA1P), non-coding RNA.	0,585	1,88E-19
10079	F3	Homo sapiens coagulation factor III (thromboplastin, tissue factor) (F3), mRNA.	0,586	1,78E-13

5220438	C20orf52	Homo sapiens chromosome 20 open reading frame 52 (C20orf52), mRNA.	0,586	4,36E-27
2970762	HCCS	Homo sapiens holocytochrome c synthase (cytochrome c heme-lyase) (HCCS), mRNA.	0,586	4,79E-15
5360424	RPS6KA2	Homo sapiens ribosomal protein S6 kinase, 90kDa, polypeptide 2 (RPS6KA2), transcript variant 2, mRNA.	0,587	1,38E-25
3390722	NICN1	Homo sapiens nicolin 1 (NICN1), mRNA.	0,588	8,97E-31
7510632	TAF10	Homo sapiens TAF10 RNA polymerase II, TATA box binding protein (TBP)-associated factor, 30kDa (TAF10), mRNA.	0,588	5,11E-28
2140634	VPS24	Homo sapiens vacuolar protein sorting 24 homolog (S. cerevisiae) (VPS24), transcript variant 2, mRNA.	0,589	7,94E-28
3290458	FEZ1	Homo sapiens fasciculation and elongation protein zeta 1 (zygin I) (FEZ1), transcript variant 1, mRNA.	0,589	1,44E-40
5810743	LOC387882	Homo sapiens hypothetical protein (LOC387882), mRNA.	0,589	5,19E-22
3060563	NR2C2AP	Homo sapiens nuclear receptor 2C2-associated protein (NR2C2AP), mRNA.	0,59	1,4E-18
2470600	KATNAL1	Homo sapiens katanin p60 subunit A-like 1 (KATNAL1), transcript variant 2, mRNA.	0,591	1,42E-21
4180612		Homo sapiens mRNA; cDNA DKFZp434C1613 (from clone DKFZp434C1613)	0,591	1,95E-30
5810685	THBS1	Homo sapiens thrombospondin 1 (THBS1), mRNA.	0,591	9,35E-23
6580121	MID1IP1	Homo sapiens MID1 interacting protein 1 (gastrulation specific G12 homolog (zebrafish)) (MID1IP1), mRNA.	0,591	1,14E-28
4540465	C11orf70	Homo sapiens chromosome 11 open reading frame 70 (C11orf70), mRNA.	0,593	5,23E-19
4070427	TTLL11	Homo sapiens tubulin tyrosine ligase-like family, member 11 (TTLL11), mRNA.	0,595	3,05E-19
2450246	OSBPL5	Homo sapiens oxysterol binding protein-like 5 (OSBPL5), transcript variant 2, mRNA.	0,595	3,49E-29
3140092	TRAK1	Homo sapiens trafficking protein, kinesin binding 1 (TRAK1), mRNA.	0,596	3,27E-25
6100022	HIST2H2AC	Homo sapiens histone cluster 2, H2ac (HIST2H2AC), mRNA.	0,597	3,3E-24
620538	ROMO1	Homo sapiens reactive oxygen species modulator 1 (ROMO1), nuclear gene encoding mitochondrial protein, mRNA.	0,599	4,78E-23
2900441	ZBTB4	Homo sapiens zinc finger and BTB domain containing 4 (ZBTB4), mRNA.	0,599	3,23E-25
7050189	PRPF19	Homo sapiens PRP19/PSO4 pre-mRNA processing factor 19 homolog (S. cerevisiae) (PRPF19), mRNA.	0,599	3,28E-18
1820592	HIST2H2AA3	Homo sapiens histone cluster 2, H2aa3 (HIST2H2AA3), mRNA.	0,6	1,63E-08
2190689	OSBPL5	Homo sapiens oxysterol binding protein-like 5 (OSBPL5), transcript variant 1, mRNA.	0,602	2,69E-32
2510253	C10orf35	Homo sapiens chromosome 10 open reading frame 35 (C10orf35), mRNA.	0,602	2,76E-27
1740717	BOLA2	Homo sapiens bolA homolog 2 (E. coli) (BOLA2), mRNA.	0,603	7,35E-17
2640292	CTGF	Homo sapiens connective tissue growth factor (CTGF), mRNA.	0,604	1,8E-10
4290088	MSRB3	Homo sapiens methionine sulfoxide reductase B3 (MSRB3), transcript variant 1, mRNA.	0,604	2,18E-19
1780367	C12orf44	Homo sapiens chromosome 12 open reading frame 44 (C12orf44), transcript variant 2, mRNA.	0,605	7,48E-22
5130332	ZNF213	Homo sapiens zinc finger protein 213 (ZNF213), mRNA.	0,608	1,09E-20
1110228	TMEM136	Homo sapiens transmembrane protein 136 (TMEM136), mRNA.	0,608	4,02E-27
4050463	TMEM218	Homo sapiens transmembrane protein 218 (TMEM218), mRNA.	0,61	3,53E-15

5670661	MGC71993	Homo sapiens similar to DNA segment, Chr 11, Brigham & Womens Genetics 0434 expressed (MGC71993), mRNA.	0,611	1,55E-27
2470484	RNASEK	Homo sapiens ribonuclease, RNase K (RNASEK), mRNA.	0,612	1,61E-14
520255	TUBB6	Homo sapiens tubulin, beta 6 (TUBB6), mRNA.	0,613	8,61E-28
3360452	COL8A1	Homo sapiens collagen, type VIII, alpha 1 (COL8A1), transcript variant 2, mRNA.	0,613	9,19E-18
4780072	TCEAL3	Homo sapiens transcription elongation factor A (SII)-like 3 (TCEAL3), transcript variant 1, mRNA.	0,614	1,71E-33
1240360	MRPL52	Homo sapiens mitochondrial ribosomal protein L52 (MRPL52), nuclear gene encoding mitochondrial protein, transcript variant 2, mRNA.	0,614	2,4E-21
70634	RABAC1	Homo sapiens Rab acceptor 1 (prenylated) (RABAC1), mRNA.	0,614	2,86E-17
6940561	IFI27L2	Homo sapiens interferon, alpha-inducible protein 27-like 2 (IFI27L2), mRNA.	0,616	4,66E-13
3940564	FAM131A	Homo sapiens family with sequence similarity 131, member A (FAM131A), mRNA.	0,616	5,61E-17
2750309	MRPL53	Homo sapiens mitochondrial ribosomal protein L53 (MRPL53), nuclear gene encoding mitochondrial protein, mRNA.	0,617	1,81E-15
1940274	IFI27L2	Homo sapiens interferon, alpha-inducible protein 27-like 2 (IFI27L2), mRNA.	0,617	3,33E-18
6520433	ZNF789	Homo sapiens zinc finger protein 789 (ZNF789), transcript variant 2, mRNA.	0,617	5,3E-15
1710202	LOC644869	PREDICTED: Homo sapiens hypothetical protein LOC644869 (LOC644869), mRNA.	0,617	5,4E-13
1340400	C6orf129	Homo sapiens chromosome 6 open reading frame 129 (C6orf129), mRNA.	0,618	4,99E-18
6380187	C21orf57	Homo sapiens chromosome 21 open reading frame 57 (C21orf57), transcript variant 1, mRNA.	0,619	1,38E-22
3390093	BOLA3	Homo sapiens bolA homolog 3 (E. coli) (BOLA3), transcript variant 2, mRNA.	0,619	7,4E-26
5080367	CKLF	Homo sapiens chemokine-like factor (CKLF), transcript variant 5, mRNA.	0,619	2,02E-24
7150433	TCTEX1D2	Homo sapiens Tctex1 domain containing 2 (TCTEX1D2), mRNA.	0,62	5,95E-35
3780095	AOX1	Homo sapiens aldehyde oxidase 1 (AOX1), mRNA.	0,62	2,42E-17
7610747	MRPL24	Homo sapiens mitochondrial ribosomal protein L24 (MRPL24), nuclear gene encoding mitochondrial protein, transcript variant 1, mRNA.	0,62	3,07E-23
540451	LOC127295	PREDICTED: Homo sapiens similar to 60S ribosomal protein L36 (LOC127295), mRNA.	0,621	4,82E-22
3120707	CUTA	Homo sapiens cutA divalent cation tolerance homolog (E. coli) (CUTA), transcript variant 5, mRNA.	0,621	3,02E-17
3940132	ITGB4	Homo sapiens integrin, beta 4 (ITGB4), transcript variant 2, mRNA.	0,622	1,79E-29
6550180	ZMAT5	Homo sapiens zinc finger, matrin type 5 (ZMAT5), transcript variant 1, mRNA.	0,623	3,24E-14
5870446	ATP5G1	Homo sapiens ATP synthase, H+ transporting, mitochondrial F0 complex, subunit C1 (subunit 9) (ATP5G1), nuclear gene encoding mitochondrial protein, transcript variant 2, mRNA.	0,623	1,25E-29
2510091	COL8A1	Homo sapiens collagen, type VIII, alpha 1 (COL8A1), transcript variant 2, mRNA.	0,623	1,45E-27
6040292	FBXO28	Homo sapiens F-box protein 28 (FBXO28), mRNA.	0,623	1,97E-16
4290075	SRA1	Homo sapiens steroid receptor RNA activator 1 (SRA1), mRNA.	0,624	4,72E-16
1570092	TUBB6	PREDICTED: Homo sapiens tubulin, beta 6 (TUBB6), mRNA.	0,624	2,47E-16

5490626	SUMF1	Homo sapiens sulfatase modifying factor 1 (SUMF1), mRNA.	0,625	4,94E-29
1240551	ACADVL	Homo sapiens acyl-Coenzyme A dehydrogenase, very long chain (ACADVL), nuclear gene encoding mitochondrial protein, transcript variant 1, mRNA.	0,625	3,03E-10
7200156	ITGB2	Homo sapiens integrin, beta 2 (antigen CD18 (p95), lymphocyte function-associated antigen 1; macrophage antigen 1 (mac-1) beta subunit) (ITGB2), mRNA.	0,626	3,69E-27
4200541	FAM113B	Homo sapiens family with sequence similarity 113, member B (FAM113B), mRNA.	0,628	2,1E-21
4250398	STK4	Homo sapiens serine/threonine kinase 4 (STK4), mRNA.	0,628	2,64E-25
6660270	MRPL17	Homo sapiens mitochondrial ribosomal protein L17 (MRPL17), nuclear gene encoding mitochondrial protein, mRNA.	0,628	2,57E-24
4780040	MRPL41	Homo sapiens mitochondrial ribosomal protein L41 (MRPL41), nuclear gene encoding mitochondrial protein, mRNA.	0,628	2,48E-20
1240521	PSMG4	Homo sapiens proteasome (prosome, macropain) assembly chaperone 4 (PSMG4), transcript variant 2, mRNA.	0,629	3,24E-22
1070671	LOC100129297	PREDICTED: Homo sapiens hypothetical protein LOC100129297 (LOC100129297), mRNA.	0,629	4,02E-08
4290014	FLAD1	Homo sapiens FAD1 flavin adenine dinucleotide synthetase homolog (S. cerevisiae) (FLAD1), transcript variant 2, mRNA.	0,63	1,77E-41
730040	LAMB3	Homo sapiens laminin, beta 3 (LAMB3), transcript variant 1, mRNA.	0,631	8E-22
1660703	MGC72080	Homo sapiens MGC72080 pseudogene (MGC72080) on chromosome 7.	0,631	7,81E-13
6760414	C19orf60	Homo sapiens chromosome 19 open reading frame 60 (C19orf60), transcript variant 2, mRNA.	0,631	4,26E-11
5310168	HLA-B	Homo sapiens major histocompatibility complex, class I, B (HLA-B), mRNA.	0,632	8,99E-20
770687	FASTK	Homo sapiens Fas-activated serine/threonine kinase (FASTK), transcript variant 4, mRNA.	0,632	3,09E-23
2060110	TDP1	Homo sapiens tyrosyl-DNA phosphodiesterase 1 (TDP1), transcript variant 1, mRNA.	0,633	6,2E-18
6060731	MAPRE1	Homo sapiens microtubule-associated protein, RP/EB family, member 1 (MAPRE1), mRNA.	0,633	5,41E-19
5050156	BCL2L2	Homo sapiens BCL2-like 2 (BCL2L2), mRNA.	0,634	1,26E-15
2760519	CKLF	Homo sapiens chemokine-like factor (CKLF), transcript variant 6, mRNA.	0,634	1,09E-16
270196	OBFC2B	Homo sapiens oligonucleotide/oligosaccharide-binding fold containing 2B (OBFC2B), mRNA.	0,634	7,28E-18
3140021	PCBD1	Homo sapiens pterin-4 alpha-carbinolamine dehydratase/dimerization cofactor of hepatocyte nuclear factor 1 alpha (PCBD1), mRNA.	0,635	4,25E-11
4150687	NDUFB2	Homo sapiens NADH dehydrogenase (ubiquinone) 1 beta subcomplex, 2, 8kDa (NDUFB2), nuclear gene encoding mitochondrial protein, mRNA.	0,636	2,71E-29
7000307	ACSL4	Homo sapiens acyl-CoA synthetase long-chain family member 4 (ACSL4), transcript variant 1, mRNA.	0,636	4,04E-13
3390577	MRRF	Homo sapiens mitochondrial ribosome recycling factor (MRRF), nuclear gene encoding mitochondrial protein, transcript variant 2, mRNA.	0,636	2,04E-33
2030044	C1orf144	Homo sapiens chromosome 1 open reading frame 144 (C1orf144), mRNA.	0,637	1,25E-35

5700309	FAHD2B	Homo sapiens fumarylacetoacetate hydrolase domain containing 2B (FAHD2B), mRNA.	0,637	7,32E-11
6220746	GLIPR1	Homo sapiens GLI pathogenesis-related 1 (GLIPR1), mRNA.	0,637	7,06E-22
7610593	TRAPPC5	Homo sapiens trafficking protein particle complex 5 (TRAPPC5), transcript variant 3, mRNA.	0,638	1,54E-17
990372	COL17A1	Homo sapiens collagen, type XVII, alpha 1 (COL17A1), mRNA.	0,638	9,58E-21
7560092	TMEM126A	Homo sapiens transmembrane protein 126A (TMEM126A), mRNA.	0,64	7,11E-20
1400484	LDOC1	Homo sapiens leucine zipper, down-regulated in cancer 1 (LDOC1), mRNA.	0,64	1,06E-18
5050242	TCEB1	Homo sapiens transcription elongation factor B (SIII), polypeptide 1 (15kDa, elongin C) (TCEB1), mRNA.	0,641	1,24E-07
4880392	KIAA1539	Homo sapiens KIAA1539 (KIAA1539), mRNA.	0,641	4,63E-22
7380164	STX4	Homo sapiens syntaxin 4 (STX4), mRNA.	0,642	1E-07
2640411	UNC84B	Homo sapiens unc-84 homolog B (C. elegans) (UNC84B), mRNA.	0,642	9,88E-26
5310286	SPA17	Homo sapiens sperm autoantigenic protein 17 (SPA17), mRNA.	0,643	1,38E-16
3190671	ATP5D	Homo sapiens ATP synthase, H+ transporting, mitochondrial F1 complex, delta subunit (ATP5D), nuclear gene encoding mitochondrial protein, transcript variant 1, mRNA.	0,644	7,47E-17
1510521	PAFAH1B3	Homo sapiens platelet-activating factor acetylhydrolase, isoform Ib, gamma subunit 29kDa (PAFAH1B3), mRNA.	0,644	1,18E-27
7330068	SF3B5	Homo sapiens splicing factor 3b, subunit 5, 10kDa (SF3B5), mRNA.	0,645	1,67E-18
6370468	BOLA2	Homo sapiens bolA homolog 2 (E. coli) (BOLA2), mRNA.	0,645	1,17E-13
6280167	LOC401115	PREDICTED: Homo sapiens hypothetical gene supported by BC038466; BC062790 (LOC401115), mRNA.	0,645	1,74E-23
2140369	NDUFA11	Homo sapiens NADH dehydrogenase (ubiquinone) 1 alpha subcomplex, 11, 14.7kDa (NDUFA11), nuclear gene encoding mitochondrial protein, mRNA.	0,645	1,03E-21
4760288	ANAPC11	Homo sapiens anaphase promoting complex subunit 11 (ANAPC11), transcript variant 4, mRNA.	0,646	1,63E-23
7210544	LOC100133328	PREDICTED: Homo sapiens misc_RNA (LOC100133328), miscRNA.	0,646	4,62E-18
3390129	C9orf103	Homo sapiens chromosome 9 open reading frame 103 (C9orf103), mRNA.	0,646	2,62E-23
6370500	AGRN	Homo sapiens agrin (AGRN), mRNA.	0,646	6,98E-17
1510543	DNASE1L1	Homo sapiens deoxyribonuclease I-like 1 (DNASE1L1), transcript variant 4, mRNA.	0,647	2,25E-14
1580021	TCTEX1D2	Homo sapiens Tctex1 domain containing 2 (TCTEX1D2), mRNA.	0,648	1,7E-14
2650164	FLJ10986	Homo sapiens hypothetical protein FLJ10986 (FLJ10986), mRNA.	0,648	4,25E-32
20435	LOC729279	PREDICTED: Homo sapiens misc_RNA (LOC729279), miscRNA.	0,648	3,03E-18
3890373	ITGB2	Homo sapiens integrin, beta 2 (complement component 3 receptor 3 and 4 subunit) (ITGB2), mRNA.	0,648	2,1E-28
3710725	ATP5E	Homo sapiens ATP synthase, H+ transporting, mitochondrial F1 complex, epsilon subunit (ATP5E), nuclear gene encoding mitochondrial protein, mRNA.	0,649	1,5E-18
6520576	BOLA3	Homo sapiens bolA homolog 3 (E. coli) (BOLA3), transcript variant 1, mRNA.	0,649	3,01E-22
7400468	AP1G2	Homo sapiens adaptor-related protein complex 1, gamma 2 subunit (AP1G2), mRNA.	0,65	4,65E-14
3890427	LOC729843	PREDICTED: Homo sapiens similar to WW domain binding protein 1 (LOC729843), mRNA.	0,65	1,49E-18

4590615	C7orf59	Homo sapiens chromosome 7 open reading frame 59 (C7orf59), mRNA.	0,65	4,92E-22
2450725	SLC3A2	Homo sapiens solute carrier family 3 (activators of dibasic and neutral amino acid transport), member 2 (SLC3A2), transcript variant 6, mRNA.	0,65	1,22E-17
290035	C11orf59	Homo sapiens chromosome 11 open reading frame 59 (C11orf59), mRNA.	0,651	2,17E-24
5670594	NMB	Homo sapiens neuromedin B (NMB), transcript variant 1, mRNA.	0,651	1,62E-15
540240	LOC440957	Homo sapiens similar to CG32736-PA (LOC440957), mRNA.	0,651	9,53E-13
2120270	COL17A1	Homo sapiens collagen, type XVII, alpha 1 (COL17A1), mRNA.	0,652	1,21E-19
6940360	ACVR1	Homo sapiens activin A receptor, type I (ACVR1), mRNA.	0,652	5,48E-16
6940377	TOMM7	Homo sapiens translocase of outer mitochondrial membrane 7 homolog (yeast) (TOMM7), nuclear gene encoding mitochondrial protein, mRNA.	0,652	1,43E-16
2000468	SRPK2	Homo sapiens SFRS protein kinase 2 (SRPK2), transcript variant 2, mRNA.	0,653	8,02E-14
4640392	MLLT6	Homo sapiens myeloid/lymphoid or mixed-lineage leukemia (trithorax homolog, Drosophila); translocated to, 6 (MLLT6), mRNA.	0,654	8,27E-17
2650274	C19orf60	Homo sapiens chromosome 19 open reading frame 60 (C19orf60), transcript variant 1, mRNA.	0,655	6,21E-16
1240176	PPP1R13L	Homo sapiens protein phosphatase 1, regulatory (inhibitor) subunit 13 like (PPP1R13L), mRNA.	0,655	9,97E-17
6270100	LAMP1	Homo sapiens lysosomal-associated membrane protein 1 (LAMP1), mRNA.	0,656	5,87E-21
150438	MID1IP1	Homo sapiens MID1 interacting protein 1 (gastrulation specific G12 homolog (zebrafish)) (MID1IP1), transcript variant 1, mRNA.	0,657	1,57E-17
4900273	LOC100130835	PREDICTED: Homo sapiens misc_RNA (LOC100130835), miscRNA.	0,657	7,58E-14
4290368	PSTPIP2	Homo sapiens proline-serine-threonine phosphatase interacting protein 2 (PSTPIP2), mRNA.	0,659	1,95E-13
4290605	SLC44A1	Homo sapiens solute carrier family 44, member 1 (SLC44A1), mRNA.	0,659	4,01E-20
1940743	RPL13	Homo sapiens ribosomal protein L13 (RPL13), transcript variant 2, mRNA.	0,659	3,61E-12
5310411	H2AFJ	Homo sapiens H2A histone family, member J (H2AFJ), transcript variant 1, mRNA.	0,659	4,88E-17
7550307	PRKCDBP	Homo sapiens protein kinase C, delta binding protein (PRKCDBP), mRNA.	0,66	4,69E-20
1300392	FAM83H	Homo sapiens family with sequence similarity 83, member H (FAM83H), mRNA.	0,66	1,43E-28
5810201	ZNF593	Homo sapiens zinc finger protein 593 (ZNF593), mRNA.	0,66	2,2E-14
3850026	TP53AP1	Homo sapiens TP53 activated protein 1 (TP53AP1), mRNA.	0,661	1,82E-14
1260010	RBM39	Homo sapiens RNA binding motif protein 39 (RBM39), transcript variant 1, mRNA.	0,661	7,28E-18
1770747	TMEM160	Homo sapiens transmembrane protein 160 (TMEM160), mRNA.	0,661	2,67E-11
3120544	METRN	Homo sapiens meteorin, glial cell differentiation regulator (METRN), mRNA.	0,661	3,33E-11
1050386	SMUG1	Homo sapiens single-strand-selective monofunctional uracil-DNA glycosylase 1 (SMUG1), mRNA.	0,661	2,09E-21
670113	TPP1	Homo sapiens tripeptidyl peptidase I (TPP1), mRNA.	0,661	3,59E-12

6330025	EXOSC6	Homo sapiens exosome component 6 (EXOSC6), mRNA.	0,662	1,34E-17
5080164	GEMIN6	Homo sapiens gem (nuclear organelle) associated protein 6 (GEMIN6), mRNA.	0,662	2,99E-20
6110731	ITPK1	Homo sapiens inositol 1,3,4-triphosphate 5/6 kinase (ITPK1), mRNA.	0,662	3,85E-16
5260349	NGFRAP1	Homo sapiens nerve growth factor receptor (TNFRSF16) associated protein 1 (NGFRAP1), transcript variant 1, mRNA.	0,663	2,19E-15
4540241	C5orf32	Homo sapiens chromosome 5 open reading frame 32 (C5orf32), mRNA.	0,663	1,02E-13
3400133	TCEB2	Homo sapiens transcription elongation factor B (SIII), polypeptide 2 (18kDa, elongin B) (TCEB2), transcript variant 1, mRNA.	0,664	6,4E-24
4230243	NHP2L1	Homo sapiens NHP2 non-histone chromosome protein 2-like 1 (S. cerevisiae) (NHP2L1), transcript variant 2, mRNA.	0,664	1,14E-17
270615	ABCC3	Homo sapiens ATP-binding cassette, sub-family C (CFTR/MRP), member 3 (ABCC3), mRNA.	0,664	9,41E-27
6940255	PLSCR3	Homo sapiens phospholipid scramblase 3 (PLSCR3), mRNA.	0,664	2,08E-19
4830458	GMPPB	Homo sapiens GDP-mannose pyrophosphorylase B (GMPPB), transcript variant 2, mRNA.	0,665	5,96E-10
6280341	PTS	Homo sapiens 6-pyruvoyltetrahydropterin synthase (PTS), mRNA.	0,665	1,88E-12
3890673	NUMA1	Homo sapiens nuclear mitotic apparatus protein 1 (NUMA1), mRNA.	0,666	1,88E-14
1070025	ATPIF1	Homo sapiens ATPase inhibitory factor 1 (ATPIF1), nuclear gene encoding mitochondrial protein, transcript variant 3, mRNA.	0,666	2,03E-20
4050437	PTS	Homo sapiens 6-pyruvoyltetrahydropterin synthase (PTS), mRNA.	0,666	4,6E-22
6960332	FOSL1	Homo sapiens FOS-like antigen 1 (FOSL1), mRNA.	0,667	5,73E-14
3400538	IGFBP7	Homo sapiens insulin-like growth factor binding protein 7 (IGFBP7), mRNA.	0,667	4,41E-16
610451	HIST2H2AA3	Homo sapiens histone cluster 2, H2aa3 (HIST2H2AA3), mRNA.	0,667	2,91E-14
5260360	LOC100131801	PREDICTED: Homo sapiens similar to hCG2036585 (LOC100131801), mRNA.	0,667	3,93E-14
6420180	TJAP1	Homo sapiens tight junction associated protein 1 (peripheral) (TJAP1), mRNA.	0,667	1,92E-28
1340537	ALKBH2	Homo sapiens alkB, alkylation repair homolog 2 (E. coli) (ALKBH2), mRNA.	0,668	2,18E-12
6620360	C12orf62	Homo sapiens chromosome 12 open reading frame 62 (C12orf62), mRNA.	0,668	1,14E-13
1450377	BLOC1S1	Homo sapiens biogenesis of lysosome-related organelles complex-1, subunit 1 (BLOC1S1), mRNA.	0,669	4,95E-05
4180315	CHMP4B	Homo sapiens chromatin modifying protein 4B (CHMP4B), mRNA.	0,67	8,17E-20
840014	TPMT	Homo sapiens thiopurine S-methyltransferase (TPMT), mRNA.	0,67	1,16E-19
2320367	NDUFA13	Homo sapiens NADH dehydrogenase (ubiquinone) 1 alpha subcomplex, 13 (NDUFA13), mRNA.	0,67	5,36E-09
2710129	D2HGDH	Homo sapiens D-2-hydroxyglutarate dehydrogenase (D2HGDH), nuclear gene encoding mitochondrial protein, mRNA.	0,67	1,09E-19
3120228	AP2S1	Homo sapiens adaptor-related protein complex 2, sigma 1 subunit (AP2S1), transcript variant AP17, mRNA.	0,671	4,74E-19
2120286	POLE4	Homo sapiens polymerase (DNA-directed), epsilon 4 (p12 subunit) (POLE4), mRNA.	0,671	1,17E-15
2360593	DDT	Homo sapiens D-dopachrome tautomerase (DDT), transcript variant 1, mRNA.	0,672	2,62E-23

520356	FXR1	Homo sapiens fragile X mental retardation, autosomal homolog 1 (FXR1), transcript variant 1, mRNA.	0,672	1,07E-18
60148	BOLA2	Homo sapiens bolA homolog 2 (E. coli) (BOLA2), mRNA.	0,673	6,09E-22
2350333	TEX2	Homo sapiens testis expressed 2 (TEX2), mRNA.	0,673	7,66E-16
1580327	SMARCD2	Homo sapiens SWI/SNF related, matrix associated, actin dependent regulator of chromatin, subfamily d, member 2 (SMARCD2), mRNA.	0,673	4,57E-18
1090221	VPS37A	Homo sapiens vacuolar protein sorting 37 homolog A (S. cerevisiae) (VPS37A), mRNA.	0,674	1,71E-12
50450	TMEM179B	Homo sapiens transmembrane protein 179B (TMEM179B), mRNA.	0,675	9,92E-17
6100382	RTKN	Homo sapiens rhotekin (RTKN), transcript variant 2, mRNA.	0,675	5,88E-29
2690601	ARPC4	Homo sapiens actin related protein 2/3 complex, subunit 4, 20kDa (ARPC4), transcript variant 2, mRNA.	0,675	6,03E-16
3800470	MBOAT7	Homo sapiens membrane bound O-acyltransferase domain containing 7 (MBOAT7), mRNA.	0,676	7,84E-11
7000692	MRPL52	Homo sapiens mitochondrial ribosomal protein L52 (MRPL52), nuclear gene encoding mitochondrial protein, transcript variant 6, mRNA.	0,676	1,32E-15
1580427	THEM2	Homo sapiens thioesterase superfamily member 2 (THEM2), mRNA.	0,676	6,47E-15
1570110	MANBAL	Homo sapiens mannosidase, beta A, lysosomal-like (MANBAL), transcript variant 2, mRNA.	0,676	6,29E-20
5420301	LOC645979	PREDICTED: Homo sapiens similar to ribosomal protein S26 (LOC645979), mRNA.	0,676	4,63E-09
1570746	LOC651816	PREDICTED: Homo sapiens similar to Ubiquitin-conjugating enzyme E2S (Ubiquitin-conjugating enzyme E2-24 kDa) (Ubiquitin-protein ligase) (Ubiquitin carrier protein) (E2-EPF5) (LOC651816), mRNA.	0,676	4,97E-18
3710040	SFN	Homo sapiens stratifin (SFN), mRNA.	0,676	6,8E-19
3120037	C5orf30	Homo sapiens chromosome 5 open reading frame 30 (C5orf30), mRNA.	0,676	4,88E-17
2940369	SKP1	Homo sapiens S-phase kinase-associated protein 1 (SKP1), transcript variant 1, mRNA.	0,677	7,37E-20
3800725	SPHK2	Homo sapiens sphingosine kinase 2 (SPHK2), mRNA.	0,677	3,29E-16
1450168	UPF1	Homo sapiens UPF1 regulator of nonsense transcripts homolog (yeast) (UPF1), mRNA.	0,677	1,48E-13
5720102	C7orf55	Homo sapiens chromosome 7 open reading frame 55 (C7orf55), nuclear gene encoding mitochondrial protein, mRNA.	0,678	1,07E-09
6290328	MAFG	Homo sapiens v-maf musculoaponeurotic fibrosarcoma oncogene homolog G (avian) (MAFG), transcript variant 1, mRNA.	0,678	1,79E-19
4880129	TOMM7	Homo sapiens translocase of outer mitochondrial membrane 7 homolog (yeast) (TOMM7), nuclear gene encoding mitochondrial protein, mRNA.	0,678	2,1E-20
5220070	HLA-F	Homo sapiens major histocompatibility complex, class I, F (HLA-F), transcript variant 1, mRNA.	0,678	6,18E-10
270605	STRA13	Homo sapiens stimulated by retinoic acid 13 homolog (mouse) (STRA13), mRNA.	0,678	2,87E-23
2640324	SLC46A3	Homo sapiens solute carrier family 46, member 3 (SLC46A3), mRNA.	0,679	8,81E-14
1410563	C18orf25	Homo sapiens chromosome 18 open reading frame 25 (C18orf25), transcript variant 2, mRNA.	0,679	8,47E-16

2570463	LOC728492	PREDICTED: Homo sapiens similar to small EDRK-rich factor 1A, telomeric, transcript variant 4 (LOC728492), mRNA.	0,679	4,59E-19
2370167	LOC100130154	PREDICTED: Homo sapiens similar to thymosin, beta 10 (LOC100130154), mRNA.	0,679	1,83E-12
4200367	C3orf54	Homo sapiens chromosome 3 open reading frame 54 (C3orf54), mRNA.	0,679	8,9E-15
7210725	MRPL55	Homo sapiens mitochondrial ribosomal protein L55 (MRPL55), nuclear gene encoding mitochondrial protein, transcript variant 5, mRNA.	0,679	3,66E-19
990193	SF3B4	Homo sapiens splicing factor 3b, subunit 4, 49kDa (SF3B4), mRNA.	0,68	6,24E-25
2190753	C11orf17	Homo sapiens chromosome 11 open reading frame 17 (C11orf17), transcript variant 1, mRNA.	0,68	2,55E-11
3890349	HIST1H4C	Homo sapiens histone cluster 1, H4c (HIST1H4C), mRNA.	0,68	9,95E-21
510577	TRIML2	Homo sapiens tripartite motif family-like 2 (TRIML2), mRNA.	0,68	4,28E-23
6760746	MRPL55	Homo sapiens mitochondrial ribosomal protein L55 (MRPL55), nuclear gene encoding mitochondrial protein, transcript variant 1, mRNA.	0,68	4,12E-12
240546	SCAND1	Homo sapiens SCAN domain containing 1 (SCAND1), transcript variant 2, mRNA.	0,68	7,76E-11
6220026	MAPRE3	Homo sapiens microtubule-associated protein, RP/EB family, member 3 (MAPRE3), mRNA.	0,681	4,86E-15
5560594	TXNDC17	Homo sapiens thioredoxin domain containing 17 (TXNDC17), mRNA.	0,681	2,73E-25
380242	G6PC3	Homo sapiens glucose 6 phosphatase, catalytic, 3 (G6PC3), mRNA.	0,681	6,52E-10
4900402	LOC651453	PREDICTED: Homo sapiens similar to ribosomal protein L36 (LOC651453), mRNA.	0,681	1,48E-06
1780678	LOC374395	Homo sapiens similar to RIKEN cDNA 1810059G22 (LOC374395), mRNA.	0,681	4,22E-22
3130291	C12orf57	Homo sapiens chromosome 12 open reading frame 57 (C12orf57), mRNA.	0,682	9,96E-20
5050608	TIMM23	Homo sapiens translocase of inner mitochondrial membrane 23 homolog (yeast) (TIMM23), nuclear gene encoding mitochondrial protein, mRNA.	0,682	1,83E-13
3120196	ALDH3A2	Homo sapiens aldehyde dehydrogenase 3 family, member A2 (ALDH3A2), transcript variant 1, mRNA.	0,682	5,01E-17
6370288	C17orf68	PREDICTED: Homo sapiens chromosome 17 open reading frame 68 (C17orf68), mRNA.	0,683	7,42E-11
4560088	LOC439949	PREDICTED: Homo sapiens hypothetical gene supported by AY007155 (LOC439949), mRNA.	0,683	1,21E-10
1990152	CSRP2	Homo sapiens cysteine and glycine-rich protein 2 (CSRP2), mRNA.	0,683	2E-12
4290349	LOC643949	PREDICTED: Homo sapiens similar to 60S acidic ribosomal protein P2 (LOC643949), mRNA.	0,684	5,6E-10
2750066	LOC100132499	PREDICTED: Homo sapiens similar to mCG7602 (LOC100132499), mRNA.	0,685	2,11E-12
3180619	LOC643438	PREDICTED: Homo sapiens misc_RNA (LOC643438), miscRNA.	0,685	2,75E-12
6130332	UCRC	Homo sapiens ubiquinol-cytochrome c reductase complex (7.2 kD) (UCRC), transcript variant 2, mRNA.	0,685	3,03E-10
2690338	RPS21	Homo sapiens ribosomal protein S21 (RPS21), mRNA.	0,686	2,14E-19
2320110	ATP6V0E1	Homo sapiens ATPase, H+ transporting, lysosomal 9kDa, V0 subunit e1 (ATP6V0E1), mRNA.	0,686	5,47E-17

5910474	PMS2L4	Homo sapiens postmeiotic segregation increased 2-like 4 pseudogene (PMS2L4), non-coding RNA.	0,686	5,23E-18
2260066	CLIP1	Homo sapiens CAP-GLY domain containing linker protein 1 (CLIP1), transcript variant 1, mRNA.	0,686	2,82E-17
6380367	BOLA2	Homo sapiens bolA homolog 2 (E. coli) (BOLA2), mRNA.	0,687	1,3E-12
3290181	CHMP2A	Homo sapiens chromatin modifying protein 2A (CHMP2A), transcript variant 1, mRNA.	0,687	6,57E-12
1470551	SEL1L3	Homo sapiens sel-1 suppressor of lin-12-like 3 (C. elegans) (SEL1L3), mRNA.	0,687	6,33E-24
4900114	MORN2	Homo sapiens MORN repeat containing 2 (MORN2), mRNA.	0,688	5,32E-12
1660341	FLJ39632	PREDICTED: Homo sapiens misc_RNA (FLJ39632), miscRNA.	0,688	1,28E-09
1300719	C14orf149	Homo sapiens chromosome 14 open reading frame 149 (C14orf149), mRNA.	0,688	2,17E-10
1110377	ATP5D	Homo sapiens ATP synthase, H+ transporting, mitochondrial F1 complex, delta subunit (ATP5D), nuclear gene encoding mitochondrial protein, transcript variant 1, mRNA.	0,688	4,03E-15
5720136	RAB34	Homo sapiens RAB34, member RAS oncogene family (RAB34), mRNA.	0,688	2,41E-15
1450192	CENPM	Homo sapiens centromere protein M (CENPM), transcript variant 2, mRNA.	0,688	1,16E-19
5690543	LQK1	PREDICTED: Homo sapiens misc_RNA (LQK1), miscRNA.	0,688	2,5E-13
4810128	PHLDA2	Homo sapiens pleckstrin homology-like domain, family A, member 2 (PHLDA2), mRNA.	0,688	6,77E-19
4560528	POP5	Homo sapiens processing of precursor 5, ribonuclease P/MRP subunit (S. cerevisiae) (POP5), transcript variant 3, mRNA.	0,688	3,06E-18
1470348	RAGE	Homo sapiens renal tumor antigen (RAGE), mRNA.	0,688	4,54E-27
6980750	PRKAA1	Homo sapiens protein kinase, AMP-activated, alpha 1 catalytic subunit (PRKAA1), transcript variant 2, mRNA.	0,689	3,23E-10
6480095	SNX27	Homo sapiens sorting nexin family member 27 (SNX27), mRNA.	0,689	1,71E-18
6840022	MANBAL	Homo sapiens mannosidase, beta A, lysosomal-like (MANBAL), transcript variant 2, mRNA.	0,689	1,86E-15
4850300	KIAA1688	Homo sapiens KIAA1688 protein (KIAA1688), mRNA.	0,689	1,01E-13
3170332	DPP9	Homo sapiens dipeptidyl-peptidase 9 (DPP9), mRNA.	0,689	1,52E-08
4280093	LOC440157	Homo sapiens hypothetical gene supported by AK096951; BC066547 (LOC440157), mRNA.	0,689	6,93E-13
6480494	MGMT	Homo sapiens O-6-methylguanine-DNA methyltransferase (MGMT), mRNA.	0,689	2,77E-18
2340494	RDH11	Homo sapiens retinol dehydrogenase 11 (all-trans/9-cis/11-cis) (RDH11), mRNA.	0,689	1,59E-07
4230066	C16orf53	Homo sapiens chromosome 16 open reading frame 53 (C16orf53), mRNA.	0,69	1,29E-11
6520201	NFATC2IP	Homo sapiens nuclear factor of activated T-cells, cytoplasmic, calcineurin-dependent 2 interacting protein (NFATC2IP), mRNA.	0,69	5,03E-10
3390072	LOC100133477	PREDICTED: Homo sapiens similar to Nop10p (LOC100133477), mRNA.	0,69	3,35E-15
2690561	RPLP1	Homo sapiens ribosomal protein, large, P1 (RPLP1), transcript variant 1, mRNA.	0,69	8,01E-08
4010086	OKL38	Homo sapiens pregnancy-induced growth inhibitor (OKL38), transcript variant 1, mRNA.	0,69	1,35E-15
2570100	ABCA7	Homo sapiens ATP-binding cassette, sub-family A (ABC1), member 7 (ABCA7), mRNA.	0,69	8,88E-10
2470333	TBPL1	Homo sapiens TBP-like 1 (TBPL1), mRNA.	0,691	4,86E-13

360626	CMIP	Homo sapiens c-Maf-inducing protein (CMIP), transcript variant Tc-mip, mRNA.	0,691	8,85E-20
1500129	DCPS	Homo sapiens decapping enzyme, scavenger (DCPS), mRNA.	0,691	2,58E-10
4490259	COX8A	Homo sapiens cytochrome c oxidase subunit 8A (ubiquitous) (COX8A), mRNA.	0,692	3,2E-27
7550722	ZMYM6	Homo sapiens zinc finger, MYM-type 6 (ZMYM6), mRNA.	0,692	6,11E-17
150040	ZNF142	Homo sapiens zinc finger protein 142 (ZNF142), transcript variant 2, mRNA.	0,692	1,74E-16
3120139	NENF	Homo sapiens neuron derived neurotrophic factor (NENF), mRNA.	0,692	2,35E-34
6770343	ETFB	Homo sapiens electron-transfer-flavoprotein, beta polypeptide (ETFB), transcript variant 2, mRNA.	0,692	1,09E-23
1240592	C7orf47	Homo sapiens chromosome 7 open reading frame 47 (C7orf47), mRNA.	0,693	8,87E-11
5670075	PAFAH1B1	Homo sapiens platelet-activating factor acetylhydrolase, isoform Ib, alpha subunit 45kDa (PAFAH1B1), mRNA.	0,693	3,74E-19
4260484	COMMD6	Homo sapiens COMM domain containing 6 (COMMD6), transcript variant 1, mRNA.	0,693	1,91E-19
5050437	SCAND1	Homo sapiens SCAN domain containing 1 (SCAND1), transcript variant 1, mRNA.	0,693	8,94E-12
5820753	RBCK1	Homo sapiens RanBP-type and C3HC4-type zinc finger containing 1 (RBCK1), transcript variant 1, mRNA.	0,693	3,84E-22
20450	LOC729580	PREDICTED: Homo sapiens hypothetical LOC729580 (LOC729580), mRNA.	0,693	1,51E-06
4920487	TCEAL4	Homo sapiens transcription elongation factor A (SII)-like 4 (TCEAL4), transcript variant 4, mRNA.	0,693	5,08E-17
730576	SPRY4	Homo sapiens sprouty homolog 4 (Drosophila) (SPRY4), mRNA.	0,693	6,9E-18
7570131	RPS18	Homo sapiens ribosomal protein S18 (RPS18), mRNA.	0,694	1,86E-15
4120025	CHCHD8	Homo sapiens coiled-coil-helix-coiled-coil-helix domain containing 8 (CHCHD8), mRNA.	0,694	6,58E-14
830739	RPP21	Homo sapiens ribonuclease P/MRP 21kDa subunit (RPP21), mRNA.	0,694	1,21E-16
670671	TMEM134	Homo sapiens transmembrane protein 134 (TMEM134), transcript variant 2, mRNA.	0,694	3,78E-09
6380220	Magmas	Homo sapiens mitochondria-associated protein involved in granulocyte-macrophage colony-stimulating factor signal transduction (Magmas), nuclear gene encoding mitochondrial protein, mRNA.	0,694	1,01E-12
620433	C1orf122	Homo sapiens chromosome 1 open reading frame 122 (C1orf122), mRNA.	0,695	5,73E-14
3310376	TIMM10	Homo sapiens translocase of inner mitochondrial membrane 10 homolog (yeast) (TIMM10), nuclear gene encoding mitochondrial protein, mRNA.	0,695	1,71E-19
4060768	DBT	Homo sapiens dihydrolipoamide branched chain transacylase E2 (DBT), nuclear gene encoding mitochondrial protein, mRNA.	0,695	7,03E-27
6420441	LOC728416	PREDICTED: Homo sapiens hypothetical LOC728416 (LOC728416), mRNA.	0,696	1,44E-09
5700451	FKBP9L	Homo sapiens FK506 binding protein 9-like (FKBP9L), mRNA.	0,696	8,51E-13
150441	TIGA1	Homo sapiens TIGA1 (TIGA1), mRNA.	0,696	1,58E-14
6370538	WBSCR22	Homo sapiens Williams Beuren syndrome chromosome region 22 (WBSCR22), mRNA.	0,696	4,57E-15
2510523	RBCK1	Homo sapiens RanBP-type and C3HC4-type zinc finger containing 1 (RBCK1), transcript variant 2, mRNA.	0,696	1,26E-16

7610184	PNKP	Homo sapiens polynucleotide kinase 3'-phosphatase (PNKP), mRNA.	0,696	2,66E-13
1300608	SNHG9	Homo sapiens small nucleolar RNA host gene 9 (non-protein coding) (SNHG9), non-coding RNA.	0,697	2,31E-11
4670021	NPEPL1	Homo sapiens aminopeptidase-like 1 (NPEPL1), mRNA.	0,697	5,04E-19
3390484	SERINC2	Homo sapiens serine incorporator 2 (SERINC2), mRNA.	0,697	3,29E-13
3370136	ACAD11	Homo sapiens acyl-Coenzyme A dehydrogenase family, member 11 (ACAD11), mRNA.	0,697	4,2E-17
2480739	SKP1A	Homo sapiens S-phase kinase-associated protein 1A (p19A) (SKP1A), transcript variant 1, mRNA.	0,697	6,04E-17
4050377	LOC648622	PREDICTED: Homo sapiens similar to ribosomal protein S27 (LOC648622), mRNA.	0,697	1,66E-17
7150017	C6orf48	Homo sapiens chromosome 6 open reading frame 48 (C6orf48), transcript variant 1, mRNA.	0,697	1,3E-11
7000086	KCTD20	Homo sapiens potassium channel tetramerisation domain containing 20 (KCTD20), mRNA.	0,697	1,82E-13
50224	DFFA	Homo sapiens DNA fragmentation factor, 45kDa, alpha polypeptide (DFFA), transcript variant 1, mRNA.	0,698	2,23E-15
3310041	PELP1	Homo sapiens proline, glutamic acid and leucine rich protein 1 (PELP1), mRNA.	0,699	2,82E-15
1470341	PLEKHB2	Homo sapiens pleckstrin homology domain containing, family B (evectins) member 2 (PLEKHB2), transcript variant 2, mRNA.	0,699	1,26E-12
7000703	POLR3K	Homo sapiens polymerase (RNA) III (DNA directed) polypeptide K, 12.3 kDa (POLR3K), mRNA.	0,699	1,49E-12
4670048	RPS26L	Homo sapiens 40S ribosomal protein S26-like (RPS26L), non-coding RNA.	0,699	5,83E-14
70162	TDG	Homo sapiens thymine-DNA glycosylase (TDG), mRNA.	0,699	3,75E-12
1660220	LOC283932	Homo sapiens hypothetical protein LOC283932 (LOC283932), mRNA.	0,7	1,39E-09
3420561	RPA2	Homo sapiens replication protein A2, 32kDa (RPA2), mRNA.	0,7	8,55E-17

Supplementary Table 6

The list of transcripts downregulated by at least 30% upon overexpression of all three miRNAs: miR-301a, miR-301b and miR-130b (overlap of supplementary tables 1, 2 and 3). Notice, that for some of the transcripts more than one probe was present in the array and only the probes for which the downregulation was observed are listed. Those transcripts that had more than one probe for the same mRNA transcript variant and the downregulation was not observed for at least one another probe are indicated in grey. The last column indicates whether a certain transcript is predicted to be a direct target by TargetScan v.6.2 algorithm.

Probe ID	Gene symbol	Definition	Target Scan
270615	ABCC3	Homo sapiens ATP-binding cassette, sub-family C (CFTR/MRP), member 3 (ABCC3), mRNA.	No
6940360	ACVR1	Homo sapiens activin A receptor, type I (ACVR1), mRNA.	Yes
2000546	C3orf10	Homo sapiens chromosome 3 open reading frame 10 (C3orf10), mRNA.	No
7380367	C9orf69	Homo sapiens chromosome 9 open reading frame 69 (C9orf69), mRNA.	Yes
510100	CBY1	Homo sapiens chibby homolog 1 (Drosophila) (CBY1), transcript variant 1, mRNA.	No
3930452	CDC2L6	Homo sapiens cell division cycle 2-like 6 (CDK8-like) (CDC2L6), mRNA.	No

5860010	CDS1	Homo sapiens CDP-diacylglycerol synthase (phosphatidate cytidylyltransferase) 1 (CDS1), mRNA.	Yes
2260066	CLIP1	Homo sapiens CAP-GLY domain containing linker protein 1 (CLIP1), transcript variant 1, mRNA.	Yes
990372	COL17A1	Homo sapiens collagen, type XVII, alpha 1 (COL17A1), mRNA.	No
2120270	COL17A1	Homo sapiens collagen, type XVII, alpha 1 (COL17A1), mRNA.	No
3360452	COL8A1	Homo sapiens collagen, type VIII, alpha 1 (COL8A1), transcript variant 2, mRNA.	No
2510091	COL8A1	Homo sapiens collagen, type VIII, alpha 1 (COL8A1), transcript variant 2, mRNA.	No
2650598	CYP4V2	Homo sapiens cytochrome P450, family 4, subfamily V, polypeptide 2 (CYP4V2), mRNA.	No
3120138	F3	Homo sapiens coagulation factor III (thromboplastin, tissue factor) (F3), mRNA.	No
10079	F3	Homo sapiens coagulation factor III (thromboplastin, tissue factor) (F3), mRNA.	No
2970762	HCCS	Homo sapiens holocytochrome c synthase (cytochrome c heme-lyase) (HCCS), mRNA.	No
5570279	HIST1H1C	Homo sapiens histone cluster 1, H1c (HIST1H1C), mRNA.	No
1820592	HIST2H2AA3	Homo sapiens histone cluster 2, H2aa3 (HIST2H2AA3), mRNA.	No
610451	HIST2H2AA3	Homo sapiens histone cluster 2, H2aa3 (HIST2H2AA3), mRNA.	No
4290148	HIST2H2AA4	Homo sapiens histone cluster 2, H2aa4 (HIST2H2AA4), mRNA.	No
5310168	HLA-B	Homo sapiens major histocompatibility complex, class I, B (HLA-B), mRNA.	No
6400270	HPRT1	Homo sapiens hypoxanthine phosphoribosyltransferase 1 (Lesch-Nyhan syndrome) (HPRT1), mRNA.	Yes
7610286	HPRT1	Homo sapiens hypoxanthine phosphoribosyltransferase 1 (Lesch-Nyhan syndrome) (HPRT1), mRNA.	Yes
3610129	HSD17B1	Homo sapiens hydroxysteroid (17-beta) dehydrogenase 1 (HSD17B1), mRNA.	No
3990170	IFI27	Homo sapiens interferon, alpha-inducible protein 27 (IFI27), transcript variant 2, mRNA.	No
1010246	IFI6	Homo sapiens interferon, alpha-inducible protein 6 (IFI6), transcript variant 2, mRNA.	No
5090215	IFI6	Homo sapiens interferon, alpha-inducible protein 6 (IFI6), transcript variant 3, mRNA.	No
3120431	IMPDH1	Homo sapiens IMP (inosine monophosphate) dehydrogenase 1 (IMPDH1), transcript variant 1, mRNA.	Yes
2100196	ISG15	Homo sapiens ISG15 ubiquitin-like modifier (ISG15), mRNA.	No
7200156	ITGB2	Homo sapiens integrin, beta 2 (antigen CD18 (p95), lymphocyte function-associated antigen 1; macrophage antigen 1 (mac-1) beta subunit) (ITGB2), mRNA.	No
3890373	ITGB2	Homo sapiens integrin, beta 2 (complement component 3 receptor 3 and 4 subunit) (ITGB2), mRNA.	No
2470600	KATNAL1	Homo sapiens katanin p60 subunit A-like 1 (KATNAL1), transcript variant 2, mRNA.	No
4880392	KIAA1539	Homo sapiens KIAA1539 (KIAA1539), mRNA.	No
730040	LAMB3	Homo sapiens laminin, beta 3 (LAMB3), transcript variant 1, mRNA.	No
6580091	LOC339352	PREDICTED: Homo sapiens misc_RNA (LOC339352), miscRNA.	No
4290088	MSRB3	Homo sapiens methionine sulfoxide reductase B3 (MSRB3), transcript variant 1, mRNA.	No
6960014	MTMR9	Homo sapiens myotubularin related protein 9 (MTMR9), mRNA.	Yes

4570091	NDUFAF3	Homo sapiens NADH dehydrogenase (ubiquinone) 1 alpha subcomplex, assembly factor 3 (NDUFAF3), nuclear gene encoding mitochondrial protein, transcript variant 1, mRNA.	No
4010086	OKL38	Homo sapiens pregnancy-induced growth inhibitor (OKL38), transcript variant 1, mRNA.	No
240400	PMEPA1	Homo sapiens prostate transmembrane protein, androgen induced 1 (PMEPA1), transcript variant 2, mRNA.	Yes
7650333	PSAP	Homo sapiens prosaposin (PSAP), transcript variant 2, mRNA.	Yes
6200086	PSAP	Homo sapiens prosaposin (PSAP), transcript variant 1, mRNA.	Yes
2760452	RPS29	Homo sapiens ribosomal protein S29 (RPS29), transcript variant 2, mRNA.	No
5360424	RPS6KA2	Homo sapiens ribosomal protein S6 kinase, 90kDa, polypeptide 2 (RPS6KA2), transcript variant 2, mRNA.	Yes
7100193	RTCD1	Homo sapiens RNA terminal phosphate cyclase domain 1 (RTCD1), mRNA.	Yes
5420326	RTCD1	Homo sapiens RNA terminal phosphate cyclase domain 1 (RTCD1), mRNA.	Yes
1980209	SEC23B	Homo sapiens Sec23 homolog B (S. cerevisiae) (SEC23B), transcript variant 2, mRNA.	No
6370133	SEC23B	Homo sapiens Sec23 homolog B (S. cerevisiae) (SEC23B), transcript variant 2, mRNA.	No
770408	SERPINE1	Homo sapiens serpin peptidase inhibitor, clade E (nexin, plasminogen activator inhibitor type 1), member 1 (SERPINE1), mRNA.	No
2940369	SKP1	Homo sapiens S-phase kinase-associated protein 1 (SKP1), transcript variant 1, mRNA.	Yes
4290605	SLC44A1	Homo sapiens solute carrier family 44, member 1 (SLC44A1), mRNA.	Yes
2640324	SLC46A3	Homo sapiens solute carrier family 46, member 3 (SLC46A3), mRNA.	No
4050161	STX6	Homo sapiens syntaxin 6 (STX6), mRNA.	Yes
2480487	STX6	Homo sapiens syntaxin 6 (STX6), mRNA.	Yes
2340626	TFB1M	Homo sapiens transcription factor B1, mitochondrial (TFB1M), mRNA.	No
7550608	TMEM9B	Homo sapiens TMEM9 domain family, member B (TMEM9B), mRNA.	Yes
3140092	TRAK1	Homo sapiens trafficking protein, kinesin binding 1 (TRAK1), mRNA.	No
510577	TRIML2	Homo sapiens tripartite motif family-like 2 (TRIML2), mRNA.	No
4640066	VAMP3	Homo sapiens vesicle-associated membrane protein 3 (cellubrevin) (VAMP3), mRNA.	No
6200332	VPS24	Homo sapiens vacuolar protein sorting 24 homolog (S. cerevisiae) (VPS24), transcript variant 2, mRNA.	Yes
2140634	VPS24	Homo sapiens vacuolar protein sorting 24 homolog (S. cerevisiae) (VPS24), transcript variant 2, mRNA.	Yes
1090221	VPS37A	Homo sapiens vacuolar protein sorting 37 homolog A (S. cerevisiae) (VPS37A), mRNA.	Yes
4670059	ZAK	Homo sapiens sterile alpha motif and leucine zipper containing kinase AZK (ZAK), transcript variant 2, mRNA.	Yes
3940088	ZBED2	Homo sapiens zinc finger, BED-type containing 2 (ZBED2), mRNA.	No
3140543	ZMAT3	Homo sapiens zinc finger, matrin type 3 (ZMAT3), transcript variant 2, mRNA.	Yes